Variations des systèmes de mousson à l'Holocène dans le modèle de l'IPSL

Charline Marzin

THESE DE DOCTORAT DE
L'UNIVERSITE PIERRE ET MARIE CURIE

Spécialité

Sciences de l'Environnement
Ecole doctorale ED 129
Laboratoire des Sciences du Climat et de l'Environnement

Présentée par

Mme Charline MARZIN

Pour obtenir le grade de

DOCTEUR de l'UNIVERSITÉ PIERRE ET MARIE CURIE

Sujet de la thèse:

Variations des systèmes de mousson à l'Holocène dans le modèle de l'IPSL

soutenue le 28 Février 2011

devant le jury composé de:

Mme Pascale BRACONNOT	*Directrice de thèse*
Mrs Sandy HARRISON	*Rapporteur*
Mr Hervé DOUVILLE	*Rapporteur*
Mme Katia LAVAL	*Examinateur*
Mr Serge JANICOT	*Examinateur*

Table des matières

Résumé

De nombreux indicateurs climatiques et expériences de modélisation montrent l'influence des paramètres de l'orbite terrestre sur les variations passées des systèmes de mousson en Asie et en Afrique. En particulier, les moussons sont amplifiées en Afrique et en Inde au début de l'Holocène, période de maximum d'insolation au sommet de l'atmosphère pendant l'été boréal. Ce travail s'intéresse à l'analyse des variations des systèmes de mousson du Sahel, d'Inde et d'Asie du sud-est au début de l'Holocène (9.5 ka BP) et à l'Holocène moyen (6 ka BP) à l'aide du modèle couplé IPSL-CM4. Il met en évidence l'effet de la précession des équinoxes et de l'influence de diverses rétroactions du climat sur la saisonnalité et les variations relatives de ces trois systèmes de mousson au cours de l'Holocène. Ainsi l'amplitude et la phase des mécanismes de réponse aux variations d'insolation diffèrent entre la mousson indienne et la mousson africaine. Ce lien entre mousson et précession est également confirmé par des simulations du dernier interglaciaire présentant des analogies orbitales avec les périodes de l'Holocène. La thèse aborde aussi le possible rôle de téléconnections entre les systèmes de mousson et entre les moussons et les moyennes latitudes. La comparaison de simulations couplées et forcées met en évidence le rôle de la rétroaction de l'océan sur le cycle saisonnier des précipitations de mousson. Le signe de cette rétroaction sur les changements paléoclimatiques diffère selon les systèmes de mousson. L'influence de la calotte résiduelle au début de l'Holocène et de l'impact du flux d'eau douce lié à la fonte des calottes en Atlantique Nord sur les moussons est discutée. Les expériences de sensibilité montrent des réponses différentes des systèmes asiatiques et africains à ces forçages. Pour compléter ces expériences, la réponse des moussons à un flux d'eau douce en Atlantique Nord est comparée pour plusieurs périodes climatiques

passées (Eémien, dernier maximum glaciaire et Holocène), présente et future. Pour comprendre les résultats, des tests de sensibilité aux variations de température de surface des océans engendrées par la fonte des calottes au dernier maximum glaciaire mettent en évidence des mécanismes de téléconnection entre l'Atlantique tropical et les moussons indienne et africaine. Les résultats des simulations à l'Holocène et au dernier maximum glaciaire sont mis en regard d'enregistrements paléoclimatiques océaniques prélevés dans l'Océan Indien en collaboration avec d'autres équipes scientifiques.

Abstract

Numerous climate indicators and modelling experiments show the influence of orbital parameters on past variations of Asian and African monsoons. In particular, the monsoon precipitation and circulation were amplified in India and Africa at the beginning of the Holocene, when the insolation received at the top of the atmosphere was maximum during boreal summer. This study analyses the variations of monsoons systems over the Sahel, India and East-Asia at the beginning of the Holocene (9.5 kyr BP) and at the Mid-Holocene (6 kyr BP) with the IPSL-CM4 coupled model. This work highlights the role of precession of equinoxes and the influence of several climate feedbacks in modifying the seasonality and the relative amplification of monsoon systems throughout the Holocene. The amplitude and the phase of the mechanisms by which monsoons respond to insolation changes vary over India and Africa. This link between monsoon and precession is also confirmed using some modelling experiments of the last interglacial period with similar orbital configurations as the Holocene. This thesis also discusses the possible role of teleconnections between monsoons subsystems and between monsoons and the mid-latitudes. The comparison between coupled and atmospheric simulations enables to show the impact of the ocean feedback on the seasonal cycle of monsoon precipitation. The sign of the ocean feedback on paleoclimate changes vary from one subsystem to the other. The impact of the reminiscent ice sheet at the beginning of the Holocene and of the freshwater flux due to ice melting in the North Atlantic on monsoons is analyzed. The sensitivity experiments show different responses of the Asian and African systems to these forcings. To complement these experiments, the impact of freshwater flux in the North Atlantic on monsoon systems is compared for several past (Eemian, Last Glacial Maximum, Early Holocene, Mid-Holocene), present and future periods. To understand the results, some sensitivity experiments to the variations of ocean

surface temperature variations due to ice sheet melting have been carried out for the Last glacial Maximum. These highlight teleconnection mechanisms between the tropical Atlantic and the Indian and African monsoons. The results of the modelling experiments at the Holocene and at the Last Glacial Maximum have been compared with paleoclimatic marine records in the Indian Ocean, in collaboration with other scientific groups.

Remerciements

Avant tout, je remercie de tout coeur Pascale Braconnot, ma directrice de thèse, non seulement pour son encadrement scientifique juste et l'opportunité qu'elle m'a donnée de travailler sur un sujet si passionnant et de présenter mes résultats lors de nombreux séminaires et conférences, mais aussi pour son extrême patience, la motivation et les encouragements qu'elle m'a toujours procurés et qui m'ont aidée à rebondir pendant les moments difficiles et à accomplir mon projet professionnel, au-delà de mes espérances. C'est pour moi aussi un modèle de carrière scientifique de femme, n'hésitant pas à s'investir avec passion dans de multiples projets tout en mettant un point d'ordre à faciliter la communication entre différentes communautés scientifiques, et ceci toujours avec le sourire.

Je remercie aussi Masa Kageyama pour avoir piqué ma curiosité avec l'étude de la mousson en période glaciaire, pour avoir supervisé cette partie de mon travail en lien avec Pascale, et elle aussi pour sa disponibilité et sa bonne humeur constante ! Je remercie toute l'équipe de direction du LSCE, ainsi que Didier Paillard, Gilles Ramstein et Elsa Cortijo qui font tout pour apporter aux thésards des conditions de travail vraiment idéales et épanouissantes. Mille mercis pour la précieuse aide technique que j'ai pu recevoir de nombreuses personnes dont Anne, Arnaud, Joséphine, Patrick, Olivier, Jean-Yves, François, Julien, Gaëlle... pour pouvoir mener à bien ces travaux. Cette thèse a été financée grâce à une bourse octroyée par le CEA (Commissariat à l'Energie Atomique). Avant Pascale, BN Goswami, Jean-Philippe Duvel, Alexandre Stegner, Laurent Mortier et Alain Lahellec ont aussi contribué à encourager ma passion pour la recherche dans ce domaine. Je remercie chaleureusement Sandy Harrison, Katia Laval, Hervé Douville et Serge Janicot qui ont accepté d'évaluer mes travaux pour la soutenance de thèse.

Je suis très reconnaissante des discussions que j'ai pu avoir avec de nombreux scientifiques à propos de ce travail, dont Hervé Douville, Jean-Yves Grandpeix, Sandy Harrison, Chris Hewitt, Brian Hoskins, Serge Janicot, Anne-Marie Lézine, Zhengyu Liu, Barbara Maher, Maria Sanchez-Goni, Joy Singarayer, J Srinivasan, Julia Slingo, Bin Wang, Pinxian Wang... qui m'ont permis d'aborder certains problèmes avec un angle différent. Les nombreuses interactions que j'ai eues pendant la thèse avec les scientifiques travaillant sur les enregistrements paléoclimatiques ont grandement enrichi ce travail, notamment avec Elise Mathien-Blard, Franck Bassinot, Jean-Claude Duplessy, Nejib Kallel, Anne-Marie Lézine, Sarah Ivory et Morteza Djamali, merci.

La compagnie de nombreux amis du monde entier croisés au cours de ces quelques années au bâtiment 712 et au LSCE en général a constitué une richesse humaine inestimable, la liste serait bien trop longue ! En particulier merci Anne pour tous ces bons moments passés ensemble, ces goûters, pique-niques, dégustations etc... qui ont insufflé un vent de gourmandise dans les couloirs ! Merci aussi à Aurélie et Joséphine, avec qui on faisait un beau tableau de femmes enceintes ! Merci à toute l'équipe rencontrée sur Le Marion Dufresne lors de la campagne AMOCINT, Catherine, Carlo, Elisabeth, Stefano, Cindy, Aurélie et Camille, cette expérience unique fut inoubliable !

Merci à Marie, Olivier, Rekha, Viju, Cath et George qui m'ont soutenue pendant la phase de rédaction que j'ai effectuée pendant que je travaillais au Met Office. Et mille mercis à Marie et Olivier pour leur relecture du manuscrit.

Je ne pense pas que j'aurais pu traverser ces si longues années d'études qui ont mené à la thèse avec autant de passion et de facilité sans mes grands-parents, aussi bien du point de vue affectif que matériel, merci, merci, merci. Mes remerciements les plus chargés d'émotion à mes parents, pour leur soutien et surtout leur confiance. J'ai pu grâce à eux faire mes propres choix et réaliser mon rêve de petite fille : devenir "météorologue" ! Etre collègues et époux peut avoir des inconvénients, mais avec Prince ça n'a été qu'avantages, je le remercie chaleureusement non seulement de tout l'amour et le soutien qui m'ont permis de dépasser mes capacités et

mes aspirations, de passer les moments difficiles, et d'élargir et enrichir considérablement mon univers, mais aussi de toute son aide scientifique et technique pour de nombreux aspects de ce travail.

Enfin je dédie cette thèse à ma fille Neha, qui bien qu'elle ne m'ait pas rendu tous les jours (les nuits) faciles pendant la thèse, elle est tout simplement ma joie de vivre et mon plus grand bonheur, qui me permet de tout relativiser et de prendre les choses du bon côté. Je lui souhaite d'être aussi fière que moi de faire ce qu'elle choisira de réaliser plus tard.

Liste des publications

Braconnot, P., C. Marzin, L. Gregoire, E. Mosquet, and O. Marti, 2008 : *Monsoon response to changes in Earth's orbital parameters : comparisons between simulations of the Eemian and of the Holocene*. Clim. Past Discuss., 4, 459–493.

Marzin, C. and P. Braconnot, 2009 : *The role of the ocean feedback on Asian and African monsoon variations at 6 kyr and 9.5 kyr BP*. Comptes Rendus Geoscience, 341 (8-9), 643– 655.

Marzin, C. and P. Braconnot, 2009 : *Variations of Indian and African monsoons induced by insolation changes at 6 and 9.5 kyr BP*. Climate Dynamics, 33 (2-3), 215–231.

Kageyama, M., J. Mignot, D. Swingedouw, C. Marzin, R. Alkama, and O. Marti, 2009 : *Glacial climate sensitivity to different states of the Atlantic Meridional Overturning Circulation : results from the IPSL model*. Climate Of The Past, 5 (3), 551–570.

Marzin, C. and P. Braconnot : *Impact of a meltwater flux and of the remnant ice sheet on monsoons at 9.5kyr BP*. Soumis à Geophys. Res. Let.

Bassinot, F.C., C. Marzin, P. Braconnot, O. Marti, E. Mathien-Blard, F. Lombard, and L. Bopp : *Holocene evolution of summer winds and marine productivity in the tropical Indian Ocean in response to insolation forcing : data-model comparison*. Soumis à Climate of the Past.

Marzin, C., N. Kallel, J.-C. Duplessy, M. Kageyama, P. Braconnot : *Impact of rapid events*

on the Indian monsoon under glacial conditions : a model/data comparison study. En préparation.

Glossaire

AMMA : Analyse Multidisciplinaire de la Mousson Africaine

AMOC : Atlantic Meridional Overturning Circulation

ANR : Agence Nationale pour la Recherche

CEA : Commissariat à l'Energie Atomique

COHMAP : COoperative Holocene MApping Project

CMAP : Climate Prediction Center Merged Analysis of Precipitation

CMIP3 : Coupled Modelling Intercomparison Project 3

CMIP5 : Coupled Modelling Intercomparison Project 5

DMG : Dernier Maximum Glaciaire

IPCC : Intergovernmental Panel on Climate Change

IPSL : Institut Pierre Simon Laplace des Sciences de l'Environnement

IRCAAM : Influence Réciproque des Climats d'Afrique de l'ouest, du sud de l'Asie et du bassin Méditerranéen

JJAS : Moyenne sur les mois de Juin, Juillet, Août et Septembre

ka : Milliers d'années avant la période industrielle

LGM : Last Glacial Maximum

LMD : Laboratoire de Météorologie Dynamique

LIM : Louvain Ice Model

LSCE : Laboratoire des Sciences du Climat et de l'Environnement

MJO : Madden-Julian Oscillation

NCEP-NCAR : National Centers for Environmental Prediction-the National Center for Atmospheric Research

OLR : Outgoing Longwave Radiation

ORCHIDEE : ORganizing Carbon and Hydrology In Dynamic EcosystEms

ORCA : Configuration of OPA with a grid covering the whole globe

OPA : Ocean general circulation model

PMIP : Paleoclimate Modelling Intercomparison Project

SAHELP : Sahara and Sahel vulnerability : lessons from the past

SST : Sea Surface Temperature

ZCIT : Zone de Convergence Intertropicale

1

Introduction

"The rainy season had arrived. Rivers overflowed their banks. Peacocks danced at eventide. The rain quelled the expanse of dust as a great ascetic quells the tide of passion. The chataka birds were unhappy. Lightning shown like a bejewelled boat of love in the pleasure-pool of the sky ; it was like a garland for the gate of the palace of paradise : like a lustrous girdle for some heavenly beauty ; like a row of nailmarks left upon the cloud by its lover the departing day."

Extract from Vasavadatta of Subandhu (late 6th century AD)

Le mot "mousson" a pour origine le mot "mausim" (saison en arabe, Fein and Stephens (1987)), les premiers marchands arabes étant familiers du renversement saisonnier des vents dans l'Océan Indien. Cette définition de changement de circulation atmosphérique est traditionnellement celle des géographes et climatologues. Les fermiers indiens ou du Sahel sont eux bien plus concernés par les pluies locales attendues lors de la saison humide. Les pluies des systèmes de mousson de par le monde nourrissent environ la moitié de la population globale

(Webster et al., 1998). Bien que la prévision de ces pluies de mousson représente un enjeu primordial pour les sociétés et économies de nombreux pays, la mousson demeure un système très complexe à prévoir et la modélisation climatique ne parvient pas à représenter toutes les facettes de cette complexité. Ainsi, de nombreuses études sont à la recherche d'une meilleure compréhension des mécanismes climatiques associés à la mousson, depuis les premières études de Halley, Blanford et Walker (Halley, 1686; Blanford, 1886; Walker, 1910).

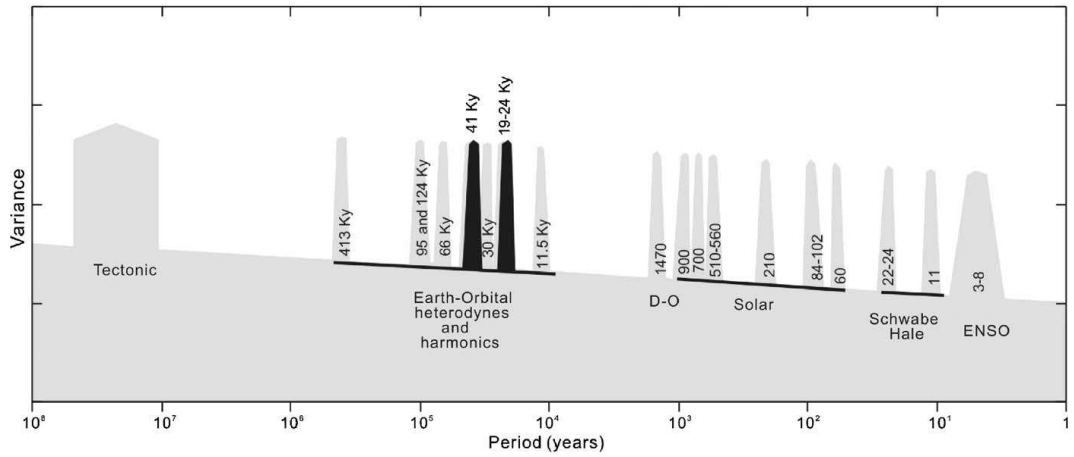

FIGURE 1.1: Spectre conceptuel de variabilité de la mousson asiatique de l'échelle annuelle à l'échelle tectonique, issue de Wang et al. (2005)

L'étude de l'évolution des moussons dans le passé permet d'améliorer la compréhension de ces systèmes et les mécanismes de réponse à divers forçages climatiques. Wang et al. (2005) synthétisent les forçages influençant la mousson à diverses échelles de temps (Fig. 1.1) tels que l'orographie, la distribution spatiale des continents, les concentrations en gaz atmosphériques, les paramètres de l'orbite terrestre, l'étendue des calottes de glace, la variabilité solaire, l'usage des sols, les émissions anthropiques parmis les principaux.

Les paramètres de l'orbite terrestre que sont l'excentricité, l'obliquité et la précession (définitions schématisées sur la figure 1.2) régulent la distribution latitudinale et saisonnière des radiations solaires incidentes au sommet de l'atmosphère (appelée insolation dans le reste du manuscrit, Berger (1978)). Les systèmes de mousson sont connus pour être sensibles à ces variations (COHMAP Members, 1988), les moussons de l'hémisphère nord étant amplifiées pendant les périodes interglaciaires de maximum d'insolation (Prell and Kutzbach, 1987). A l'échelle

du dernier Quaternaire, d'autres facteurs climatiques peuvent altérer la relation entre l'intensité des moussons et celle de l'insolation, tels que la présence de calotte de glace, et la fonte plus ou moins rapides de celles-ci.

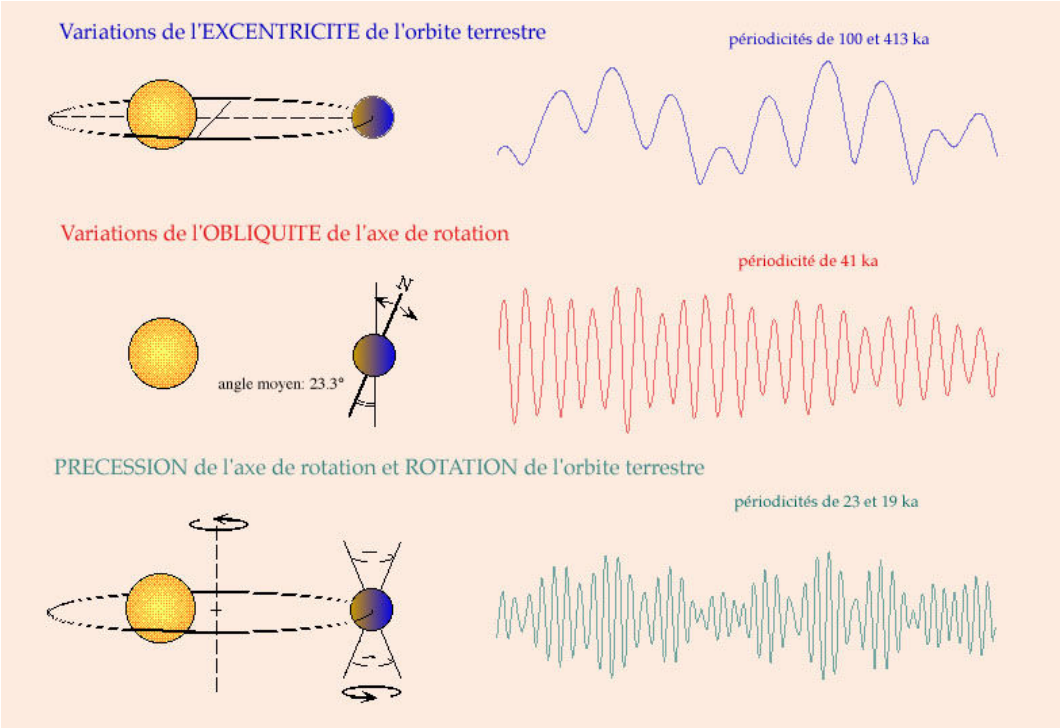

FIGURE 1.2: Schéma des paramètres de l'orbite terrestre : l'excentricité, l'obliquité et la précession. Figure provenant du site internet http ://planet-terre.ens-lyon.fr.

La modélisation du climat passé permet d'étudier en détail la réponse des moussons à ces forçages et de les comparer aux données paléoclimatiques disponibles. Cet exercice permet d'en apprendre plus sur certains mécanismes clés de la mousson et sert de d'évaluation pour les modèles. Les premières expériences de modélisation de la mousson passée furent pour analyser l'effet principal de la précession des équinoxes (ce qui détermine les changements de saisons astronomiquement parlant) au début de l'Holocène (Kutzbach, 1981; Kutzbach and Ottoblies-ner, 1982; Kutzbach and Gallimore, 1988). Ensuite, le projet d'intercomparaison de modélisation paléoclimatique (PMIP, Joussaume and Taylor (1995)) s'est focalisé sur deux périodes de référence : l'Holocène moyen à 6 ka BP (6000 ans avant la période préindustrielle, par la suite 6 ka) pour comprendre la réponse du climat au changement du cycle saisonnier d'insolation ; et le dernier maximum glaciaire à 21 ka, pour comprendre la réponse du climat à la présence

de larges calottes de glace et de concentrations plus faibles en gaz à effet de serre. De plus, cet exercice d'intercomparaison s'appuie sur de nombreuses données paléoclimatiques et synthèses de données pour ces deux périodes climatiques.

Les grandes variations des systèmes de mousson sont aujourd'hui relativement bien comprises. L'objectif de cette thèse est d'étudier plus en détail les variations relatives de plusieurs systèmes de mousson suivant différents types de forçages climatiques. Nous nous intéressons dans cette étude principalement aux variations des moussons indienne, africaine et d'Asie du sud-est pendant l'Holocène. Pour ce faire, des simulations de climats passés ont été réalisées à l'aide du modèle de climat couplé océan-atmosphère IPSL-CM4 (Marti et al., 2010). En particulier, l'analyse des simulations au début de l'Holocène (9.5 ka) et au milieu de l'Holocène (6 ka) permettent d'étudier l'impact des changements de précession des équinoxes sur le climat. Les variations de précession induisent en plus de changements de gradients d'insolation, des changements de saisonnalité et de longueurs de saisons (Joussaume and Braconnot, 1997; Tuenter et al., 2005). Le début de l'Holocène présente aussi un intérêt pour étudier l'influence de la fonte de la calotte réminiscente sur la Laurentide et la Fennoscandie à cette époque sur les systèmes de mousson. Par la suite, ce travail s'intéresse de façon plus générale à l'interaction entre les hautes latitudes et les systèmes de mousson, le Dernier Maximum Glaciaire (DMG) ainsi que d'autres périodes climatiques sont alors considérés. Le schéma 1.3 synthétise l'ensemble des périodes climatiques abordées ainsi que les types de forçages imposés.

A l'aide de ces expériences de modélisation, ce travail vise à détailler la compréhension des réponses différenciées de plusieurs systèmes de mousson aux forçages évoqués ci-dessus. Quels sont les mécanismes et rétroactions du système climatique permettant d'expliquer ces variations de mousson ? Sont-elles proportionnelles aux variations d'insolation ? Les sous-systèmes de mousson évoluent-ils de la même manière ? Quel est l'importance du phasage de l'insolation sur le cycle saisonnier des moussons ? Quelles téléconnections entre les systèmes de mousson et d'autres phénomènes climatiques sont affectées par les différences de forçage ? Et comment ces résultats peuvent être mis en regard d'enregistrements paléoclimatiques spécifiques ? Est-ce-que la prise en compte de forçages climatiques supplémentaires tels la présence de calotte et la fonte de celles-ci a une influence sur les variations des moussons ? Les systèmes de mousson

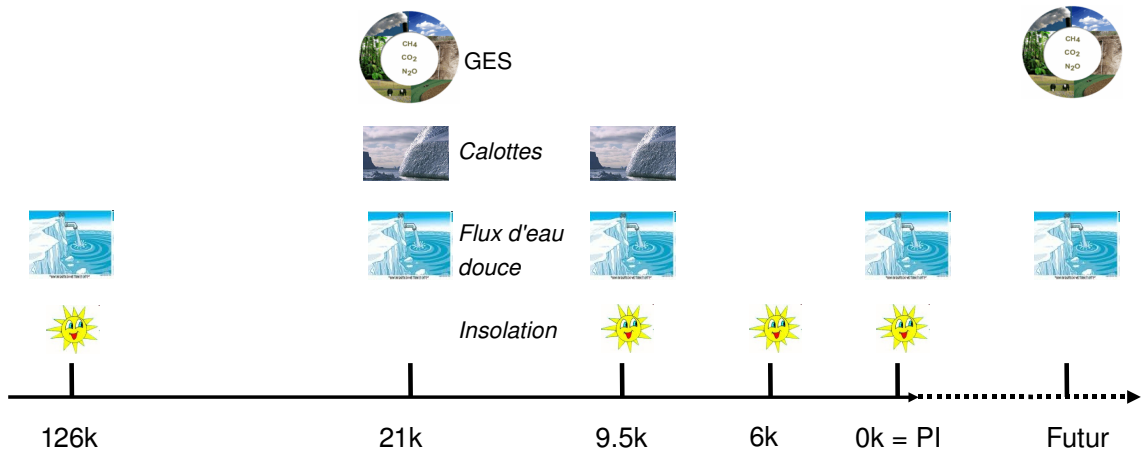

FIGURE 1.3: Schéma représentant les différentes périodes climatiques considérées : 126 ka pendant l'Eémien, 21 ka au Dernier Maximum Glaciaire, 9.5 ka au début de l'Holocène, 6 ka au milieu de l'Holocène, 0 ka la période préindustrielle qui sert de référence, et le futur sous l'influence des émissions anthropogéniques de gaz à effet de serre. ainsi que les différents types de forçages imposés : différences d'insolation, de flux d'eau douce dans l'Atlantique nord, d'extension des calottes de glace et de concentrations de gaz à effet de serre (GES).

retenus dans cette étude sont discutés dans le chapitre 2 ainsi que leur évolution passée connue à partir des enregistrements paléoclimatiques. Le modèle IPSL-CM4 utilisé pour les expériences numériques y est présenté avec une évaluation de la représentation des systèmes de mousson dans ce modèle.

Le chapitre 3 est tout d'abord consacré à l'étude de la réponse des moussons aux variations d'insolation à l'Holocène (ainsi qu'une analogie avec l'Eémien, la période interglaciaire précédente) dans les simulations couplées océan-atmosphère, en terme de cycle saisonnier moyen puis en terme de variabilité. De plus, les résultats d'une collaboration visant à comparer les résultats de simulation avec des enregistrements marins dans l'Océan Indien couvrant la période de l'Holocène y sont présentés. Le chapitre 4 tente de mettre en évidence l'impact d'une possible téléconnection entre l'Inde, la Méditerranée et l'Afrique de l'Ouest sur les amplifications relatives des systèmes de mousson à l'Holocène. De manière plus générale, l'importance de l'interaction des systèmes de mousson tropicaux avec les moyennes latitudes est abordée. Le chapitre 5 aborde le rôle de la rétroaction de l'océan à l'aide d'expériences complémentaires réalisées avec le modèle atmosphérique forcé par les températures océaniques, puis la sensibilité de la réponse des moussons à un flux d'eau douce en Atlantique Nord et à la calotte de glace

qui perdure au début de l'Holocène. Une étude de comparaison modèle/données de la sensibilité de la mousson indienne au flux d'eau douce d'Atlantique Nord en climat glaciaire (au DMG) permet d'expliquer les variations abruptes de la mousson observées dans les enregistrements paléoclimatiques et apporte un complément aux résultats de l'Holocène. La sensibilité des systèmes de mousson à l'intensité de la circulation thermohaline est ensuite comparée entre les climats interglaciaires, glaciaires et futurs. Finalement, la conclusion permet de synthétiser et discuter les principaux résultats présentés, puis de mentionner les perspectives qu'ouvrent ce travail de thèse.

Ce manuscrit est organisé autour d'articles principaux qui contiennent les résultats détaillés ainsi que la bibliographie et les méthodes permettant de répondre à chaque problématique. Ainsi, chaque chapitre présente une partie d'introduction pour remettre en contexte les thématiques et la démarche scientifique permettant d'articuler les différentes études et de résumer les résultats scientifiques détaillés par la suite dans le chapitre. En plus de résultats principaux sous forme d'articles déjà publiés, soumis ou en préparation, chaque chapitre présente des parties complémentaires qui permettent d'explorer d'autres aspects des problèmes abordés, non publiés à ce jour. Ces compléments font partie intégrante des questionnements scientifiques que j'ai pu développer au cours de cette thèse et qui ont amené une richesse de perspectives pour la poursuite de ce travail. Les articles auxquels j'ai contribué en lien avec ces problématiques sont présentés en annexe.

2

Systèmes de mousson : évolution dans le passé et représentation dans le modèle de l'IPSL

2.1 Evolution passée des moussons dans les enregistrements paléoclimatiques

Le terme mousson se réfère à un renversement saisonnier de la circulation de surface dans les tropiques et les subtropiques. Les gradients saisonniers de température et de chauffage entre les deux hémisphères et les continents et les océans ont pour conséquence la migration vers le nord de la zone de convergence intertropicale pendant l'été boréal et la mise en place de l'alternance d'une saison sèche et d'une saison humide. Le concept de mousson globale a été

introduit par Trenberth et al. (2000) et Wang and Ding (2006, 2008) ont repris en détail ce concept de renversement de circulation atmosphérique à grande échelle dans les Tropiques. Bien que la mousson globale réagisse en premier lieu au forçage solaire, des différences locales sont attribuées aux sous-systèmes en fonction de la distribution géographique et de l'orographie. La Fig. 2.1 représente l'indice de mousson globale déterminé par Wang and Ding (2008) et met en évidence les sous-systèmes suivants : le Sahel, l'Inde, l'Asie du sud-est, le nord de l'Australie, l'Amérique du nord et l'Amérique du sud. Les analyses considérées dans cette thèse portent une attention particulière aux trois premiers systèmes, qui sont historiquement les plus étudiés mais aussi les plus importants en terme d'énergétique du climat et d'impact sur les populations.

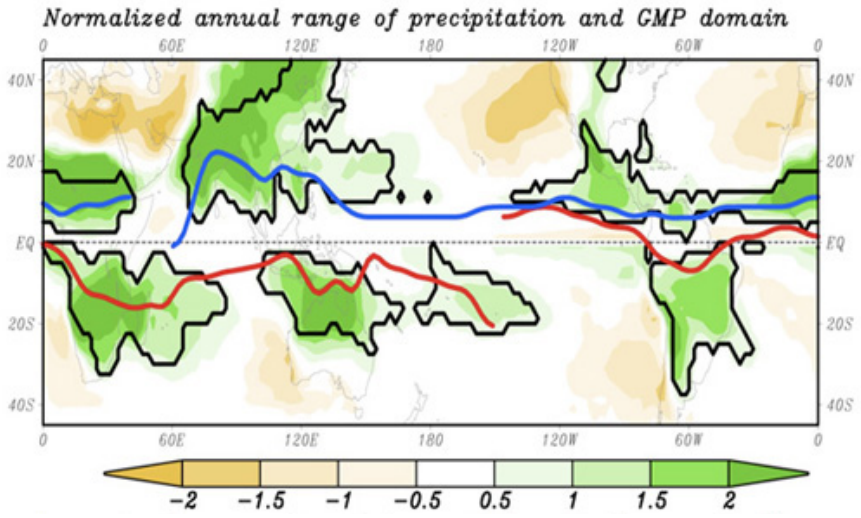

FIGURE 2.1: Variation saisonnière des précipitations (été moins hiver, normalisé par la moyenne annuelle, couleur). Domaine de précipitation de mousson globale : variation saisonnière $\geq 2mm/jour$ et 70% de la moyenne annuelle (contours noirs). Position de la ZCIT en été (juillet-août, ligne bleue) et en hiver (janvier-février, ligne rouge). Figure issue de Wang and Ding (2008)

Nous présentons tout d'abord la manière dont l'évolution passée de ces systèmes de mousson est retracée à l'aide d'enregistrements paléoclimatiques et les principaux résultats que suggèrent l'interprétation de ces indicateurs paléoclimatiques pour la période de l'Holocène. Une bibliographie plus spécifique à chaque étude est donnée en introduction de chapitre ou d'article dans la suite de ce manuscrit.

Il existe une large diversité d'enregistrements paléoclimatiques provenant de prélèvements

sur les continents et les océans qui permettent de retracer des variations climatiques en relation avec la température, la végétation, les précipitations ou les circulations atmosphérique et océanique. De nombreuses paléoreconstructions réalisées en Asie et en Afrique sur des proxies de précipitations, de vents, de niveaux des lacs et de végétation ont indiqué une intensification des systèmes de mousson au début et au milieu de l'Holocène induite par le forçage orbital (Wright et al., 1993). Les variations de la précession des équinoxes sont principalement responsables de la distribution méridionale et saisonnière de rayonnement solaire reçu au sommet de l'atmosphère à l'échelle de temps de l'Holocène. Ce renforcement des moussons résulterait de l'amplification du cycle saisonnier d'insolation dans l'hémisphère nord, engendrant une augmentation du gradient continent-océan et un déplacement plus au nord de la zone de convergence intertropicale (ZCIT).

La première moitié de l'Holocène (9000 à 5000 BP) représente une période clé en Afrique. Les paléodonnées montrent qu'à cette époque, les conditions de l'Afrique du Nord étaient plus humides et qu'il y avait présence de végétation et de lacs sur le Sahara. C'est pourquoi on l'a appelé le « Sahara vert ». L'analyse de différentes sources de données attestent que l'on est entré dans une période plus humide à l'Holocène, au sortir de la période glaciaire (Wright et al., 1993). De nombreux indicateurs climatiques sont témoins de l'expansion de la mousson africaine à cette époque. Les niveaux des lacs étaient maximum (Gasse, 2000), les données palynologiques et paléobotaniques permettent de retracer l'évolution complexe de la végétation dans cette zone aujourd'hui désertique (Jolly et al., 1998; Lezine et al., 2007; Watrin et al., 2009). L'avènement de cette période humide a permis l'adaptation de nombreux mammifères dans le Sahara et a encouragé les débuts d'agriculture et d'élevage (Petit-Maire, 1999). Un effort international de reconstruction des conditions climatiques a été réalisé pour l'Holocène moyen (Prentice and Webb, 1998; Jolly et al., 1998; Hoelzmann et al., 1998) et sert de référence à toute étude du climat de l'Afrique à l'Holocène, en particulier pour la comparaison aux résultats des modèles climatiques dans le cadre de PMIP.

Le débat actuel repose surtout sur l'étude de la fin de la période humide en Afrique et la sensibilité des écosystèmes aux variations d'insolation. deMenocal et al. (2000) et Adkins et al.

(2006) montrent une transition abrupte des apports terrigènes dans les sédiments de l'Atlantique tropical vers 5 ka, indiquant la fin brutale de la période humide en Afrique de l'Ouest. La rétroaction positive de la végétation sur le climat est invoquée pour expliquer l'évolution rapide de la mousson africaine par rapport à l'insolation. Certaines études de modélisation soutiennent cette thèse (Claussen et al., 1999), tandis que l'étude de Liu et al. (2007) propose une relation plus complexe entre l'évolution de la végétation et celle des précipitations au Sahel. Cependant, d'autres reconstructions suggèrent une évolution plus régulière de la mousson africaine au cours de l'Holocène (Lezine, 2009; Kropelin et al., 2008; Weldeab et al., 2007). Bien que le travail de cette thèse ne traite pas directement cette problématique, il a participé au fondement du projet ANR SAHELP (Sahara and Sahel vulnerability : lessons from the past) dirigé par Anne-Marie Lézine et dont l'objectif est de mieux cerner la vulnérabilité de l'Afrique sèche à la fin de la période humide et les relations entre climat, systèmes hydrologiques et végétation.

Les proxies mettant en évidence le renforcement de la mousson asiatique au début de l'Holocène abondent également. Des travaux de synthèse avec une approche multiproxies ont été réalisés et constituent une approche plus globale des variations de la mousson asiatique à l'Holocène. La migration des civilisations et leur adaptation aux variations climatiques témoignent d'une période de transition au cours de l'Holocène quand l'intensité et l'étendue de la mousson indienne ont diminué (Gupta et al., 2006). En effet, les variations de la mousson indienne influencent les réseaux hydrologiques. Ainsi les débuts de culture et d'élevage en Inde correspondent à la période d'amplitude et d'extension vers le nord maximum de la mousson, tandis que la diminution au cours de l'Holocène a engendré des migrations de populations vers des zones plus productives et des systèmes d'adaptation tels la construction de réservoirs artificiels (Gupta, 2004; Gupta et al., 2006). Les proxies de précipitation (provenant de spéléothèmes, dépôts minéraux précipités dans une grotte) et de vents (upwelling) (provenant de sédiments marins) indiquent une mousson indienne amplifiée et plus étendue vers le nord-ouest au début de l'Holocène (Wang et al., 2005; Prasad and Enzel, 2006; Fleitmann et al., 2007), cependant Prasad and Enzel (2006) montrent que le phasage de l'évolution de la mousson indienne au cours de l'Holocène varie selon l'emplacement et la nature (terrestre ou marin) des échantillons. De plus, Staubwasser (2006) et Ramesh (2001) insistent sur le fait que la distribution spatiale des précipitations était différente de l'actuel et a évolué au cours de l'Holocène. Ainsi,

les précipitations ont diminué dans le nord de l'Inde au cours de l'Holocène tandis qu'elles ont augmenté à la pointe sud de la péninsule.

La mousson d'Asie du sud-est était aussi plus intense au début de l'Holocène. An et al. (2000) passe en revue les données de niveau des lacs, de pollens et de sédiments éoliens (loess) et montre que la période de mousson la plus active pendant l'Holocène dépend fortement des régions considérées. Les fameux enregistrements de spéléothèmes des grottes Hulu et Sanbao (Wang et al., 2001b; Wang and Ding, 2008) montrent un lien direct entre les variations de la précession et celles des précipitations de mousson d'Asie du sud-est à l'échelle du Quaternaire. Cependant, l'interprétation de ces enregistrements est débattue. Maher (2008) suggère qu'ils seraient plus représentatifs des précipitations de la mousson indienne, les données provenant du plateau de loess n'étant pas en accord avec celles des spéléothèmes pour l'Holocène. Clemens et al. (2008) suggèrent que ces enregistrements seraient plus représentatifs d'une combinaison de mousson d'été et d'hiver. Bien que l'effet de l'insolation sur l'évolution de la mousson asiatique ait été maintes fois mis en évidence, il existe à l'actuel un vif débat quant aux mécanismes dynamiques d'impact de la précession sur la mousson. La première hypothèse de "phasage nul" défendue à l'origine par Kutzbach (1981); Ruddiman (2006) suggère que la mousson asiatique est directement en phase avec les variations de l'insolation d'été de l'hémisphère nord. La seconde hypothèse développée par Clemens et al. (1991) propose le rôle dominant du flux de chaleur latente provenant de l'hémisphère sud en plus de l'effet de l'insolation de l'hémisphère nord sur les fluctuations passées de la mousson. (Liu and Shi, 2009) résument et discutent les différentes hypothèses concernant le phasage et les mécanismes de réponse de la mousson asiatique au forçage par la précession et concluent que d'autres effets doivent être pris en compte et que le débat n'est pas clos.

Les systèmes de mousson présentent aussi une variabilité à l'échelle centenaire et millénaire qui peut engendrer des variations de climat plus ou moins brutales (Gasse and Vancampo, 1994; Haug et al., 2001; Gupta et al., 2003). La fréquence de ces évènements peut souvent être reliée à la variabilité de la couverture de glace ou de température de l'Atlantique Nord (Bond et al., 1997; Schulz et al., 1998; Weldeab et al., 2007). Cependant, cette relation est encore débattue (Risebrobakken) et d'autres facteurs, tels que la variabilité solaire (Bond et al., 2001; Fleitmann

et al., 2003) et la variabilité interne des Tropiques (Brown et al., 2007) pourraient aussi expliquer les évènements rapides observés au cours de l'Holocène.

Les données paléoclimatiques servent de référence pour évaluer et discuter les résultats de modélisation des climats passés. Malheureusement, peu d'études synthétisent et comparent les enregistrements de plusieurs systèmes de mousson sur une période donnée. La datation et le phasage des enregistrements représentent une difficulté majeure ce qui ne facilite pas les comparaisons modèle-données. De plus, les relations entre proxies et variables climatiques sont établies par rapport au climat actuel et font l'hypothèse que celles-ci restent invariables dans le temps. Cependant, les circulations atmosphérique et océanique peuvent avoir été décalées ou modifiées par rapport à l'actuel. La saisonnalité de certains phénomènes climatiques et les mécanismes de téléconnection peuvent aussi avoir été modifiés, ce qui biaise alors les interprétations des enregistrements. La modélisation apporte une approche globale de l'analyse des variations climatiques passées et peut apporter des solutions aux problèmes de datation et d'interprétation des différents proxies. Bien que les paléoreconstructions soient essentielles et soient le seul moyen que l'on ait de valider les modèles à l'échelle climatique, elles représentent les phénomènes climatiques de façon beaucoup plus indirectes et locales que les observations actuelles et le degré de confiance que l'on a dans ces reconstructions lors de comparaison aux résultats de simulations (elles-mêmes biaisées par définition) doit tenir compte de ces difficultés. Ces comparaisons sont un processus itératif d'aller-retour pour mieux comprendre et interpréter les données et évaluer et améliorer les modèles.

Le travail de modélisation présenté par la suite permet ainsi d'avancer la compréhension des mécanismes de variations des moussons dans le passé, en se focalisant sur les différences d'évolution entre les sous-systèmes de mousson, certaines rétroactions du système climatique et les effets de saisonnalité. Le modèle utilisé est présenté dans la partie suivante, ainsi que les caractéristiques des principales expériences de simulation. Les caractéristiques des sous-systèmes de mousson retenus et leur représentation dans le modèle de l'IPSL sont présentées dans la partie 2.4.

2.2 Présentation du modèle IPSL-CM4

Les différentes études présentées dans cette thèse s'appuient sur des simulations numériques réalisées avec le modèle de climat de l'IPSL. Le modèle IPSL-CM4 est un modèle de circulation générale permettant de coupler les différentes grandes composantes du système climatique que sont l'océan, l'atmosphère, la glace de mer, et les surfaces terrestres. Aucun flux n'est corrigé. La version utilisée dans ce manuscrit (Marti et al., 2005, 2010) est celle qui a servi à réaliser l'ensemble de simulations du projet d'intercomparaison CMIP3 (Meehl et al., 2007) et qui ont servi de support au Groupe d'Experts Intergouvernemental sur l'Evolution du Climat (Solomon et al., 2007) pour projeter et comprendre les changements du climat induits par l'activité humaine. La même version a participé à la deuxième phase du projet PMIP pour les climats de l'Holocène moyen et du dernier maximum glaciaire (Braconnot et al., 2007a).

Ce modèle couple les points de grille du modèle de circulation générale atmosphérique LMDz (Hourdin et al., 2006) développé au Laboratoire de Météorologie Dynamique avec le modèle de circulation générale océanique OPA (Madec et al., 1998). Sur les continents, le modèle de surface ORCHIDEE (Krinner et al., 2005) est couplé au modèle d'atmosphère. Un modèle de dynamique et de thermodynamique de glace de mer, LIM (Fichefet and Maqueda, 1997) est inclus dans le modèle océanique. Les modèles d'océan et d'atmosphère s'échangent la température de surface, la couverture de glace de mer, le moment cinétique ainsi que les flux d'énergie et d'eau douce par l'intermédiaire du coupleur OASIS (Terray et al., 1995) développé au CERFACS. Aucun de ces flux ne nécessite de correction. Ce modèle simule les phénomènes de l'échelle de l'heure au siècle et au delà et peut être utilisé aussi bien pour étudier le changement climatique que la variabilité climatique. Le schéma des différentes composantes de ce modèle est présenté sur la Fig. 2.2.

La partie dynamique de la composante atmosphérique est discrétisée en différences finies sur une grille de type Arakawa-C. La résolution est de 96x72 points en longitude et latitude et comporte 19 niveaux sur la verticale, dont les coordonnées sont hybrides. La dynamique permet de résoudre les équations primitives de l'atmosphère (équation de continuité, du mouvement, thermodynamique et hydrostatique) selon Sadourny and Laval (1984). La physique

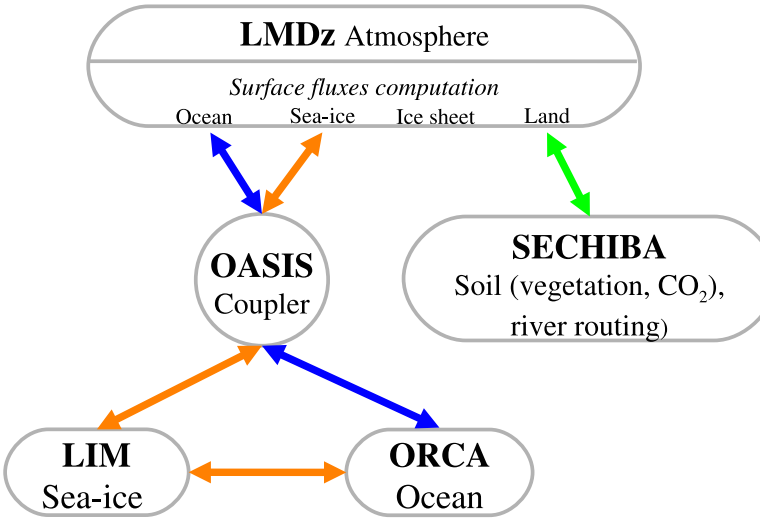

FIGURE 2.2: Schéma des composantes du modèle de l'IPSL

qui représente les processus non résolus à l'échelle de la maille, est calculée sur une colonne d'air en une dimension. Le schéma de convection introduit dans le modèle IPSL-CM4 est celui d'Emanuel (1991). Le schéma de nuages (Bony and Emanuel, 2001) utilise une distribution log-normale dont la largeur est une fonction interactive de l'intensité de la convection. La condensation est paramétrée séparément pour les nuages convectifs et les nuages stratiformes. La paramétrisation de Lott (1999) permet de bien prendre en compte l'effet des montagnes sur la circulation atmosphérique.

La composante océanique a une résolution de deux degrés (ORCA2). La diffusion verticale turbulente est paramétrée à partir de l'énergie cinétique turbulente (TKE, Blanke and Delecluse (1993)). Le modèle de glace de mer utilisé est LIM (Fichefet and Maqueda, 1997), qui représente les aspects dynamiques et thermodynamiques de la glace de mer et de la neige subjacente. Seule la composante thermodynamique d'ORCHIDEE (Krinner et al., 2005), SECHIBA, est active dans les simulations présentées ici. Ce modèle biophysique décrit les phénomènes rapides d'échanges d'eau et d'énergie entre la surface et l'atmosphère. Sont également calculés dans cette partie la conductance stomatique du couvert et sa productivité primaire brute. La végétation et le cycle foliaire sont prescrits dans toutes les simulations considérées dans cette thèse. La fermeture du bilan d'eau avec l'océan est réalisée grâce à un schéma d'écoulement

de rivière qui est ajouté au modèle de surface. Un schéma de routage des rivières inclu dans le modèle de surface amène les rivières aux points d'embouchure observés dans le monde réel pour les 50 plus grands fleuves. Les calottes de glace sont aussi représentées dans le modèle et sont fixées au niveau des observations de leur position actuelle (sauf mentionné). L'albédo très fort des surfaces terrestres englacées est ainsi pris en compte. Les différentes études menées au cours de cette thèse s'intéressent principalement aux variables atmosphériques du modèle ainsi qu'à l'albédo et la couverture neigeuse du modèle de surface continentale et aux températures et salinités de surface du modèle d'océan.

2.3 Simulations de référence

Une simulation du climat préindustriel sert de référence dans notre étude (elle est mentionnée par 0 ka par la suite). Cette période a été choisie car elle a servi de référence dans plusieurs études de modélisation climatique (Braconnot et al., 2007a). Les conditions préindustrielles sont celles recommandées par PMIP pour les conditions de surface et de végétation et le taux de CO_2. La végétation est prescrite aux conditions actuelles, prenant en compte deux types de surface anthropisées. Le rôle de la dynamique de la végétation avait été analysé avec une version antérieure du modèle (Braconnot et al., 1999) et ne sera pas directement abordé ici car la végétation dynamique n'était pas prête au début de cette thèse. Les impacts de l'utilisation des sols et de la végétation dynamique ont été développés et étudiés par ailleurs dans les travaux de thèse d'Edouard Davin et Marie-Noëlle Boillez respectivement. La climatologie est réalisée sur un échantillon de 100 ans correspondant au milieu de la simulation (qui fait maintenant environ 1000 ans), après stabilisation du bilan de surface et de l'océan. Le détail des autres expériences de simulation réalisées et analysées est donné pour chaque étude par la suite. De plus, certaines simulations ont été réalisées à l'aide d'une version plus récente du modèle d'atmosphère, ou en prescrivant la fonte des calottes, ceci est précisé en temps voulu.

2.4 Systèmes de mousson considérés et leur représentation dans le modèle de l'IPSL

La comparaison des sorties de modèle aux observations et réanalyses permet de mettre en évidence les mécanismes bien représentés dans le modèle, les biais et les insuffisances de modélisation. Cette comparaison est indispensable pour mener par la suite une analyse cohérente des différents climats, et pour comparer les résultats obtenus aux paléodonnées et à d'autres résultats de modèles en connaissance de cause. Pour cela, nous présentons ici la vision des systèmes de mousson abordée dans cette étude en comparant la simulation de référence du climat préindustriel à des observations et réanalyses correspondant aux dernières décennies du climat actuel. J'ai vérifié mais ceci n'est pas montré ici que les différences entre les simulations du climat préindustriel et du climat du 20ème siècle sont mineures concernant les systèmes de mousson, au regard des différences entre les résultats du modèle et les données actuelles. La climatologie des précipitations observées provient du Climate Prediction Center Merged Analysis of Precipitation (CMAP, Xie and Arkin (1997)), celles de la température de surface et des vents sont issues des réanalyses NCEP-NCAR (Kalnay et al., 1996; Kistler et al., 2001), l'OLR (flux infrarouge au sommet de l'atmosphère, indicateur de la couverture nuageuse) provient des données interpolées du National Oceanic and Atmospheric Administration (NOAA) (Liebmann and Smith, 1996). Cette version du modèle a participé à plusieurs projets de comparaison de modèles, aussi bien dans le cadre de la représentation de climats passés (PMIP) que présent et futurs (Solomon et al. (2007), tableaux dans chapitres 8 et 10).

La moyenne de variables atmosphériques sur la saison de juin à septembre (JJAS) permet d'englober toute la saison des pluies pour les trois systèmes considérés. Trop souvent le mois de septembre n'est pas inclus alors qu'il contribue de façon non négligeable au total des précipitations de mousson. De plus, de fortes variations interannuelles ou entre différents climats passés peuvent avoir lieu en fin de saison comme nous le verrons par la suite. La figure 2.3 représente la comparaison de plusieurs variables entre les observations et réanalyses et la climatologie de 100 ans de simulation du climat préindustriel : les précipitations, l'OLR, la température de surface et les vents à 850 et 200hPa. La structure de la ZCIT en été est bien représentée au niveau

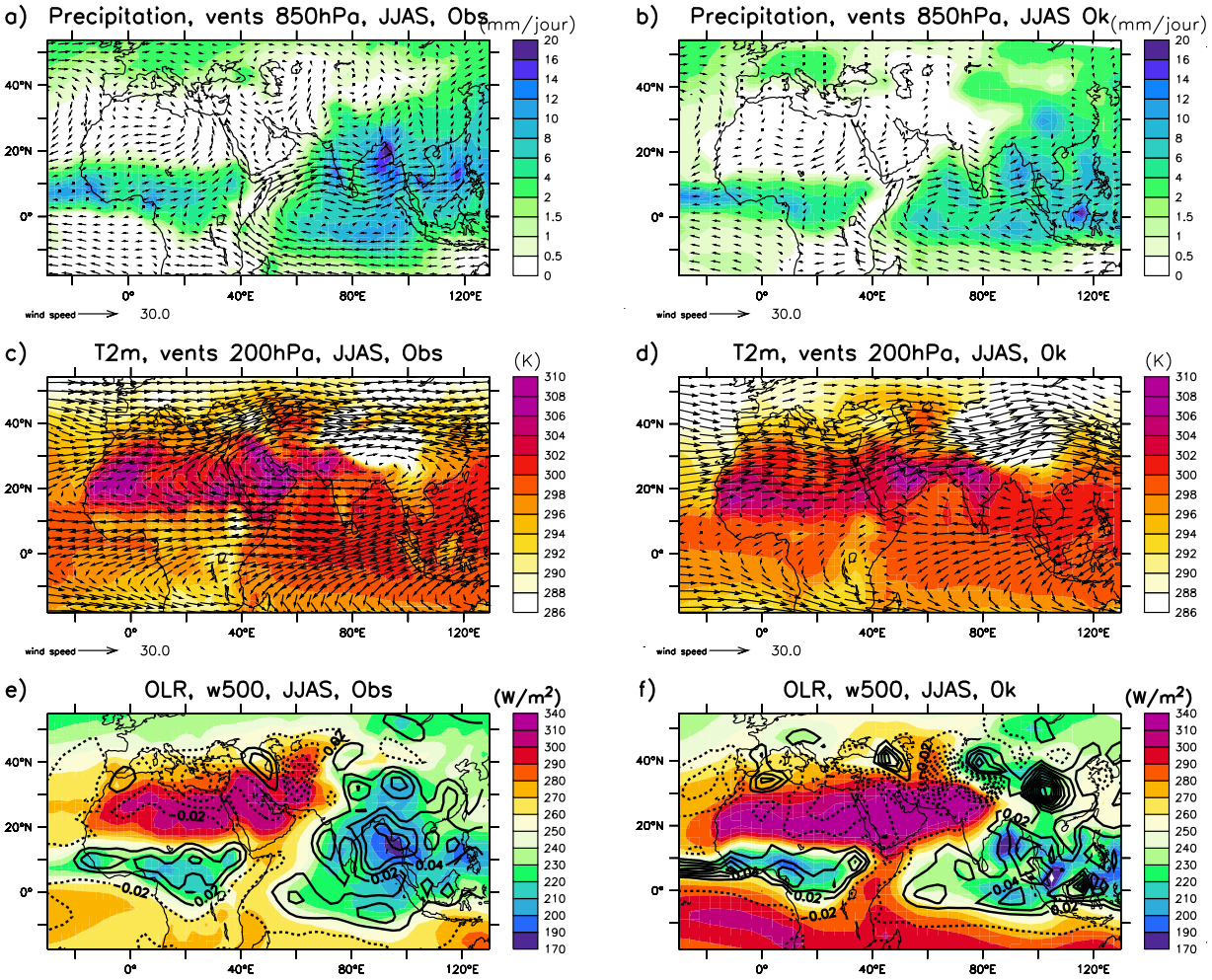

FIGURE 2.3: Précipitation et vents à 850hPa pour (a) CMAP et réanalyses NCEP-NCAR et (b) 0 ka, simulation de référence. Températures à 2 mètres du sol et vents à 200hPa pour (a) réanalyses NCEP-NCAR et (b) 0 ka. OLR et vitesse verticale à 500hPa pour (a) NOAA et réanalyses NCEP-NCAR et (b) 0 ka, simulation de référence.

de l'équateur, surtout sur les océans comme l'attestent les cartes de précipitation (Marti et al., 2010; Braconnot et al., 2007a). Globalement, l'amplitude des précipitations est plus faible pour la simulation, par exemple sur l'océan Indien et sur l'océan Pacifique. La distribution spatiale des précipitations sur le Sahel est correcte mais d'amplitude insuffisante et ne s'étend pas suffisamment vers le Nord (5°de latitude de différence) (Cook and Vizy, 2006), et n'atteint pas le lac Tchad, région cruciale pour la comparaison avec les paléodonnées des lacs. De même, les principales structures de la mousson indienne sont bien représentées, avec un maximum dans le Golfe du Bengale et au sud-ouest de la péninsule indienne. Cependant elles ne pénètrent pas

assez sur les continents au niveau des Ghats occidentaux et du nord-est de l'Inde. De plus, le modèle présente trop de précipitation sur la partie nord de l'Himalaya.

Les caractéristiques des précipitations de mousson sont relativement correctes à grande échelle cependant le modèle présente un défaut majeur quant à l'amplitude et à l'extension vers le nord des systèmes de mousson. Ces biais sont présents dans le modèle forcé LMDZ4-OR et sont renforcés dans le modèle couplé (Marti et al., 2010). Ils sont associés à des conditions trop froides sur les moyennes latitudes (Swingedouw et al., 2007) et sur l'Himalaya qui ne permettraient pas de développer suffisamment la dépression thermique dans cette région. De plus, un biais chaud à l'est de l'Atlantique ne favorise pas la mousson africaine. La thèse de Didier Swingedouw (Swingedouw, 2006) a montré l'association entre le décalage des zones dépressionnaires vers le sud avec la stratification en eau douce au nord et l'inhibition des plongées d'eau en mer de Labrador, expliquant la faible circulation thermohaline. Une autre hypothèse pour expliquer ce biais de precipitations saisonnières serait une mauvaise représentation des interactions avec le sol. En effet les sols sont trop secs au Sahel et au nord-ouest de l'Inde ainsi l'évaporation continentale est trop faible. En particulier, dans cette version du modèle, l'évaporation présente des instabilités numériques et a tendance à assécher et refroidir trop fort les zones semi-arides. De plus, l'épaisseur de neige est trop importante, en particulier en été. J'ai participé lors de ma thèse à élaborer et analyser des tests de sensibilité des systèmes de mousson à l'albédo des zones semi-arides et à l'albédo de neige en collaboration avec Nathalie de Noblet. Ceux-ci ne sont pas présentés ici car les résultats bien que positifs étaient prématurés à l'époque. Mais ils ont contribué à développer la nouvelle version du modèle couplé IPSL-CM5 et à améliorer la représentation des systèmes de mousson.

Dans les tropiques, l'OLR (flux de rayonnement infrarouge sortant au sommet de l'atmosphère) est bien corrélée aux zones de précipitation et d'ascendance, tandis qu'aux plus hautes latitudes, ce rayonnement infrarouge est plutôt indicatif de la température de surface. Les systèmes convectifs représentés par les zones de faible OLR sont moins étendus dans le modèle et là où il pleut moins sur le continent (péninsule indienne et Sahel), la température de surface est plus élevée d'environ 8 Kelvin. Les structures de SST (température de surface des océans) sont bien respectées mais on remarque l'important biais froid du modèle sur l'Atlantique Nord.

La zone dépressionnaire au nord de l'Himalaya est plus froide et contraste encore plus avec le continent excessivement chaud. Les zones ascendantes correspondent bien aux zones de précipitation et les zones de subsidence qui nous intéresseront par la suite au niveau de la Méditerranée et au sud-est de la mer d'Aral sont correctement positionnées. Un maximum de convection est localisé sur le centre de la Chine, ceci est un biais récurrent de plusieurs modèles couplés.

Dans le modèle, les structures dynamiques de la circulation atmosphérique à 200hPa sont représentées, cependant le jet d'ouest et le jet d'est tropical sont décalés vers le sud (figure 2.3 c et d). Les flux de mousson d'été à 850 hPa entre l'Afrique de l'ouest, l'Inde et l'Asie du sud-est sont différents, principalement du fait de l'orographie et des distributions continent/océan locales (Wang et al., 2003; Wang, 2006) qui engendrent des gradients méridiens et horizontaux de pression de surface et de température troposphérique essentiels au développement saisonnier des moussons. Concernant la mousson indienne, le contraste de température de surface terre/océan est insuffisant pour expliquer le cycle saisonnier de la mousson indienne, tandis que l'orographie, les gradients de température troposphérique (Yanai et al., 1992; He et al., 2003; Xavier et al., 2007) et le flux de chaleur latente sur la Baie du Bengale (Gadgil, 2003; Srinivasan, 2006) sont primordiaux. La mousson d'Asie du sud-est est un système plus subtropical, et la mousson est le résultat de la migration de la bande de pluie Meiyu sur le continent asiatique (Wang et al., 2003; Wang, 2006). La circulation de mousson et la nature des évènements convectifs est aussi singulièrement différente entre les systèmes asiatiques et l'Afrique. Sur le Sahel, la couche de mousson est beaucoup plus mince et représente un système quasi zonal très sensible au gradient d'albédo de surface (Hall and Peyrille, 2006; Janicot, 2009; Lafore et al., 2010). Cook and Vizy (2006) ont comparé la représentation de la mousson africaine dans les modèle de l'AR4, cette étude montre que malgré le biais de précipitation sur le Sahel, les structures de la circulation atmosphérique, la position des jets au-dessus de l'Afrique de l'ouest sont bien représentées dans le modèle.

Une attention particulière à la saisonnalité des évènements climatiques est apportée dans ce travail. Pour ce faire, j'ai réalisé des climatologies journalières de 100 ans. La Fig. 2.4 montre que malgré le biais sur l'amplitude des précipitations en Inde et au Sahel et un décalage systématique du démarrage des moussons, le phasage est relativement bien respecté par rapport

aux observations, avec notamment un phasage correct des maxima de précipitations qui met en évidence les différences de saisonnalité et de longueurs de saison entre les trois sous-systèmes. Ces climatologies journalières permettent par la suite d'analyser les changements de longueur de saison de mousson.

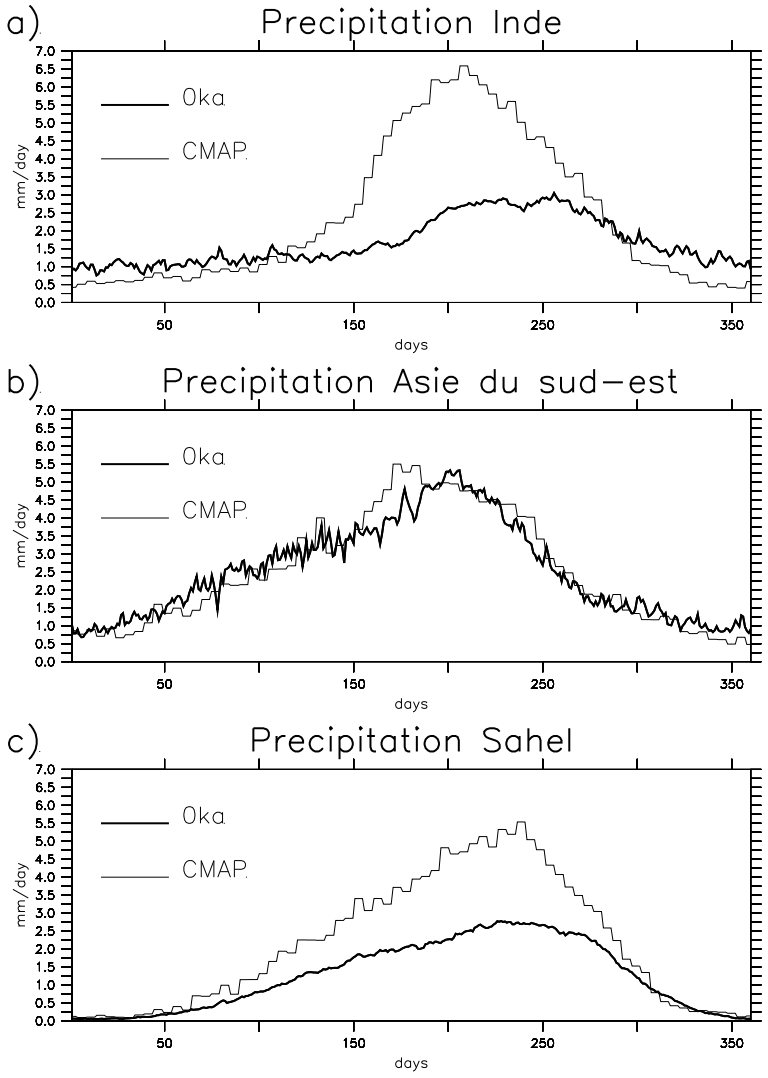

FIGURE 2.4: Cycle saisonnier des précipitations continentales sur (a) l'Inde (70-100°E, 10-35°N), (b) l'Asie du sud-est (105-135°E, 20-45°N) et (c) le Sahel (20°O-30°E, 5-17°N) pour les données CMAP (pentad, trait fin) et pour 0 ka (journalières, trait gras).

Pour conclure, les structures dynamiques et convectives sont globalement bien respectées, avec cependant des défauts systématiques de précipitation sur les continents. Sur le seul critère

d'amplitude des précipitations d'été sur le continent indien, ce modèle est l'un des moins performants de CMIP3 (Kripalani et al., 2007), même si les caractéristiques de la circulation tridimensionnelle sont présentes. En revanche, cette simulation est très satisfaisante sur les océans tropicaux. Les résultats de la simulation couplée pour l'Holocène Moyen (6 ka) ont été comparés aux résultats d'autres modèles ainsi qu'aux synthèses de données paléoclimatiques dans le cadre de PMIP. Cette version du modèle permet de bien représenter l'amplification des moussons à cette période, bien que comme pour les autres modèles, l'extension vers le nord de la bande de mousson au Sahel n'atteigne pas le niveau suggéré par les données (Braconnot et al., 2007a). En conclusion, le modèle de l'IPSL-CM4 représente un outil utile pour l'étude des variations des systèmes de mousson dans le passé. Malgré les biais importants signalés, on a une confiance relative sur la dynamique et la sensibilité à des changements de climat.

3

Réponses des moussons aux variations de paramètres orbitaux

3.1 Résumé

De nombreuses études ont mis en évidence la relation qui existe entre les moussons et les variations lentes de l'insolation induites par les paramètres orbitaux. Elles ont été synthétisées dans COHMAP Members (1988) et Wright et al. (1993). Les premières études de paléomodélisation ont étudié le climat du maximum d'insolation à l'Holocène, à 9 ka (Kutzbach, 1981; Kutzbach and Ottobliesner, 1982; Kutzbach and Gallimore, 1988; Mitchell et al., 1988). Prell and Kutzbach (1987) ont mis en évidence la relation qui existe entre les moussons et les variations d'insolation de l'hémisphère nord en été lors des 150000 dernières années. Ensuite, le projet PMIP a choisi comme période de référence l'Holocène moyen (6 ka). Ainsi de nombreuses études de modélisation ont montré que les moussons de l'hémisphère nord sont amplifiées en

été en réponse au forçage par l'insolation à l'Holocène moyen (Wright et al., 1993; Kutzbach and Liu, 1997; Claussen and Gayler, 1997; Hewitt and Mitchell, 1998; Braconnot et al., 2000b; Texier et al., 2000; Voss and Mikolajewicz, 2001; Liu et al., 2004). Le projet PMIP (Joussaume and Taylor, 1995) a permis de comparer dans une première phase les résultats de plusieurs modèles atmosphériques (Joussaume et al., 1999; Braconnot et al., 2000a, 2002) et dans une deuxième phase ceux de modèles couplés océan-atmosphère à l'Holocène moyen (Zhao et al., 2005; Braconnot et al., 2007a,b). A cette période, le cycle saisonnier d'insolation est plus contrasté dans l'hémisphère nord qu'à l'actuel, ainsi les continents sont plus chauffés en été, ce qui intensifie le gradient de température terre/océan. Ce mécanisme est d'un commun accord la principale explication à l'amplification des systèmes de mousson dans les Tropiques, tandis que certaines rétroactions telles celles de l'océan et de la végétation peuvent nuancer l'amplification des moussons. Cependant, les mécanismes de variation des moussons sont complexes et doivent tenir compte des dernières avancées de la compréhension des systèmes de mousson actuels.

Cette étude s'intéresse à une question supplémentaire : est-ce que les variations des sous-systèmes de mousson sont en phase avec les changements d'insolation ou font l'objet d'un déphasage lié à leur saisonnalité ? Pour y répondre, deux périodes sont analysées : l'Holocène moyen (6 ka) et le début de l'Holocène (9.5 ka), qui diffèrent principalement par la précession des équinoxes. En effet, Braconnot and Marti (2003) ont mis en évidence le fait que la précession, qui module la phase du maximum d'insolation en été, a une conséquence importante sur les précipitations de la mousson indienne ainsi que sur la circulation atmosphérique et océanique associée. La mousson est affectée différemment selon que le maximum de différence d'insolation soit au début ou à la fin de l'été. A 9.5 ka, le solstice d'été a lieu quand la Terre est proche du périhélie (le point de l'orbite terrestre le plus proche du soleil), tandis qu'à l'actuel, elle est proche de l'aphélie (le point de l'orbite terrestre le plus éloigné du soleil) ce qui nous procure des étés longs et doux. Ainsi, à 9.5 ka, le maximum de différence d'insolation est en phase avec le cycle saisonnier actuel si l'on adopte une définition des saisons basée sur les solstices et équinoxes. A 6 ka, l'équinoxe d'automne a lieu quand la Terre est proche du périhélie, le maximum de différence d'insolation par rapport à l'actuel est ainsi plus tardif qu'à 9.5 ka. En plus de cette différence de saisonnalité, l'amplitude du changement d'insolation est plus forte à 9.5 ka. Le forçage orbital est présenté plus en détail dans Marzin and Braconnot (2009b). Peu

d'études différencient la réponse des différents systèmes de mousson à ces variations de forçage d'insolation. Nous proposons ici d'analyser les différentes réponses des moussons indienne et africaine aux changements d'insolation à 6 et 9.5 ka.

L'étude Marzin and Braconnot (2009b) présentée dans la partie suivante, détaille les différentes configurations de l'orbite terrestre et leur impact sur le cycle saisonnier d'insolation et sur les longueurs de saison entre les périodes 0, 6 et 9.5 ka, ainsi que les caractéristiques des expériences de modélisation. L'objectif de cette étude est d'analyser à l'aide du modèle IPSL-CM4 les réponses des moussons indienne et africaine à ces changements d'insolation, en terme d'amplification du cycle hydrologique et de la circulation de mousson mais aussi de phasage du cycle saisonnier des précipitations. Une attention particulière est apportée à la longueur des saisons et au choix de calendrier utilisé pour réaliser les moyennes mensuelles (calendrier fixe, similaire au calendrier actuel ou calendrier céleste basé sur la définition astronomique de longueur des mois et saisons) qui peuvent influencer les résultats (Joussaume and Braconnot, 1997). Pour ce faire, les résultats sont analysés à partir des sorties journalières.

Le principal résultat est que les deux systèmes de mousson sont plus amplifiés à 9.5 ka qu'à 6 ka par rapport à l'actuel, mais que l'amplification est plus importante entre 6 et 9.5 ka pour la mousson indienne que pour la mousson africaine. Une des hypothèses repose sur le fait que le système de mousson qui est le plus en phase avec le changement d'insolation est favorisé par effet de résonance. Ainsi la mousson indienne qui est pleinement développée à l'actuel au mois de juillet est relativement favorisée par un maximum d'insolation en juillet à 9.5 ka tandis que la mousson africaine qui est plus tardive est relativement favorisée par le maximum de différence d'insolation en août à 6 ka. De plus, la longueur des saisons de mousson est affectée. La saison des pluies est plus longue à 9.5 ka pour les deux moussons bien que l'été soit plus court du point de vue de l'insolation qu'à l'actuel, et à 6 ka, le démarrage des moussons est plus tardif qu'à 9.5 ka. Les flux de mousson sont renforcés en été pour les deux systèmes de mousson à 6 et 9.5 ka et il est démontré que l'intensification des précipitations est principalement due à plus d'advection d'air humide plutôt qu'à un recyclage local plus actif. Cette étude montre aussi l'importance du gradient méridien de température troposphérique pour la mousson indienne ainsi que le rôle de la fonte de la couverture neigeuse sur le Plateau Tibétain pour le démarrage plus précoce de la

mousson indienne à 9.5 ka. Elle pose aussi les premières questions concernant le lien entre la convection au-dessus de l'Inde, la subsidence autour de la Méditerranée et leur connection avec le développement de la mousson au Sahel.

Il est important de vérifier si les résultats de l'influence de la précession sur les systèmes de mousson à l'Holocène sont aussi valides dans un autre contexte orbital. Ainsi, les analyses de Marzin and Braconnot (2009b) ont été étendues à l'Eémien et sont présentées dans l'annexe A.1 (Braconnot et al., 2008). Un ensemble de trois simulations correspondant à l'Eémien mais ayant les mêmes caractéristiques de précession que les périodes de l'Holocène choisies a été réalisé. L'excentricité étant plus forte à cette époque, l'effet de la précession est amplifiée, ainsi les cycles saisonniers d'insolation sont plus contrastés dans l'hémisphère nord à 122 et 126 ka. Les résultats confirment le rôle de la précession sur l'amplification relative des systèmes de mousson. Il est montré que la réponse en terme de température et de salinité dans l'océan indien est différente en fonction du phasage de l'insolation en été. De plus, la contribution des moussons à l'énergétique des régions tropicales dépend aussi de la précession.

Les analyses précédentes abordent les variations du cycle saisonnier, qu'en est-il des changements de variabilité et de régimes de précipitation ? Bien que le coeur de ce travail de thèse ne soit pas consacré à la variabilité, un complément d'étude est présenté dans la partie 3.3 pour explorer quelques diagnostiques de variabilités interannuelle et intrasaisonnière des moussons et comment elles varient entre les trois périodes d'étude de l'Holocène. De même que pour le cycle saisonnier, ces analyses montrent que l'effet de la précession agit sur la variabilité et sur les régimes de précipitation de façon différente pour chaque sous-système étudié.

Les résultats présentés dans cette première partie ne prennent en compte que le forçage par l'insolation. Le fait de ne pas prendre en compte la rétroaction de la végétation est une limite importante de cette étude pour la comparaison avec les enregistrements paléoclimatiques. Cependant, Hely et al. (2009) a utilisé les simulations couplées de l'IPSL-CM4 à l'Holocène (9.5 ka, 6 ka, 4 ka et 0 ka) pour forcer le modèle de végétation LPJ-GUESS et analyser les changements de végétation sur l'Afrique de l'ouest au cours de l'Holocène. Les résultats de cette étude indiquent que le modèle de l'IPSL représente bien l'intensification de la mousson

africaine pendant la période humide et que l'assèchement au cours de l'Holocène démarre plus tôt et est plus graduel à l'est de l'Afrique tandis qu'il est plus tardif à l'ouest. Ceci est en accord avec les changements de précipitation observés dans le modèle couplé entre les simulations 6 et 9.5 ka sur ces régions. La partie est de l'Afrique suit ainsi plus le rythme de déclin de la mousson indienne au cours de l'Holocène. Cette corrélation entre l'intensité de la mousson indienne et les pluies sur l'est de l'Afrique a aussi été mise en évidence à l'échelle interannuelle (Camberlin, 1995, 1997). De plus, Hely et al. (2009) montre que le modèle de végétation forcé par l'IPSL-CM4 est en accord avec les données polliniques de l'est du Sahara et du Sahel.

Bien que délicate, la comparaison des résultats de modélisation aux données paléoclimatiques est essentielle. Elle peut être abordée en synthétisant de nombreux proxies pouvant apporter une vision plus globale du changement de mousson à une certaine époque. Cet effort considérable a été réalisé dans le cadre de COHMAP (COHMAP Members, 1988; Wright et al., 1993) puis de PMIP pour l'Holocène Moyen (Prentice et al., 1996; Harrison et al., 1998; Wang et al., 2005). De plus, une étroite interaction entre les modélisateurs et les personnes ayant analysé des données spécifiques permet de discuter et de sélectionner l'information apportée par les enregistrements appropriée aux variables délivrées par la modélisation et de confronter les différents indices de mousson considérés par ces deux approches. Les simulations couplées à l'Holocène de cette thèse ont ainsi été discutées et comparées avec les enregistrements sédimentaires marins de l'Océan Indien de la thèse d'Elise Mathien-Blard (Mathien-Blard, 2009), dirigée par Franck Bassinot au LSCE. Elise Mathien-Blard a traité, analysé et interprété les échantillons d'enregistrements provenant de sédiments marins de plusieurs régions de l'Océan Indien. Ma contribution fut de comparer ces résultats aux variables atmosphériques et de surfaces océaniques des simulations à 0, 6 et 9.5 ka. Une sélection des résultats de cette collaboration sont présentés dans la partie 3.4. Les gradients de salinité est-ouest et nord-sud dans la partie supérieure de l'Océan Indien déduits des données concordent avec les zones de changements de précipitation en été visibles entre la simulation du début de l'Holocène et celle de l'actuel. De plus, l'augmentation de l'activité de l'upwelling de la marge d'Oman et la diminution de l'upwelling à la pointe sud de l'Inde au début de l'Holocène sont en accord avec les variations de circulation de surface obtenues à l'aide du modèle couplé. Les résultats en rapport

aux variations d'upwelling ont été soumis à Climate of the Past (annexe A.2). Pascale Braconnot, Olivier Marti et Laurent Bopp ont complété cette étude par une analyse de la circulation et de la productivité océanique dans les simulations.

3.2 Variations des moussons indienne et africaine dues aux changements d'insolation à 6 et 9.5 ka

Clim Dyn
DOI 10.1007/s00382-009-0538-3

Variations of Indian and African monsoons induced by insolation changes at 6 and 9.5 kyr BP

Charline Marzin · Pascale Braconnot

Received: 11 February 2008 / Accepted: 28 January 2009

Abstract This study investigates the role of insolation in controlling the Indian and African monsoon evolutions during the Holocene using coupled ocean-atmosphere simulations of 0, 6, 9.5 kyr BP climates, for which only the variations of Earth's orbital configuration are considered. The two monsoon systems are enhanced at 6 and 9.5 kyr BP, compared to 0 kyr BP, as a result of the intensified seasonal cycle of insolation in the Northern Hemisphere. The analysis of daily climatologies indicates that even though the length of the "celestial" summer season is shorter at 9.5 kyr BP, the rainy season is longer than at present. Emphasis is put on the impact of the precession on the seasonality, which partly explains why the relative amplification of the Indian and African monsoon varies between 9.5 and 6 kyr BP. Moreover, the changes in snow cover over the Tibetan Plateau play a critical role in reinforcing the 9.5 kyr BP monsoon in India during spring. The results suggest that the teleconnection between convection over India and subsidence over the Mediterranean regions, through the Rodwell and Hoskins mechanism, has an impact on the development of the African monsoon at 9.5 kyr BP.

Keywords Monsoon · Holocene · Modeling · Paleoclimate

C. Marzin (✉) · P. Braconnot
LSCE/IPSL, UMR CEA-CNRS-UVSQ 1572,
Orme des merisers, bat. 712, Gif-sur-Yvette, France
e-mail: charline.marzin@lsce.ipsl.fr

1 Introduction

Monsoon systems are key-components of tropical climate variability, from intraseasonal to Milankovitch time scales. Monsoon regions are characterized by a seasonal reversal of atmospheric circulation and an associated increase in land precipitation during the summer, responding to a seasonal meridional gradient of heating (Wang 2006). This study is focused on two subsystems of the global monsoon, the Indian and the West African (hereafter the African monsoon) monsoons, in order to better understand the different mechanisms that dictate their relative variations during the Early to Mid-Holocene.

Several studies attest that monsoons in the Northern Hemisphere were more intense at the beginning of the Holocene and then decreased to their present values (Wright et al. 1993). Indian and African monsoons have thus undergone important changes during the Holocene. At the beginning of the Holocene, the flourishment of the Indus valley civilization (northwestern part of India) and its migration towards the Ganga plain in the Mid-Holocene indicates their adaptation to climate conditions (Gupta et al. 2006). Different paleoclimate records, such as proxies of lake levels, vegetation and oceanic circulation, show that the maximum in Indian monsoon intensity occured during the beginning of the Holocene and that it decreased regularly during the Holocene to the present dry climate (Lezine et al. 2007; Prasad and Enzel 2006; Fleitmann et al. 2007; Wang et al. 2005). However, the African monsoon seems to have decreased differently. A long humid period referred to as the "Green Sahara" is observed from the Early Holocene until 5–4 kyr BP (Gasse 2000; Liu et al. 2007). Lakes and pollen data suggest that during that time there was a humid period in now arid regions (Jolly et al. 1998; Hoelzmann et al. 1998). An abrupt change to

Published online: 18 February 2009

the present dry conditions then followed (deMenocal et al. 2000; Prentice and Webb 1998).

The main forcing of the monsoon evolution during the Holocene is the changes in the seasonal cycle of insolation due to precession and obliquity. So far, most of the studies analysed the monsoon response to insolation forcing (increased summer insolation in the Northern Hemisphere) and the role of atmosphere, ocean, vegetation and their interactions (Wright et al. 1993; Joussaume et al. 1999; Kutzbach and Liu 1997; Hewitt and Mitchell 1998; Braconnot et al. 2000b; Claussen and Gayler 1997; Texier et al. 1997; Voss and Mikolajewicz 2001). Numerous studies have been performed for the Mid-Holocene monsoon thanks to the Paleo-Modeling Intercomparison Project (PMIP) (Joussaume et al. 1999; Braconnot et al. 2000a, 2007b). These analyses show that models are able to represent monsoon reinforcements due to insolation variations, and that oceanic and vegetation feedbacks are essential to explain the paleodata (Braconnot et al. 2007c). Other studies have also enlarged their analysis to include the remote impacts of several climatic phenomena on the development of the monsoon during the Holocene (Kitoh and Murakami 2002; Liu et al. 2000, 2006; Otto-Bliesner 1999; Zhao et al. 2007). Prell and Kutzbach (1987) first compared the relative evolution of Indian and African monsoons for the past 150.000 years using a simple atmospheric general circulation model. Liu et al. (2003) did an extensive study on the variations of several monsoon systems of the Northern and Southern Hemisphere between several periods of the Holocene, and the impact of the ocean feedbacks. deNoblet et al. (1996) studied the spatial distribution of rainfall anomalies and the increase (decrease) of high (low) precipitation events for several periods.

However, these studies have not adressed in detail the relative decay of Indian and African monsoons during the Holocene and their mechanisms. Also the effect of the precession on the lengths of the seasons and on the seasonality of the climatic events is crucial at this time scale and acts as a pace maker of the hydrological changes in the Tropics. We thus adress in this study the different mechanisms and the possible lags of Indian and African monsoons variations for three key periods of the Holocene. Here, we compare their responses to the insolation forcing of the Early Holocene (9.5 kyr BP), the Mid-Holocene (6 kyr BP) and the preindustrial climate (0 kyr BP) using an ocean-atmosphere coupled model. The orbital configuration at 9.5 and 6 kyr BP differs mainly due to precession, which influences the seasonal contrast in insolation. Braconnot and Marti (2003) have emphasized the role of the seasonal timing of the insolation forcing on the response of Indian monsoon. We analyse this precessionnal effect as well as the changes in the length of the seasons due to different orbital configurations. We analyse processes based on recent monsoon understanding, focusing on the role of the snow cover of the Tibetan Plateau and the teleconnection between Indian and African monsoons.

In Sect. 2, we introduce the modeling experiment, the orbital configurations and the seasonal cycles of insolation corresponding to the three selected periods. Then we present the results for the changes in terms of precipitation over the land, the main large-scale circulation changes, and changes in the length and the timing of the rainy season in Sect. 3. In Sect. 4, we focus on interesting feedbacks, such as the role of the Tibetan Plateau snow cover and the teleconnection between Indian and African monsoons. Results and perspectives are discussed in the last section.

2 Model, experiments and major characteristics of the monsoon

2.1 The coupled ocean-atmosphere model and monsoon systems in the control simulation

The simulations are performed with the version of the IPSL coupled model (Marti et al. 2005) used for future climate projections as part of the WCRP/CMIP3 multi-ensemble experiments (Meehl et al. 2007) that served as a basis for the last IPCC assessment (Solomon et al. 2007). IPSL_CM4 couples the grid point atmospheric general circulation model LMDz (Hourdin et al. 2006) developed at Laboratoire de Météorologie Dynamique (LMD, France) to the oceanic general circulation model ORCA (Madec et al. 1998) developed at the Laboratoire d'Océanographie et du Climat (LOCEAN, France). On the continent, the land surface scheme ORCHIDEE (Krinner et al. 2005) is coupled to the atmospheric model. Only the thermodynamic component of ORCHIDEE is active in the simulations presented here. The closure of the water budget with the ocean is achieved via a river routing scheme implemented in the land surface model. A sea-ice model (Fichefet and Maqueda 1997), which computes ice thermodynamics and dynamics, is included in the ocean model. The ocean and atmospheric models exchange surface temperature, sea-ice cover, momentum, heat and fresh water fluxes once a day, using the OASIS coupler (Terray et al. 1995) developed at CERFACS (France). None of these fluxes are corrected. In its present configuration, the model is run at medium resolution. The atmospheric grid is regular, with a resolution of 3.75° in longitude, 2.5° in latitude, and 19 vertical levels. The ocean model grid has approximately 2° resolution (0.5° near the equator) with 182 points in longitude, 149 points in latitude and 31 vertical 1evels.

The large scale features of the tropical circulation are reproduced qualitatively well in this model (Braconnot

et al. 2007b; Marti et al. 2005). The comparison with observation datasets shows good dynamic structures and reasonable seasonal cycles of temperature and precipitation over Indian Ocean and Tropical Atlantic. Figure 1 shows that the model captures well the climatological features of JJAS precipitation compared to the CPC Merged Analysis of Precipitation (CMAP) long term mean dataset (Xie and Arkin 1997). However, precipitation is too low over the Indian continent, with a tendency of the rain band to remain over the ocean (Kripalani et al. 2007). The Indian monsoon onset is also slightly delayed compared to observations. Nevertheless, the overall dynamic structures, such as the mid-latitude westerly jet and the tropical easterly jet at the top of the troposphere, are represented with a proper vertical structure in the atmosphere and in the ocean. The monsoon patterns, as well as the seasonal cycle, are reasonably reproduced but the amplitude of precipitation north of 8°N is lower than observed. A cold bias in mid-latitude and a warm bias in the Guinean Gulf contribute to this deficit of precipitation. In addition, the tropical interannual variability is quite satisfactorily reproduced in the model (Guilyardi 2006; Leloup et al. 2007). Finally, the simulated changes at the Mid-Holocene share most of the features of the Paleo-Modeling Intercomparison Project (PMIP) simulations (Zhao et al. 2005; Braconnot et al. 2007b). Despite the underestimation of precipitation over the continent, the IPSL_CM4 model is suitable for experiments to study the variability of monsoon systems at orbital time scales.

2.2 Insolation forcing, length of the seasons and calendar

Changes in insolation due to slow variations of the Earth's orbital parameters are the major driver of climate variability during the Holocene. Precession and obliquity are the two parameters that shape the insolation forcing over this period. Here, we restrict our analysis to three key periods in the Holocene, the Early Holocene (9.5 kyr BP), the Mid-Holocene (6 kyr BP) and the preindustrial period (0 kyr BP) in order to study the variations of the precession and its effect on the seasonality of the tropical climate. They correspond to key periods chosen for model intercomparisons within the PMIP project (Braconnot et al. 2007b; Crucifix et al. 2002).

Figure 2 illustrates the orbital configurations for these three climates. Orbital parameters are calculated from Berger (1978). Because of the precession, the summer solstice (SS) was close to the perihelion during the Early Holocene period. The axial tilt (i.e. obliquity) was also larger compared to present day (Fig. 2). According to Kepler's laws, the season closer to the perihelion is shorter. As a result, the time spent between equinoxes and solstices varies for different climates and so do the date of a particular position along the orbit. The opposite configuration at 9.5 kyr BP compared to 0 kyr BP leads to a shorter summer (summer solstice to autumnal equinox) with more insolation in the Northern Hemisphere and a longer winter (winter solstice to vernal equinox) with less insolation. At 6 kyr BP, the axial tilt is slightly reduced compared to 9.5 kyr BP but still larger than at the present day (Fig. 2). The difference with 9.5 kyr BP is that the autumnal equinox is near the perihelion. This leads to a shift in the timing of the seasonal variations. These different orbital configurations result in changes in the seasonal and meridional distribution of incoming solar radiation at the top of the atmosphere (insolation), as well as changes in the lengths of the seasons.

To analyse the seasonal cycle of a climatic variable, one has to be careful with the choice of the calendar used for monthly averages. Indeed, the lengths of the seasons are altered by the precession variations. To compare the timing of two different climate seasonal cycles, an absolute time reference has to be defined as well as a calendar for the monthly averages. The usual reference date for the PMIP simulations is the Vernal Equinox (VE) fixed on 21 March at noon (Braconnot et al. 2007b). Table.1 shows the lengths of the seasons for the different periods. In the present climate, summer is longer than winter. At 9.5 kyr

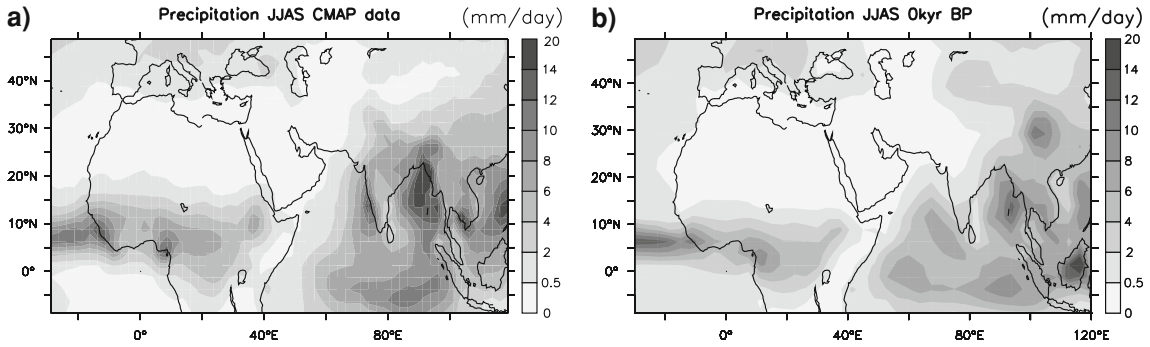

Fig. 1 Precipitation (mm/day) averaged from June to September (JJAS) for **a** CMAP dataset climatology from years 1979 to 2000; **b** preindustrial (0 kyr BP) simulation

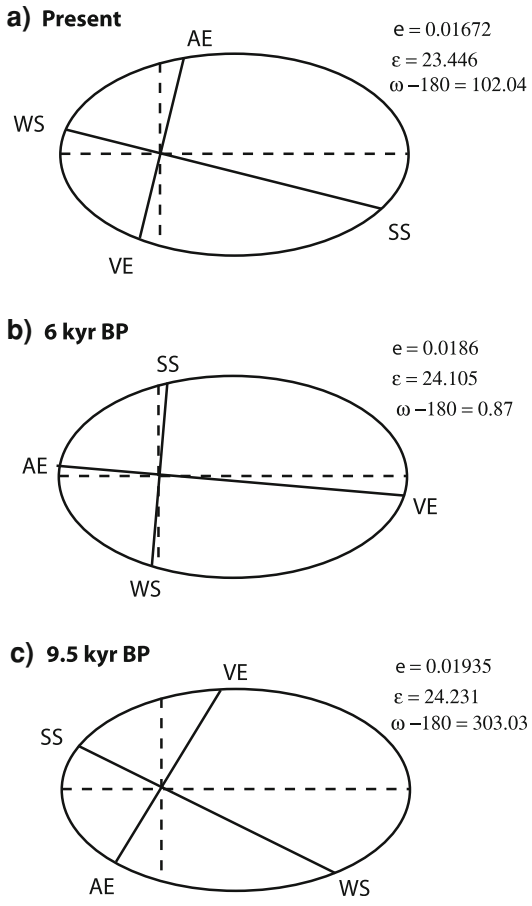

Fig. 2 Earth's orbital elements for preindustrial, 6 and 9.5 kyr BP periods, where e is the eccentricity, ε is the obliquity and ω is the longitude of the perihelion. WS stands for winter solstice, VE for vernal equinoxe, SS for summer solstice and AE for autumnal equinoxe

BP, the spring and summer seasons were shorter than the autumn and winter seasons, whereas the summer and autumn seasons were longer than the winter and spring seasons at 6 kyr BP.

Monthly values are generally based on the modern calendar definition (or fixed calendar), which does not take into account the changes in the lengths of the seasons for other climates. For example, if the reference date for two climates is fixed for the vernal equinox, the autumnal equinox dates will be different, so that the changes that occur in autumn will be slightly underestimated with this modern calendar in the Northern Hemisphere (Braconnot et al. 2007b). As an alternative, a "celestial" definition of the months is consistent with a definition of seasons based on insolation. For some of the analyses presented below, we adopted the Kutzbach and Gallimore (1988) definition of calendar discussed in Joussaume and Braconnot (1997). For each periods, the beginning and end of the months correspond to the same celestial longitudes from the VE along the Earth's orbit as for the modern months. The corresponding dates in the year and lengths of the months are reported in Table 2. Each period has its corresponding celestial calendar and as a result, the monthly means are phased according to the solstices and equinoxes and the seasonal evolutions can be compared. Joussaume and Braconnot (1997) quantified the impact of the choice of different calendars to compare two climates and showed that it can lead to biases up to 10% of the signal.

The celestial definition of the calendar has been used to compute the monthly mean changes in insolation (Fig. 3) induced by the changes in orbital parameters. Precession controls the seasonal variations of insolation whereas obliquity controls the contrast between low and high latitudes. The magnitude of the seasonal cycle was enhanced in the Northern Hemisphere at 9.5 kyr BP compared to present (Fig. 3b), with more insolation during summer and less during winter, while it was damped in the Southern Hemisphere. These changes in insolation are associated with increased winter cooling and summer warming in the Northern Hemisphere. Insolation averaged from 10 to 50°N is amplified by almost 10% (40 W m^{-2}) during summer and is in phase with the present seasonal cycle of insolation (i.e. maximum change at the SS, Fig. 3c). The seasonal cycle at 6 kyr BP was also enhanced over the Northern Hemisphere summer, but with a shift in the amplification of insolation towards autumn (Fig. 3d). The magnitude of the insolation change during the Northern Hemisphere summer is larger at the northern high latitudes. This is explained by the fact that 10% of the insolation changes at 9.5, compared to 0 kyr BP, are due to the effect of obliquity. The effect of obliquity alone on the seasonal cycle of insolation is similar at 6 and at 9.5 kyr BP. During the Mid-Holocene, a maximum insolation occurs between the summer solstice and the autumnal equinox and this shift is even more important within the Tropics. The difference in insolation averaged over the Northern Hemisphere (10–50°N, Fig. 3c) lags the change in insolation at 9.5 kyr BP

Table 1 Lengths of the seasons in days and dates of equinoxes and solstices (according to modern calendar) at 0, 6 and 9.5 kyr BP

	WS date	Winter length	VE date	Spring length	SS date	Summer length	AE date	Autumn length
0 kyr BP	23/12	88	21/03	91	22/06	92	25/09	89
6 kyr BP	19/12	92	21/03	92	23/06	88	21/09	88
9.5 kyr BP	18/12	93	21/03	89	20/06	87	17/09	91

Table 2 Number of days per month for the celestial calendar and date of the first day of the january month (according to the present dates) at 0, 6 and 9.5 kyr BP

	Starting date	01	02	03	04	05	06	07	08	09	10	11	12
0 kyr BP	01/01	30	30	30	30	30	30	30	30	30	30	30	30
6 kyr BP	27/12	31	32	31	31	30	29	29	28	29	29	30	31
9.5 kyr BP	26/12	32	32	31	30	29	28	28	28	29	30	31	32

by about one month. The maximum amplification is reduced at 6 kyr BP (25 W m^{-2}) compared to 9.5 kyr BP. We will then consider both the changes in the magnitude and timing of the seasonal cycle when analysing the impact of insolation forcing on the African and Indian monsoons.

2.3 Simulations of 9.5 and 6 kyr BP climates

Three simulations were performed with IPSL-CM4 for the climates of 9.5 and 6 kyr BP, and of the preindustrial periods considering only the variations of the orbital parameters described above. Simulations for the 0, 6, and 9.5 kyr BP climates are 990, 800, and 270 years long, respectively, and are stable (the trend of global surface temperature is less than 0.02 K/century). Initial conditions are from Levitus (1982) climatology for the ocean model and the 1st January representative of a present day climate for the atmosphere. We compute the mean climatologies from the last 100 years of each simulation in order to analyse the seasonal variations in the characteristics of the Indian and African monsoons. These experiments use a 360-day calendar. When possible we use the celestial definition of calendar in order to avoid misinterpretations of the changes in autumn between the simulations. However, the use of the "celestial calendar" is only possible for the climate variables for which we have stored daily outputs. This explains why some of our analyses also consider the modern calendar.

We first analyse the response of the African and Indian monsoon systems to the three different solar forcings in terms of precipitation, which is the basic variable to evaluate the changes in monsoon activity. We consider the averaged precipitation from June to September (JJAS) in order to account for the whole rainy season for both African and Indian monsoons in all three climates. Indian and African monsoons are considerably enhanced at 9.5 and 6 kyr BP compared to the preindustrial simulation (Fig. 4a, b). Precipitation over the Sahel is intensified and

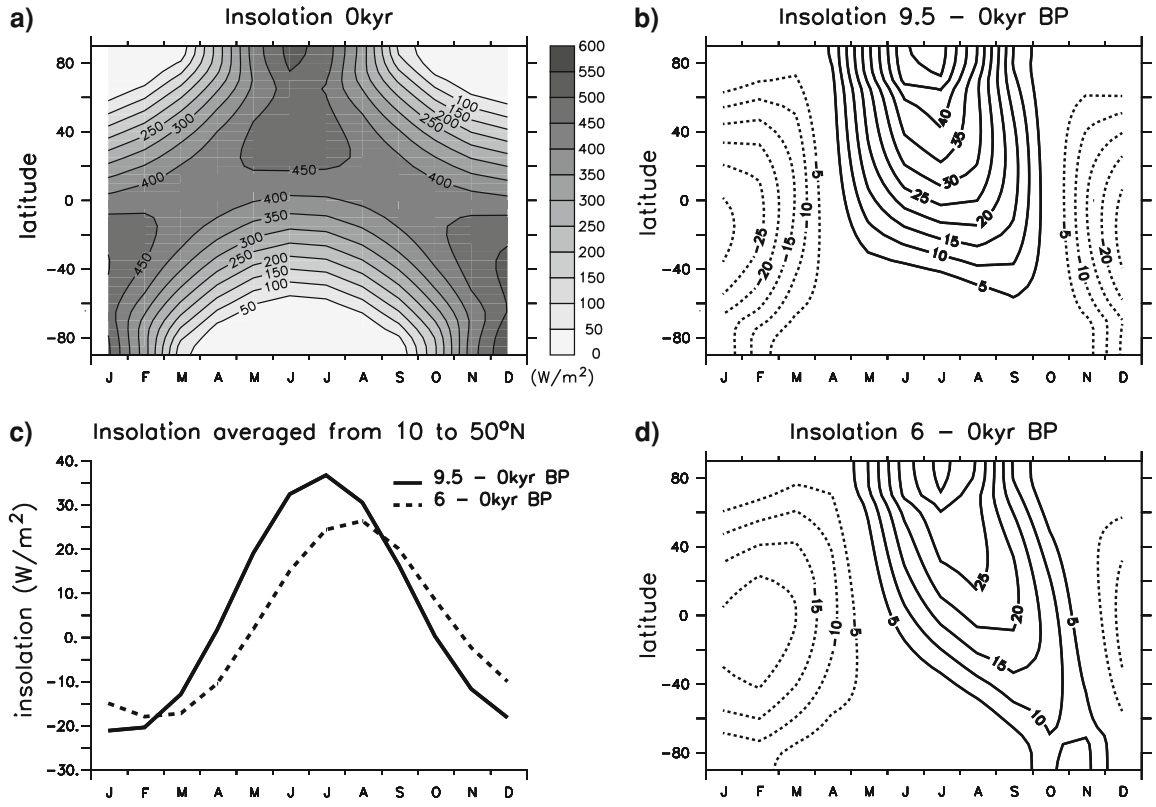

Fig. 3 Incoming solar radiation at the top of the atmosphere (W/m^2) averaged over the longitude and plotted as a function of months, for **a** present, **b** 9.5–0 kyr BP, **d** 6–0 kyr BP; **c** insolation averaged from 10–50°N and plotted a s a function of months for 9.5-0 kyr BP (*line*) and 6-0 kyr BP (*dash*). The celestial calendar is used to compute the monthly means

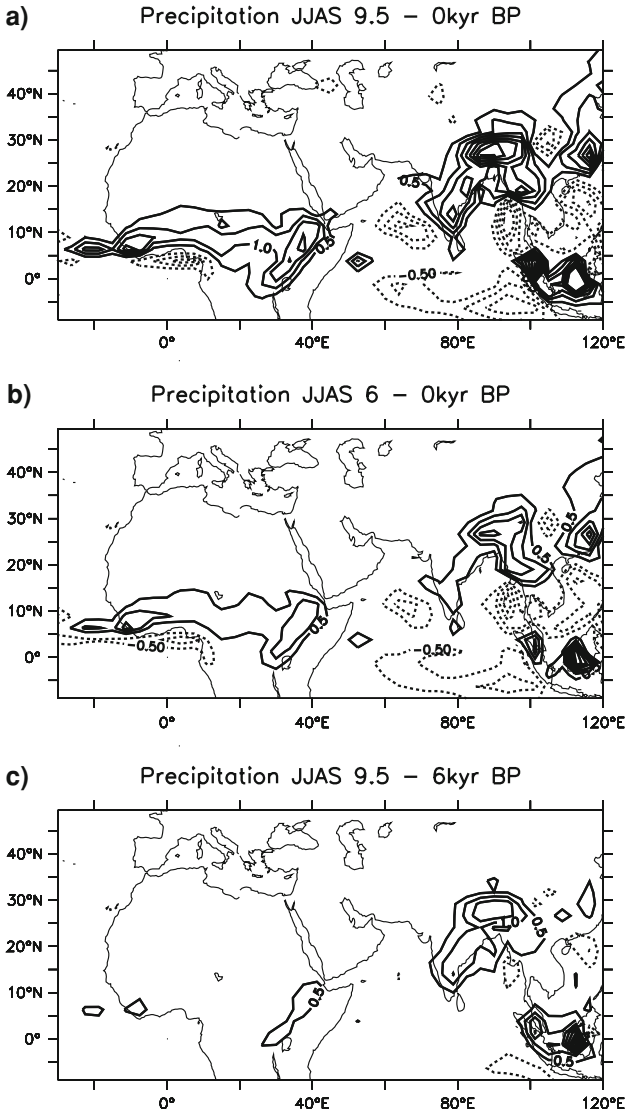

Fig. 4 Differences of precipitation (mm/day) averaged from June to September (JJAS) for **a** 9.5–0 kyr BP, **b** 6–0 kyr BP, **c** 9.5–6 kyr BP. The celestial calendar is used to compute the monthly means

shifted northward, which is characterized by a negative anomaly along 4°N and a maximum positive anomaly around 9°N. In the Indian sector, precipitation is enhanced and penetrates further inland over North–East India both at 9.5 and 6 kyr BP. It is also intensified over South and Central India at 9.5 kyr BP. Figure 4c shows the difference in the responses of the two monsoon sytems between the Early and Mid-Holocene. The Indian monsoon is stronger at 9.5 than at 6 kyr BP, whereas the African monsoon is similar for those two periods. This raises the question of a potentially different response of Indian and African monsoons to insolation over these two periods.

In terms of seasonal evolution of monsoons, Fig. 5a and b show the differences in the seasonal cycle of rainfall averaged over the land only [over Sahel (20°W–30°E; 5–17°N) and India (70–100°E; 10–35°N]. The amplification of Indian and African monsoons is larger and occurs earlier in the season at 9.5 than at 6 kyr BP. This is consistent with the variations in the seasonality and amplitude of insolation forcings between two periods. The next section will focus on mechanisms and more detailed characteristics of these monsoon amplifications at the Early and Mid-Holocene.

3 Variations of Indian and African monsoon characteristics

3.1 Large scale circulation changes

Variations in the seasonal cycle of insolation are transmitted via thermodynamic changes and the dynamic circulation and involve the whole troposphere and air-sea interactions. Although the land-sea surface temperature contrast enhancement is often claimed to be the main factor driving the monsoon changes during the Holocene in paleoclimatology studies, it has been proved to be not sufficiant to trigger the complex onset of the Indian monsoon (Schneider and Lindzen 1976; Srinivasan 2006). The complex role of large scale heating of the Tibetan Plateau and of latent heating over the ocean should also be considered for the Holocene variations of monsoon as for the

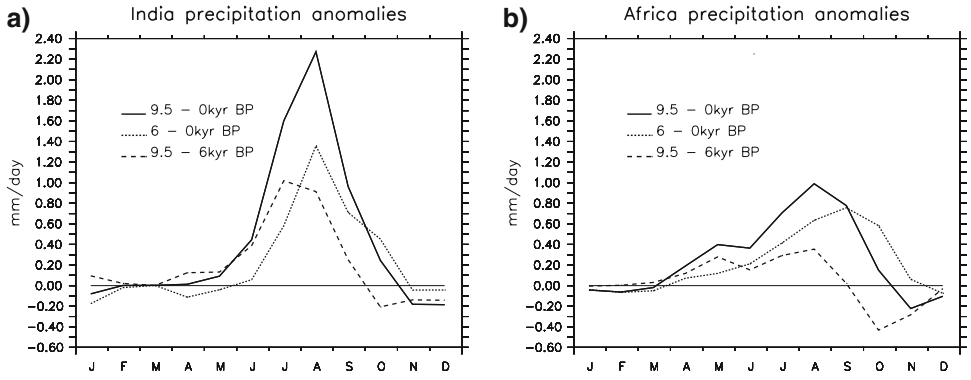

Fig. 5 Monthly land precipitation differences between 9.5 and 0, 6 and 0 and 9.5 and 6 kyr BP, averaged over **a** India (70–100°E, 10–35°N) and **b** Sahel (20°W–30°E, 5–17°N). The celestial calendar is used to compute the monthly means

present day. Studies by Li and Yanai (1996) and Xavier et al. (2007) emphasize the role of the meridional gradient in tropospheric temperature (TT) in driving the Asian monsoon. Xavier et al. (2007) defined an Indian monsoon index based on the reversal of this gradient during boreal summer and autumn. This index is used to determine the onset and withdrawal of the monsoon, and its integral is well correlated with integrated rainfall over India. However, there is no direct correlation between the temperature amplitude and the rainfall intensity. We characterized this gradient by considering a similar index of the Indian monsoon named DeltaTT based on the difference in TT (averaged from 200 to 500 hPa) between a large northern box (60–120°E, 10-45°N) and a large southern box (60–120°E, 25°S–10°N). The monsoon starts (withdraws) when this gradient becomes positive (negative) in spring (autumn). We compare the seasonal evolution of this gradient for the three climates (Fig. 6). The differences in DeltaTT between present and Early and Mid-Holocene track the differences in the insolation seasonal cycle, with a

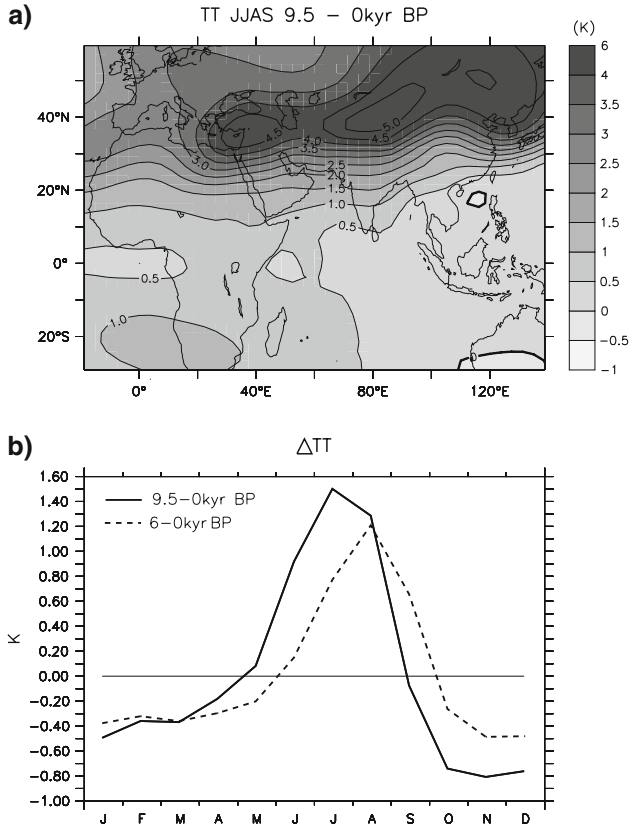

Fig. 6 Tropospheric temperature (TT) averaged from 200 to 500 hPa, **a** averaged from June to September (JJAS) for 9.5–0 kyr BP; **b** TT seasonal gradient (DeltaTT, the annual averages are removed) between northern box (60–120°E, 10–45°N) and southern box (60–120°E, 25°S–10°N) for 9.5–0 kyr BP (*line*) and 6–0 kyr BP (*dash*). The modern calendar is used to compute the monthly means

meriodional gradient of TT increased by 1.5 K from 0 to 9.5 kyr BP and by 1.2 K from 0 to 6 kyr BP, as well as a lag between 9.5 and 6 kyr BP. Most of the differences between those periods come from a stronger heating (cooling) at the troposphere over the northern box during spring and summer (autumn and winter), whereas the oceanic southern box does not show such large temperature variations (Fig. 6a), which is consistent with the enhanced (damped) seasonal cycle of insolation in the Northern Hemisphere (Southern Hemisphere).

The large scale meridional tropospheric gradient is associated with an amplification of the contrast in land-sea surface temperature at 9.5 and 6 kyr BP. This feature is well depicted between the Gulf of Guinea and North Africa and between the Indian continent and the Indian Ocean (Fig. 7a, b). This is associated with a deepening of the heat-lows over the Tibetan Plateau and the Sahara (Fig. 7c, d). Monsoon systems are amplified over the Sahel and India as this large meridional temperature gradient is consistent with a more northerly monsoon and these experiments demonstrate that this change is ultimately forced by the insolation changes. Monsoon flows are intensified over the Arabian Sea, the South Indian Ocean and the western coast of Africa (Fig. 7e, f). The surface winds are also weaker south of the Indian subcontinent. The dynamic structure of the Indian monsoon flow is shifted northward and penetrates further inland. Deep convection and subsidence zones are represented by low and high values of the outgoing longwave radiation (OLR) respectively (Fig. 7a, b). This radiative variable is a more reliable proxy for the large scale deep convective zones as it is less affected by small structures than precipitation. The large scale OLR structures on Fig. 7a and b highlight deeper convective activity over the Sahel and North India, less convection over the western African coast and over the southern part of the Bay of Bengal. Interestingly, the large scale subsidence anomaly observed around the Mediterannean Sea at 9.5 kyr BP is not as large at 6 kyr BP. This difference will be further analysed in Sect. 4.2.

Several studies have discussed how the response of the ocean to insolation forcing affects the change in the African and Indian monsoons (Liu et al. 2004; Braconnot et al. 2007c; Ohgaito and Abe-Ouchi 2007). At 6 kyr BP, this feedback is positive for the African monsoon. The ocean remains cool in spring compared to the land which enhances the beginning of the monsoon and of the building up of a SST gradient with warmer SST to the north of 5°N that maintains the ITCZ quite north in Autumn (Kutzbach and Liu 1997; Braconnot et al. 2000b; Zhao et al. 2005). It is more complex for the Indian monsoon. The warming of the Indian Ocean has been shown to dampen the response of the Indian monsoon over land (Braconnot et al. 2007c; Ohgaito and Abe-Ouchi 2007). The SST patterns at 9.5 and

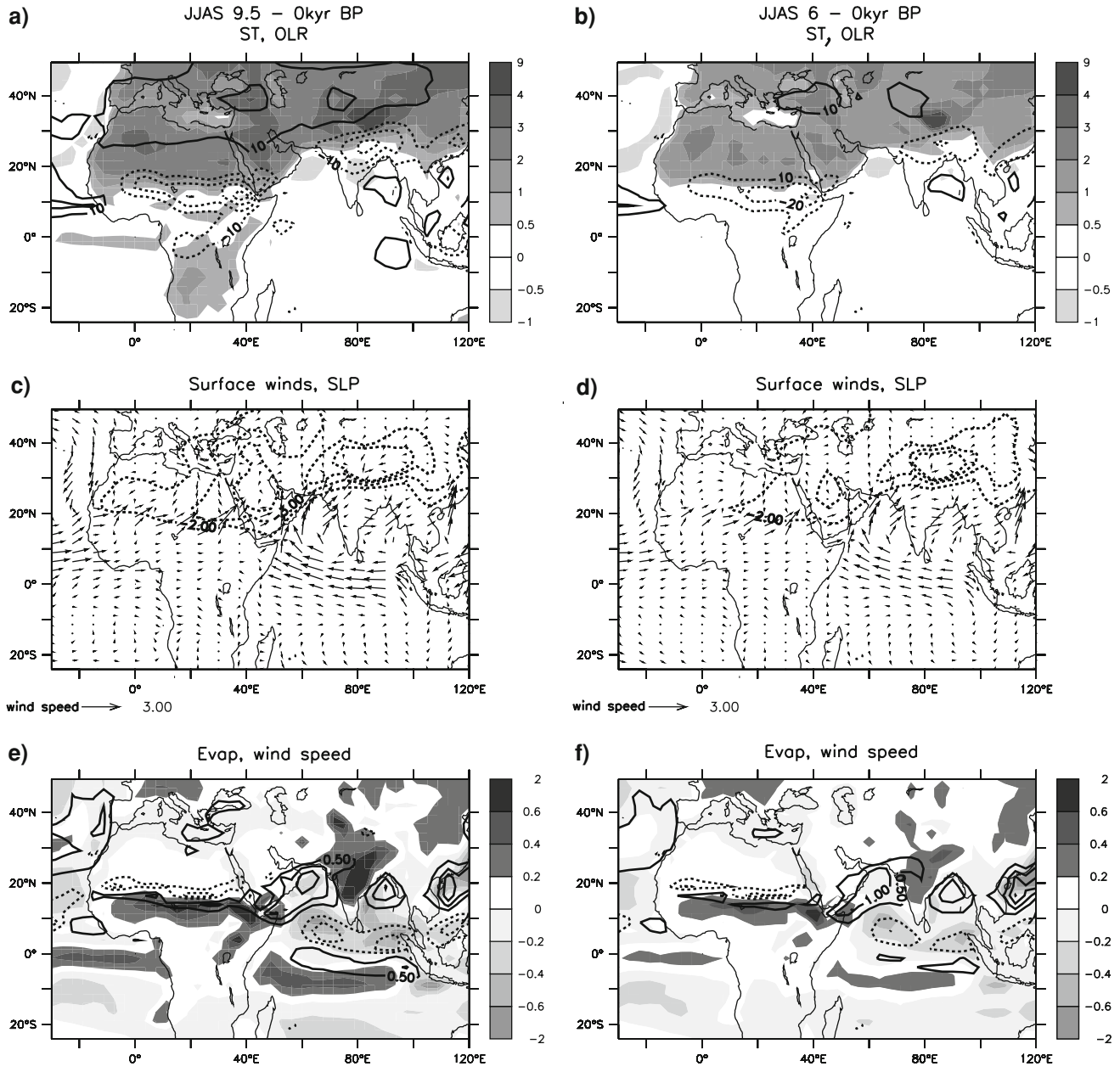

Fig. 7 **a**, **b** Surface temperature (ST) in kelvin (*shade*) and outgoing longwave radiation (OLR) in W/m^2 (*contour*) averaged from June to September (JJAS) for 9.5-0 and 6-0 kyr BP respectively; **c**, **d** surface horizontal wind (*arrows*) and sea level pressure (SLP) in hPa (*contour*) averaged over JJAS for 9.5–0 and 6–0 kyr BP respectively; **e**, **f** evaporation (*Evap*) in mm/day (*shade*) and surface horizontal wind speed in m/s (*contour*) for 9.5–0 and 6–0 kyr BP, respectively.The celestial calendar is used to compute the monthly means

6 kyr BP compared to present (Fig. 7a, b), seem to confirm these effects, but additional simulations would be required to properly assess the role of the ocean, which is beyond the scope of this paper.

3.2 Moisture sources of monsoon precipitation

To first order, two mechanisms are responsible for the enhancement of monsoon rainfall: a stronger advection of humidity over land or a stronger local recycling (precipitation of the evaporated water from the land). Figure 7e and f show the differences in evaporation and wind speed during summer between 9.5, 6 and 0 kyr BP. Evaporation is amplified where precipitation is increased in India and Africa, both at 6 and 9.5 kyr BP, due to local recycling. Over the equatorial Indian Ocean, evaporation patterns follow surface wind speed patterns. However, over the Arabian Sea and the Bay of Bengal, there is less evaporation, despite intensified flow. This is the result of stronger winds, thereby amplifying coastal upwellings and

cooling the surface temperature, thereby increasing air stability and reducing evaporation. To quantify this effect, we average over these regions and for JJAS several terms of the evaporation equation as below:

$$E = \rho C_e V (q_{\text{surf}} - q_{\text{air}}) \quad (1)$$

where E is the evaporation flux, ρ is the air density, C_e the exchange coefficient, V the surface wind speed, q_{surf} the surface air humidity and q_{air} the air humidity at the first vertical level. At 9.5 kyr BP compared to present, E is reduced by 6.9% over the Arabian Sea (58–70°E, 16–22°N). The effect of the strong increase in the wind speed (18.2%) over this region is compensated by the decrease in the air humidity gradient at the surface (−18.5%) and by the fact that the temperature profile at the surface is more stable, due to the cooling of the surface (by 0.6°C) thus reducing the exchange coefficient (−2.9%). The enhancement of the coastal upwelling along the Arabian peninsula (Fig. 7e) contributes to this cooling. Over the Bay of Bengal, the mixed layer depth is shallower (not shown) due to runoff and precipitation during summer season, stronger winds result in a cooling of the sea surface temperature, and therefore the evaporation is reduced. On the contrary, the mixed layer depth is deeper in the equatorial Indian Ocean, and we observe stronger evaporation corresponding to stronger winds between 9.5 and 0 as well as 6 and 0 kyr BP.

The available moisture over the continent results from moisture advection and local recycling over the Sahel and the Indian continent. To first order, the contribution of moisture advection to precipitation over land is estimated by the ratio $(P-E)/P$ (Table 3). In order to estimate the relative impact of changes in local recycling and moisture advection, we computed for each period this ratio considering the changes in precipitation and evaporation. In the preindustrial simulation, moisture advection accounts for about 30% of precipitation over India and Sahel, but it can be up to 46% for India and 41% for Sahel at 9.5 kyr BP. The changes in precipitation between 9.5 and 0 and 6 and 0 kyr BP are mainly due to the enhancement of inland moisture advection (about 80% in India and 65% in Sahel). In fact, even if the evaporation over the Bay of Bengal and the Arabian Sea is reduced, there is more moisture transported from the equatorial Indian Ocean to the continent. Over Sahel, the moisture is advected from the Tropical Atlantic. As a result, the enhancement of the monsoon flow is the main mechanism triggered by the change in insolation at the beginning of the Holocene. This is valid for both 9.5 and 6 kyr BP climates.

3.3 Characteristics of the length and intensity of the monsoon season

In order to better characterize the changes in monsoons, considering the monsoon intensity, the length of the rainy season and a possible seasonal shift in monsoon peak between the different periods, we adopt a definition of the monsoon season based on daily values. We have computed daily climatologies of 100 years for each climate. Figure 8 shows the seasonal evolution of precipitation averaged over Sahel (20°W–30°E; 5–17°N) and India (70–100°E; 10–35°N). As discussed in the previous section, this diagnostic shows a stronger enhancement of the Indian monsoon at the beginning of Holocene than at the Mid-Holocene (the maximum of precipitation is doubled from 0 to 9.5 kyr BP), and almost the same enhancement of the African monsoon for both periods. If a simple threshold of 2 mm/day is used to define the beginning and the end of the rainy season, the length of the rainy season is 102 days at 0 kyr BP, 110 days at 6 kyr BP, and 119 days at 9.5 kyr BP in India, whereas over Sahel it is 107 days at 0 kyr BP, 131 days at 6 kyr BP and 133 days at 9.5 kyr BP. Thus, the rainy season is longer at 9.5 than at 6 kyr BP in India, whereas it is equivalent in Africa for both periods. If we consider the Vernal Equinox as a reference, this figure also indicates that the African monsoon is shifted by 10 days (with the threshold of 2 mm/day) at 6 kyr BP for both the onset and the withdrawal of the monsoon. Indian monsoon onset occurs later (by 11 days in terms of number of days after the VE) at 6 compared to 9.5 kyr BP but it seems to end at the same time (only 2 days difference in terms of number of days after the autumnal equinox). According to the season definition (the time between solstices and

Table 3 Ratio of JJAS precipitation due to water advection, estimated by $P - E/P$ averaged over the land only in Sahel (20°W–30°E, 5–17°N) and India (70–100°E, 10–35°N) and changes between 9.5 and 0, 6 and 0 and 9.5 and 6 kyr BP

(Pi − Ei)/Pi	0 kyr BP	6 kyr BP	9.5 kyr BP
India	0.28	0.39	0.46
Africa	0.33	0.39	0.41
((Pj − Pi) − (Ej − Ei))/(Pj − Pi)	9−0 kyr BP	6−0 kyr BP	9−6 kyr BP
India	0.77	0.79	0.76
Africa	0.65	0.64	0.67

The celestial calendar is used to compute the monthly means

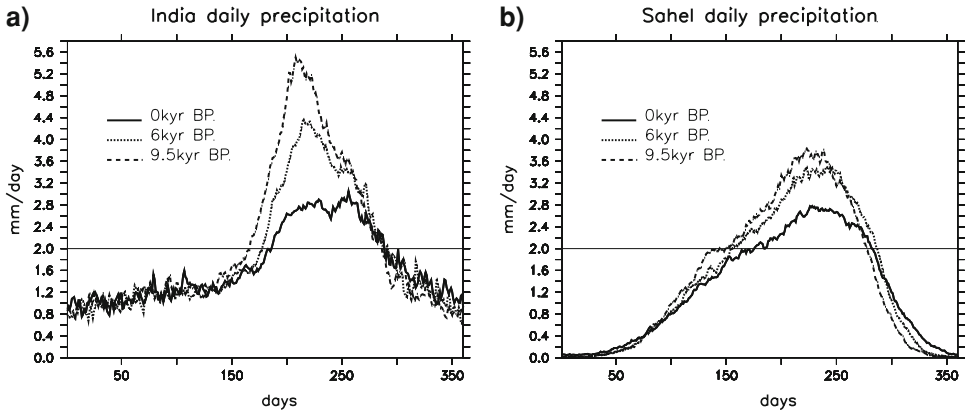

Fig. 8 Daily land precipitation averaged over **a** India (70–100°E, 10–35°N) and **b** Sahel (20°W–30°E, 5–17°N) at 9.5, 6 and 0 kyr BP

equinoxes), the summer season is shorter at 9.5 than at 6 kyr BP, but surprisingly, the monsoon season is longer. This highlights the crucial role of the meridional and seasonal contrast of the heating and of the different feedbacks.

Another way of highlighting the different behaviour of the two monsoon systems is to average JJAS precipitation over land only for the Sahel (20°W–30°E, 5–17°N) and the Indian (70–100°E, 10–35°N) regions (Fig. 9), which are the two regions most affected by the variations of the northern edge of the monsoon belt. The increase in precipitation (27%) from 0 to 6 kyr BP is similar for Indian and African monsoons, whereas from 6 to 9.5 kyr BP, Indian precipitation is amplified by 16% but African precipitation is increased by only 4%. The two monsoon subsystems do not respond the same way to the 9.5 and 6 kyr BP insolation forcings.

Braconnot and Marti (2003) discussed the impact of the precession on the timing of the Indian monsoon and showed that the Indian monsoon enhancement was more

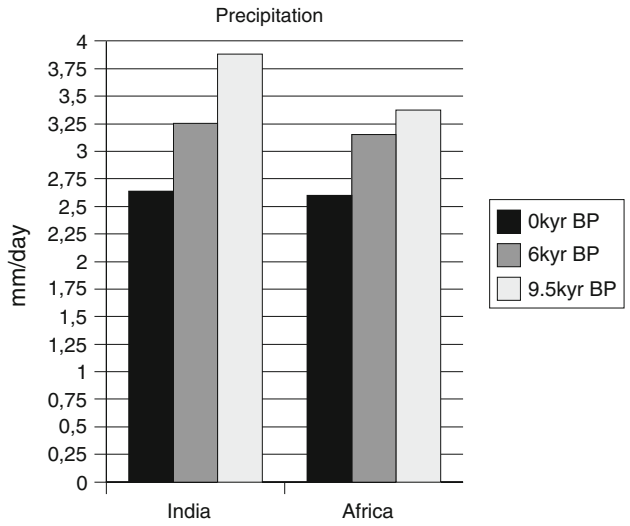

Fig. 9 JJAS land precipitation averaged over Sahel (20°W–30°E, 5–17°N) and India (70–100°E, 10–35°N) at 9.5, 6 and 0 kyr BP. The celestial calendar is used to compute the monthly means

sensitive to an amplification of the insolation in phase with the solstice, as it is the case at 9.5 kyr BP. Concerning our study, the Indian monsoon maximum intensity occurs today during July–August, so its amplification is favored when the insolation forcing is in phase with this maximum, as it is the case at 9.5 kyr BP. Similarly, the African monsoon maximum precipitation occurs today during August-September, and would produce a more resonant response to forcings in phase with its evolution. The fact that the change in insolation is maximum in August–September at 6 kyr BP partly explains why the African monsoon remains relatively stronger than the Indian monsoon. Thus, the relative amplifications of Indian and African monsoons are partly driven by the changes in seasonality of insolation due to the precession variations, as the maximum amplification occurs when the change in insolation is in phase with the development of the phenomenon considered. This is similar to the response of an oscillator (Braconnot and Marti 2003). The following sections will give further insight on the origin of the different responses of Indian and African monsoons.

4 Additional features impacting the relative changes of the African and Indian monsoon

4.1 Snow feedback over the Tibetan Plateau

The heating of the Tibetan Plateau is a key feature of monsoon development. Several studies (Yanai and Li 1994; Liu and Yanai 2001) have shown that the snow mass and snow cover over the Tibetan Plateau could alter the Indian monsoon characteristics. The Indian monsoon onset is partly triggered by the build up in sensible heating over the Tibetan Plateau (combined with the latent heat source over the Bay of Bengal) that occurs when the major snow cover is melted. For the modern climate, several studies (Wu and Kirtman 2007; Fasullo 2004; Yanai et al. 1992) show an anticorrelation between the Eurasian snow cover

in winter and spring and monsoon rainfall during boreal summer at an interannual time scale. Here, we investigate if changes in the seasonal cycle of the snow cover over the Himalayas affects the development of sensible heating over the Tibetan Plateau and thereby the development of the monsoon. Figure 10 indicates that the snow mass over the Tibetan Plateau is larger during winter and spring at 9.5 and 6 than at 0 kyr BP, whereas it is reduced in summer, following the enhanced seasonal cycle of insolation. Because precession introduces a lag in the seasonal cycle of insolation at 6 kyr BP, snow cover is larger at 6 than at 9.5 kyr BP in June and July. This snow cover contributes to the spring cooling and could delay the monsoon onset, even though the insolation forcing is sufficiently large to rapidly melt the snow at the end of spring and trigger the monsoon.

To further quantify the feedback of the snow cover on the build up of the diabatic heat source, we used a simple model of the response of the system to the insolation forcing derived from Braconnot et al. (2007b). Here, in order to only consider the surface albedo feedback on the radiative budget, we use clear sky (cs) variables. The difference in net shortwave radiation at the top of the atmosphere between the paleo (pal) and the reference (0k) periods is represented by $SW_{ncspal} - SW_{ncs0k}$. It is the sum of the forcing (considering the albedo constant) and the feedback due to the albedo change. Following Hewitt and Mitchell (1996), we compute the insolation forcing SWf as

$$SWf = (1 - \alpha_{0k})(SW_{dncspal} - SW_{dncs0k}) \quad (2)$$

where SW_{dncs} is the downward (dn) incoming solar radiation for clear sky at the top of the atmopshere, and α0k the planetary albedo of the control simulation. This forcing represents the effect of the change in insolation with the assumption that the planetary albedo is not affected by the climate change.

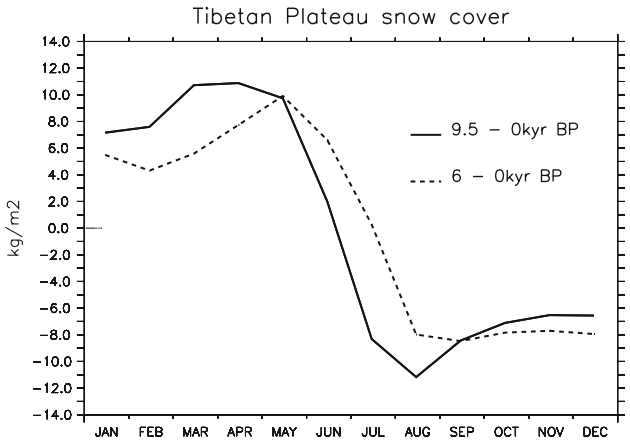

Fig. 10 Differences of seasonal anomaly of snow mass averaged over the Tibetan Plateau (65–95°E, 25–45°N). The modern calendar is used to compute the monthly means

The albedo feedback is then considered to be at the first order the difference between the net shortwave radiation and the shortwave forcing (Braconnot et al. 2007a):

$$\text{Albedo effect} = (SW_{ncspal} - SW_{ncs0k}) - SWf \quad (3)$$

where SW_{ncs} is the net shortwave radiation for clearsky at the top of the atmosphere.

The albedo effect between 9.5 and 0 and 6 and 0 kyr BP is plotted on Fig. 11 as well as SWf and the sensible heat flux (all the fluxes are considered positive downward). At 9.5 kyr BP, the sensible heating of the atmosphere is reduced in winter due to the larger snow cover compared to present. During summer, sensible heating is increased to 7 W/m^2, from May to September, and contributes to the large elevated heat source driving the monsoon. Here the sensible flux evolution does not follow the seasonal cycle of insolation as it does over a desertic area (over the Sahara for example, not shown), but is delayed by more than one month, due the high albedo of snow cover. The quantified albedo effect evolves seasonally in anti-phase with the

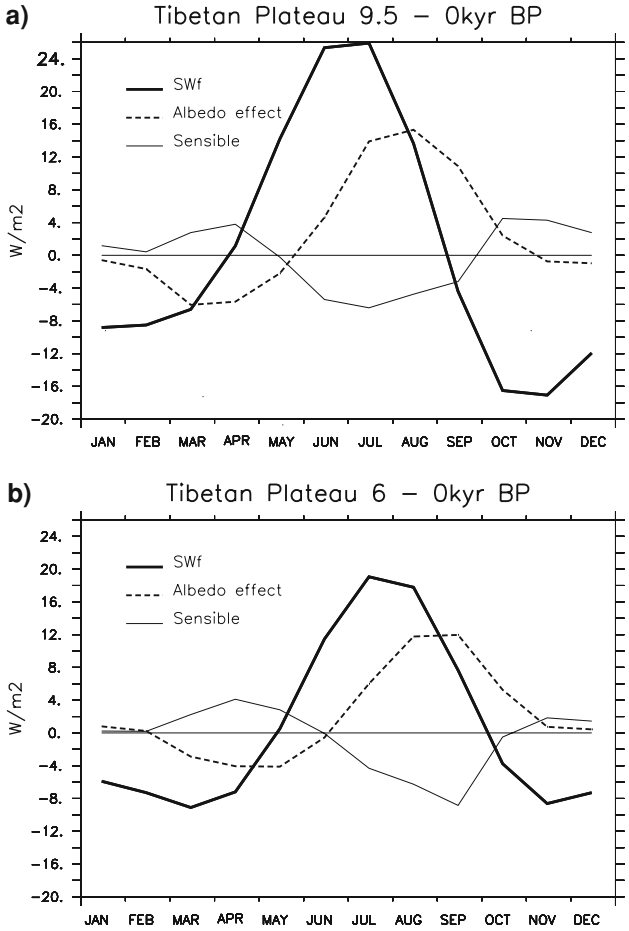

Fig. 11 Shortwave radiative forcing, sensible flux and albedo effect in W/m^2 (all the fluxes are positive downward) averaged over the Tibetan Plateau (65–95°E, 25–45°N) for **a** 9.5–6 kyr BP and **b** 6–0 kyr BP. The modern calendar is used to compute the monthly means

sensible heat flux difference and it has a large contribution to the difference in radiative heating of the atmosphere (Fig. 11). During spring, snow cover remains thick, and the energy is used to melt the snow. This is thus a time when the albedo is still active and prevents the surface warming. Then, during the beginning of summer when the surface albedo is sufficiently low, the surface provides energy to the atmosphere through sensible heating. The reduction in snow cover at that time amplifies the insolation forcing and strengthens the monsoon. The feedback of the albedo of the snow cover counteracts the effect of the forcing. This explains the delay between the radiative forcing and the heating response. Thus, the additionnal snow cover in winter do not act here to delay the monsoon onset as for the present day interannual variability.

The delay in the response of surface heating compared to the insolation forcing, is the same between the Early Holocene and present and between the Mid-Holocene and present. The difference is that the albedo reduction effect is maximum in July–August at 9.5 kyr BP, whereas it is maximum in August-September at 6 kyr BP. The positive feedback of Tibetan Plateau snow cover in July is an additional effect that helps explain the early onset of the Indian monsoon at 9.5, compared to 6 kyr BP, and its relative amplification. Compared to present, the build up of sensible heating over the Tibetan Plateau becomes stronger during May at 9.5 kyr BP, which is synchronous to the establishment of the meridional gradient in tropospheric temperature (the absolute gradient is not shown in Fig. 6). At 6 kyr BP, it occurs in June with a one month lag compared to the build up of the tropospheric temperature gradient. It thus only contributes in strengthening the second half of the monsoon season. This shows that the timing of the snow albedo feedback is critical, and that the effect of the snow cover does not simply result from the winter snow cover. This feedback explains how the snow may affect the monsoon intensity. This stresses that the impact of the snow cover is critical in spring at the time of the onset of the monsoon.

4.2 Teleconnection between Indian and African regions

The Indian and African monsoon systems are connected through the large scale circulation to other remote regions. In addition to ocean and snow feedbacks, monsoon teleconnections could also contribute to relative differences in the development of monsoon subsystems under different climates. Figure 7a shows the large scale clear sky signal over the Mediterranean Sea at 9.5 kyr BP. These positive anomalies in OLR are significant between 9.5 and 0 kyr BP with a maximum over Turkey and at the North–West of the Tibetan Plateau and are proportionally weaker between 6 and 0 kyr BP. The vertical velocity at 500 hPa indicates a downward motion over the same regions (Fig. 13c, d). This signal corresponds to a large anomaly in subsidence and is the main striking difference between the 9.5 and 6 kyr BP climatologies.

To give an insight on the origin of the strengthening in subsidence over the Mediterranean Sea in this simulation, we have plotted the seasonal evolution of OLR averaged over two regions (50–80°E, 35–50°N; and 5–40°E, 30–45°N, respectively; Fig. 12). The intensity of the OLR changes between the three climates for the two regions is proportional to the intensity of the changes in precipitation over India (Fig. 8) and not to the Sahel. The correlation is not a proof that the Indian monsoon drives the subsidence. However, it suggests that the subsidence is larger when the Indian monsoon is stronger.

The full structure also involves a rising cell over Africa with an Hadley-type circulation (Fig. 13a, b) and a reinforcement of the northerly surface winds over the Sahara

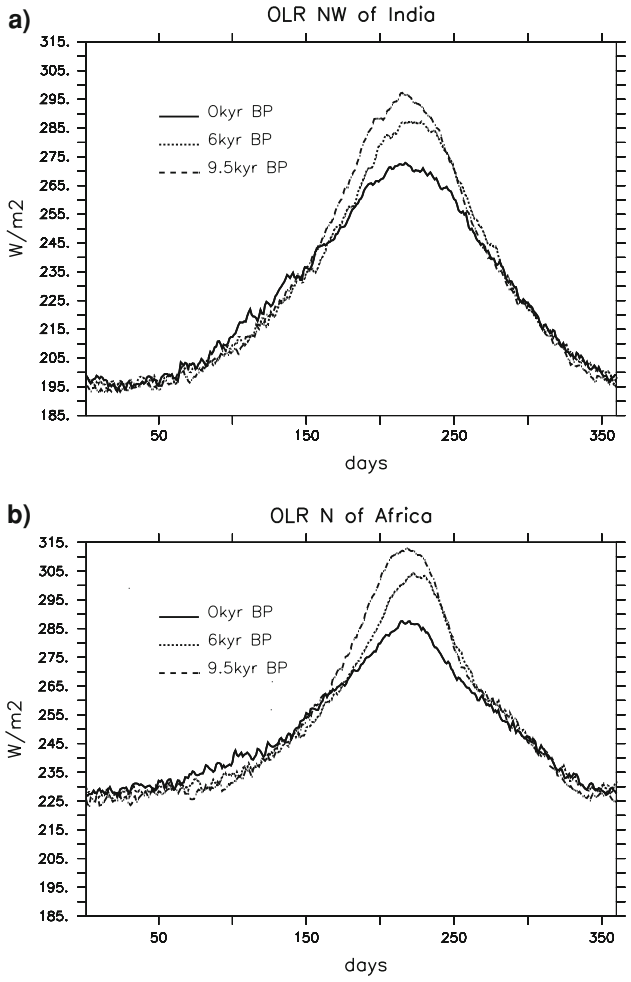

Fig. 12 OLR daily climatology averaged (**a**), over North–West of India (50–80°E, 35–50°N) and (**b**), over North of Africa (5–40°E, 30–45°N) at 9.5, 6 and 0 kyr BP

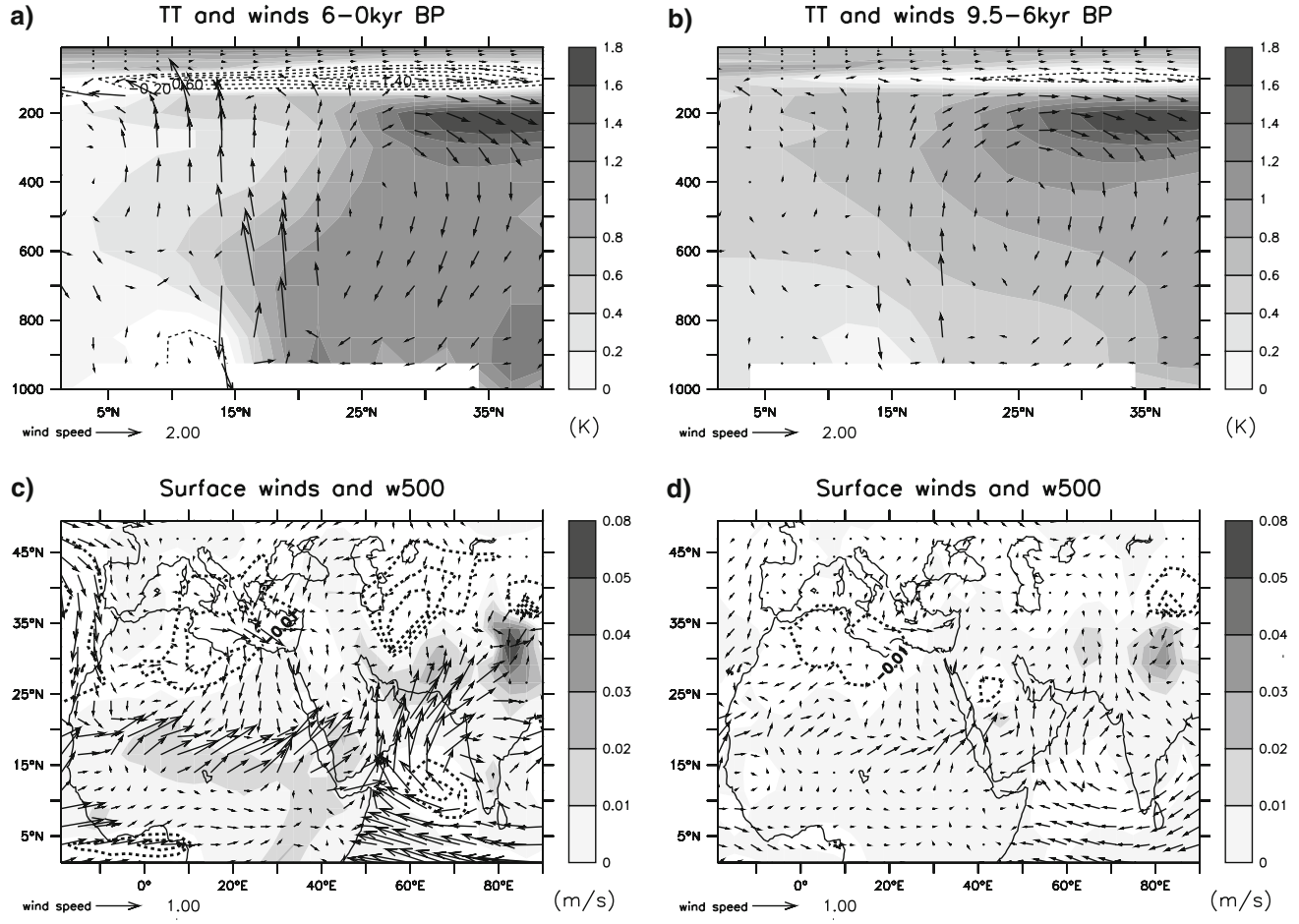

Fig. 13 **a**, **b** Differences of JJAS temperature and winds zonally averaged from 0 to 30°N between 6 and 0 and between 9.5 and 6 kyr BP; **c**, **d** differences of JJAS surface winds and vertical speed at 500 hPa (w500) between 6 and 0 and between 9.5 and 6 kyr BP. The modern calendar is used to compute the monthly means

(Fig. 13c, d). This surface winds reinforcement is proportional to the changes in OLR and to Indian precipitation whereas the ascent over West Africa is similar between 9.5 and 6 kyr BP. Moreover, the two vertical profiles of temperature differences between 6 and 0 and between 9.5 and 6 kyr BP are significantly different (Fig. 13a, b). While the former tends to destabilize the temperature profile, the latter is stabilizing and contributes to inhibate the convection over Sahel.

These patterns share some similarities with the subsidence anomalies discussed by Rodwell and Hoskins (1996). The Rodwell and Hoskins mechanism establishes the connection between the large heating over the Indian region during the monsoon season and its impact on subsidence over the Mediterranean Sea through westward propagation of Rossby waves. The interaction between the propagating thermal structures and the westerly jet causes adiabatic descent over the region located to the North–West of the Tibetan Plateau and the Mediterranean region. This teleconnection seems to be active in our simulations and explains the correlation between the OLR over the Mediterranean region and the Indian precipitation.

This teleconnection between India and the Mediterranean Sea could influence the African monsoon. Indeed, Rodwell and Hoskins (1996) interpreted this teleconnection as a mechanism for the desertification of Northern Africa, but it could also interact with the African monsoon. Other studies highlight changes in surface moisture transport and the temperature of the Mediterranean Sea as being also crucial in controlling the link between the Mediterranean climate and the African monsoon (Hall and Peyrille 2006; Peyrille et al. 2007). In our simulations, the strengthening in subsidence over the Mediterranean Sea is associated with a strengthening in the Easterly jet over Africa towards the Atlantic Ocean. The mid-latitude westerly jet is considerably slower between 9.5 and 6 kyr BP, and the descending motion over the subsidence zones (Fig. 13) is associated with cyclonic patterns of the 200 hPa winds (not shown).

A hypothesis for the weak amplification of African monsoon between 6 and 9.5 kyr BP in response to the

insolation could be that interactions with the large subsidence over North Africa prevent the Sahel precipitation from extending northward. However, this hypothesis is difficult to assess in this study and it involves mechanisms of African monsoon which are not fully understood in the studies of the present climate. For example, the evolution of the heat low in the Sahara desert, ventilation processes and the Mediterranean Sea links with the convection over Sahel are complex (Chou and Neelin 2003; Su and Neelin 2005; Peyrille et al. 2007). In particular, Chou and Neelin (2003) present an extensive analysis of the different mechanisms limiting the northward extent of monsoon systems, including the interactive Rodwell and Hoskins mechanism. Additional experiments isolating these different mechanisms would be of significant help to better understand the differences of evolution of monsoons for paleoclimates.

5 Conclusions and discussion

In this study, we investigated the role of the insolation forcing on the variations of Indian and African monsoons during the Holocene. We compared the simulations for the 0, 6, 9.5 kyr BP climates using the IPSL-CM4 climate model, for which only differences in orbital configuration are considered. These simulations permit an analysis of the detailed mechanisms of the different responses of monsoon systems. Indian and African monsoon precipitation are amplified at 6 and 9.5 kyr BP, compared to the 0 kyr BP control simulation, as a result of the intensified seasonal cycle of insolation. The amplitude and timing of the monsoons are clearly consistent with the seasonal cycle of insolation at 6 and 9.5 kyr BP. The main difference between the two monsoon subsystems is that the Indian monsoon is significantly amplified between 6 and 9.5 kyr BP whereas the African monsoon presents almost the same activity during those two periods. The changes in the timing of the seasonal cycle of insolation due to precession variations can qualitatively explain this different behaviour. The amplification of the Indian monsoon is relatively favoured at 9.5 kyr BP as the maximum insolation difference is in phase with its actual development, whereas African monsoon is favoured at 6 kyr BP due to the delayed amplification of insolation during late summer. This simple analogy with the response of an oscillator highlights the different behaviour of the two monsoon systems between Early and Mid-Holocene in the model and the fact that precession changes have different impacts on different monsoon subsytems. This result is consistent with the study of Braconnot and Marti (2003) that was using a very different version of the IPSL model.

The analysis of daily climatologies indicates that even if the length of the "celestial" summer season is shorter at 9.5 kyr BP, the rainy season is longer than at present. This reveals the major influence of the seasonal and meridional contrast in heating on monsoon development. The reconstruction of monthly climatologies based on a "celestial" calendar definition allows us to compare the timing of onsets and withdrawals of monsoons and to better emphasize the links and lags between the periods in a consistent framework. Those results demonstrate the important role of the precession on the seasonality of the climate phenomena.

Several atmospheric mechanisms explaining the monsoon responses are highlighted. The amplification of monsoons is accompanied by a northward extension of precipitation between 9.5 and 0 and 6 and 0 kyr BP due to a reinforced monsoon flux over the Arabian Sea and the Eastern Tropical Atlantic. The advection of moisture contributes more to the precipitation increases than local recycling through evaporation, which is consistent with the multi-model analysis by Zhao et al. (2005). The monsoon dynamics are consistent with and most likely initiated by the meridional gradient in tropospheric temperature, which is intensified in summer at 6 and 9.5 kyr BP in phase with the insolation variations. The Tibetan Plateau snow cover also plays an important role in the Indian monsoon characteristics for those three climates. We point out the positive feedback of the radiative effect of snow cover on the timing of the onset and the strength of the Indian monsoon at 9.5 kyr BP, which partly explains the earlier onset at 9.5 than at 6 kyr BP. The key factor appears to be the timing of the snow feedback, which is critical in spring and early summer for the Indian monsoon. The Tibetan snow cover mechanism for the Indian monsoon is plausible and consistent with previous studies.

Along with the very weak differences in convection over Sahel between 9.5 and 6 kyr BP, there is a striking and assymetric pattern of stronger subsidence over the Mediterranean Sea. We show that it is related to the Rodwell and Hoskins mechanism, that involves the teleconnection between the highly convective Indian region and the desertic zone around the Mediterranean Sea. Several connections in the dynamic fields strongly support the idea that strong convection over India could prevent the full development of the African monsoon. This study demonstrates that the teleconnective link from the Indian monsoon to the Mediterranean/north African OLR and tropospheric temperatures is clear. The results are consistent with this link having an influence on the north African monsoon. This teleconnection should receive more attention in order to understand global monsoon changes induced by Earth's orbital parameters. However, further studies are needed to confirm this, several experiments are required to isolate the impact of the strong convection over India on the Mediterranean subsidence and the African monsoon extent, in addition to theoretical work.

Of course, to fully assess the timing of the evolution of the Indian and African monsoons across the Holocene, the effects of the vegetation interaction and of the continental ice sheet that remains at 9.5 kyr BP should be also considered. We believe that in our coupled ocean–atmosphere experiments, we capture the first order response of the monsoon to the insolation forcing and that our major conclusions on seasonality, snow cover and teleconnection between India and Mediterranea would remain the same with these additional feedbacks. This is further attested by the fact that the response of the coupled system to insolation forcing is able to represent the trend of monsoon variations depicted by paleoclimatology data significantly. In particular, the faster decrease of the Indian monsoon, compared to the African monsoon, is consistent with some datasets (Fleitmann et al. 2007; Lezine et al. 2007). In these studies, the wet period in the Indian region tends to end at around 7.5 kyr BP and is shorter than for the Sahel region (Gasse 2000). Inspired by this study, we have also compared the evolution of Indian and African monsoons during the Holocene and the Eemian, the last interglacial period, using corresponding periods in terms of precession (Braconnot et al. 2008).

It is unclear to what extent the results of this study could be model dependent, it would be worth examining if the same mechanisms can explain the monsoon decay during the Holocene using other models. However, the mechanisms highlighted here are consistent with recent studies based on observations to better understand monsoon characteristics and all the PMIP2 simulations of Mid-Holocene have monsoon changes with similar characteristics in their seasonal development as the ones discussed here (Zhao et al. 2005; Braconnot et al. 2007b). Even though some of our results may be affected by model biases, they clearly highlight that the timing of different feedbacks is a critical factor in explaining the differences between different monsoon subsystems and should be examinated further. They also show that additional experiments are still needed to better understand climate teleconnections and how the response of the ocean alter the feedbacks in different regions.

Acknowledgments Charline Marzin is funded by a grant from the Commissariat a l'Energie Atomique. Computer time was provided by the Centre National de la Recherche Scientifique (IDRIS computing center) and the Commissariat a l'Energie Atomique (CCRT computing center). CMAP Precipitation data is provided by the NOAA/OAR/ESRL PSD, Boulder, Colorado, USA, from their Web site at http://www.cdc.noaa.go. This work is a contribution to the French "ANR blanc" PICC project and to the "ANR Vulnérabilité Climat et Milieu" SAHELP project. We would like to thank Prince K. Xavier, Sonke Zaehle and Alessandro Tagliabue for technical assistance and proof reading of this manuscript. The reviewers of this paper have greatly contributed to improve the quality and the presentation of this study.

References

Berger AL (1978) Long-term variations of daily insolation and quaternary climatic changes. J Atmos Sci 35(12):2362–2367

Braconnot P, Marti O (2003) Impact of precession on monsoon characteristics from coupled ocean atmosphere experiments: changes in Indian monsoon and Indian ocean climatology. Mar Geol 201(1–3):23–34

Braconnot P, Joussaume S, de Noblet N, Ramstein G (2000a) Mid-Holocene and last glacial maximum African monsoon changes as simulated within the Paleoclimate modelling intercomparison project. Glob Planet Change 26(1–3):51–66

Braconnot P, Marti O, Joussaume S, Leclainche Y (2000b) Ocean feedback in response to 6 kyr BP insolation. J Clim 13(9):1537–1553

Braconnot P, Hourdin F, Bony S, Dufresne JL, Grandpeix JY, Marti O (2007a) Impact of different convective cloud schemes on the simulation of the tropical seasonal cycle in a coupled ocean-atmosphere model. Clim Dyn 29(5):501–520

Braconnot P, Otto-Bliesner B, Harrison S, Joussaume S, Peterchmitt JY, Abe-Ouchi A, Crucifix M, Driesschaert E, Fichefet T, Hewitt CD, Kageyama M, Kitoh A, Laine A, Loutre MF, Marti O, Merkel U, Ramstein G, Valdes P, Weber SL, Yu Y, Zhao Y (2007b) Results of PMIP2 coupled simulations of the Mid-Holocene and last glacial maximum—Part 1: experiments and large-scale features. Clim Past 3(2):261–277

Braconnot P, Otto-Bliesner B, Harrison S, Joussaume S, Peterchmitt JY, Abe-Ouchi A, Crucifix M, Driesschaert E, Fichefet T, Hewitt CD, Kageyama M, Kitoh A, Loutre MF, Marti O, Merkel U, Ramstein G, Valdes P, Weber L, Yu Y, Zhao Y (2007c) Results of PMIP2 coupled simulations of the Mid-Holocene and last glacial maximum—Part 2: feedbacks with emphasis on the location of the ITCZ and mid- and high latitudes heat budget. Clim Past 3(2):279–296

Braconnot P, Marzin C, Gregoire L, Mosquet E, Marti O (2008) Monsoon response to changes in earth's orbital parameters: comparisons between simulations of the eemian and of the holocene. Clim Past Discuss 4:459–493

Chou C, Neelin JD (2003) Mechanisms limiting the northward extent of the northern summer monsoons over North America, Asia, and Africa. J Clim 16(3):406–425

Claussen M, Gayler V (1997) The greening of the Sahara during the Mid-Holocene: results of an interactive atmosphere-biome model. Glob Ecol Biogeogr Lett 6(5):369–377

Crucifix M, Loutre MF, Tulkens P, Fichefet T, Berger A (2002) Climate evolution during the Holocene: a study with an Earth system model of intermediate complexity. Clim Dyn 19(1):43–60

de Menocal P, Ortiz J, Guilderson T, Adkins J, Sarnthein M, Baker L, Yarusinsky M (2000) Abrupt onset and termination of the African Humid Period: rapid climate responses to gradual insolation forcing. Quatern Sci Rev 19(1–5):347–361

deNoblet N, Braconnot P, Joussaume S, Masson V (1996) Sensitivity of simulated Asian and African summer monsoons to orbitally induced variations in insolation 126, 115 and 6kBP. Clim Dyn 12(9):589–603

Fasullo J (2004) A stratified diagnosis of the Indian monsoon-Eurasian snow cover relationship. J Clim 17(5):1110–1122

Fichefet T, Maqueda MAM (1997) Sensitivity of a global sea ice model to the treatment of ice thermodynamics and dynamics. J Geophys Res 102(C6):12,609–12,646

Fleitmann D, Burns SJ, Mangini A, Mudelsee M, Kramers J, Villa I, Neff U, Al-Subbary AA, Buettner A, Hippler D, Matter A (2007) Holocene ITCZ and Indian monsoon dynamics recorded in stalagmites from Oman and Yemen (Socotra). Quatern Sci Rev 26(1–2):170–188

Gasse F (2000) Hydrological changes in the African tropics since the Last Glacial Maximum. Quatern Sci Rev 19(1–5):189–211

Guilyardi E (2006) El Nino-mean state-seasonal cycle interactions in a multi-model ensemble. Climate Dyn 26(4):329–348

Gupta AK, Anderson DM, Pandey DN, Singhvi AK (2006) Adaptation and human migration, and evidence of agriculture coincident with changes in the Indian summer monsoon during the Holocene. Curr Sci 90(8):1082–1090

Hall NMJ, Peyrille P (2006) Dynamics of the west African monsoon. J Phys IV 139:81–99

Hewitt CD, Mitchell JFB (1996) Gcm simulations of the climate of 6 kyr bp: mean changes and interdecadal variability. J Clim 9(12):3505–3529

Hewitt CD, Mitchell JFB (1998) A fully coupled GCM simulation of the climate of the Mid-Holocene. Geophys Res Lett 25(3):361–364

Hoelzmann P, Jolly D, Harrison SP, Laarif F, Bonnefille R, Pachur HJ (1998) Mid-Holocene land-surface conditions in northern Africa and the Arabian Peninsula: A data set for the analysis of biogeophysical feedbacks in the climate system. Global Biogeochem Cycles 12(1):35–51

Hourdin F, Musat I, Bony S, Braconnot P, Codron F, Dufresne JL, Fairhead L, Filiberti MA, Friedlingstein P, Grandpeix JY, Krinner G, Levan P, Li ZX, Lott F (2006) The LMDZ4 general circulation model: climate performance and sensitivity to parametrized physics with emphasis on tropical convection. Clim Dyn 27(7–8):787–813

Jolly D, Prentice IC, Bonnefille R, Ballouche A, Bengo M, Brenac P, Buchet G, Burney D, Cazet JP, Cheddadi R, Edorh T, Elenga H, Elmoutaki S, Guiot J, Laarif F, Lamb H, Lezine AM, Maley J, Mbenza M, Peyron O, Reille M, Reynaud-Farrera I, Riollet G, Ritchie JC, Roche E, Scott L, Ssemmanda I, Straka H, Umer M, Van Campo E, Vilimumbalo S, Vincens A, Waller M (1998) Biome reconstruction from pollen and plant macrofossil data for Africa and the Arabian peninsula at 0 and 6000 years. J Biogeogr 25(6):1007–1027

Joussaume S, Braconnot P (1997) Sensitivity of paleoclimate simulation results to season definitions. J Geophys Res 102(D2):1943–1956

Joussaume S, Taylor KE, Braconnot P, Mitchell JFB, Kutzbach JE, Harrison SP, Prentice IC, Broccoli AJ, Abe-Ouchi A, Bartlein PJ, Bonfils C, Dong B, Guiot J, Herterich K, Hewitt CD, Jolly D, Kim JW, Kislov A, Kitoh A, Loutre MF, Masson V, McAvaney B, McFarlane N, de Noblet N, Peltier WR, Peterschmitt JY, Pollard D, Rind D, Royer JF, Schlesinger ME, Syktus J, Thompson S, Valdes P, Vettoretti G, Webb RS, Wyputta U (1999) Monsoon changes for 6000 years ago: results of 18 simulations from the Paleoclimate Modeling Intercomparison Project (PMIP). Geophys Res Lett 26(7):859–862

Kitoh A, Murakami S (2002) Tropical pacific climate at the Mid-Holocene and the last glacial maximum simulated by a coupled ocean-atmosphere general circulation model. Paleoceanography 17(3):1047

Krinner G, Viovy N, de Noblet-Ducoudre N, Ogee J, Polcher J, Friedlingstein P, Ciais P, Sitch S, Prentice IC (2005) A dynamic global vegetation model for studies of the coupled atmosphere-biosphere system. Glob Biogeochem Cycles 19(1):GB1015

Kripalani RH, Oh JH, Kulkarni A, Sabade SS, Chaudhari HS (2007) South Asian summer monsoon precipitation variability: coupled climate model simulations and projections under IPCC AR4. Theor Appl Climatol 90(3–4):133–159

Kutzbach JE, Gallimore RG (1988) Sensitivity of a coupled atmosphere mixed layer ocean model to changes in orbital forcing at 9000 years BP. J Geophys Res 93(D1):803–821

Kutzbach JE, Liu Z (1997) Response of the African monsoon to orbital forcing and ocean feedbacks in the middle Holocene. Science 278(5337):440–443

Leloup JA, Lachkar Z, Boulanger JP, Thiria S (2007) Detecting decadal changes in ENSO using neural networks. Clim Dyn 28(2–3):147–162

Levitus S (1982) Climatological Atlas of the World Ocean. Professional paper, NOAA/GFDL

Lezine AM, Tiercelin JJ, Robert C, Saliege JF, Cleuziou S, Inizan ML, Braemer F (2007) Centennial to millennial-scale variability of the Indian monsoon during the early Holocene from a sediment, pollen and isotope record from the desert of Yemen. Palaeogeogr Palaeoclimatol Palaeoecol 243(3–4):235–249

Li CF, Yanai M (1996) The onset and interannual variability of the Asian summer monsoon in relation to land sea thermal contrast. J Clim 9(2):358–375

Liu XD, Yanai M (2001) Relationship between the Indian monsoon rainfall and the tropospheric temperature over the Eurasian continent. Q J R Meteor Soc 127(573):909–937

Liu XD, Liu ZY, Kutzbach JE, Clemens SC, Prell WL (2006) Hemispheric insolation forcing of the Indian Ocean and Asian monsoon: local versus remote impacts. J Clim 19(23):6195–6208

Liu Z, Otto-Bliesner B, Kutzbach J, Li L, Shields C (2003) Coupled climate simulation of the evolution of global monsoons in the Holocene. J Clim 16(15):2472–2490

Liu Z, Harrison SP, Kutzbach J, Otto-Bliesner B (2004) Global monsoons in the Mid-Holocene and oceanic feedback. Clim Dyn 22(2–3):157–182

Liu Z, Wang Y, Gallimore R, Gasse F, Johnson T, deMenocal P, Adkins J, Notaro M, Prenticer IC, Kutzbach J, Jacob R, Behling P, Wang L, Ong E (2007) Simulating the transient evolution and abrupt change of Northern Africa atmosphere-ocean-terrestrial ecosystem in the Holocene. Quatern Sci Rev 26(13–14):1818–1837

Liu ZY, Kutzbach J, Wu LX (2000) Modeling climate shift of El Nino variability in the Holocene. Geophys Res Lett 27(15):2265–2268

Madec G, Delecluse P, Imbard M, Levy C (1998) OPA version 8.1 ocean general circulation model reference manual. LODYC/IPSL, Paris, France, 11

Marti O, Braconnot P, Bellier J, Bony S, Brockmann P, Cadule P, Caubel A, Denvil JL S andDufresne, Fairhead MA L and Filiberti, Foujols MA, Fichefet T, Friedlingstein P, Goosse H, Grandpeix JY, Hourdin F, Krinner G, Lvy C, Madec G, Musat I, deNoblet N, Polcher J, Talandier C (2005) The new IPSL climate system model: IPSL-Cm4. Note du Ple de Modlisation n26: ISSN 1288–1619

Meehl GA, Covey C, Delworth T, Latif M, McAvaney B, Mitchell JFB, Stouffer RJ, Taylor KE (2007) The WCRP CMIP3 multimodel dataset—a new era in climate change research. Bull Amer Meteor Soc 88(9):1383–+

Ohgaito R, Abe-Ouchi A (2007) The role of ocean thermodynamics and dynamics in Asian summer monsoon changes during the Mid-Holocene. Clim Dyn 29(1):39–50

Otto-Bliesner BL (1999) El nino la nina and sahel precipitation during the middle holocene. Geophys Res Lett 26(1):87–90

Peyrille P, Lafore JP, Redelsperger JL (2007) An idealized two-dimensional framework to study the West African monsoon. Part I: Validation and key controlling factors. J Atmos Sci 64(8):2765–2782

Prasad S, Enzel Y (2006) Holocene paleoclimates of India. Quatern Res 66(3):442–453

Prell WL, Kutzbach JE (1987) Monsoon variability over the past 150,000 years. J Geophys Res 92(D7):8411–8425

Prentice IC, Webb T (1998) BIOME 6000: reconstructing global Mid-Holocene vegetation patterns from palaeoecological records. J Biogeogr 25(6):997–1005

Rodwell MJ, Hoskins BJ (1996) Monsoons and the dynamics of deserts. Quart J Roy Meteor Soc 122(534):1385–1404

Schneider EK, Lindzen RS (1976) Influence of stable stratification on thermally driven tropical boundary-layer. J Atmos Sci 33(7):1301–1307

Solomon S, Qin D, Manning M, Chen Z, Marquis M, Averyt KB, Tignor M, Miller HL (eds) (2007) IPCC 2007: climate change 2007: the physical basis. Contribution of Working Group I to the Fourth Assessment Report of the Intergovernmental Panel on Climate Change. Cambridge University Press, Cambridge

Srinivasan J (2006) Holocene precipitation and theories of monsoon. J Geol Soc India 68(3):527–532

Su H, Neelin JD (2005) Dynamical mechanisms for african monsoon changes during the Mid-Holocene. J Geophys Res 110(D19): D19,105

Terray L, Sevault E, Guilyardi E, Thual O (1995) The OASIS coupler user guide version 2.0.

Texier D, de Noblet N, Harrison SP, Haxeltine A, Jolly D, Joussaume S, Laarif F, Prentice IC, Tarasov P (1997) Quantifying the role of biosphere-atmosphere feedbacks in climate change: coupled model simulations for 6000 years BP and comparison with palaeodata for northern Eurasia and northern Africa. Clim Dyn 13(12):865–882

Voss R, Mikolajewicz U (2001) The climate of 6000 years bp in near-equilibrium simulations with a coupled aogcm. Geophys Res Lett 28(11):2213–2216

Wang B (ed) (2006) The Asian Monsoon. Springer/Praxis Publishing Co., Heidelberg/Chichester

Wang PX, Clemens S, Beaufort L, Braconnot P, Ganssen G, Jian ZM, Kershaw P, Sarnthein M (2005) Evolution and variability of the Asian monsoon system: state of the art and outstanding issues. Quatern Sci Rev 24(5–6):595–629

Wright H, Kutzbach J, Webb III T, Ruddiman W, Street-Perrot F, Bartlein P (eds) (1993) Global climates since the last glacial maximum. University of Minnesota Press

Wu RG, Kirtman BP (2007) Observed relationship of spring and summer East Asian rainfall with winter and spring Eurasian snow. J Clim 20(7):1285–1304

Xavier PK, Marzin C, Goswami BN (2007) An objective definition of the Indian summer monsoon season and a new perspective on the ENSO-monsoon relationship. Q J R Meteor Soc 133(624):749–764

Xie PP, Arkin PA (1997) Global precipitation: a 17-year monthly analysis based on gauge observations, satellite estimates, and numerical model outputs. Bull Am Meteorol Soc 78:2539–2558

Yanai M, Li CF (1994) Mechanism of heating and the boundary-layer over the Tibetan Plateau. Mon Weather Rev 122(2):305–323

Yanai MH, Li CF, Song ZS (1992) Seasonal heating of the Tibetan Plateau and its effects on the evolution of the Asian summer monsoon. J Meteor Soc Japan 70(1B):319–351

Zhao Y, Braconnot P, Marti O, Harrison SP, Hewitt C, Kitoh A, Liu Z, Mikolajewicz U, Otto-Bliesner B, Weber SL (2005) A multi-model analysis of the role of the ocean on the African and Indian monsoon during the Mid-Holocene. Clim Dyn 25(7–8):777–800

Zhao Y, Braconnot P, Harrison SP, Yiou P, Marti O (2007) Simulated changes in the relationship between tropical ocean temperatures and the western African monsoon during the Mid-Holocene. Clim Dyn 28(5):533–551

3.3 Impact de la variation des paramètres orbitaux sur la variabilité des systèmes de mousson

3.3.1 Changements de variabilité intrasaisonnière et de distribution des pluies

Les variations des moyennes saisonnières de précipitation ne sont qu'un aspect des changements climatiques. A l'échelle de l'Holocène, les systèmes de mousson sont influencés par des forçages externes comme les variations d'insolation, mais il ne faut pas oublier que ces changements représentent une moyenne d'évènements haute fréquence. La mousson indienne est connue pour sa forte variabilité à l'échelle de 10 à 20 jours et de 30 à 60 jours, alternant des périodes de mousson actives et calmes et résultant d'oscillations méridiennes de la ZCIT (Goswami, 2005). La mousson d'Asie du sud-est est aussi marquée par une variabilité intrasaisonnière à l'échelle de 10-30 jours et 30-60 jours (Hsu, 2005). La variabilité des précipitations sur le Sahel est dominée par les échelles de temps de 10-25 et 25-60 jours dont les fluctuations peuvent représenter jusqu'à plus de 30% de la moyenne saisonnière (Sultan et al., 2003; Maloney and Shaman, 2008). Cependant, la variabilité intrasaisonnière est mal représentée de façon systématique dans les modèles climatiques (Xavier et al., 2010), c'est pourquoi une étude détaillée des différences de variabilité intrasaisonnière dans nos simulations aurait peu de sens. Il est toutefois intéressant d'analyser les changements à l'échelle intrasaisonnière de façon à mieux comprendre les variations climatologiques préalablement discutées.

Les séries temporelles de précipitations journalières pour les moussons indienne, d'Asie du sud-est et africaine ont été réalisées pour la période JJAS sur 31 années pour chaque climat. Les transformées de Fourier de ces séries ont été calculées puis lissées de façon à obtenir des spectres plus lisibles (Fig. 3.1). Les signaux ne sont pas suffisamment distincts pour les moussons africaine et d'Asie du sud-est, cependant on observe une forte augmentation de la variabilité à toute échelle de temps à 9.5 ka pour la mousson indienne (Fig. 3.2 a). Ceci suggère que le renforcement de la mousson indienne à 9.5 ka est associée à un renforcement de la variabilité interne.

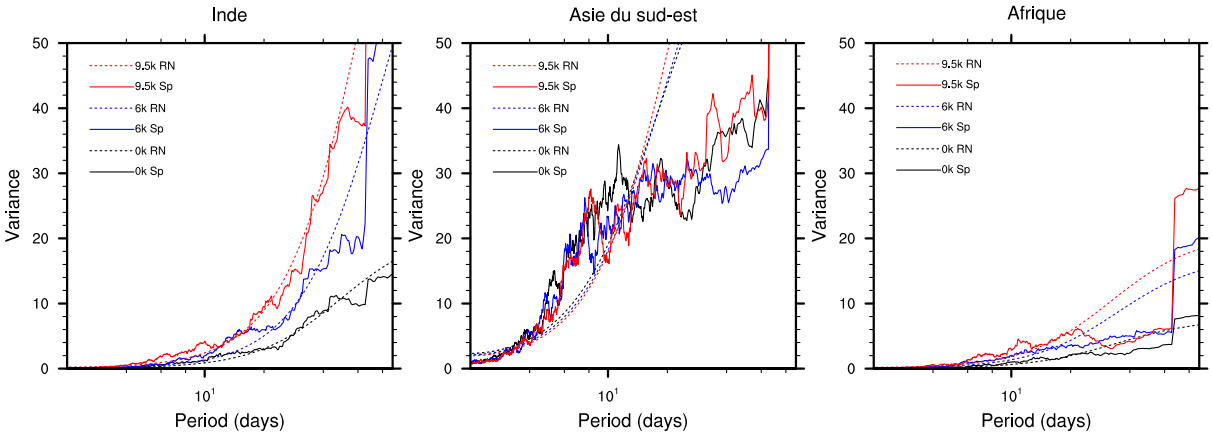

FIGURE 3.1: Transformée de Fourier de 31 ans de précipitations journalières de juin à septembre pour 0, 6 et 9.5 ka moyennées sur (a) l'Inde (70-100°E, 10-35°N), (b) l'Asie du sud-est (105-135°E, 20-45°N) et (c) le Sahel (20°O-20°E, 7-18°N). Les courbes en pointillé représentent le spectre du bruit rouge correspondant à chaque série temporelle.

Une autre approche consiste à analyser l'intensité des évènements précipitants. deNoblet et al. (1996) ont montré à l'aide de simulations atmosphériques que l'amplification des moussons à 6 ka et 126 ka est principalement due à une augmentation de la fréquence des évènements précipitants de plus de 5mm/jour et une diminution de ceux de moins de 5mm/jour. Les densités de probabilité calculées pour les précipitations journalières sur 30 ans de JJAS (Fig. 3.2) montrent que le même résultat est obtenu à 6 et 9.5 ka par rapport à l'actuel pour les trois systèmes de mousson. La distribution des pluies est décalée vers les évènements plus précipitants et diminuée pour les évènements faibles dans tous les cas. Ceci est en accord avec les résultats de Zheng and Braconnot (soumis) qui montrent que la majorité des modèles PMIP présentent une augmentation des régimes fortement convectifs à 6 ka sur le Sahel et une diminution des évènements de faible précipitation, et que ces variations sont principalement dues à l'advection de grande échelle. Ce qui est intéressant dans notre analyse, c'est que les variations de cette distribution se font de façon différente pour les trois systèmes entre les trois périodes. On observe une différence significative entre les distributions de 6 et 9.5 ka pour la mousson indienne, avec un décalage du pic de distribution ainsi qu'une occurrence plus fréquente des évènements intenses et une réduction des évènements faibles. Le profil de distribution n'est cependant pas modifié entre 6 et 9.5 ka pour la mousson africaine et seulement légèrement décalé pour l'Asie du sud-est. Ces différences relatives d'intensité des évènements entre systèmes de mousson sont similaires à celles du cycle annuel des précipitations et sont donc bien à l'origine des différences

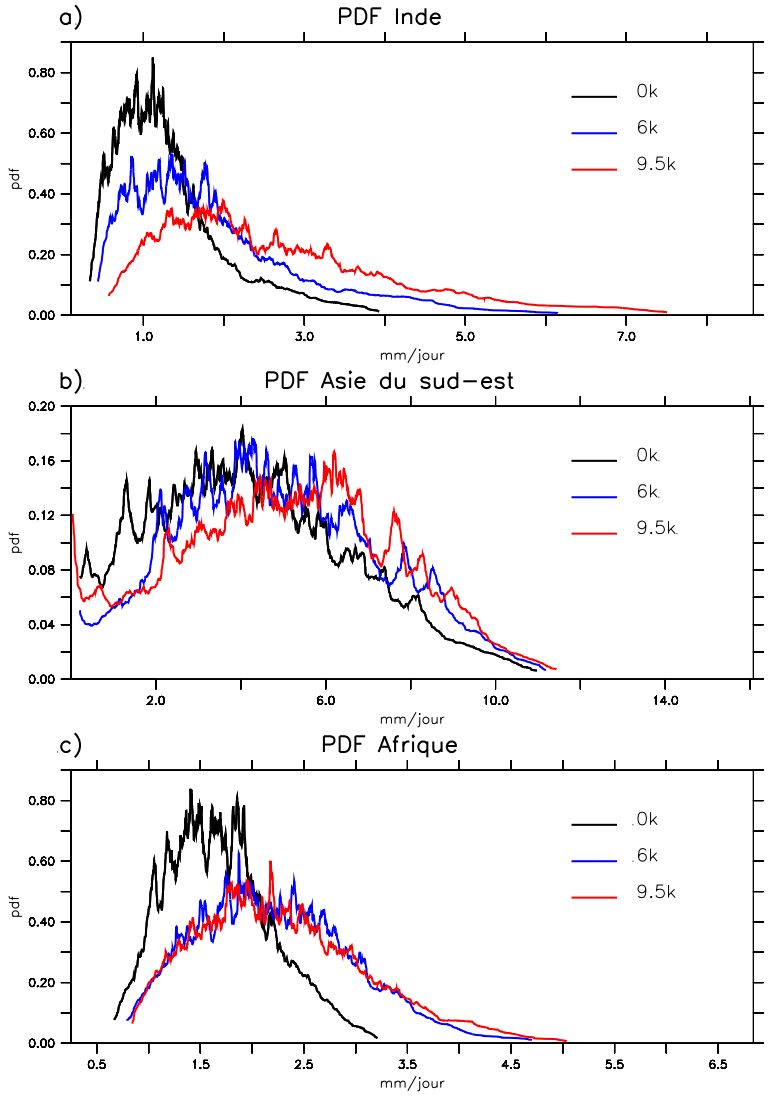

FIGURE 3.2: Densité de probabilité de 31 ans de précipitations journalières de juin à septembre pour 0, 6 et 9.5 ka moyennées sur (a) l'Inde (70-100°E, 10-35°N), (b) l'Asie du sud-est (105-135°E, 20-45°N) et (c) le Sahel (20°O-20°E, 7-18°N)

simulées d'état moyen.

3.3.2 Changements de variabilité interannuelle

De façon à compléter la vision générale des variations des caractéristiques des systèmes de mousson entre 0, 6 et 9.5 ka, nous abordons brièvement les changements de variabilité interannuelle dans nos simulations. Ces analyses seront complétées par les résultats d'une thèse en

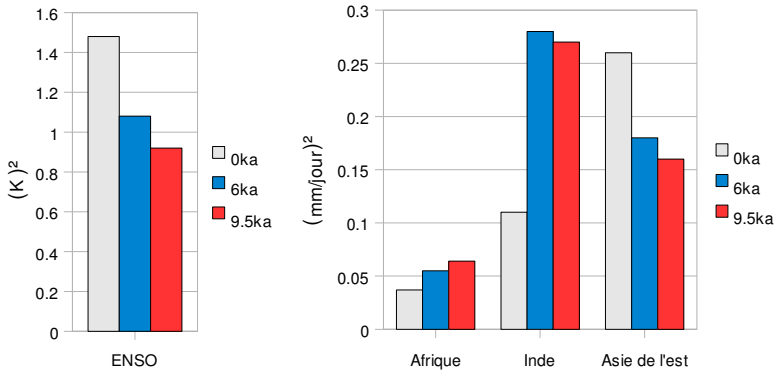

FIGURE 3.3: Variance des SSTs de la région Niño3 moyennées sur JJAS pour 0, 6 et 9.5 ka et variance des précipitations continentales pour les trois régions de mousson, le Sahel, l'Inde, et l'Asie du sud-est

cours sur les variations des caractéristiques du phénomène ENSO (El Niño Southern Oscillation) au cours de l'Holocène et dans le cadre du projet de recherche ELPASO qui vise à utiliser les enregistrements du passé ainsi que les simulations des climats passés pour mieux comprendre la variabilité d'ENSO et ses téléconnections (Braconnot et al., 2010, soumis). Dans une revue de l'importance des variations du climat tropical dans les paléoclimats, Chiang (2009) met en évidence le fait que les phénomènes climatiques présentant une forte variabilité interannuelle sont susceptibles d'être plus sensibles aux changements climatiques. L'analyse suivante tente de vérifier ce lien entre les changements de climatologie et la variabilité interannuelle.

Les moussons indienne et africaine sont connues pour leurs variations extrêmes d'une année à l'autre qui peuvent avoir des impacts socio-économiques dramatiques. La variabilité interannuelle de ces moussons est étroitement liée au principal mode de variabilité dans les tropiques, ENSO, ainsi qu'aux conditions de surfaces océaniques locales. La figure 3.3 présente la variance des précipitations des trois systèmes de mousson calculée sur 100 ans de simulation pour les trois périodes, 0, 6 et 9.5 ka. Il est à nouveau notable que les trois systèmes de mousson ont des réponses différentes au forçage orbital en terme de variabilité interannuelle. La variance des précipitations au Sahel est très faible et varie peu pour 0, 6 et 9.5 ka. La variance de la mousson indienne augmente d'environ 0.2 entre 0 et 6 ka et est à un niveau similaire à 9.5 ka. La variance de la mousson d'Asie du sud-est diminue entre 0, 6 et 9.5 ka.

Zhao et al. (2005) montre que la variabilité des pluies au nord du Sahel est augmentée à 6 ka

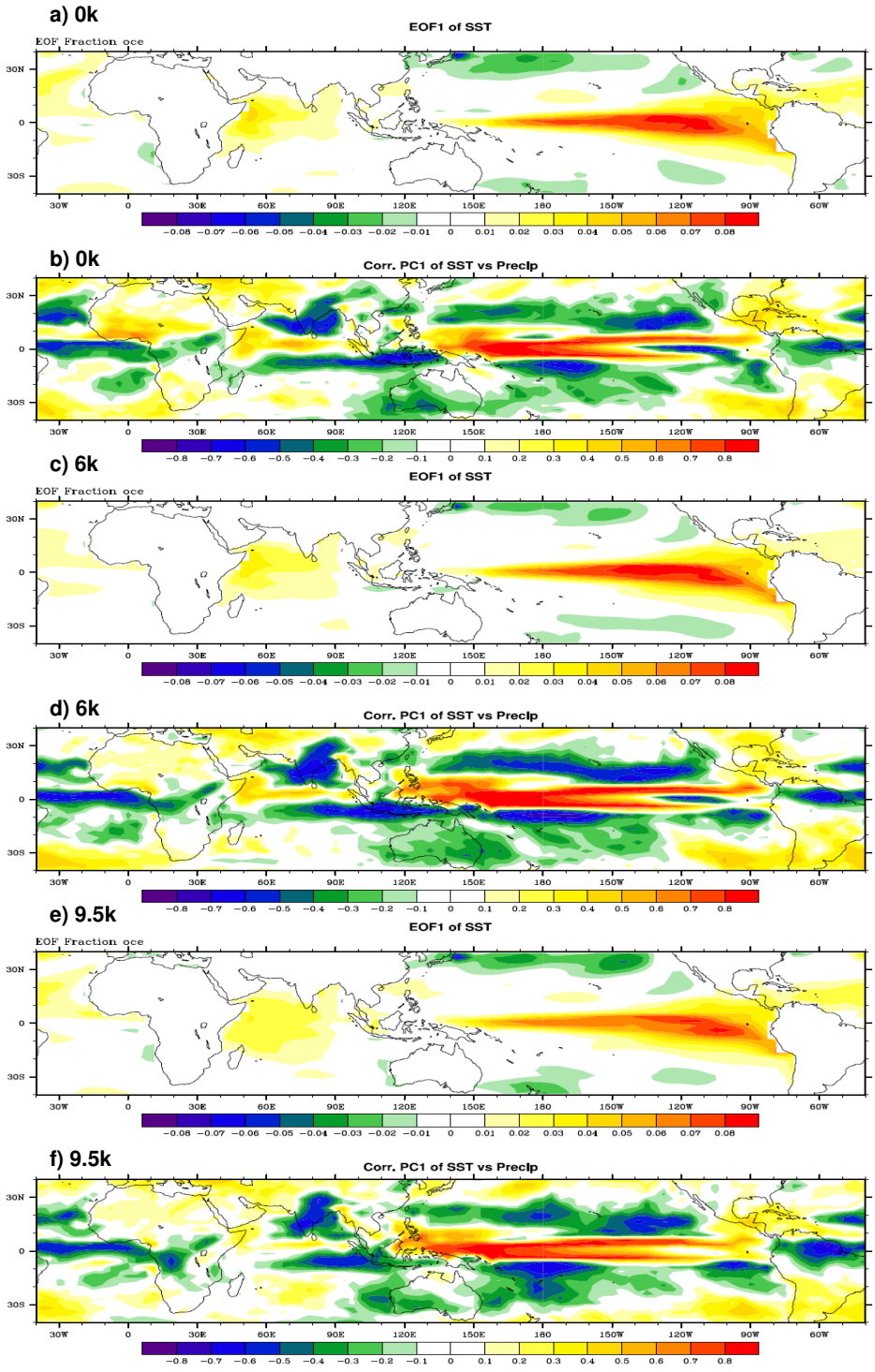

FIGURE 3.4: Premier mode de variabilité (EOF1) des SSTs pour (a) 0k, (c) 6k, (e) 9.5k. Corrélation entre la première composante principale de ce mode et les précipitations pour (b) 0k, (d) 6k, (f) 9.5k.

tandis qu'elle est diminuée au sud, en lien avec le déplacement de la ZCIT vers le nord. Cette étude montre aussi que la variabilité sur le Sahel est d'autant plus corrélée au dipôle de SST

dans l'Atlantique tropical à l'Holocène moyen qu'à l'actuel. Zhao et al. (2005) montre aussi que la variabilité du dipôle de l'Océan Indien est diminuée à 6 ka, mais que l'impact sur les précipitations de mousson n'est pas significatif. Nous proposons ici d'étudier le lien entre la variabilité des systèmes de mousson et celle d'ENSO.

Pour ce faire, une analyse en composantes principales a été effectuée pour les SST dans les tropiques. La figure 3.4 présente le premier mode de variabilité (EOF 1) pour chaque climat. Le phénomène ENSO est représenté de façon relativement correcte dans le modèle de l'IPSL-CM4 (Marti et al., 2010; Guilyardi, 2006), cependant la fréquence des évènements est trop régulière autour de la période de 2 ans et la structure de variance des SST est trop confinée à l'Equateur et étendue vers l'ouest, ceci est visible sur la Fig. 3.4a. L'amplitude de ce premier mode de variabilité est diminuée à 6 et à 9.5 ka. Ceci se retrouve aussi dans la diminution de la variance des SST moyennées sur la zone Niño3 (Fig. 3.3). Cet affaiblissement de la variabilité d'ENSO est en accord avec différents types de paléoenregistrements (Cole, 2001; Koutavas et al., 2006; Brown et al., 2008). La comparaison multi-modèles des changements d'ENSO à l'Holocène Moyen effectuée par Zheng et al. (2008) dans le cadre de PMIP2 montre que les modèles représentent de façon systématique un affaiblissement d'ENSO à 6 ka. Ceci est principalement dû à l'amplification du système de mousson asiatique qui perturbe la circulation de Walker sur le Pacifique et induit des anomalies de vents d'est et des anomalies d'upwelling dans le Pacifique central et ouest qui atténuent le développement d'évènements El Niño. Ce mécanisme semble se vérifier aussi à 9.5 ka, où la mousson indienne est d'autant plus amplifiée et l'amplitude de la variabilité d'ENSO diminuée par rapport à 6 ka.

De façon à analyser les changements d'interaction des systèmes de mousson avec ENSO ; la corrélation entre la première composante principale des SSTs de la zone Niño3 et les précipitations dans les tropiques est présentée pour les trois périodes climatiques dans la Fig. 3.4. Le modèle représente une forte corrélation négative entre ENSO et la mousson indienne (≥ 0.5) à l'actuel. Ceci est observé dans les observations des dernières décennies bien qu'un changement de lien entre ces deux phénomènes soit apparu dans les années 1980-1990 (Torrence and Webster, 1999; Wang, 2006). La mousson africaine est elle aussi négativement corrélée avec ENSO (Janicot et al., 2001; Rowell, 2001; Giannini et al., 2003) mais le modèle ne parvient

pas à capturer cette téléconnection correctement et présente une corrélation de signe opposé à 0 ka (Fig. 3.4 b). Ceci a été montré précédemment par Zhao et al. (2007). La corrélation des précipitations de mousson indienne avec ENSO est plus forte à 6 et 9.5 ka qu'à l'actuel, surtout sur les zones où la mousson est amplifiée (centre et nord-est de l'Inde, Fig. 3.4 d et f).

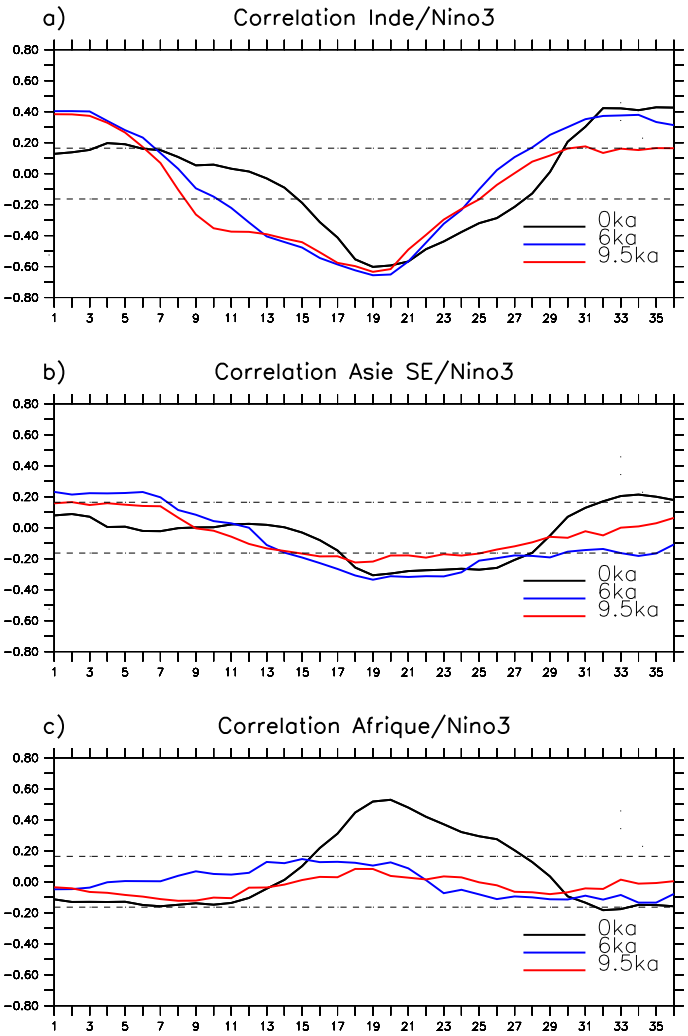

FIGURE 3.5: Corrélation glissante entre les précipitations de mousson JJAS de l'année 0 (mois 18 à 21) et les SSTs de la région Niño3 de l'année précédente (mois 1 à 12) à l'année suivante (mois 25 à 36) pour (a) l'Inde, (b) l'Asie du sud-est, (c) l'Afrique. Les traits en pointillé représentent les niveaux de significativité à 90% des corrélations.

Les analyses précédentes sont basées sur la variabilité des SST de la zone Niño3 pour la période JJAS, or la variabilité d'ENSO est maximale en hiver et la téléconnection avec les systèmes de mousson asiatique varie en fonction de la saison (chapitre 6, Wang (2006)). La climatologie des corrélations glissantes entre les précipitations JJAS (année 0) des 3 systèmes

de mousson et les SST de la zone Niño3 est calculée entre janvier de l'année -1 et décembre de l'année +1 (Fig. 3.5). A l'actuel, la corrélation avec la mousson indienne est maximale en été de l'année 0. A 6 et 9.5 ka, cette corrélation est amplifiée et étendue à l'hiver et au printemps de la même année. Les corrélations ne sont pas significatives pour l'Asie du sud-est, sauf en été où la faible corrélation négative est atténuée à 9.5 ka. Pour la mousson africaine, la corrélation est maximale et du mauvais signe en été comme il a été montré auparavant, et celle-ci devient nulle à toute période de l'année à 6 et 9.5 ka. Ceci est en accord avec l'étude de Zhao et al. (2007) qui montre l'affaiblissement de la téléconnection entre ENSO et la mousson africaine dans la plupart des modèles PMIP2.

En conclusion, ces analyses montrent qu'en plus de modifications du cycle saisonnier des systèmes de mousson, les changements d'insolation ont aussi un impact sur la distribution des régimes de pluie et sur les caractéristiques des variabilités intrasaisonnière et interannuelle. La distribution des régimes de pluie indique les mêmes changements relatifs entre les différents systèmes de mousson que ceux pour le cycle saisonnier, la mousson indienne étant plus impactée entre 6 et 9.5 ka que la mousson africaine. Les analyses de changements de variabilité interannuelle montrent que les sous-systèmes répondent de façon diverses alors que l'amplitude du phénomène ENSO est largement diminuée au début et au milieu de l'Holocène. Le fait que l'amplitude et le phasage de téléconnections telle que celle entre ENSO et la mousson indienne puissent avoir été modifiés dans le passé doit être considéré lors de l'interprétation des enregistrements paléoclimatiques, et ceci peut aider à mieux comprendre les variations observées à l'actuel à l'échelle décennale.

3.4 Comparaison modèle/données dans l'Océan Indien à l'Holocène

3.4.1 Motivations et proxies de paléoreconstruction de la mousson

Une comparaison modèle/données a été réalisée en collaboration avec Elise Mathien-Blard et Franck Bassinot dans le but de mieux comprendre les changements d'hydrologie de surface et

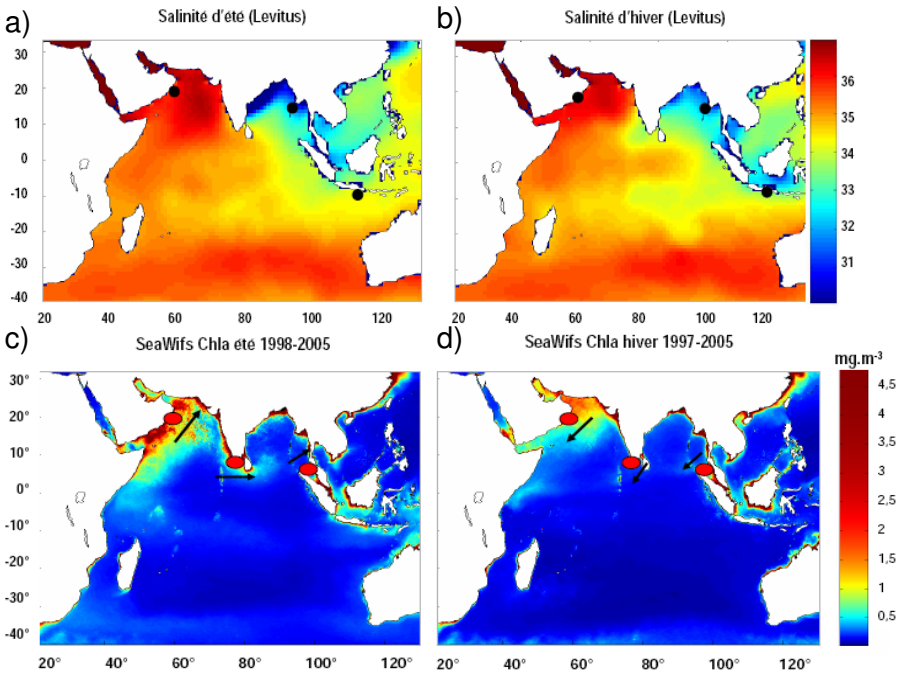

FIGURE 3.6: Distribution d'été et d'hiver de la salinité d'après les données Levitus 1998 (Levitus, 1998) (a et b) et de la chlorophylle d'après les données satellites de SeaWiFs (c et d) dans l'Océan Indien. Les climatologies sont calculées sur la période 2002-2005 pour la salinité et 1998-2005 pour la chlorophylle.

de circulation atmosphérique de l'Océan Indien au cours de l'Holocène. Le travail concernant les paléoreconstructions a été réalisé par Elise Mathien-Blard et Franck Bassinot, une partie des résultats ainsi que les Fig. 3.6, Fig. 3.7 a, c et Fig. 3.9 a, c sont extraits de la thèse d'Elise intitulée "Révision du paléothermomètre Mg/Ca et son application sur l'hydrologie de surface de l'Océan Indien Tropical au cours de l'Holocène". J'ai analysé les simulations couplées du modèle IPSL-CM4 à 0, 6 et 9.5 ka discutées auparavant pour cette comparaison.

Le système de mousson indienne induit d'importants gradients Est/Ouest et Nord/Sud de salinité dans l'Océan Indien. La Mer d'Arabie est caractérisée par des salinités élevées (de l'ordre de 36 psu) tandis que la Baie du Bengale est caractérisée par des salinités faibles (de l'ordre de 33 psu, Fig. 3.6 a et b), due aux fortes précipitations de mousson en été et aux apports fluviaux des fleuves se déversant dans la Baie du Bengale. L'Océan Indien est aussi l'une des régions qui a la plus importante productivité biologique. Ces gradients de salinité peuvent être reconstruits à partir de carottes sédimentaires en calculant la composition isotopique de l'oxygène de l'eau de mer ($\delta^{18}O$sw) à partir de la composition isotopique de l'oxygène de la calcite des

foraminifères (G. ruber) et de la température obtenue d'après le rapport Mg/Ca des tests de foraminifères (à l'aide de la procédure de correction du thermomètre Mg/Ca développée par Elise Mathien-Blard et Franck Bassinot (Mathien-Blard and Bassinot, 2009)). G. ruber est une espèce de foraminifère planctonique présente tout au long de l'année avec une représentation plus importante pendant la mousson d'été. Les mesures de $\delta^{18}O$sw de 3 sites de carottes sédimentaires ont été utilisées pour analyser les gradients hydrographiques de l'Océan Indien : un enregistrement provenant de la Mer d'Arabie, un de la Baie du Bengale, et un autre de l'archipel d'Indonésie, à la sortie de la Mer de Timor (Fig. 3.6 a et b). Les résultats sont discutés dans la partie 3.4.2.

Une deuxième partie de cette comparaison a concerné la variation des vents saisonniers de l'Océan Indien qui peut être reconstruite à partir de proxies d'upwellings côtiers de mousson. Deux sites représentatifs d'upwelling de mousson d'été ont été sélectionnés : la marge d'Oman (carotte sédimentaire ODP117-723A) et la pointe sud de l'Inde (carotte sédimentaire MD77-191). La figure 3.6 c montre la forte concentration en chlorophylle le long de la marge d'Oman. Cette productivité est associée au pompage d'Eckman dû aux vents de sud-ouest qui engendre l'upwelling côtier et les remontées d'eau enrichie en sels nutritifs rendant ces eaux très fertiles. L'upwelling de la côte sud-ouest de l'Inde est aussi maximum en été (Fig. 3.6 c), et résulte d'une interaction complexe entre ces trois mécanismes : le pompage d'Eckman dû aux vents d'ouest, l'advection latérale d'eaux nutritives sur la côte ouest et l'approfondissement locale de la couche de mélange à cette saison. La productivité maximale à la pointe sud de l'Inde est associée principalement au développement de l'upwelling en été (Levy et al., 2007). Un des proxies les plus utilisés pour retracer l'intensité de la mousson est l'abondance de G. bulloides. Une forte abondance de G. bulloides est l'indicateur de l'activité intense de ce processus d'advection. Les proxies représentatifs d'upwellings qui ont été mesurés par Elise Mathien-Blard pour cette étude sont le pourcentage de G. bulloides, le flux de G. bulloides et le rapport G. bulloides/G. ruber.

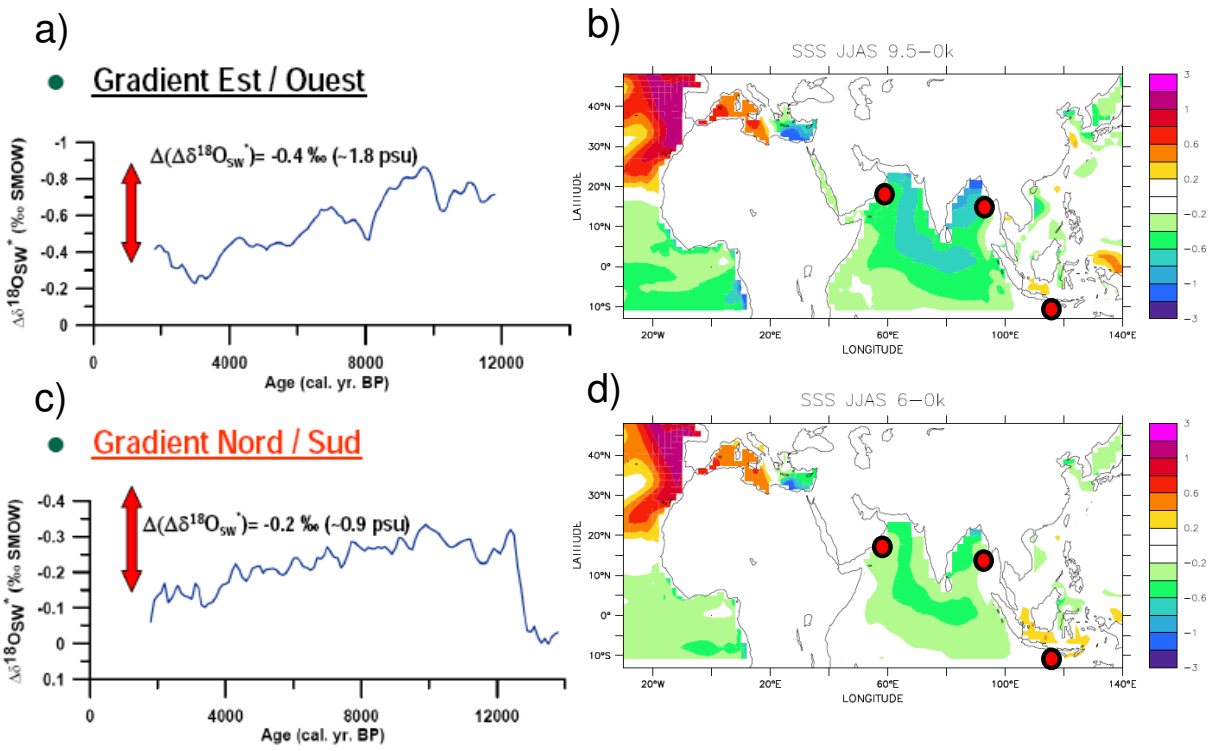

FIGURE 3.7: (a) Différences de $\delta^{18}Osw$ entre le site en Mer d'Arabie et le site en Mer d'Andaman, à l'est de la Baie du Bengale, en fonction du temps, (c) différences de salinité entre le site en Mer d'Andaman et le site de l'archipel indonésien. Différences de salinité moyennée sur JJAS dans les simulations couplées entre (b) 9.5 et 0k et (d) 6 et 0k.

3.4.2 Evolution des gradients hydrographiques

Les carottes sédimentaires situées en Mer d'Arabie (carotte sédimentaire ODP117-723A, 19°03'N, 57°37'E) et dans la Mer d'Andaman (carotte sédimentaire MD77-176, (14°31'N, 93°08'E) sont idéales pour reconstruire l'évolution du gradient de salinité est-ouest, représentatifs de l'intensité de la mousson indienne (Duplessy, 1982). L'évolution du $\delta^{18}Osw$ entre la Baie du Bengale et la Mer d'Arabie au cours de l'Holocène est représenté sur la figure 3.7 a. Ce gradient est toujours négatif, indiquant que la Baie du Bengale a toujours reçu plus d'eau douce que la Mer d'Arabie, et il décroît au cours de l'Holocène. L'enregistrement en Mer d'Arabie montre qu'elle se dessale au cours de l'Holocène tandis que la Baie du Bengale se resale (non montré). Ces enregistrements indiquent que le gradient est-ouest de salinité était maximum au début de l'Holocène, correspondant à la période de maximum d'insolation, la différence avec

le début de l'Holocène étant d'environ 1.8 psu. Ce résultat est en accord avec d'autres enregistrements marins qui montrent l'intensification de la mousson indienne d'été au début de l'Holocène (Gasse and Vancampo, 1994; Overpeck et al., 1996; Ramesh, 2001; Sarkar et al., 2000).

Le gradient nord-sud est quant à lui mesuré entre le site de la Mer d'Andaman et celui de l'archipel indonésien au nord-est de Sumatra (carotte sédimentaire BAR94-24, 9°39'S, 118°20'E). L'évolution du $\delta^{18}O$sw sur la figure 3.7 c indique aussi une diminution au cours de l'Holocène, avec un maximum de plus de 0.9 psu au début de l'Holocène. L'évolution du $\delta^{18}O$sw est opposée entre les deux sites (non montré). Ce résultat vient renforcer l'hypothèse d'amplification du système de mousson dû au forçage d'insolation au début de l'Holocène et l'hypothèse de migration vers le nord de la ZCIT suggérées à partir d'autres paléo-enregistrements (spéléothèmes de la marge d'Oman, (Fleitmann et al., 2003)).

Il est difficile de comparer exactement les résultats de chaque site aux simulations couplées du modèle IPSL-CM4 à cause de la faible résolution du modèle et des biais de représentation de ruissellement présents dans le modèle. Cependant, la comparaison avec les changements de ces gradients de salinité à grande échelle entre nos périodes simulées est très utile (Fig. 3.7). Les gradients est-ouest et nord-sud sont bien amplifiés, principalement dû aux apports d'eau douce plus importants dans la Baie du Bengale (Fig. 3.7 b et d). En effet, les précipitations de mousson sont principalement augmentées sur le continent indien, avec un maximum au nord-est de l'Inde (Fig. 3.8). Les données sont ainsi en accord avec l'extension vers le nord et l'intensification du système de mousson décrit dans la partie 3.2. Cependant, le modèle présente un variation de salinité inverse aux données dans la Mer d'Arabie. L'amplitude de variation de ces gradients entre le début et la fin de l'Holocène est moindre dans les simulations par rapport à ce que suggèrent les données (environ -0.3 psu par rapport à -1.8 psu pour le gradient est-ouest, et 0.7 psu par rapport à 0.9 psu pour le gradient nord-sud). Ces différences de gradients sont moins évidentes entre 6 et 0 ka qu'entre 9.5 et 0 ka, tout comme le suggère les données.

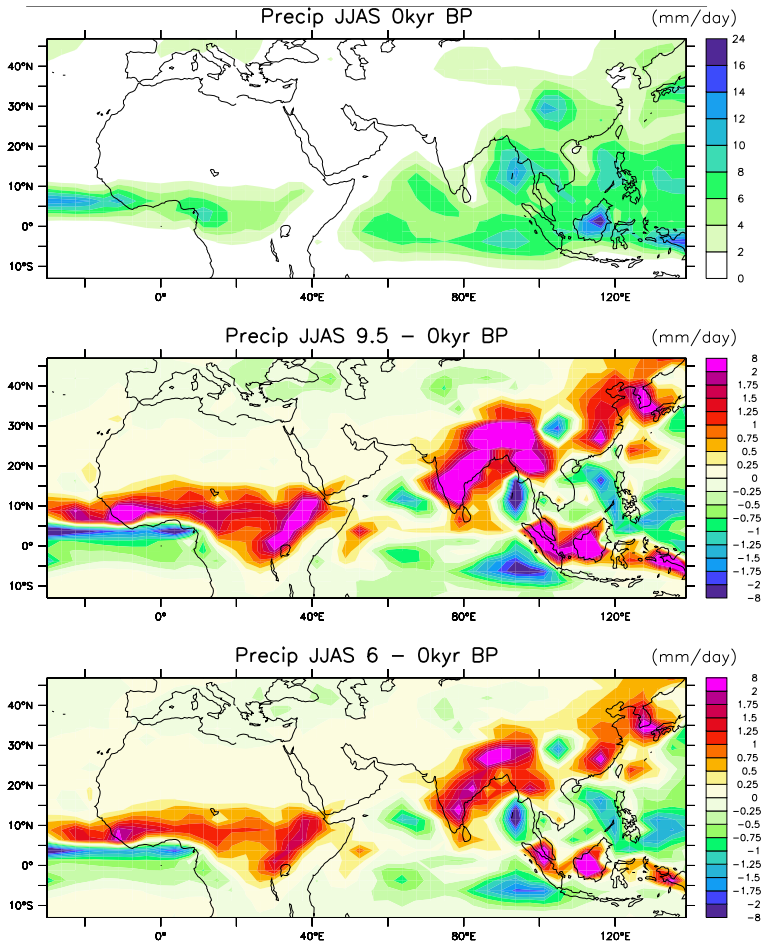

FIGURE 3.8: Précipitations moyennées sur JJAS pour (a) 0k, (b) différence entre 9.5 et 0k, (c) différence entre 6 et 0k.

3.4.3 Evolution des vents de mousson/upwellings

Les variations des proxies d'upwelling pour la marge d'Oman et la pointe sud de l'Inde au cours de l'Holocène sont indiqués sur la figure 3.9 a et c. La productivité le long de l'Arabie est diminuée au cours de l'Holocène, avec un maximum vers 7 et 9 ka, indiquant une intensification de l'upwelling côtier et une intensification des vents de mousson du sud-ouest au début de l'Holocène. Ces résultats sont en accord avec d'autres enregistrements d'upwelling de la Mer d'Arabie (Ivanochko et al., 2005), et avec l'hypothèse que la circulation de surface de la mousson indienne était amplifiée au début de l'Holocène en réponse à la plus forte insolation d'été.

De façon plus inattendue, la productivité à la pointe sud de l'Inde augmente graduellement au cours de l'Holocène suggérant un affaiblissement de l'upwelling au début de l'Holocène

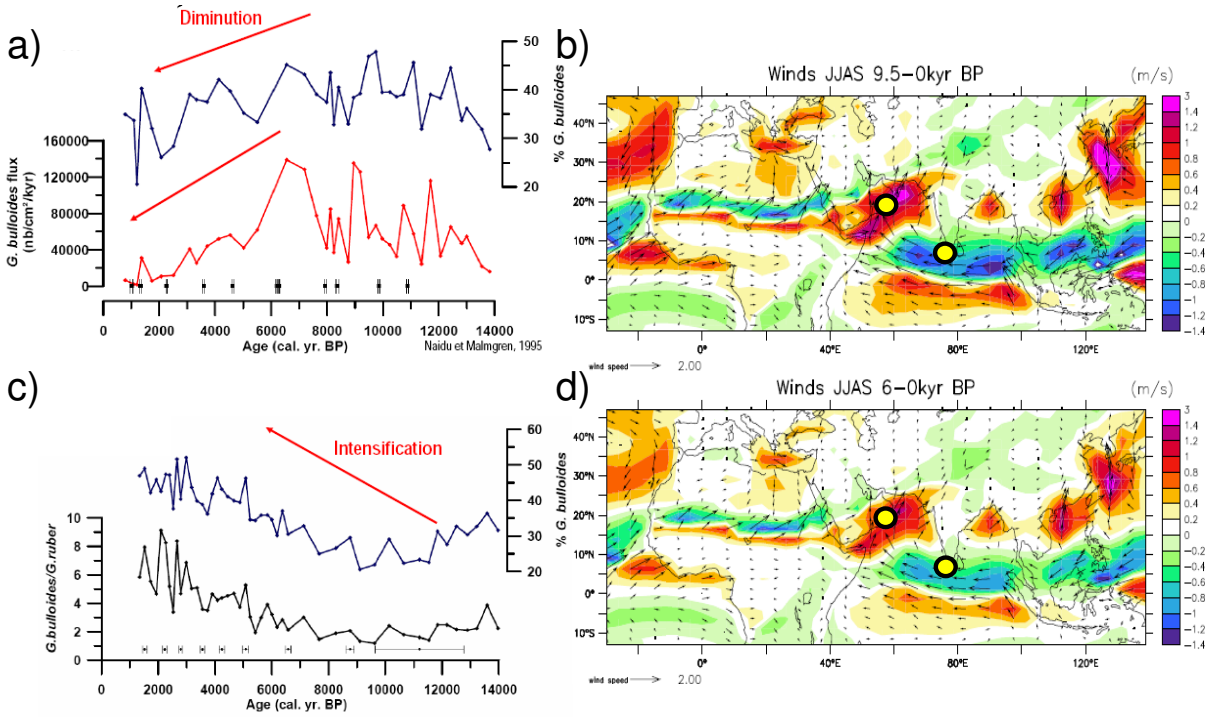

FIGURE 3.9: Flux et pourcentage de G. Bulloides en fonction du temps pour (a), le site en Mer d'Arabie, (c) le site de la pointe sud de l'Inde. Différences de circulation à 10 mètres dans les simulations couplées entre (b) 9.5 et 0k, (d) 6 et 0k.

(Fig. 3.9 c). En faisant l'hypothèse que la productivité est toujours contrôlée par la circulation d'été, ceci suggère que les vents d'ouest étaient plus faibles sur cette région. Un mécanisme permettant d'interpréter l'évolution inverse de ces deux upwellings au cours de l'Holocène serait une migration importante du flux de mousson et de la ZCIT vers le nord au début de l'Holocène par rapport à l'Holocène récent. Les simulations couplées permettent de reproduire ces variations de circulation de surface. Les figures 3.9 b et d montrent que le flux de mousson de surface est amplifié et décalé vers le nord sur la Mer d'Arabie, engendrant une intensification des vents de sud-ouest le long de l'Arabie et une anomalie de vent d'est au sud du continent indien. Ces anomalies de vents de surface sont en accord avec l'interprétation faite des deux enregistrements d'upwelling.

La comparaison des résultats des simulations couplées de l'IPSL-CM4 avec ces enregistrements marins permet de valider l'hypothèse d'amplification du système de mousson indienne dû au forçage par l'insolation. Le fait que les variations soient plus fortes à 9.5 qu'à 6 ka dans les simulations et les données souligne l'importance de la variation de la précession entre ces deux périodes pour cet océan. Ces résultats ont été soumis à Climate of the Past (annexe A.2). Des expériences supplémentaires ont été réalisées et analysées par Laurent Bopp à l'aide du modèle de biogéochimie marine PISCES (Aumont and Bopp, 2006; Gehlen et al., 2007). Deux simulations, à 6 et 0 ka, sont forcées par les conditions aux limites provenant des simulations couplées de l'IPSL-CM4. Les résultats non présentés ici montrent une augmentation de la productivité en Mer d'Arabie et une réduction à la pointe sud de l'Inde. Bien que l'interaction entre les vents de surface et la productivité soit complexe, ces expériences supplémentaires confirment le fait que les anomalies de vents du sud-ouest le long de la marge d'Oman et de vents d'ouest à la pointe sud de l'Inde expliquent bien les variations de productivité obtenues à partir des carottes sédimentaires. Les sorties du modèle d'océan sont aussi analysées pour comparer les variations de la profondeur de couche de mélange aux enregistrements.

En conclusion, la comparaison des simulations du modèle de l'IPSL-CM4 avec les enregistrements paléoclimatiques de salinité et d'upwellings de l'Océan Indien permettent de confirmer l'intensification et l'extension vers le nord du système de mousson indienne au début de l'Holocène. Les enregistrements offrent une possibilité d'évaluation du modèle, et mettent en évidence certains biais, ainsi la simulation des variations de salinité dans la Mer d'Arabie ne semble pas réaliste.

4

Téléconnection Inde-Méditerranée-Afrique

4.1 Introduction

L'interaction entre les systèmes de mousson et les moyennes latitudes est abordée dans cette partie. Ces téléconnections sont de plus en plus étudiées, leur importance ayant été démontrée à différentes échelles de temps. L'étude Marzin and Braconnot (2009b) présentée au chapitre 3 met en évidence une subsidence accrue au début de l'Holocène sur la Méditerranée. Ce phénomène rappelle le mécanisme de Rodwell et Hoskins (Rodwell and Hoskins, 1996) qui relie la convection en Inde aux conditions désertiques au nord-ouest de l'Inde et sur l'est de la Méditerranée. La question se pose quant à l'influence de cette téléconnection sur l'extension de la mousson africaine à 9.5 ka. La faible amplification de la mousson africaine entre 6 et 9.5 ka fait l'objet de plusieurs hypothèses : l'effet de la saisonnalité Marzin and Braconnot (2009b), l'effet de la réduction de l'upwelling équatorial dans l'Atlantique (Marzin and Braconnot, 2009a), qui sera abordé dans la partie suivante, et le possible impact de la subsidence

accrue sur la Méditerranée. Cette dernière hypothèse est investie plus en détail dans ce chapitre.

Le mécanisme de Rodwell et Hoskins est tout d'abord rappelé dans la partie 4.2, ainsi que l'interprétation qu'en ont fait plusieurs études basées sur des données pour expliquer les téléconnections entre le climat méditerranéen et la mousson indienne à diverses échelles de temps. Sont présentées ensuite les caractéristiques de l'intensification de la subsidence au début de l'Holocène et de la corrélation avec l'amplification de la mousson indienne dans les simulations couplées et forcées. La partie suivante pose la question de savoir si l'amplification de la mousson indienne et le changement de climat méditerranéen a un impact sur le développement de la mousson au Sahel. Cependant, l'analyse des résultats des simulations couplées ne permettent pas de déterminer s'il y a un lien de causalité entre ces phénomènes climatiques. J'ai essayé de développer un protocole expérimental pour tester la sensibilité du climat méditerranéen et du Sahel à l'amplification de la mousson indienne entre 6 et 9.5 ka. L'intention de ces tests est présentée dans la partie 4.4, mais ce travail n'a malheureusement pas pu aboutir dans le temps imparti à cette thèse. Cette partie se présente ainsi sous forme de discussion.

4.2 Le mécanisme de Rodwell et Hoskins

Rodwell and Hoskins (1996) ont réalisé des simulations à l'aide d'un modèle simple de façon à expliquer les zones de subsidence observées au sud-est de la mer d'Aral et sur l'est de la Méditerranée (Fig. 4.1 a). Une subsidence limite le développement de systèmes convectifs et pourrait donc expliquer le climat désertique de ces régions (Eshel and Farrell2004). Ces auteurs rejettent l'influence d'une cellule de Hadley locale sur ces zones désertiques, la branche descendante de la circulation de Hadley en été étant positionnée dans l'hémisphère sud. Ils proposent un mécanisme reliant la forte convection en Inde en été avec ces zones de subsidence.

Rodwell and Hoskins (1996) ont calculé les termes principaux de l'équation de la thermodynamique à partir de réanalyses et montrent que dans les régions d'ascendance tropicales, le terme de chauffage diabatique (le flux de chaleur latente dû à la convection) est entièrement contrebalancé par le refroidissement adiabatique dû à l'ascendance. Cependant, dans les zones

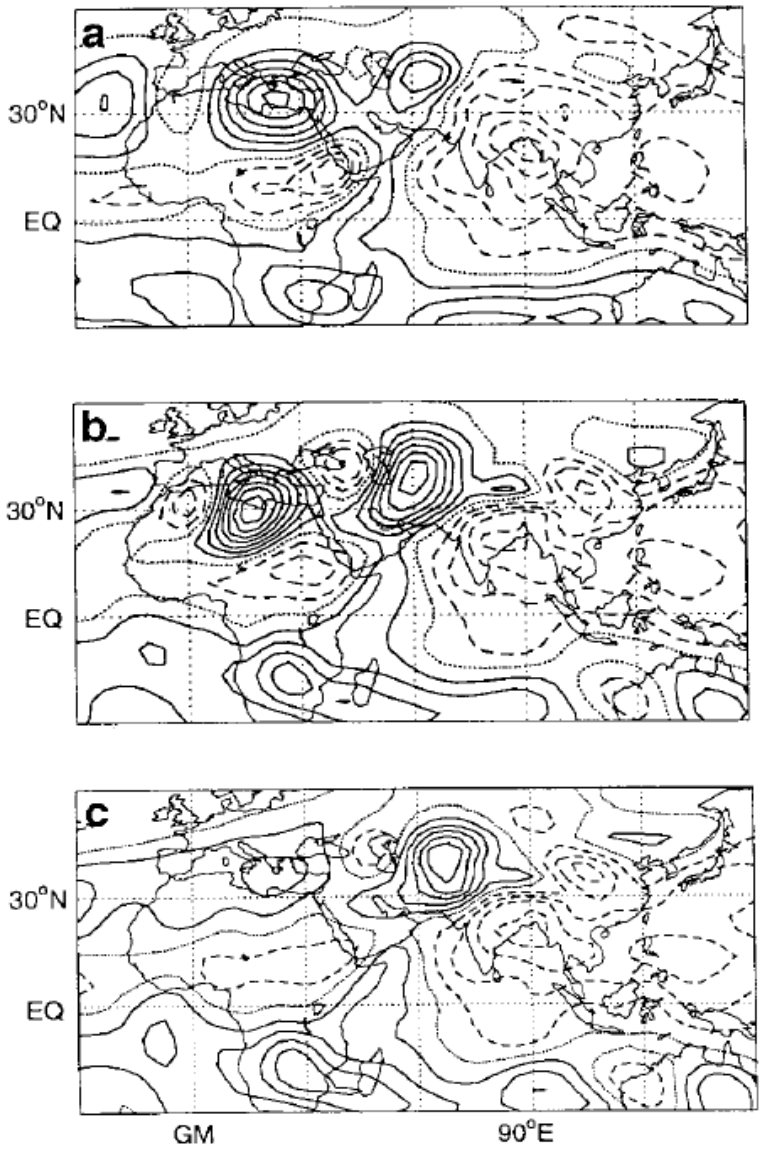

FIGURE 4.1: Figure provenant de Hoskins et al. (1999) et adaptée à l'origine de Rodwell and Hoskins (1996). Vitesse verticale à 477 hPa, ω, (a) des réanalyses ECMWF moyennée de juin à août, (b) du 16ème jour de la simulation de Rodwell and Hoskins (1996) forcée par le flux de chaleur latente, (c), pareil que (b) mais en empêchant le refroidissement adiabatique sur la région méditerranéenne/nord-africaine. Les contours sont de 0.5 hPa.

de subsidence subtropicales, le chauffage adiabatique est contrebalancé par le refroidissement radiatif et surtout par le terme d'advection horizontale de la température, celui-ci étant essentiel à la localisation des zones désertiques.

Suivant les premières expériences de mousson idéalisées de Gill (1980) qui présentaient

une zone de subsidence à l'ouest par propagation d'ondes de Rossby, Rodwell and Hoskins (1996) ont imposé un chauffage diabatique représentatif de l'important flux de chaleur latente produit sur la zone de la mousson asiatique à l'aide de leur modèle simple. Ce seul forçage permet d'obtenir une représentation fidèle des zones de subsidence sur le sud-est de la mer d'Aral et l'est de la Méditerranée (Fig. 4.1 b). Une série d'expériences sans orographie utilisant un processus de linéarisation (Hoskins and Rodwell, 1995) et imposant un chauffage diabatique centré sur l'Inde autour de 25°N montre que la mousson asiatique engendre une subsidence à l'ouest associée à une structure dite de Rossby "pure". Les expériences non-linéaires montrent que la structure thermale engendrée par le mode de Rossby interagit avec la partie sud du jet d'ouest, ce qui renforce la subsidence. Cependant, la localisation exacte des zones de subsidence n'est obtenue qu'en incluant l'orographie dans ces simulations, le rôle de l'Atlas étant particulièrement déterminant. Rodwell and Hoskins (1996, 2001) ont aussi démontré que la subsidence adiabatique engendrée par la propagation d'onde de Rossby seule est renforcée par un refroidissement radiatif local, comme le démontre l'expérience présentée sur la Fig. 4.1 c (pas de refroidissement diabiatique imposé autour de la Méditerranée).

Rodwell and Hoskins (1996) discute l'importance de ce mécanisme pour expliquer l'existence de ces zones désertiques subtropicales. Cependant ceci n'explique pas la présence du Sahara ouest et du désert d'Arabie qui sont régis par d'autres mécanismes. D'autres études ont analysé cette téléconnection entre l'Inde et l'est de la Méditerranée à plusieurs échelles de temps. Ziv et al. (2004) ont mis en évidence une corrélation significative entre l'est de la Méditerranée et la mousson asiatique à l'échelle synoptique. Raicich et al. (2003) a étudié la relation entre les moussons indienne et africaine et montre que leurs variations à l'échelle interannuelle sont corrélées avec les distributions de pression de surface autour de l'est de la Méditerranée. Janicot et al. (2009) suggère qu'un lien entre la mousson indienne et le Sahel serait aussi important à l'échelle intrasaisonnière. Par ailleurs, Chatfield et al. (2004) ont mis en évidence l'apport de la pollution en ozone troposphérique de l'Inde sur le continent africain par l'anticyclone d'altitude de la mousson asiatique. De manière encore plus intéressante pour notre étude, l'évolution concomitante des zones désertiques de l'est de la Méditerranée et de l'intensité de la mousson asiatique a été établie à l'échelle paléoclimatologique. Des indicateurs de niveaux des lacs sur l'est du Sahara synthétisés par Lezine and Casanova (1991) suggèrent que

des évènements humides retracés sur les derniers 140000 ans sont corrélés avec les périodes de minimum d'insolation de l'hémisphère nord, qui correspondent à des périodes de faible intensité de mousson asiatique.

Webster et al. (1998) évoque aussi cette relation entre l'est de la Méditerranée et la mousson indienne, la qualifiant de "mousson transverse". Cette étude représente la divergence des vents associée à la mousson en trois circulations : la mousson latérale, de l'Asie à l'Océan Indien sud, la mousson transverse, de l'Asie à l'est de la Méditerranée, et la mousson de Walker, de l'Asie au Pacifique est. Selon les auteurs, les forts gradients de flux de chaleur latente et de forçage radiatif maintiennent ces circulations (la mousson transverse représentant les plus forts gradients). Chou and Neelin (2003) ont généralisé le concept développé par Rodwell et Hoskins pour tenir compte de l'interaction entre la zone convective et la zone de subsidence. Ce mécanisme de Rodwell et Hoskins interactif est un des mécanismes qu'ils ont considéré pour étudier les facteurs limitant l'extension vers le nord des systèmes de mousson. Wu et al. (2009) a aussi complété la compréhension de la formation et de l'interaction entre les zones humides à l'est des continents et les zones arides à l'ouest de continents, en invoquant l'effet combiné de plusieurs forçages, la distribution des océans et des continents, l'effet de brise de mer locale sur les côtes, l'orographie locale et la rétroaction positive entre le forçage diabatique et la génération de vorticité dans les basses couches.

4.3 Résultats des simulations couplées à l'Holocène

4.3.1 Téléconnection Inde-Méditerranée

L'analyse des simulations couplées à 0, 6 et 9.5 ka permet de mettre en évidence ce lien entre la convection sur l'Inde et la subsidence autour de la Méditerranée. De plus, j'ai vérifié que ce lien persiste dans les simulations atmosphériques forcées par les SST du modèle couplé de référence (0fk, 6fk, 9.5fk, le détail de ces simulations est décrit dans la partie 5.2), pour illustrer le caractère atmosphérique de cette téléconnection. Les différences de climatologie de l'OLR et de la vitesse verticale à 500 hPa entre 9.5 et 0 ka et 9.5 et 6 ka sont présentées dans la

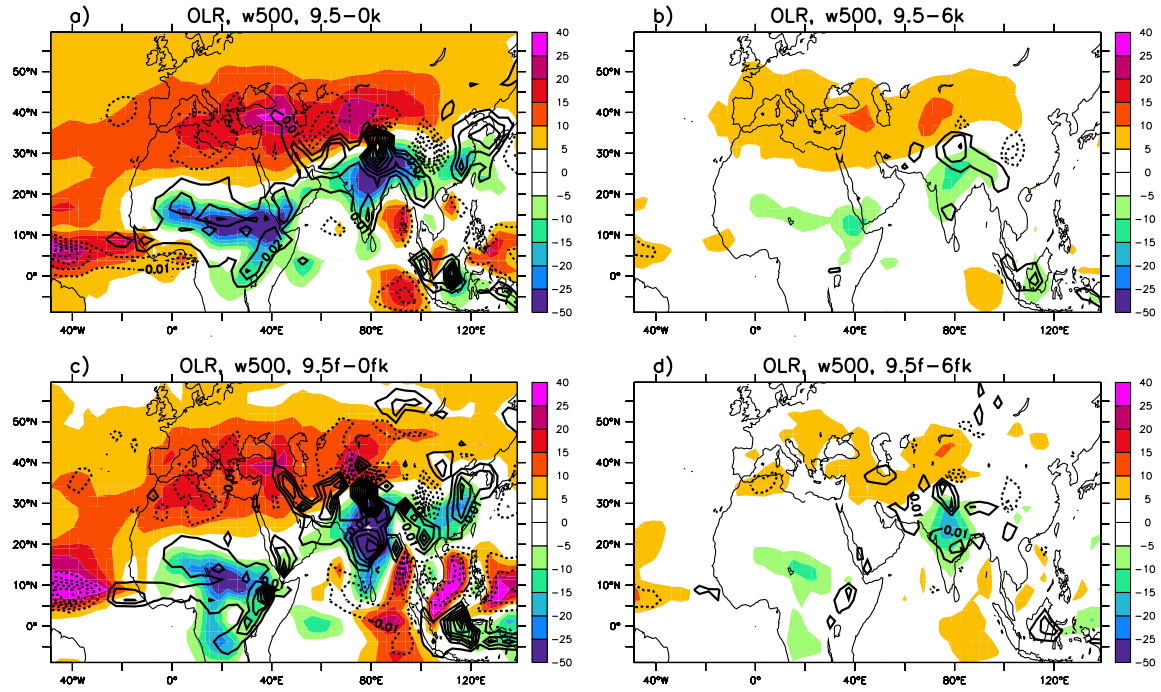

FIGURE 4.2: Différences JJAS d'OLR ($W.m^{-2}$, couleurs) et de vitesse verticale à 500 hPa ($m.s^{-1}$, contours) dans les simulations couplées entre (a) 9.5 et 0 ka et (b) 9.5 et 6 ka, et dans les simulations forcées entre (c) 9.5 et 0 ka et (d) 9.5 et 6 ka.

figure 4.2 pour les simulations couplées et forcées. Il faut tout d'abord rappeler que le modèle de l'IPSL-CM4 représente le positionnement et l'intensité des zones de subsidence au nord-est de l'Inde et sur l'est de la Méditerranée (Fig. 2.3) dans la simulation de référence, bien que trop intenses. Ces zones de subsidence sont renforcées à 6 et 9.5 ka, d'autant plus à 9.5 ka dans les deux types de simulation, de même que la couverture nuageuse et l'ascendance au dessus de l'Inde sont amplifiées. Marzin and Braconnot (2009b) ont montré dans les simulations couplées que le renforcement de cette subsidence et de la convection en Inde varient de façon proportionnelle entre les trois périodes, indiquant peut-être une téléconnection entre ces deux zones. De plus, les caractéristiques spatiales du signal de vitesse verticale à 500 hPa sont similaires aux expériences de Rodwell et Hoskins mettant en évidence l'impact de la convection en Inde sur les zones désertiques de la Méditerranée par propagation d'ondes de Rossby vers l'ouest. Le fait que ces mêmes résultats soient visibles dans les simulations "paléo" forcées par les SST actuelles rendent l'hypothèse de la téléconnection par la circulation atmosphérique seule plausible.

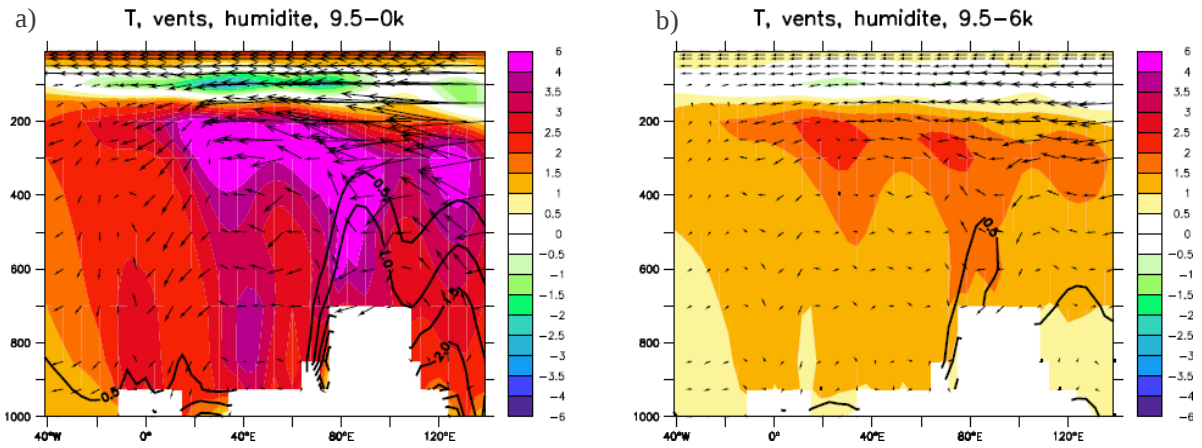

FIGURE 4.3: Différences JJAS de vent zonal et de vent vertical (multiplié par 100), de température (couleurs) et d'humidité spécifique (contours), moyennés entre 30 et 40 °N, entre (a) 9.5 et 0k et (b) 9.5 et 6k.

La figure 4.3 représente la coupe zonale des anomalies de circulation atmosphérique, de température et d'humidité spécifique de l'Inde à la Méditerranée, entre 9.5 et 0k, et entre 9.5 et 6k. Les différences de forçage par l'insolation engendre un large réchauffement de la troposhère, avec un maximum en haut de la troposphère au-dessus de l'Asie ainsi qu'un important ralentissement du jet d'ouest subtropical. Des anomalies de vents d'est dans les plus basses couches sont aussi observées entre 9.5 et 0 ka, et de façon moindre entre 9.5 et 6 ka et relient la plus forte ascendance au-dessus de l'Inde et de l'Asie de l'est au renforcement des zones de subsidences autour de 20 et 50°nord, en accord avec la notion de mousson transverse de Webster et al. (1998), et l'interprétation des réanalyses NCEP de Ziv et al. (2004).

La subsidence renforcée à l'est de la Méditerranée et à l'est de la Mer Caspienne inhibe le développement de systèmes convectifs, rendant ces zones plus arides en été en terme de précipitations (Fig. 3.8). Ceci reflète que le résultat de ces simulations est conforme à plusieurs enregistrements paléoclimatiques qui indiquent une période estivale plus aride sur ces régions au début de l'Holocène. En effet, Tzedakis (2007) et Tzedakis et al. (2009) montrent à l'aide d'enregistrements palynologiques que les conditions arides du sud de l'Europe sont associées à des périodes de déplacement maximum de la ZCIT vers le nord. D'autres indicateurs de végétation et de niveau des lacs établissent des conditions estivales très arides sur le Moyen Orient au début de l'Holocène (Zeist and Bottema, 1991; Wick et al., 2003). De plus, Goni et al. (2008)

ont analysé l'extension méridionale des forêts de l'Europe de l'ouest pendant la dernière période glaciaire, et suggèrent aussi une corrélation entre l'extension des forêts en Méditerranée et l'amplification de la mousson asiatique (pics d'émission de méthane). Djamali et al. (2010) propose que le retardement de la colonisation postglaciaire des forêts au Moyen-Orient pourrait être dû à l'influence de la mousson indienne. Il suggère que le déplacement vers le nord-est de l'influence de la mousson indienne au début de l'Holocène aurait défavorisé les précipitations de fin de printemps et de début d'été sur le Moyen-Orient, essentielles au développement de ces forêts. Le désert en Asie centrale est aussi influencé par la forte convection sur l'Inde lors de la mousson. Chen et al. (2008) ont montré que l'aridité de ce désert évolue de façon opposée à l'intensité de la mousson indienne, pendant le maximum d'humidité sur le flan du Plateau Tibétain au début de l'Holocène, le désert atteignait son maximum d'aridité.

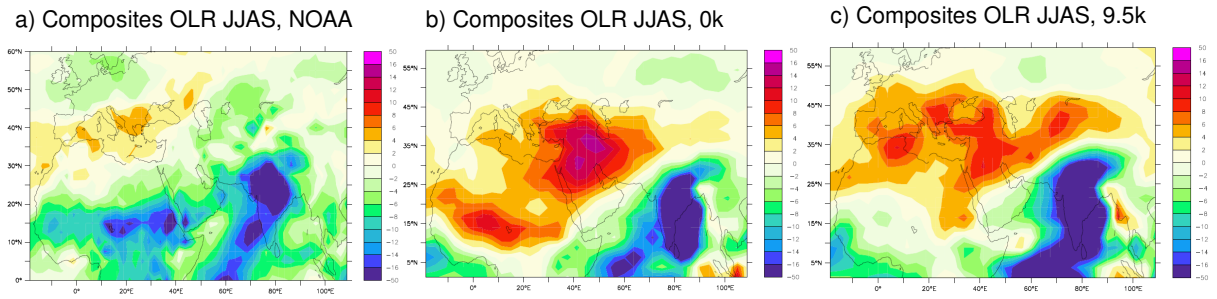

FIGURE 4.4: Différences JJAS d'OLR entre les composites des années de mousson indienne plus forte et celles de mousson indienne plus faible, pour (a) les observations NOAA (29 ans), (b) 0k (100 ans) et (c) 9.5k (100 ans).

Cependant, le renforcement du flux infrarouge sortant est aussi simplement une réponse à la plus forte insolation qui réchauffe les continents, de façon à contrebalancer ce forçage radiatif. Il est impossible dans ces simulations de découpler cet effet de l'influence de la téléconnection avec l'Inde. Une manière de mettre à part l'impact de l'insolation sur cette subsidence est de regarder la variabilité interannuelle de la mousson indienne pour vérifier si celle-ci est bien associée aux zones de subsidence, sans différence de forçage par l'insolation. J'ai ainsi calculé des composites d'années de moussons indiennes fortes et d'années de moussons faibles en me basant sur 100 ans de série temporelle d'OLR (supérieure ou inférieure à l'écart-type) pour chaque simulation couplée 0 et 9.5 ka (Fig. 4.4 b et c) et sur 29 ans de données d'OLR NOAA (Liebmann and Smith, 1996) (Fig. 4.4 a). Les composites à 0 et 9.5k confirment bien que plus

la mousson indienne est amplifiée, plus l'anomalie d'OLR est importante à l'est de la Méditerranée et de la Mer Caspienne. Cette relation est observée dans les composites des données NOAA mais d'amplitude moindre. Ces différences de composite indiquent aussi la possible téléconnection Inde/Méditerranée-Asie centrale à l'échelle interannuelle. De plus, l'amplitude des variations entre les deux climats 0, 6 et 9.5 ka est supérieure à celle de la variabilité interannuelle seule.

4.3.2 Influence sur la mousson d'Afrique de l'ouest

Ayant mis en évidence la subsidence renforcée à 9.5 ka autour de la Méditerranée et la relative faible intensité de la mousson africaine à 9.5 ka, la question se pose de savoir si l'un est influencé par l'autre. Marzin and Braconnot (2009b) montre que l'intensification entre les trois périodes est proportionnelle à l'insolation et à l'intensité de la mousson indienne, tandis que la mousson africaine n'est pas plus amplifiée à 9.5 qu'à 6 ka. L'hypothèse proposée suite à cette étude était que la forte amplification de la mousson indienne et le renforcement de la subsidence sur la Méditerranée pourrait limiter le développement de la mousson africaine à 9.5 ka et ainsi apporter un mécanisme supplémentaire pour expliquer les différences de réponse entre les sous-systèmes.

Peu d'études ont analysé les relations entre la mousson indienne et africaine et encore moins ont pu mettre en évidence un mécanisme de téléconnection robuste. Le mécanisme de Rodwell et Hoskins est souvent invoqué mais sans test de sensibilité à l'aide d'un GCM. Ziv et al. (2004) a calculé dans les réanalyses une corrélation de 0.33 entre les vitesses verticales au-dessus des deux systèmes de mousson à l'échelle inter-journalière, avec un délai de 2 jours. Ward (1998) et Raicich et al. (2003) trouvent une corrélation positive entre les précipitations JAS sur l'Inde et le Sahel à l'échelle interannuelle. La corrélation négative concomitante des deux moussons avec la circulation de surface sur l'est de la Méditerranée suggère le rôle primordial des vents étésiens (harmattans) sur le développement de la mousson au Sahel. Janicot et al. (2009) suggère une relation entre les deux systèmes de mousson à l'échelle intrasaisonnière, cette étude est appuyée par des expériences à l'aide d'un modèle simple de dynamique sèche mettant en

évidence l'influence d'une phase active de la mousson indienne sur le Sahel, avec un déphasage de deux semaines. Une corrélation est aussi mise en évidence à l'échelle interannuelle et intra-saisonnière entre les précipitations en Inde et sur l'est de l'Afrique (Camberlin, 1995, 1997). Cependant, des études plus récentes montrent que ce lien est plus complexe (Camberlin et al., 2010; Vizy and Cook, 2003).

Ce lien entre les deux systèmes de mousson n'est pas bien représenté dans la simulation de référence, comme en témoigne les composites d'OLR sur les figures 4.4 a et b. Le signe des différences d'OLR est opposé sur le Sahel entre les observations et la simulation. Nous savons déjà que la variabilité interannuelle de la mousson africaine est mal représentée dans le modèle de l'IPSL-CM4, aussi bien en terme de téléconnection avec ENSO (partie 3.3, Joly et al. (2007)) qu'entre les SSTs du Golfe de Guinée et le dipôle de précipitation entre la côte et le Sahel (Cook and Vizy, 2006). Ce biais présente un limite considérable à l'analyse de l'interaction entre les deux systèmes de mousson. Cependant, le signal sur le Sahel semble s'inverser à 9.5 ka indiquant peut-être une meilleure représentation de ce lien suite à la progression de la mousson indienne sur le continent réduisant le biais de la simulation de référence. Le projet IRCAAM (IRCAAM, compte-rendu de fin de projet, Bielli et al. (2010)), dirigé par Hervé Douville, a quantifié l'importance de la bonne représentation du climat tropical et des climats de mousson pour améliorer la variabilité extratropicale, à l'aide d'analyses d'observations et de réanalyses, mais aussi de simulations utilisant la technique de nudging. Ce projet a aussi confirmé le lien entre la mousson africaine et indienne à l'échelle intra-saisonnière via la Madden-Julian Oscillation (MJO). Cependant, un lien statistique entre les systèmes de mousson et le bassin méditerranéen à l'échelle interannuelle tel que mis en évidence par Raicich et al. (2003) n'est pas présent de façon robuste dans les simulations des modèles CMIP3, soulignant la complexité de l'analyses de ces téléconnections.

Il est difficile d'évaluer si les variations de la mousson africaine entre 0, 6 et 9.5 ka sont influencées par la subsidence sur la Méditerranée, beaucoup d'autres phénomènes entrant en jeu. D'après la bibliographie discutée ci-dessus, s'il y avait un lien, cette subsidence devrait plutôt favoriser plutôt qu'inhiber la mousson africaine, invalidant l'hypothèse suggérée dans Marzin and Braconnot (2009b). L'intensité et l'extension de la mousson africaine sont sujettes

à de nombreux facteurs qui sont résumés dans les études Hall and Peyrille (2006), et Janicot et al. (2010) et Lafore et al. (2010) suite au projet AMMA. Ainsi la climatologie de la mousson africaine peut être influencée par, entre autre, les SSTs de la Mer Méditerranée (Rowell, 2003; Fontaine et al., 2010), les SSTs du Golfe de Guinée et l'upwelling équatorial (Okumura and Xie, 2004) qui contrôlent l'advection d'humidité sur le Sahel, la dépression thermique saharienne (Lavaysse et al., 2009), l'albédo et l'humidité des sols Douville et al. (2001). Roca et al. (2005) a aussi mis en évidence le rôle d'intrusion d'air sec en altitude provenant des moyennes latitudes et favorisant les systèmes convectifs sur l'Afrique de l'ouest.

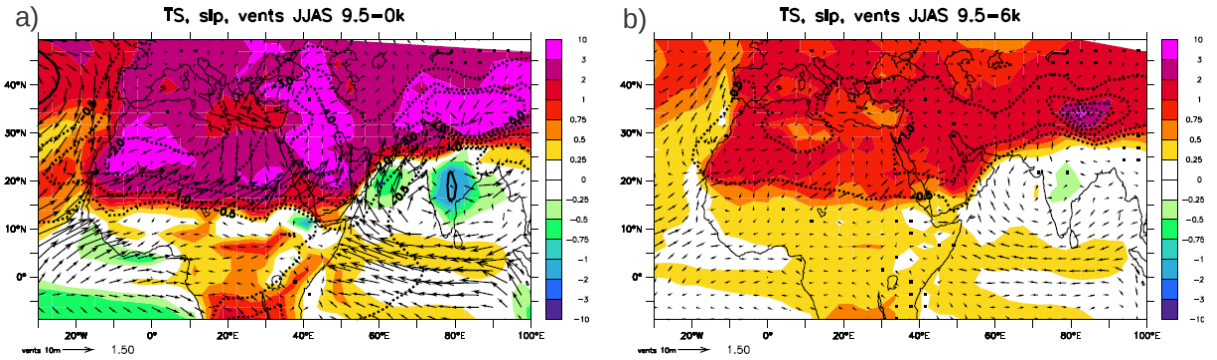

FIGURE 4.5: Différences JJAS de température (couleurs), de pression (contours, interval de 0.5 hPa) et de vents de surface (vecteurs) entre (a) 9.5 et 0 ka, (b) 9.5 et 6 ka.

De façon à déterminer le facteur limitant l'amplification de la mousson africaine, les différences de température de surface, de circulation de surface et de pression sont tracées sur la figure 4.5 entre 9.5 et 0 ka et entre 9.5 et 6 ka. A 9.5 ka, le flux de mousson et le front inter-tropical sont intensifiés ainsi que la dépression thermique sur le Sahara. Les vents étésiens sont augmentés sur l'Afrique du nord-est, intensifiant le phénomène de ventilation de la Méditerranée. Les SSTs de la Méditerranée sont plus élevées. Toutes ces caractéristiques sont aussi présentes pour les différences entre 9.5 et 6 ka, mais d'amplitude moindre. En particulier, le front inter-tropical et le flux de mousson sur la côte du Golfe de Guinée sont très faiblement amplifiés. Entre 9.5 et 6 ka, on remarque un réchauffement de l'Atlantique tropical. Ceci pourrait expliquer la faible amplification de la mousson africaine à 9.5 par rapport à 6 ka. Cette hypothèse sera analysée plus en détail dans la partie 5.2.

La figure 4.6 représente les différences de circulation atmosphérique 3D au-dessus de la partie ouest et est de l'Afrique de l'ouest. Sur la partie ouest à 9.5 ka, les vents d'ouest apportant

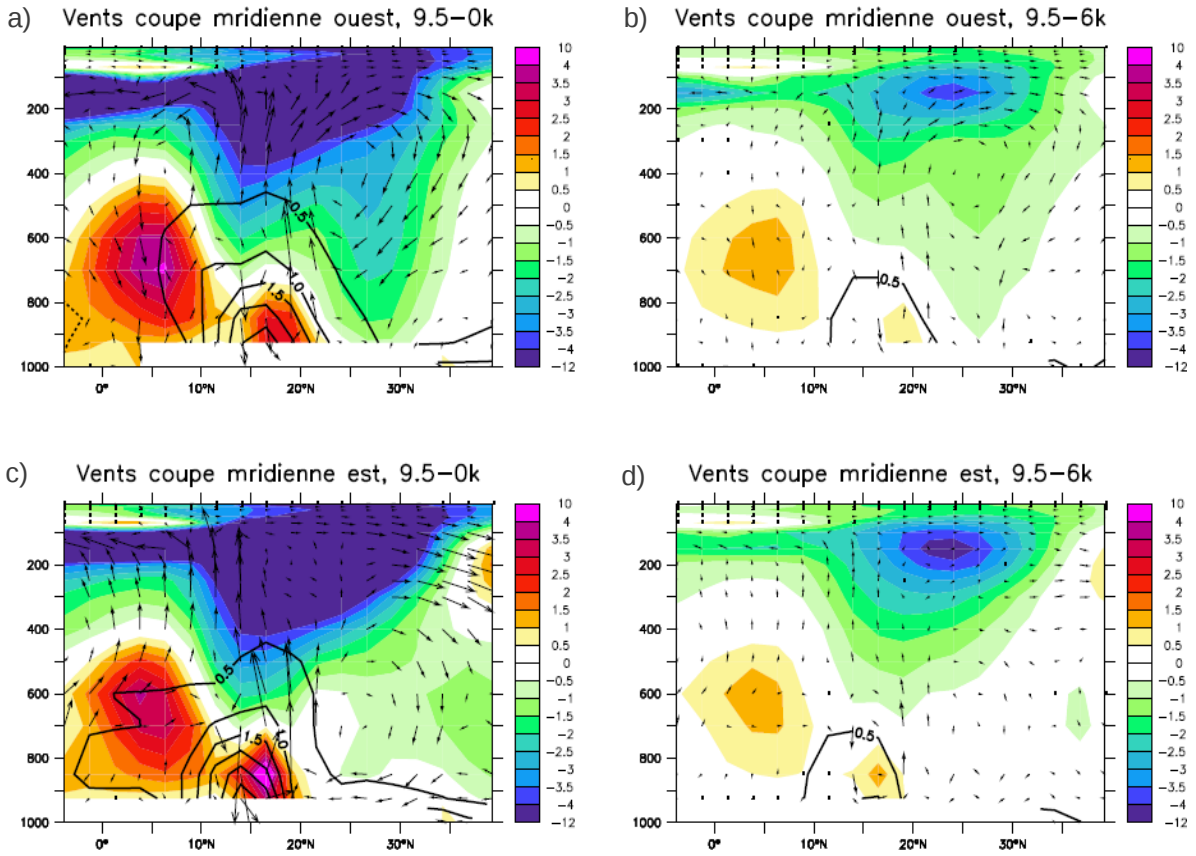

FIGURE 4.6: Différences JJAS des vents, de la composante horizontale u (couleur) et d'humidité spécifique (contours) moyenné de 10°O à 15°E entre (a) 9.5 et 0 ka et (b) 9.5 et 6 ka, puis moyenné de 15°E à 35°E entre (c) 9.5 et 0 ka et (d) 9.5 et 6 ka.

de l'humidité de l'Atlantique sont fortement renforcés, le jet d'est africain est lui diminué ainsi que le jet d'ouest suptropical tandis que le jet d'est à 200 hPa est accéléré. La plus forte subsidence entre 30 et 40°N est observée dans les deux régions. On retrouve l'intensification des harmattans sur la partie est. Entre 9.5 et 6 ka, le jet d'est africain et le flux de mousson sont par contre très faiblement modifiés. Il est difficile de conclure sur ce qui peut principalement causer les variations de la mousson africaine entre 6 et 9. ka, si ce n'est l'effet de la précession sur le cycle saisonnier de la mousson africaine (Marzin and Braconnot, 2009b). Aussi bien pour analyser ces téléconnections à l'échelle interannuelle ou paléoclimatique, la plus grande difficulté réside dans le fait que les variations des systèmes de mousson résultent de multiples forçages et interactions du système climatique. La partie suivante présente une tentative d'isoler l'impact de l'amplification de la mousson indienne à 9.5 ka sur le bassin méditerranéen et le

Sahel.

4.4 Test de cette téléconnection

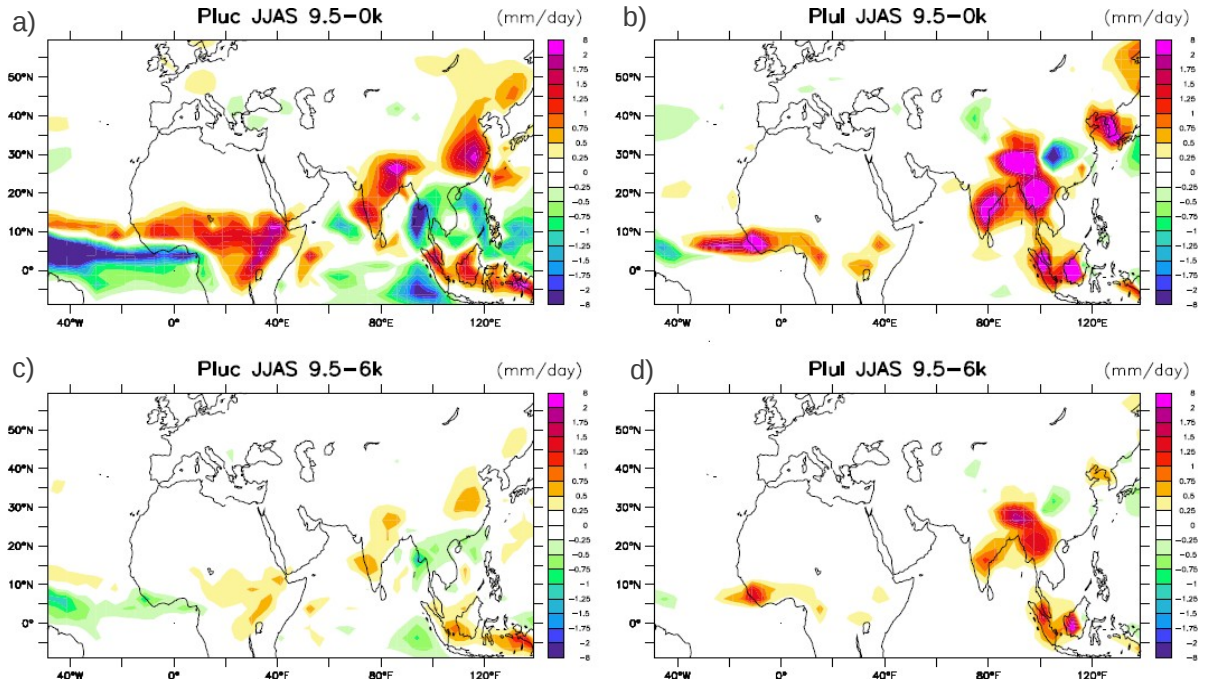

FIGURE 4.7: Différences de précipitations convectives et stratiformes entre (a) et (b) 9.5 et 0 ka et (c) et (d) 9.5 et 6 ka.

De façon à isoler le seul effet de l'activité convective au-dessus de l'Inde sur la Méditerranée et l'Afrique du Nord, j'ai élaboré une méthode expérimentale permettant de modifier la convection sur cette zone spécifique, à l'aide du modèle atmosphérique LMDZ-OR. Plusieurs méthodes auraient pu être retenues. Avec les conseils et l'aide de Jean-Yves Grandpeix, j'ai choisi de perturber le modèle de façon conservative en prescrivant une anomalie de profil vertical de température avant de résoudre la convection profonde et stratiforme. En effet, les variations des précipitations sur les deux systèmes de mousson résultent d'une combinaison d'amplification de pluies convectives et stratiformes (Fig. 4.7). Les différences de précipitations convectives sont plus intenses sur l'est de l'Afrique et le centre de l'Inde tandis que les variations de précipitations stratiformes sont plus marquées sur la côte ouest du Sahel et le sud-est et nord-est de l'Inde. La principale question à laquelle j'ai essayé de répondre étant si l'amplification extrême de la mousson indienne à 9.5 ka a ou non une influence directe sur la Méditerranée et un effet

d'inhibition sur le développement de la mousson africaine. La simulation de référence est une simulation forcée par une climatologie de SST avec des conditions orbitales correspondant à 9.5 ka. L'idée ensuite est d'imposer une réduction de l'activité de la mousson indienne au niveau de celle de 6 ka pour voir l'impact sur la Méditerranée et l'Afrique du Nord, et de réaliser un ensemble de test en modifiant les conditions initiales et les anomalies de profils de température. Une vingtaine d'années de simulations de référence à 9.5 et 6 ka ont été réalisées.

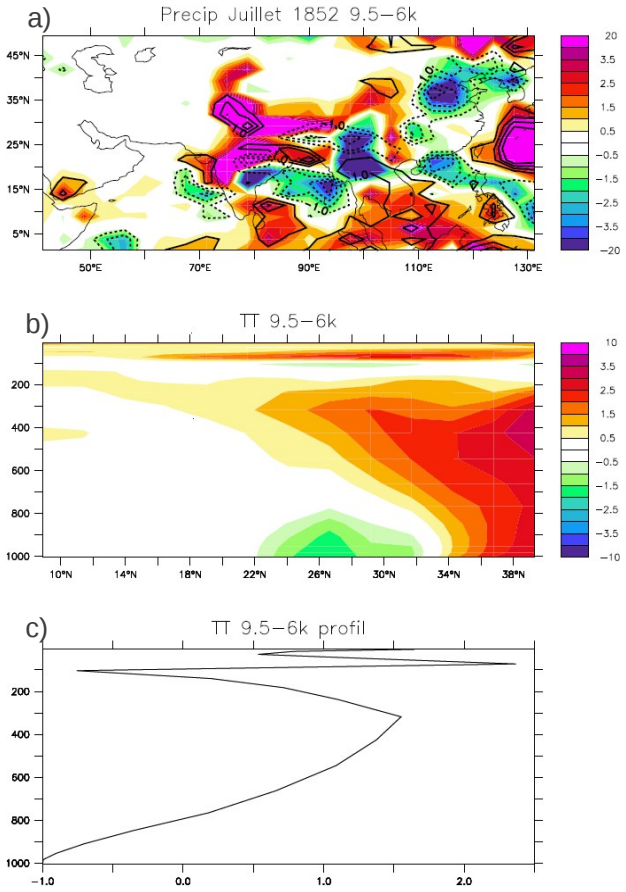

FIGURE 4.8: (a) Différences de précipitations (couleurs) et d'OLR (contours) entre 9.5 et 6 ka pour l'année de simulation 1852 ; (b) différence de température troposphérique moyennée de 70 à 95°E entre 9.5 et 6 ka ; (c) Profil de différence de température troposphérique moyenné entre 70 et 95°E et 22 à 32°N entre 9.5 et 6 ka.

Ensuite, un cas test a été sélectionné où la différence de convection en juillet sur le nord-est de l'Inde entre 9.5 et 6 ka était importante (Fig. 4.8). Les différences de température troposphérique moyennées de 70 à 95°E présentent un réchauffement de la moyenne et haute troposhère et un refroidissement des basses couches de 22 à 32°N dû aux précipitations plus importantes. L'anomalie de profil de température moyenné de 20 à 34°N est celui qui a été

soustrait à chaque pas de temps au profil de température dans les simulations test en partant du début du mois de juillet de cette année choisie.

Après avoir résolu plusieurs difficultés numériques et de mise en place du protocole, de nombreux tests de un mois ont été réalisés, en imposant l'anomalie de profil de température avant de passer dans le schéma de convection profonde ou de convection stratiforme, ou bien avant les deux. D'autres profils d'anomalies ont été appliqués. Malheureusement, aucun de ces tests n'a permis de recréer une diminution de la convection raisonnable et limitée à une région sans entraîner des effets de bord importants, et encore moins d'obtenir un signal significatif sur la Méditerranée et le Sahel. Je pense que le problème vient du fait d'imposer une anomalie moyennée sur une région et sur un mois entier. Je suggèrerais pour poursuivre ce travail de se concentrer sur des évènements convectifs particuliers et les conditions qui les déclenchent, et d'améliorer le protocole expérimental pour imposer une anomalie hétérogène de façon à éviter les effets de bord. ou bien de tenter d'autres méthodes moins conservatives, comme imposer une divergence, multiplier le flux de chaleur sensible ou latente sur une région ou des techniques de nudging.

Cette partie n'a pas aboutit à un mécanisme compréhensif de la possible téléconnection entre la mousson indienne et africaine et n'a pas quantifier le rôle des différents forçages ayant pu inhiber la mousson africaine à 9.5 ka. Cependant, une partie de la multitude d'études récentes tentant de répondre aux questionnements liés à l'interdépendance des systèmes de mousson et à leur influence sur les extratropiques à été discutée. Une compréhension complète de ces interactions et de leur représentation dans les modèles reste encore à atteindre. En attendant, la modélisation des climats passés peuvent être d'une aide précieuse pour renseigner sur ces mécanismes et leur biais de représentation en exacerbant un aspect ou l'autre des forçages qui régissent ces téléconnections et en validant les résultats à l'aide d'enregistrements paléoclimatiques.

5

Influence de l'océan et des calottes de glace

5.1 Résumé

Le rôle de l'interaction océan-atmosphère sur les variations des systèmes de mousson est investi plus en profondeur dans ce chapitre. La rétroaction climatique de l'océan sur les variations des moussons à l'Holocène est tout d'abord étudiée, de façon à évaluer si cette rétroaction a le même impact à 9.5 ka que celui mis en évidence dans des études précédentes pour le milieu de l'Holocène. Par ailleurs, d'autres forçages que l'insolation ont pu influencer l'évolution des moussons au cours de l'Holocène. J'ai analysé des simulations qui ont été réalisées pour tester la sensibilité du climat à la fonte des glaciers à 6 et 9.5 ka et à la présence d'une calotte de glace réminiscente à 9.5 ka. Ces tests de sensibilité permettent de tester la validité des résultats présentés précédemment dans des conditions légèrement modifiées.

L'avènement des modèles couplés océan-atmosphère a permis d'étudier le rôle de l'océan

dans les variations passées du climat tropical. La comparaison des deux exercices d'intercomparaison de modèles PMIP entre les résultats des modèles atmosphériques seuls et ceux des modèles couplés permet de mettre en évidence la rétroaction des conditions de surface océanique sur l'évolution des moussons à 6 ka et 21 ka (Braconnot et al., 2007a,b). Le rôle de cette rétroaction a été analysé dans nos simulations à l'aide du modèle couplé IPSL-CM4 et de sa composante atmosphérique LMDZ. La partie (Marzin and Braconnot, 2009a) présente la méthodologie abordée ainsi que les différences de résultat entre les moussons asiatiques et africaine pour les trois périodes d'études : 0, 6 et 9.5 ka.

De façon à isoler l'impact de l'océan, j'ai réalisé des simulations forcées par 20 ans de SST journalières provenant de la simulation couplée 0k, et qui ne prennent en compte que les variations de paramètres orbitaux entre les périodes étudiées. La différence entre les simulations couplées et ces simulations forcées met en évidence l'impact de l'interaction océan-atmosphère en réponse aux variations d'insolation. Plusieurs études précédentes ont mis en évidence l'impact de la rétroaction de l'océan sur le délai de réponse des systèmes de mousson au changement d'insolation à 6 ka (Kutzbach and Liu, 1997; Hewitt and Mitchell, 1998; Braconnot et al., 2000b; Liu et al., 2004; Zhao et al., 2005; Ohgaito and Abe-Ouchi, 2007). En accord avec celles-ci, notre étude montre que la rétroaction de l'océan est positive pour la mousson africaine, un dipôle de SST dans l'Atlantique tropical favorisant le démarrage de la mousson aussi bien à 6 qu'à 9.5 ka. Les cycles saisonniers des SST et de la couche de mélange de l'Océan Indien et du Pacific ouest sont aussi affectés à 6 et 9.5 ka. Les SSTs sont plus élevées en fin de saison, ce qui favorise la convection sur l'océan et induit ainsi une rétroaction négative de l'océan sur les précipitations de mousson indienne et d'Asie du sud-est. Cette rétroaction est d'autant plus négative à 9.5 qu'à 6 ka pour la mousson indienne. Ces résultats montrent que les systèmes de mousson sont affectés de façon singulièrement différente par la réponse de l'océan aux variations d'insolation à l'Holocène.

D'autres facteurs ont pu influencer les systèmes de mousson au début de l'Holocène. Cette période d'insolation maximum a engendré la fonte de vastes calottes de glace de l'hémisphère nord, se traduisant par un apport important d'eau douce et fraîche dans l'Atlantique Nord qui a pu perturber l'effet de la précession. Des tests de sensibilité ont été effectués pour évaluer

l'impact de cette fonte des glaces sur les moussons. De façon à étudier l'impact de ce flux d'eau douce, les simulations couplées à 6 et 9.5 ka ont été réalisées avec et sans paramétrisation de fonte des icebergs (cette paramétrisation thermodynamique des glaciers est détaillée dans Swingedouw et al. (2006)). De plus, une expérience de sensibilité du climat à la présence de restes de la calotte fennoscandienne et de la Laurentide à 9.5 ka a été réalisée (les simulations présentées jusqu'alors considérant les délimitations des calottes de glace actuelles). L'analyse que j'ai faite de ces simulations fait l'objet d'une publication soumise présentée dans la partie 5.3 dont les résultats sont résumés ci-dessous.

La partie 5.3 présente les mécanismes de réponse des systèmes de mousson à ces deux types de forçage. La fonte des icebergs induit un refroidissement de l'Atlantique Nord et un réchauffement de l'Atlantique sud tropical et a pour effet de diminuer les précipitations de mousson en Inde et au Sahel, mais pas en Asie du sud-est. La présence de plus larges calottes de glace à 9.5 ka induit un refroidissement global de l'hémisphère nord. La mousson d'Asie du sud-est est affaiblie, tandis que la mousson africaine l'est seulement légèrement. La réponse de la mousson indienne à ces calottes est plus ambiguë, car elle est diminuée en début de saison et amplifiée par la suite. En Asie du sud-est, les précipitations sont considérablement diminuées tout au long de l'année. Les deux forçages introduisent des perturbations importantes du jet d'ouest. Les changements des moussons asiatiques reflètent l'extension des centres de refroidissement de la couche troposphérique au niveau des moyennes latitudes. Une fois de plus, ces expériences de sensibilité montrent que les systèmes de mousson sont affectés différemment par ces forçages climatiques.

De la même façon, les systèmes de mousson présentent de fortes variations en période glaciaire. Les données suggèrent que ces variations sont en lien avec les évènements abrupts de l'Atlantique Nord. En effet, de nombreux indicateurs paléoclimatiques indiquent la concomitance des évènements de débâcle glaciaire dans l'Atlantique Nord (évènements de Heinrich) avec ceux de plusieurs régions influencées par la mousson (Porter and An, 1995; Schulz et al., 1998; Leuschner and Sirocko, 2000; Wang et al., 2001a; Altabet et al., 2002; Rashid et al., 2007) qui dominent la dernière période glaciaire. De façon à mieux comprendre les interactions entre les moussons et le climat de l'Arctique et de l'Atlantique Nord, nous présentons par la

suite dans la partie 5.4 une étude détaillée de la réponse des moussons à une expérience de flux d'eau douce dans l'Atlantique Nord en condition glaciaire. Il existe plusieurs études de modélisation de réponse des systèmes de mousson à un flux d'eau douce dans l'Atlantique Nord, mais la plupart ont ont été réalisées dans des conditions climatiques actuelles. Notre étude a été réalisée avec des conditions climatiques correspondant au dernier maximum glaciaire, ce qui permet de comparer de façon plus réaliste les résultats d'expériences de modélisation avec les enregistrements paléoclimatiques.

Kageyama et al. (2009) (annexe A.3) détaille l'impact du flux d'eau douce sur l'affaiblissement de la circulation thermohaline. Ma contribution (partie 5.3) présente une première partie de l'analyse de la réponse de la mousson indienne à ce forçage. La diminution des pluies de mousson sur le continent indien est associé à un affaiblissement du gradient méridien de température troposphérique, et ce dernier évolue de façon synchrone avec la diminution de la circulation thermohaline. A la suite de ce travail, j'ai participé en collaboration avec Masa Kageyama, Nejib Kallel et Jean-Claude Duplessy, à la comparaison de ces résultats de simulations à un enregistrement de l'hydrologie de la Baie du Bengal sur les 40000 dernières années (partie 5.4.1). L'affaiblissement de la mousson indienne en réponse au flux d'eau douce en Atlantique Nord dans les simulations glaciaires permet de justifier l'hypothèse de synchronisation des variations d'hydrologie de la Baie du Bengale avec celles de l'enregistrement des carottes de glace du Groenland. De façon à analyser la téléconnection entre le forçage de l'Atlantique Nord et les moussons, j'ai proposé à Masa Kageyama de réaliser des études de sensibilité pour isoler la zone de changements de SST qui influence le plus les variations d'intensité des systèmes de mousson. L'analyse que j'ai faite de ces tests démontre que le dipôle de SST en Atlantique tropical associé au déplacement de la ZCIT vers le sud est essentiel et agit bien plus efficacement sur les perturbations de moyennes latitudes que les changements de SST dans l'Atlantique Nord eux-mêmes. Ces expériences permettent d'apporter une alternative aux hypothèses préalablement citées dans la littérature, invoquant le lien direct entre le refroidissement de l'Atlantique Nord et la mousson indienne via le refroidissement de l'Eurasie (Goswami et al., 2006; Feng and Hu, 2008) ou bien le lien via les variations de SST dans le Pacifique est (Zhang and Delworth, 2005; Lu and Dong, 2008).

La section 5.4.2 présente les compléments à cette étude, notamment l'ensemble des tests de sensibilité effectués ainsi que les mécanismes de réponse des moussons africaine et d'Asie du sud-est à un évènement de type Heinrich. L'intensité de la mousson africaine est aussi affectée par le flux d'eau douce en Atlantique nord, d'une part par le dipôle d'anomalies de SSTs dans l'Atlantique tropical, et d'autre part par le refroidissement autour de la Mer Méditerranée. Cependant, il n'y a pas de changement au niveau de l'Asie du sud-est. Ceci est aussi observé dans d'autres études de modélisation (Zhang and Delworth, 2005; Vellinga and Wood, 2002), voir figures dans Clement and Peterson (2008)) et suscite des interrogations pour l'interprétation des enregistrements paléoclimatiques qui représentent des fluctuations climatiques abruptes sur cette région.

Après avoir étudié l'impact du flux d'eau douce en Atlantique nord sur les moussons au début de l'Holocène et au dernier maximum glaciaire, la question se pose de savoir si ce forçage induit la même réponse pour tous les systèmes de mousson et pour différents climats. En se basant sur l'étude de Swingedouw et al. (2009) qui compare l'impact d'une expérience de flux d'eau douce pour plusieurs conditions climatiques (Eemien 126 ka, dernier maximum glaciaire 21 ka, moyen Holocène 6 ka, préindustriel 0 ka et futur), nous analysons la réponse des systèmes de mousson dans ces expériences en ajoutant celle du début de l'Holocène présentée dans la partie 5.3. L'objectif est de déterminer si l'impact du flux d'eau douce sur les systèmes de mousson varie selon les périodes climatiques étudiées, glaciaire ou interglaciaire, ou sous l'influence du réchauffement climatique. Les résultats montrent que toutes les simulations ont en commun un affaiblissement des moussons africaine et indienne associées au refroidissement de l'hémisphère nord et au dipôle de SST dans l'Atlantique tropical, mais que celles-ci ne sont pas linéaires au flux d'eau douce, ni à la diminution de l'intensité de la circulation thermohaline, sauf dans le cas de la seule variation des paramètres orbitaux (0 ka, 6 ka, 9.5 ka et 126 ka). Le climat tropical est plus sensible au flux d'eau douce en conditions glaciaires et en conditions de réchauffement climatique. Il serait intéressant de poursuivre ce travail en réalisant des tests supplémentaires aux zones de changements de SST pour ces différents climats, comme ceux réalisés pour la période glaciaire. Les interactions entre les hautes latitudes et les tropiques sont encore loin d'être totalement comprises. Une large comparaison de résultats de modèles à des expériences de flux d'eau douce permettrait de faciliter l'interprétation des enregistrements

paléoclimatiques et d'expliquer les mécanismes de téléconnection.

5.2 Impact de la rétroaction de l'océan sur les variations des moussons asiatique et africaine à 6 et 9.5 ka

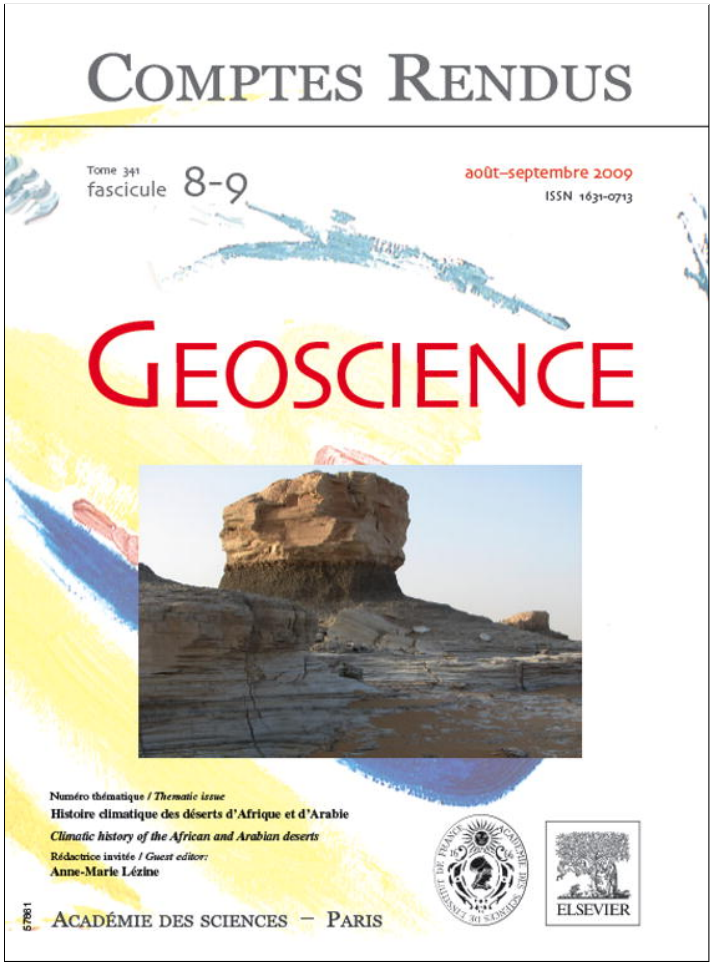

Available online at www.sciencedirect.com
ScienceDirect
C. R. Geoscience 341 (2009) 643–655
Comptes Rendus Geoscience

External geophysics, climate and environment

The role of the ocean feedback on Asian and African monsoon variations at 6 kyr and 9.5 kyr BP

Charline Marzin *, Pascale Braconnot

Laboratoire des sciences du climat et de l'environnement, unité mixte CEA–CNRS–UVSQ, Orme des Merisiers, bâtiment 712, 91191 Gif-sur-Yvette cedex, France

Received 24 May 2009; accepted after revision 1 September 2009
Available online 9 October 2009

Written on invitation of the Editorial Board

Abstract

The role of ocean feedback on monsoon variations at 6 and 9.5 kyr Before Present (BP) compared to present-day is investigated by using sets of simulations computed with the IPSL–CM4 ocean–atmosphere coupled model and simulations with the atmospheric model only with the SST prescribed to the present-day simulation for the coupled model. This work is complementary to the study by Marzin and Braconnot (2009) who have analyzed in detail the response of Indian and African monsoons to changes in insolation at 6 and 9.5 kyr BP using the IPSL–CM4 coupled model. The monsoon rainfall was intensified at 6 and 9.5 kyr BP compared to 0 kyr BP as a result of the intensified seasonal cycle of insolation in the Northern Hemisphere. In this paper, the impact of the ocean feedback is analysed for the Indian, East-Asian and African monsoons. The response of the ocean to the 6 and 9.5 kyr BP insolation forcing shares similarities between the two periods, but we highlight local differences and a delay in the response of the surface ocean between 6 and 9.5 kyr BP. The ocean feedback is shown to be positive for the early stage of the African monsoon. A dipole of SST in the tropical Atlantic favouring the earlier build-up of the monsoon in the 6 and 9.5 kyr BP coupled simulations. However, it is strongly negative for the Indian and East Asian monsoons, and of stronger amplitude at 9.5 than at 6 kyr BP over India. In these Asian regions, the convection is more active over the ocean than over the continent during the late monsoon season due to the ocean feedback. The results are consistent with previous studies about 6 kyr BP climate. In addition, it is shown that the ocean feedback is not sufficient to explain the relative amplifications of the different monsoon systems within the three periods of the Holocene, but that the mechanisms such as the effect of the precession on the seasonal cycle of monsoons as discussed in Marzin and Braconnot (2009) are more plausible. ***To cite this article: C. Marzin, P. Braconnot, C. R. Geoscience 341 (2009).***

Résumé

Le rôle de la rétroaction de l'océan sur les changements de mousson à 9500 et 6000 ans BP. Le rôle de la rétroaction de l'océan sur les changements de mousson à 9500 et 6000 ans BP (Before Present) par rapport à l'Actuel est analysé à l'aide de deux ensembles de simulations, un réalisé avec le modèle couplé océan–atmosphère IPSL–CM4 et l'autre avec le modèle atmosphérique seulement, forcé par les températures de surface de mer, issues de la simulation couplée à 0 BP. Ce travail est complémentaire de l'étude de Marzin et Braconnot (2009) qui ont analysé en détail la réponse des moussons indienne et africaine aux changements d'insolation à 6000 et 9500 ans BP, avec le modèle couple IPSL–CM4. Les pluies de mousson étaient plus intenses à 6000 et 9500 ans BP, résultant de l'amplification du cycle saisonnier d'insolation dans l'hémisphère nord. Le rôle de la rétroaction de

* Corresponding author.
E-mail address: charline.marzin@lsce.ipsl.fr (C. Marzin).

1631-0713/$ – see front matter © 2009 Published by Elsevier Masson SAS on behalf of Académie des sciences.
doi:10.1016/j.crte.2009.09.001

l'océan est analysé dans cet article pour les moussons indienne, d'Asie du Sud-Est et africaine. La réponse de l'océan au forçage par l'insolation à 6000 et 9500 ans est similaire ; cependant, nous soulignons des différences locales ainsi que le délai de la réponse de l'océan de surface, entre ces périodes. Cette rétroaction est positive pour le début de la mousson africaine. Un dipôle de température de surface de l'océan dans l'Atlantique tropical favorise une mise en place de la mousson plus précoce à 6000 et 9500 ans BP dans les simulations couplées. Cependant, elle est fortement négative pour les moussons indienne et d'Asie du Sud-Est, et de plus grande amplitude à 9500 qu'à 6000 ans BP sur l'Inde. Dans ces régions d'Asie, la convection est plus active sur l'océan que sur le continent vers la fin de la saison de mousson, à cause de la rétroaction de l'océan. Les résultats concordent avec les précédentes études sur le climat à 6000 ans BP. De plus, il est montré que la rétroaction de l'océan ne permet pas d'expliquer les amplifications relatives des différents régimes de moussons entre ces différentes périodes, tandis que les mécanismes tel l'effet de la précession sur le cycle saisonnier des moussons démontrés par Marzin et Braconnot (2009), sont plus plausibles. ***Pour citer cet article : C. Marzin, P. Braconnot, C. R. Geoscience 341 (2009).***

Keywords: Indian monsoon; East-Asian monsoon; African monsoon; Modelling; Paleoclimates; Holocene; Ocean feedback

Mots clés : Mousson indienne ; Mousson africaine ; Mousson d'Asie du Sud-Est ; Modélisation ; Paléoclimats ; Holocène ; Rétroaction océan

1. Introduction

Monsoon systems are critical features of the global climate. They are characterized in the Northern Hemisphere by a humid season in summer and a dry season in winter, as well as a seasonal reversal of winds. This study is focused on three main regions, the Indian monsoon, the East-Asian monsoon and the North-African monsoon. It has been shown that they are responsive to changes in insolation induced by variations of Earth's orbital parameters [16,18,34]. Paleoclimate records suggest that these monsoon systems have significantly evolved during the Holocene and that they were enhanced in the Northern Hemisphere during the Early to Mid Holocene compared to present-day [9,10,13,15,19,28,29,33].

This work is complementary to the study by Marzin and Braconnot [25] who have analyzed in detail the response of Indian and African monsoons to changes in insolation at 6 and 9.5 kyr BP using the IPSL–CM4 ocean–atmosphere coupled model. Monsoon rainfall was intensified at 6 and 9.5 kyr BP, compared to 0 kyr BP, as a result of the intensified seasonal cycle of insolation in the Northern Hemisphere. These three periods of the Holocene were chosen for their orbital parameters' differences, the precession being the most varying parameter throughout the Holocene. This results in a warmer boreal summer for 9.5 kyr BP in phase with the present-day insolation maximum and in a delayed warming (by approximately one month) for 6 kyr BP compared to present-day. This previous study showed that the relative response of the Indian and African monsoon is a function of precession. When the maximum change in insolation occurs in phase with the development of the monsoon system, the amplification is larger, which explains why in their simulations the decrease of the Indian monsoon is more gradual during the Holocene than that of the African monsoon which is larger in the second half of the Holocene. The role of precession on the timing and on the relative amplification of monsoon seasonal cycle is highlighted. Stronger moisture advection, enhanced meriodional gradient of tropospheric temperatures and the feedback of the Tibetan Plateau snow cover were the mechanisms analyzed to explain the monsoon variations and the differences between the subsystems. However, Marzin and Braconnot [25] did not isolate the role of the ocean feedback. We address this issue in this paper by comparing the results of the coupled simulations with the corresponding forced simulations, for which sea surface temperature (SSTs) are taken from the present-day coupled simulation. This study focuses on the African, Indian and East-Asian monsoons.

Several modeling studies have shown that the ocean feedback introduces a delay in the response to the change in summer insolation at the Mid-Holocene [3,12,18,21]. In the tropical Atlantic, the dipole of SST anomalies described by Kutzbach and Liu [18] indicates the role of the evaporation feedback in strengthening the ocean warming north of 5° N. Zhao et al. [35] have compared the role of ocean circulation changes on monsoon evolution for several coupled models which participated in the second phase of the Paleoclimate Modeling Intercomparison Project.

Braconnot et al. [4,5] further analyze how the dipole is created and maintained. In addition to the evaporation feedback, they show that the change in the Ekman transport also plays a role. The larger the dipole, the larger the monsoon change [6]. Liu et al. [20] investigated the role of ocean feedback on global

monsoons evolution for several time slices of the Holocene. These studies have also demonstrated a positive ocean feedback for the African monsoon during the Mid-Holocene whereas it is negative for the Asian monsoon. Several studies have highlighted a dampening of the Asian monsoon due to ocean feedback [5,27], a warmer Indian Ocean and western Pacific during late summer inducing reduced convection over the land.

Braconnot and Marti [1], Braconnot et al. [7] further showed that the seasonal cycle of SST in the Indian Ocean depends on precession. It involves a feedback loop between the monsoon winds, precipitation, river runoff and mixed layer depth. In late summer the west Indian Ocean warming creates a dipole across the Indian Ocean which delays the southward withdrawal of monsoon over the ocean [35]. Braconnot et al. [3] have also shown that the changes in the meridional ocean heat transport is as large as the atmospheric heat transport in the Tropics.

In this study we investigate the impact of the ocean feedback on the African, Indian and East-Asian monsoon amplifications at 6 and 9.5 kyr BP. The models used for the coupled and forced simulations are presented in section 2, as well as the experiments and the radiative forcing changes at 6 and 9.5 kyr BP. The monsoon responses in the coupled simulations are described in section 3. In section 4, we examine the impact of the ocean feedback and interesting regional features. A summary is given in section 5.

2. Model, experiments and insolation variations

2.1. IPSL–CM4 coupled model

The coupled simulations are performed with the version of the IPSL coupled model [23,24] used for future climate projections as part of the WCRP/CMIP3 multi-ensemble experiments [26] that served as a basis for the last IPCC assessment [31]. IPSL–CM4 couples the grid point atmospheric general circulation model LMDz [14] developed at Laboratoire de Météorologie Dynamique (LMD, France) to the oceanic general circulation model ORCA [22] developed at the Laboratoire d'Océanographie et du Climat (LOCEAN, France). On the continent, the land surface scheme ORCHIDEE [17] is coupled to the atmospheric model. Only the thermodynamic component of ORCHIDEE is active in the simulations presented here. The closure of the water budget with the ocean is achieved via a river routing scheme implemented in the land surface model. A sea-ice model [8], which computes ice thermodynamics and dynamics, is included in the ocean model. The ocean and atmospheric models exchange surface temperature, sea-ice cover, momentum, heat and fresh water fluxes once a day, using the OASIS coupler [32] developed at CERFACS (France). None of these fluxes are corrected. In its present configuration, the model is run at medium resolution. The atmospheric grid is regular, with a resolution of 3.75° in longitude, 2.5° in latitude, and 19 vertical levels. The ocean model grid has approximately 2° resolution (0.5°near the equator) with 182 points in longitude, 149 points in latitude and 31 vertical levels.

The representation of monsoon systems in the coupled model IPSL–CM4 is discussed in detail in Marzin and Braconnot [25]. The global dynamic features of monsoon circulation are well reproduced; however, the rainfall over the land in Sahel and India is underestimated and does not penetrate north enough. The amplitude and seasonal cycle of East-Asian monsoon precipitation are well represented in this model.

2.2. Experimental design

Three simulations were performed with IPSL–CM4 for the climates of 9.5 kyr BP, 6 kyr BP and of the preindustrial periods (hereafter 9.5k, 6k and 0k respectively) considering only the variations of the orbital parameters described below. The vegetation cover and green gas concentrations are kept to modern values. Climatologies are computed from the last 100 years of each simulation. The methodology to separate the ocean feedback from the total response is to run the same simulations with the atmosphere-land component of the model. Following Braconnot et al. [2], we extracted 20 years of daily SST from the control simulation with the coupled model and prescribed them in all the atmospheric alone simulations. In these simulations, the SST is prescribed the same as the modern control coupled simulation so that we consider only the atmopsheric response to the orbital parameters variations (hereafter 9.5fk, 6fk, 0fk for the forced simulations). These experiments are integrated for 20 years and averaged over these 20 years for the monthly climatologies. By sub-tracting the sets of coupled simulations by the atmospheric simulations, we can extract the ocean feedback on the climatic response to orbital parameters variations during the Holocene.

With this methodology, the coupled control simulation would be the reference for the paleo simulations either with the coupled model or with the atmosphere model alone. However, the version of the atmospheric model we used for the SST-forced simulations is slightly different from the one of the coupled model.

We thus ran also a control simulation with the atmosphere model alone to check that we discuss the role of the ocean feedback and not the difference between two model versions. This introduces a bias between the two sets of simulations. We have to take this into account while looking at the ocean feedback. However, the differences are not significant enough to qualitatively affect the results presented here.

2.3. Insolation variations

Changes in insolation due to slow variations of the Earth's orbital parameters are the major driver of climate variability during the Holocene. Precession and obliquity are the two parameters that shape the insolation forcing over this period. The values of the orbital parameters for the 0, 6 and 9.5 kyr BP climates are given in Marzin and Braconnot [25]. Precession controls the seasonal variations of insolation, whereas obliquity controls the contrast between low and high latitudes. With the summer solstice close to the perihelion at 9.5 kyr BP ($\varpi - 180 = 303.03$), the magnitude of the seasonal cycle of insolation was enhanced in the Northern Hemisphere at 9.5 kyr BP compared to present-day and in phase with the present seasonal cycle (Fig. 1). As a result, summer seasons were warmer and shorter and winter seasons cooler and longer. At 6 kyr BP, the autumnal equinox is near the perihelion ($\varpi - 180 = 0.87$). This leads to a shift in the timing of the seasonal variations. The difference in insolation averaged over the Northern Hemisphere (10°–50° N, Fig. 1) lags the change in insolation at 9.5 kyr BP by about one month. The maximum amplification is reduced at 6 kyr BP (25 W m^{-2}) compared to 9.5 kyr BP. The change in obliquity has almost no impact between 6k ($\varepsilon = 24.105$) and 9.5k ($\varepsilon = 24.231$) but explains the difference in the high latitudes compared to the control. We will then consider both the changes in the magnitude and timing of the seasonal cycle when analysing the impact of insolation forcing on the African and Asian monsoons. To take into account the changes in the length of the seasons, we should have used a celestial definition of the calendars for each climate, as in Joussaume et al. [16], Marzin and Braconnot [25], but for convenience we used the modern definition of calendar, as it does not change qualitatively the results presented here.

3. Large-scale characteristics of the different periods

3.1. Monsoon responses in the coupled simulations

In response to increased boreal summer insolation averaged from June to September (JJAS), the model produces higher temperatures over the northern Hemisphere continent (Fig. 2) both at 6 and 9.5k compared to present-day. However, the ocean remains cool in summer, except in the northern Atlantic and northern Pacific. This results from the latitudinal gradient in the insolation forcing and the thermal inertia of the ocean. In addition, the melting of sea ice in high latitude strengthens the warming there. The land-sea temperature contrast is enhanced, as well as the seasonal

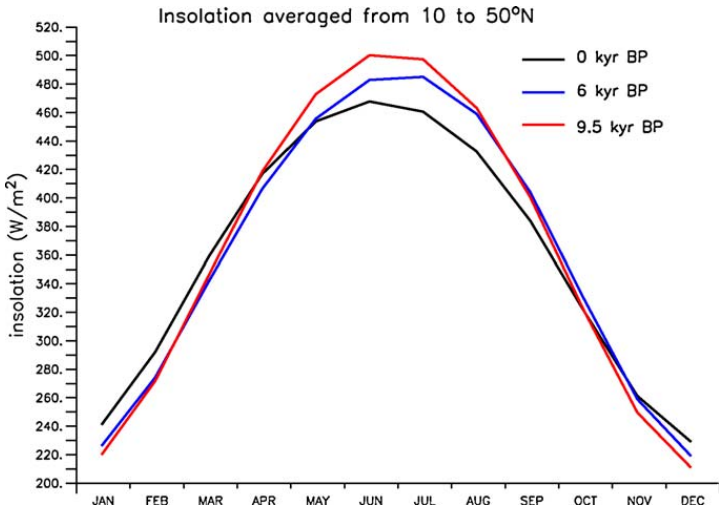

Fig. 1. Incoming solar radiation at the top of the atmosphere (W/m^2) averaged from 10 to 50° N and plotted as a function of months, for 0, 6 and 9.5 kyr BP. The celestial calendar is used to compute the monthly means.

Fig. 1. Rayonnement solaire incident au sommet de l'atmosphère (W/m^2) moyenné de 10 à 50° N et tracé en fonction des mois pour les périodes d'il y a 0, 6000 et 9500 ans (0 ka, 6 ka et 9,5 ka). Les moyennes mensuelles sont calculées en utilisant le calendrier céleste.

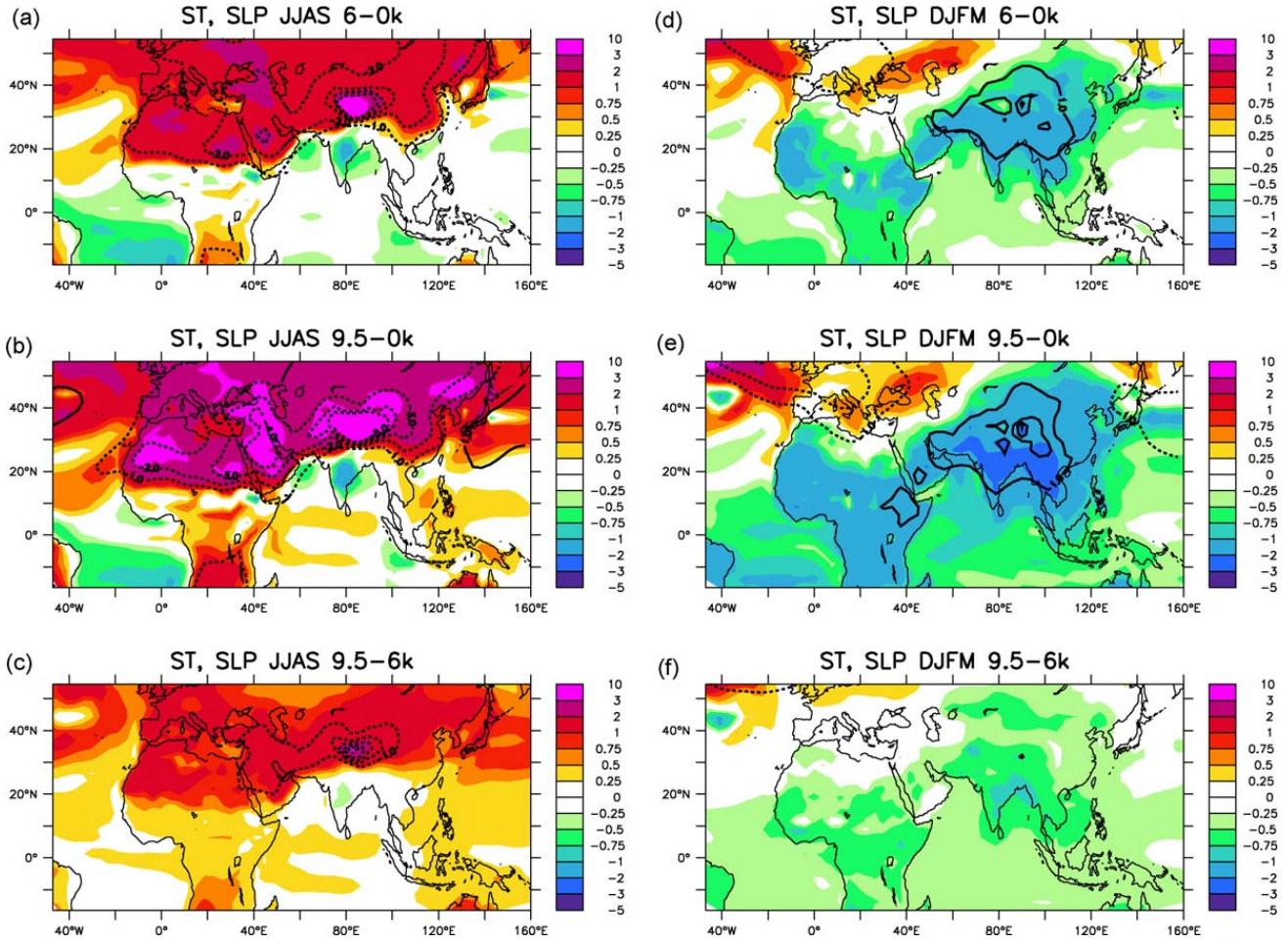

Fig. 2. Surface temperature (K) and sea level pressure (hPa) differences for JJAS between (a) 6–0 kyr BP (b) 9.5–0 kyr BP (c) 9.5–6 kyr BP coupled simulations; and (d), (e), (f) for DJFM.

Fig. 2. Différences de température de surface (K) et de pression au niveau de la mer (hPa) pour l'été boréal (gauche moyenne JJAS) et l'hiver boréal (droite, moyenne DJFM) entre (a, d) 6–0 ka (b, e) 9,5–0 ka (c, f) 9,5–6 ka.

contrast of temperatures. Low pressure centres are intensified over the Himalaya and the Sahara, favouring the advection of moist monsoon flow into the continent and thus increasing precipitation (Fig. 3). Monsoon regions present a cooling anomaly due to local recycling and cloudiness. The local SST patterns will be discussed more in detail in the next subsection.

The amplification of monsoon systems at 6 and 9.5k is clearly seen on Fig. 3. Precipitation are increased by 1 to more than 2 mm/day over the Sahel, East Africa, the whole Indian continent and the eastern part of China. As for the surface temperatures, the change is even more visible at 9.5 than at 6k. The surface winds indicate a strengthening of the monsoon flow, and it has been shown in Marzin and Braconnot [25] that 80% of the changes are due to advection processes and the rest to local recycling. Marzin and Braconnot [25] highlighted the impact of the tropospheric temperature meridional gradient on the amplification of the Indian monsoon; this is also valid for the East Asian monsoon [11].

The most important result brought out by Marzin and Braconnot [25] is the relative difference of amplification of the Indian and African monsoons between 6 and 9.5k. The increase in precipitation between 6 and 9.5k is relatively stronger over the Indian region than over Africa. On Fig. 3, the response over East Asia is similar to the African monsoon, with a small amplification between 6 and 9.5k and a larger delay in the Late Holocene. Several hypothesis and mechanisms have been detailed in Marzin and Braconnot [25] to explain these differences. The precession plays an important role on the seasonal cycle of insolation to favour one monsoon system more than the other according to the seasonal cycle of the phenomena. The positive feedback of the snow cover over the Tibetan Plateau contributes to enhance the Indian monsoon at 9.5k. In addition, the

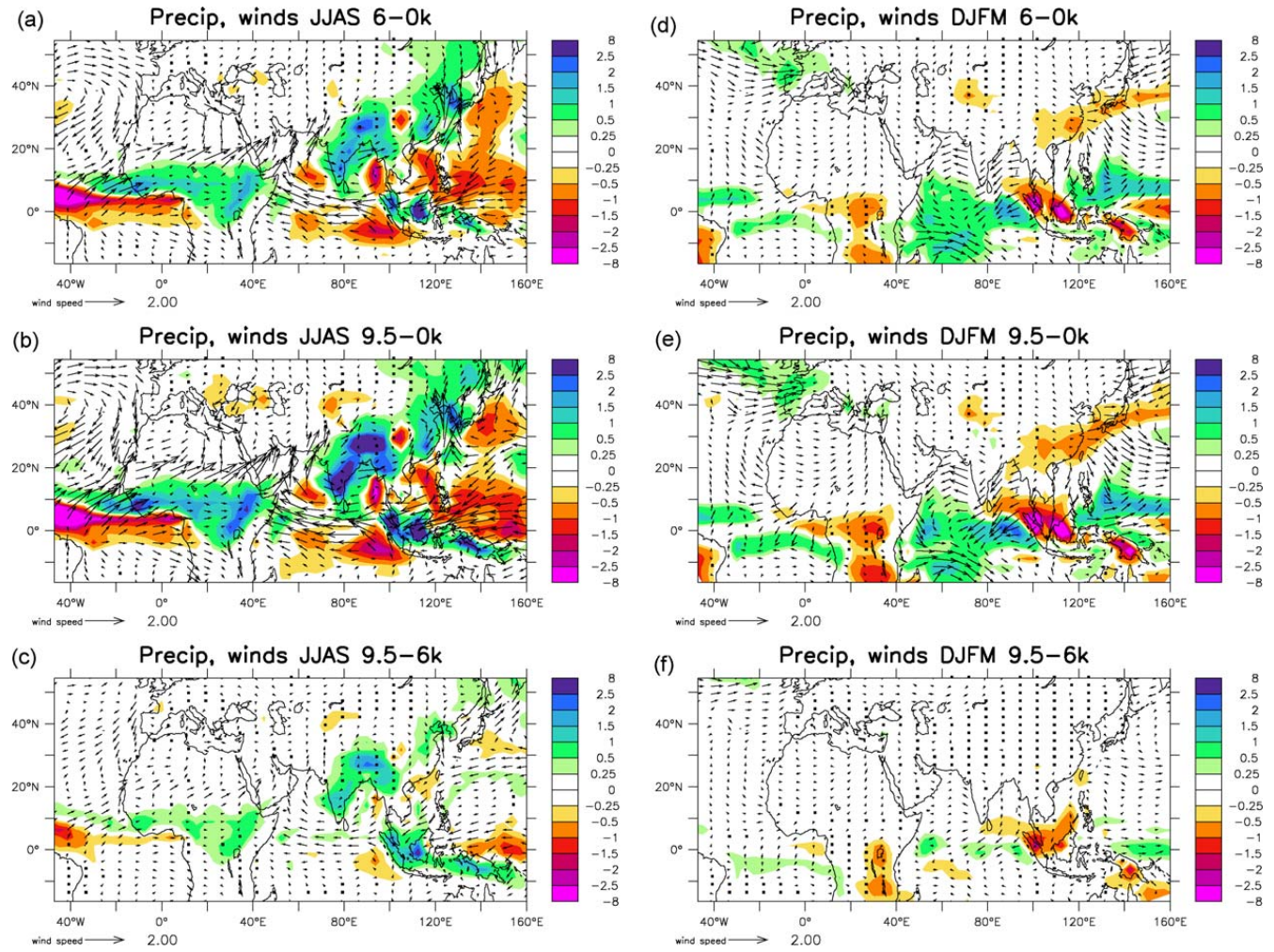

Fig. 3. Precipitation (mm/day) and surface winds (m/s) differences for JJAS between (a) 6–0 kyr BP (b) 9.5–0 kyr BP (c) 9.5–6 kyr BP coupled simulations; and (d), (e), (f) for DJFM.

Fig. 3. Différences de précipitation (mm/j) et de vent de surface (m/s) pour l'été boréal (gauche moyenne JJAS) et l'hiver boréal (droite, moyenne DJFM) entre (a, d) 6–0 ka (b, e) 9,5–0 ka (c, f) 9,5–6 ka.

teleconnection between India, the Mediterranean Sea and North Africa has been investigated, showing that the strength of the increased subsidence around the Mediterranean Sea is well correlated with the strength of the Indian monsoon as would be expected from the triggering of Rossby wave by the convection over India [30].

During the Northern Hemisphere winter, the reduced insolation averaged from December to March (DJFM) results in a large cooling over the ocean and a maximum cooling over Africa and Asia at 6 and 9.5k (Fig. 2). The large high-pressure centre is amplified over the Himalaya and favours advection from the land to the ocean. This results in a stronger convergence over the tropical oceans, with more precipitation and a southward shift of the ITCZ in the tropical Atlantic, The Indian Ocean and the equatorial western Pacific (Fig. 3). This large scale features are in good agreement with previous modelling intercomparison studies for the Mid-Holocene [5,21,35].

3.2. *Response of the ocean*

The summer SST variations between 6 and 0k and 9.5 and 0k are similar at the global scale, with a maximum warming in mid and high latitudes in the Northern Hemisphere that is directly related to the insolation forcing (Fig. 2a and b). The amplitude of these SST variations is increased at 9.5 compared to 6k over the northern Atlantic and Pacific oceans, following the differences in the magnitude of insolation. However, between 6 and 9.5k, the tropical oceans SST patterns are significantly different in some places, highlighting shifts in seasonality between the two periods and feedbacks from the response of the ocean circulation to the local insolation forcing and the large scale

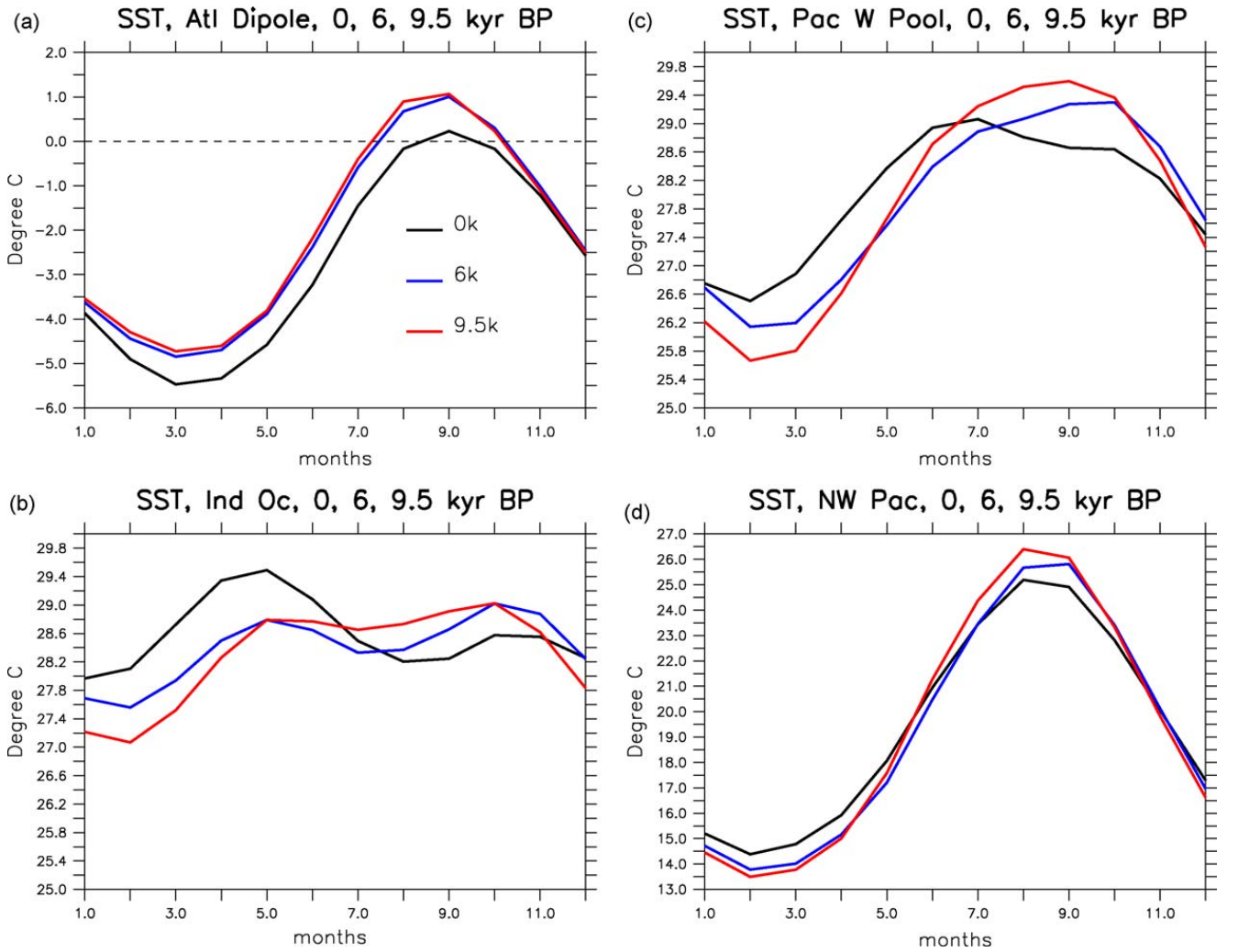

Fig. 4. Monthly SSTs (°C) averaged over (a) difference between northern tropical Atlantic (60° W–20° W, 10° N–20° N) and southern tropical Atlantic (30° W–0° E, 10° S–5° N), (b) Indian Ocean (60° E–100° E, 0° N–10° N), (c) western Pacific warm pool (110° E–150° E, 5° N–15° N), (d) north western Pacific (110° E–150° E, 25° N–35° N).

Fig. 4. Cycle annuel des températures de surface de la mer pour (a) la différence entre les moyennes obtenues pour l'océan Atlantique tropical Nord (60° O–20° O, 10° N–20° N) et l'océan Atlantique tropical Sud (30° W–0°E, 10° S–5° N), (b) l'océan Indien (60° E–100° E, 0° N–10° N), (c) la « *warm pool* » de l'Ouest Pacifique (110° E–150° E, 5° N–15° N) et (d) le Pacifique Nord-Ouest (110° E–150° E, 25° N–25° N).

dynamics. Between 6 and 0k, an overall ocean cooling is observed in the tropical oceans, as shown in previous studies [35], but between 9.5 and 0k, a warming is observed over the equatorial Atlantic, the tropical Indian Ocean and the tropical Pacific. This signal is highlighted in the difference between 9.5 and 6k simulations (Fig. 2c).

Following Zhao et al. [35], we plotted the seasonal evolution of SST over key boxes in the Atlantic Ocean, the Indian Ocean, the warm pool and the North-West Pacific. Fig. 4a shows that the warming of the tropical ocean occurs later in autumn at 6k compared to 9.5k due to the delayed response of the ocean to insolation forcing. Also, the difference between the Early and Mid-Holocene are as large as the differences between these periods and the control. Over the tropical Atlantic, (Fig. 2a and b) show a SST gradient anomaly with a warmer northern tropical Atlantic box (60° W–20° W, 10° N–20° N) and a colder southern tropical Atlantic box (30° W–0° E, 10° S–5° N) between 6 and 0k and 9.5 and 0k. This is associated with a northward shift of the ITCZ induced by a stronger surface wind convergence over the northern tropical Atlantic (Fig. 3). This dipole in the Atlantic is driven by the insolation forcing meridional gradient. Zhao et al. [35] further show that it is reinforced by a wind-evaporation feedback in the northern box and by changes in the ocean circulation. Fig. 4a represents the seasonal cycle of the SST gradient over the tropical Atlantic for the three periods. The amplification of this gradient of about 0.5 °C compared

to 0k from spring to autumn is the same for the Mid and the Early Holocene. Therefore, the ocean feedback does not explain differences in the strength of the African monsoon between these two time periods. The monsoon intensification between 6 and 9.5k is mainly driven by continental warming. At 9.5k, a warming anomaly occurs along the Equator and contributes to the warming of the southern Atlantic box, counteracting the effect of the insolation on the northern box. This anomaly is directly related to the reduction of the equatorial upwelling forced by the westerly surface wind anomaly (Fig. 3). As already mentioned in several publications (see Marzin and Braconnot [25]), the strengthening of the African monsoon results from increased moisture advection from Atlantic Ocean. However, the source region is located to the north of the Equator strengthening the northern branch of the monsoon flow and decreasing the branch from the Gulf of Guinea and the interhemispheric transport across the Equator. Therefore, the southeasterly trade wind is less intense which prevents the full development of the summer upwelling along the Equator [18]. This effect is stronger at 9.5k.

Another significant feature at 9.5k compared to 6k is the warming of the tropical Indian Ocean and Pacific. Fig. 4b, c and d represent the seasonal cycle of SST for the three periods over the Pacific warm pool, the Indian Ocean and the North-West Pacific. The SST warming occurs later than July at 6k compared to 0k, with a cooling before. However, at 9.5k, the warming starts earlier and is larger in the three regions. Zhao et al. [35] have shown that over the selected region of the Indian Ocean, there is a significant contribution of the wind-evaporation feedback to the warming and that the variations of the mixed layer depth increase the rate of warming in this area.

The mixed layer depth difference for JJAS between 9.5k and 0k plotted on Fig. 5 gives more insight in the SST features described above. A large deepening of the mixed layer is observed along the equatorial Atlantic, and is consistent with the weakening of the trade winds and of the equatorial upwelling between 9.5 and 0k. The shallowing observed over the northern tropical Atlantic is more related to a negative anomaly of the wind stress curl (verified but not shown). Another feature is the large shallowing of the mixed layer depth over the whole northern Indian Ocean. Braconnot and Marti [1], Braconnot et al. [7] have shown that it is related to the decrease of the salinity at the surface, due to the increase of precipitation and runoff at the beginning of the Holocene. The stratification reduces the thermal inertia of the upper layer of the ocean and enables a stronger response to the insolation warming in autumn (Fig. 4b). Braconnot et al. [7] have discussed more in

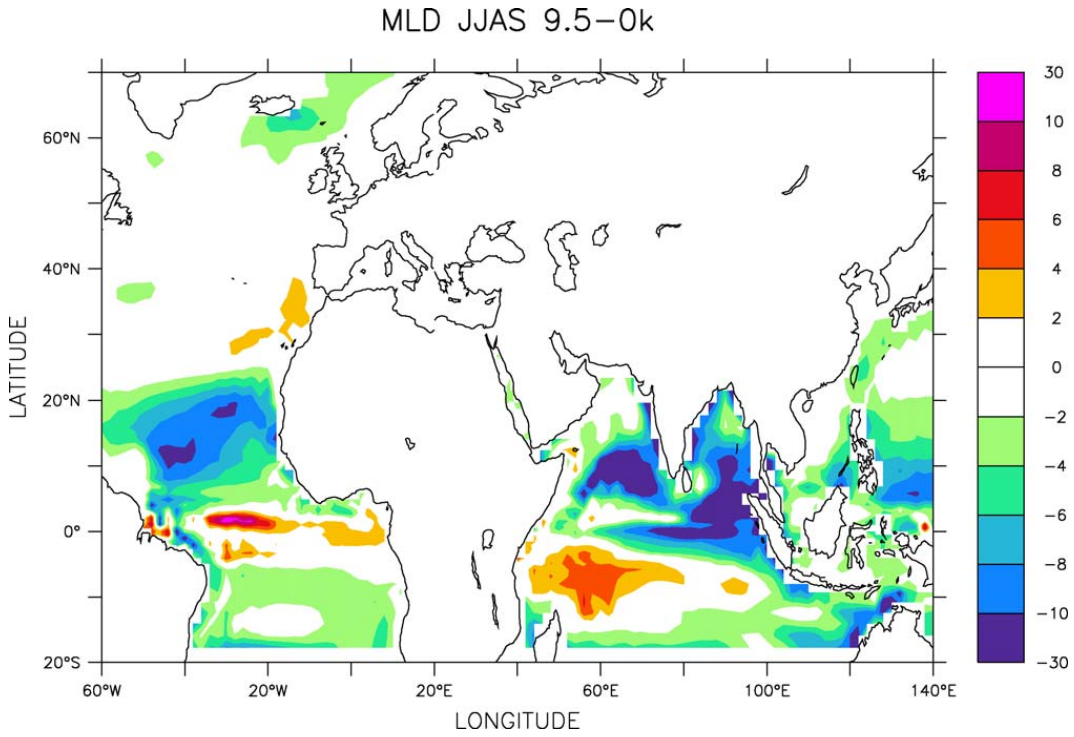

Fig. 5. Mixed layer depth (*m*) difference between 9.5 kyr and 0 kyr averaged for JJAS.

Fig. 5. Différence de profondeur de la couche de mélange (*m*) pour JJAS entre 9,5 ka et 0 ka.

detail the differences in the temperature and salinity seasonal cycles between 6 and 9.5k and the impact of the precession. Fig. 4b shows that at present-day, the SST maximum is reached in April before the onset of the monsoon. Then SST decreases and a secondary maximum occurs in autumn. Due to direct insolation forcing and feedbacks, the spring warming is damped at 6 and 9.5k and the secondary maximum in August is amplified. The reduced SST in summer also disappears at 9.5k. The warming over the north-western Pacific and over the warm pool are more directly linked to the insolation forcing (not shown). The impact of the ocean interaction on the tropical response to changes in insolation is significant. Over the warm pool SST maximum is reached in April at 0k. From the Early to Mid Holocene, the warming is such that the SST maximum is reached during boreal summer or in autumn and that SST are larger than at present during the summer monsoon season. This warming slightly damps the land sea contrast in this region.

4. Impact of the ocean feedback on monsoon systems

4.1. Summer and winter response of the global climate and monsoons to the ocean feedback

To isolate the ocean feedback on the change in precipitation from the direct insolation impact, we analyse the climate produced by the atmospheric model when SSTs are prescribed to those of the 0k coupled simulation in all the simulations. The impact of the response of the ocean to the insolation forcing is then obtained by the difference between the climate change with the atmosphere and the coupled models. To be consistent with 20 years of SSTs chosen to force the atmospheric model, the climatology used for the 0k coupled simulation is averaged over the same 20 years. Because of the small change between the versions of the atmospheric model, we need to take into account the difference between the control simulations by subtracting the climate change from the coupled simulations from the climate change from the forced simulations. The ocean feedback effect on summer and winter precipitation is presented on Fig. 6. The first significant feature is the positive ocean feedback over the tropical Atlantic, which is a common feature for most of the models [5,35]. This is associated with a northward shift of the ITCZ driven by the SST dipole anomaly described in the previous section. Over Sahel, we cannot conclude about the ocean feedback on the precipitation change from the JJAS average; however, Fig. 7a shows that it is positive in the first part of the monsoon season as discussed in the next section. The ocean feedback impact over Sahel is not significantly different between 6 and 9.5k suggested by the fact that the change in the dipole across 5° N is similar at 6 and 9.5k.

Over Asia, the ocean feedback on precipitation seems more complex. It is strongly negative over North India, with an Indian monsoon less amplified in the coupled simulations than in the forced simulations. This negative feedback of the ocean is associated with a strong positive feedback increasing precipitation over the Indian Ocean and the western tropical Pacific. At 9.5k, this moisture convergence over the ocean is associated with a warming to the South of the Indian subcontinent and of the western tropical Pacific (Fig. 2b). Higher SSTs are observed particularly at the end of the summer towards autumn both at 6k and 9.5k (Fig. 4b and c). This triggers an intensified Hadley-type circulation, reducing convection over North India. This negative ocean feedback is still effective between 6 and 9.5k (Fig. 6c), even though its magnitude is reduced at 6k.

Over East Asia, the ocean feedback is strongly negative between 6 and 0k and 9.5 and 0k, but is not significantly different between 6 and 9.5k. The reduced precipitation over North-East China is associated with more moisture convergence to the east over the ocean and to the south over the western tropical Pacific. This is associated with a warming anomaly over the North-West Pacific and the western tropical Pacific, reducing the East–West and North–South land sea contrast.

During boreal winter, a clear southward shift of the ITCZ is observed over the tropical Atlantic, the western Indian Ocean and the tropical Pacific. It is driven by the intensified interhemispheric gradient of temperature due to the cooling of the Northern Hemisphere. For the change between 9.5k and 0k, there is a large dipole structure of precipitation with increased rainfall over the tropical western Pacific and reduced rainfall over eastern tropical Indian Ocean. The difference between the coupled and forced simulations in winter is due to colder ocean and a reduced evaporation over the ocean.

4.2. Seasonal timing of the monsoon response to ocean feedback

The impact of SST changes on the seasonal timing of monsoon is also investigated by analyzing the changes in the seasonal cycle of rainfall for monsoon regions and the changes in SST seasonal cycle in key regions. The positive ocean feedback on precipitation over Sahel

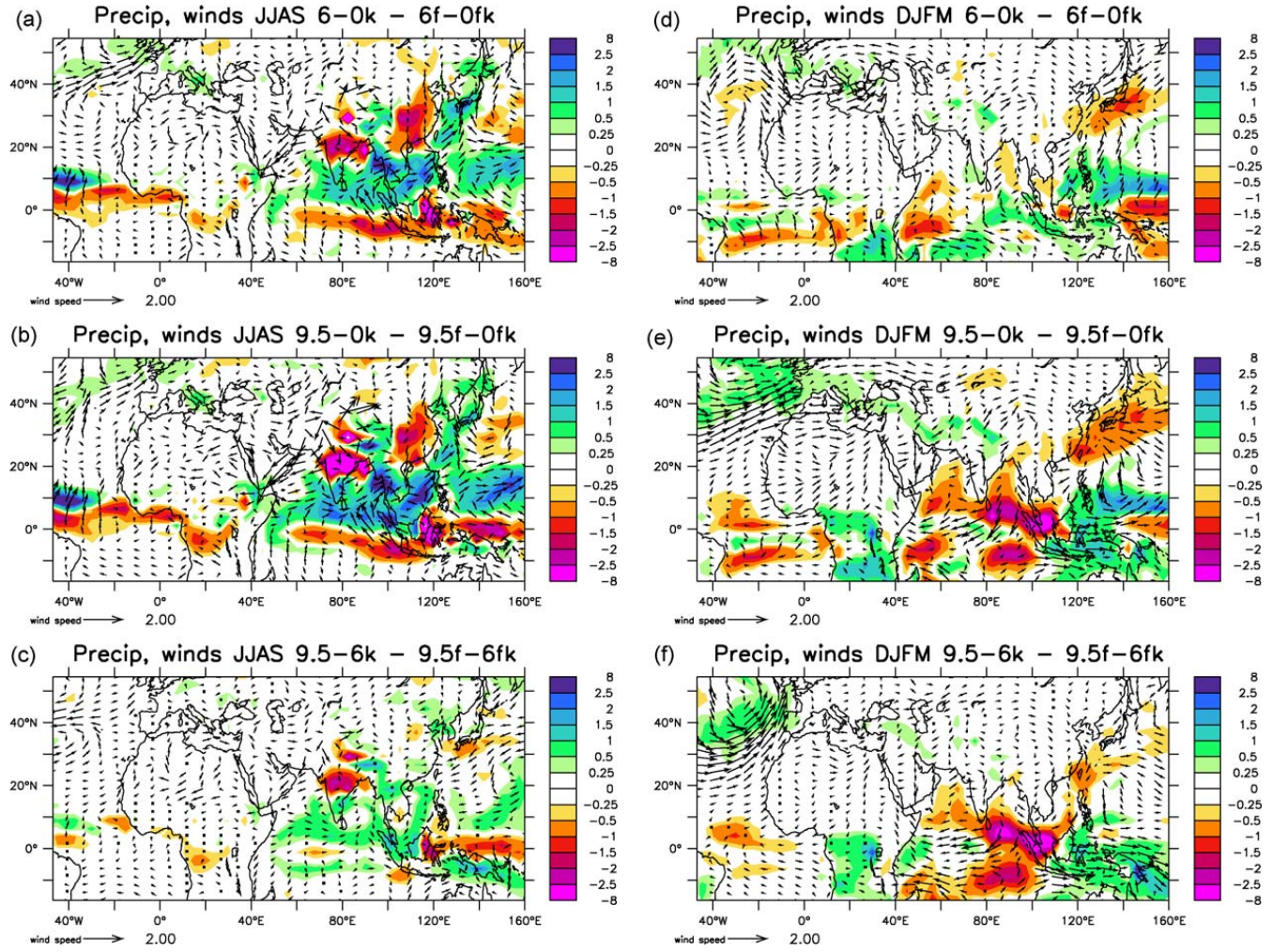

Fig. 6. Differences between coupled simulations and forced simulations of precipitation (mm/day) and surface winds (m/s) differences for JJAS between (a) 6–0 kyr BP (b) 9.5–0 kyr BP (c) 9.5–6 kyr BP; and (d), (e), (f) for DJFM.

Fig. 6. Différence de précipitation (mm/j) et de vent de surface (m/s) entre les simulations couplées et les simulations forcées pour JJAS (gauche) et DJFM (droite) et (a, d) 6–0 ka (b, e) 9,5–0 ka (c, f) 9.5–6 ka.

(Fig. 7a) seems to be predominant in the first part of the monsoon season, in June–July. Later, there is no difference for the change between 6 and 0 and 9.5 and 0k for the coupled and forced simulations. The cold tropical SST and the strengthening of the Atlantic dipole favours an earlier onset of the monsoon. The ocean feedback in August is slightly negative. It is however not possible to analyse further the simulations, since the slight difference between the versions of the atmospheric model used in the coupled and forced simulations produce different lengths of the African monsoon because of small changes in the land surface scheme. The gradient of SST between a northern tropical Atlantic box and a southern tropical Atlantic box (Fig. 4a) is very weak between 6 and 9.5k.

The seasonal cycle of precipitation changes over India in both coupled and forced simulations indicates the large negative feedback of the ocean in this region (Fig. 7b). However, at the beginning of the monsoon season, the ocean feedback on precipitation seems to be positive in June for the 6-0k difference. The SST seasonal cycle shape is considerably changed compared to present-day over the Indian Ocean (Fig. 4b). The dominant peak in spring at present-day becomes secondary at 6 and 9.5k compared to the SST peak in autumn. As a consequence, the Indian Ocean is cooler in spring and beginning of summer at 6k favouring the moisture advection towards the land. From July, it becomes warmer, especially at 9.5k, and favours the retreat of the moisture convergence over the ocean, reducing land precipitation over India. The negative ocean feedback does not affect the proportional change of precipitation over India between 6 and 9.5 kyr BP. The increase is consistent with the insolation forcing

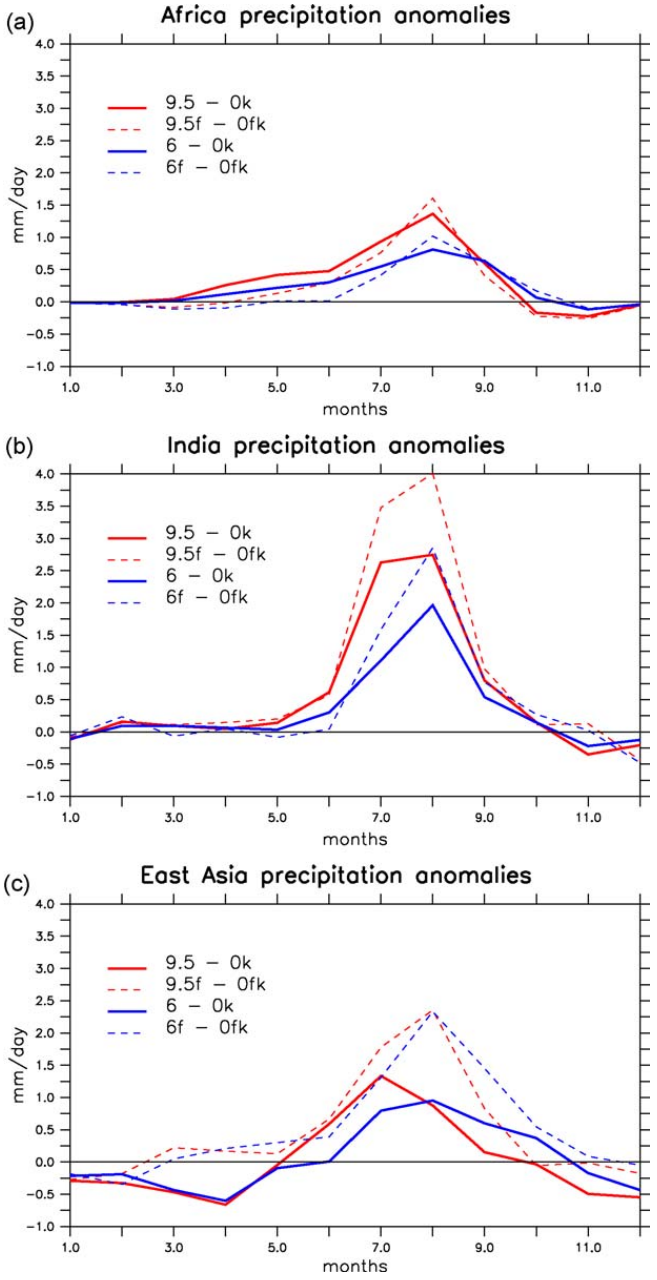

Fig. 7. Monthly land precipitation averaged over (a) North Africa (20° W–20° E, 7° N–18° N), (b) India (70° E–95° E, 10° N–35° N), (c) East Asia (105° E–125° E, 20° N–40° N).

Fig. 7. Évolution saisonnière des précipitations continentales moyennées sur (a) le Nord de l'Afrique (20° O–20° E, 7° N–18° N), (b) l'Inde (70° E–95° E, 10° N–35° N), et (c) l'Est de l'Asie (105° E–125° E, 20° N–40° N).

and the delay in the ocean response compared to Early Holocene.

The ocean feedback over East Asian monsoon is more complex and is not directly related to the surrounding surface ocean temperatures. It is strongly negative throughout the monsoon season (Fig. 7c), with a peak in August corresponding to a maximum warming of the tropical western Pacific and the north-western Pacific between 9.5 and 0k (Fig. 4c). However, the feedback is of similar amplitude between 6 and 9.5k (Fig. 6). As a conclusion on the relative amplifications between the monsoon subsystems, the ocean feedback does not explain the dominant amplification of the Indian monsoon between 6 and 9.5k in the coupled simulations, as it is also in this region that the negative feedback of the ocean is the strongest. The role of the precession and of the snow cover feedback over the Tibetan Plateau detailed in Marzin and Braconnot [25] are more plausible.

5. Conclusions

The role of the ocean feedback on monsoon precipitation during the Holocene is investigated by comparing 2 sets of experiments: coupled ocean–atmosphere simulations at 0, 6 and 9.5k and atmosphere-only simulations for the same periods forced by the SSTs of the control coupled simulation. The amplification of the Indian, East Asian and African monsoon systems is seen at 6 and 9.5k for both sets of simulations. Their relative amplification responding to different seasonal insolation forcings is specific to each system. The Indian monsoon is largely amplified between 6 and 9.5k, whereas the difference in land precipitation between these two periods is small over Sahel and East Asia. Mechanisms and the role of precession on these seasonal amplifications are detailed in Marzin and Braconnot [25] for the coupled simulations.

In the coupled simulations, the ocean responds to the seasonal insolation forcing by a delayed cooling in winter and warming in summer. Also, following the seasonal shift in the minimum and maximum of insolation forcing between Early and Mid Holocene, the ocean response is delayed by about one month at 6k. The Atlantic dipole anomaly with warmer SST to the north of 5° N and colder SST to the south of it strengthens the early stage of the African monsoon. The amplification of this dipole is similar at 6k and 9.5k, because the large insolation of 9.5k is partly compensated by higher SST along the Equator resulting from a damping of the equatorial upwelling. The effect of precession on the surface ocean changes is more highlighted in the Indian Ocean, the warm pool and the north-western Pacific with a maximum warming from July to September at 9.5k, and a warming at 6k that is smaller in amplitude but more delayed towards autumn. The results at 6k are consistent with Zhao et al. [35].

The ocean feedback on monsoon precipitation is shown to be consistent with previous studies [5,21,27,35]. It is positive at 6 and 9.5k over Sahel, especially in the first part of the monsoon season and strongly negative throughout the season for the Indian and East Asian monsoons. Ohgaito and Abe-Ouchi [27] have shown that the thermodynamic effect of the ocean feedback was dominant for the Asian monsoon changes and that the negative feedback was more important during early summer. This is also true in our case for the Indian monsoon but not for the East Asian monsoon. Our results are overall consistent with their findings even though a detailed comparison is not possible because of the difference in the area of interest.

The originality in this study relies on the fact that the three monsoon systems respond in different ways to insolation forcing and to ocean feedback for the three periods. The monsoon amplification is small between 6 and 9.5k over Sahel and East Asia whereas it is large over the Indian continent [25]. The ocean feedback over precipitation is positive for the African monsoon but of similar amplitude at 6 and 9.5k. Over the East-Asian area, it is negative but also of similar amplitude at 6 and 9.5k. However, the strong effect of the negative ocean feedback on the Indian monsoon is even larger at 9.5k than at 6k. Even though the ocean feedback plays a role on the amplitude and timing of the monsoon response to insolation changes, it does not explain the relative amplifications of the monsoon systems within the three periods [25]. These are related to the direct impact of the precession and to land surface processes.

Our results show that the ocean response in the Tropics results from a combination of direct insolation forcing, and feedbacks involving fresh water forcing and changes in the large scale atmospheric and ocean dynamics. The response of the mixed layer depth is large in some places, such as in the Indian Ocean, and locally affects the ocean inertia. The impact on the ocean biology needs to be analysed in depth to better understand the signature of the monsoon variations in time as reported from different marine proxies [33].

References

[1] P. Braconnot, O. Marti, Impact of precession on monsoon characteristics from coupled ocean atmosphere experiments: changes in Indian monsoon and Indian ocean climatology, Mar. Geology 201 (1–3) (2003) 23–34.

[2] P. Braconnot, S. Joussaume, O. Marti, N. de Noblet, Synergistic feedbacks from ocean and vegetation on the African monsoon response to Mid-Holocene insolation, Geophys. Res. Lett. 26 (16) (1999) 2481–2484.

[3] P. Braconnot, O. Marti, S. Joussaume, Y. Leclainche, Ocean feedback in response to 6 kyr BP insolation, J. Climate 13 (9) (2000) 1537–1553.

[4] P. Braconnot, S. Harrison, S. Joussaume, C. Hewitt, A. Kitoh, J. Kutzbach, Z. Liu, B. Otto-Bliesner, J. Syktus, L. Weber, The second phase of the Paleoclimate Modeling Intercomparison Project (PMIPII), Clivar Exchanges 8 (2003) 19–20.

[5] P. Braconnot, B. Otto-Bliesner, S. Harrison, S. Joussaume, J.Y. Peterchmitt, A. Abe-Ouchi, M. Crucifix, E. Driess-Chaert, T. Fichefet, C.D. Hewitt, M. Kageyama, A. Kitoh, A. Laine, M.F. Loutre, O. Marti, U. Merkel, G. Ramstein, P. Valdes, S.L. Weber, Y. Yu, Y. Zhao, Results of PMIP2 coupled simulations of the Mid-Holocene and Last Glacial Maximum - Part 1: experiments and large-scale features, Clim. Past 3 (2) (2007) 261–277.

[6] P. Braconnot, B. Otto-Bliesner, S. Harrison, S. Joussaume, J.Y. Peterchmitt, A. Abe-Ouchi, M. Crucifix, E. Driess-Chaert, T. Fichefet, C.D. Hewitt, M. Kageyama, A. Kitoh, M.F. Loutre, O. Marti, U. Merkel, G. Ramstein, P. Valdes, L. Weber, Y. Yu, Y. Zhao, Results of PMIP2 coupled simulations of the Mid-Holocene and Last Glacial Maximum - Part 2: feedbacks with emphasis on the location of the ITCZ and mid- and high latitudes heat budget, Clim. Past 3 (2) (2007) 279–296.

[7] P. Braconnot, C. Marzin, L. Gregoire, E. Mosquet, O. Marti, Monsoon response to changes in earth's orbital parameters: comparisons between simulations of the Eemian and of the Holocene, Clim. Past Discuss. 4 (2008) 459–493.

[8] T. Fichefet, M.A.M. Maqueda, Sensitivity of a global sea ice model to the treatment of ice thermodynamics and dynamics, J. Geophys. Res. 102 (C6) (1997) 12,609–12,646.

[9] D. Fleitmann, S.J. Burns, A. Mangini, M. Mudelsee, J. Kramers, I. Villa, U. Neff, A.A. Al-Subbary, A. Buettner, D. Hippler, A. Matter, Holocene ITCZ and Indian monsoon dynamics recorded in stalagmites from Oman and Yemen (Socotra), Quatern. Sci. Rev. 26 (1–2) (2007) 170–188.

[10] F. Gasse, Hydrological changes in the African tropics since the Last Glacial Maximum, Quatern. Sci. Rev. 19 (1–5) (2000) 189–211.

[11] H.Y. He, C.H. Sui, M.Q. Jian, Z.P. Wen, Lan GD, The evolution of tropospheric temperature field and its relationship with the onset of Asian summer monsoon, J. Meteorol. Soc. Japan 81 (5) (2003) 1201–1223.

[12] C.D. Hewitt, J.F.B. Mitchell, A fully coupled GCM simulation of the climate of the Mid-Holocene, Geophys. Res. Lett. 25 (3) (1998) 361–364.

[13] P. Hoelzmann, D. Jolly, S.P. Harrison, F. Laarif, R. Bonnefille, J.J. Pachur, Mid-Holocene land-surface conditions in northern Africa and the Arabian Peninsula: A data set for the analysis of biogeophysical feedbacks in the climate system, Global Biogeochem. Cycles 12 (1) (1998) 35–51.

[14] F. Hourdin, I. Musat, S. Bony, P. Braconnot, F. Codron, J.L. Dufresne, L. Fairhead, M.A. Filiberti, P. Friedlingstein, J.Y. Grandpeix, G. Krinner, P. Levan, Z.X. Li, F. Lott, The LMDZ4 general circulation model: climate performance and sensitivity to parametrized physics with emphasis on tropical convection, Climate Dyn. 27 (7–8) (2006) 787–813.

[15] D. Jolly, I.C. Prentice, R. Bonnefille, A. Ballouche, M. Bengo, P. Brenac, G. Buchet, D. Burney, J.P. Cazet, R. Cheddadi, T. Edorh, H. Elenga, S. Elmoutaki, J. Guiot, F. Laarif, H. Lamb, A.M. Lezine, J. Maley, M. Mbenza, O. Peyron, M. Reille, I. Reynaud-Farrera, G. Riollet, J.C. Ritchie, E. Roche, L. Scott, I. Ssemmanda, H. Straka, M. Umer, E. Van Campo, S. Vilimumbalo, A. Vincens, M. Waller, Biome reconstruction from pollen and plant

macrofossil data for Africa and the Arabian peninsula at 0 and 6000 years, J. Biogeography 25 (6) (1998) 1007–1027.

[16] S. Joussaume, K.E. Taylor, P. Braconnot, J.F.B. Mitchell, J.E. Kutzbach, S.P. Harrison, I.C. Prentice, A.J. Broccoli, A. Abe-Ouchi, P.J. Bartlein, C. Bonfils, B. Dong, J. Guiot, K. Herterich, C.D. Hewitt, D. Jolly, J.W. Kim, A. Kislov, A. Kitoh, M.F. Loutre, V. Masson, B. McAvaney, N. McFarlane, N. de Noblet, W.R. Peltier, J.Y. Peterschmitt, D. Pollard, D. Rind, J.F. Royer, M.E. Schlesinger, J. Syktus, S. Thompson, P. Valdes, G. Vettoretti, R.S. Webb, U. Wyputta, Monsoon changes for 6000 years ago: Results of 18 simulations from the Paleoclimate Modeling Intercomparison Project (PMIP), Geophys. Res. Lett. 26 (7) (1999) 859–862.

[17] G. Krinner, N. Viovy, N. de Noblet-Ducoudre, J. Ogee, J. Polcher, P. Friedlingstein, P. Ciais, S. Sitch, I.C. Prentice, A dynamic global vegetation model for studies of the coupled atmosphere-biosphere system, Global Biogeochem. Cycles 19 (1) (2005) GB1015.

[18] J.E. Kutzbach, Z. Liu, Response of the African monsoon to orbital forcing and ocean feedbacks in the Middle Holocene, Science 278 (5337) (1997) 440–443.

[19] A.M. Lézine, J.J. Tiercelin, C. Robert, J.F. Saliège, S. Cleuziou, M.L. Inizan, F. Braemer, Centennial to millennial-scale variability of the Indian monsoon during the Early Holocene from a sediment, pollen and isotope record from the desert of Yemen, Palaeogeogr. Palaeoclimatol. Palaeoecol. 243 (3–4) (2007) 235–249.

[20] Z. Liu, B. Otto-Bliesner, J. Kutzbach, L. Li, C. Shields, Coupled climate simulation of the evolution of global monsoons in the Holocene, J. Climate 16 (15) (2003) 2472–2490.

[21] Z. Liu, S.P. Harrison, J. Kutzbach, B. Otto-Bliesner, Global monsoons in the Mid-Holocene and oceanic feedback, Climate Dyn. 22 (2–3) (2004) 157–182.

[22] G. Madec, P. Delécluse, M. Imbard, C. Levy, OPA version 8.1 ocean general circulation model reference manual, LODYC/IPSL, Paris, France, 11, 1998.

[23] O. Marti, P. Braconnot, J. Bellier, S. Bony, P. Brockmann, P. Cadule, A. Caubel, S. Denvil, J.L. Dufresne, L. Fairhead, M.A. Filiberti, M.A. Foujols, T. Fichefet, P. Friedlingstein, H. Goosse, J.Y. Grandpeix, F. Hourdin, G. Krinner, C. Levy, G. Madec, I. Musat, N. de Noblet, J. Polcher, C. Talandier, The New IPSL Climate System Model: IPSL-Cm4, Note du Pôle de Modélisation n° 26: ISSN 1288-1619, 2005.

[24] O. Marti, P. Braconnot, J. Dufresne, J.-L. Bellier, R. Benshila, S. Bony, P. Brockmann, P. Cadule, A. Caubel, F. Codron, S. Denvil, L. Fairhead, T. Fichefet, M.A. Foujols, P. Friedlingstein, H. Goosse, J.Y. Grandpeix, E. Guilyardi, F. Hourdin, A. Idelkadi, M. Kageyama, G. Krinner, C. Levy, G. Madec, I. Musat, D. Swingedouw, C. Talandier, Key features of the IPSL ocean atmosphere model and its sensitivity to atmospheric resolution, Climate Dyn. 2009. DOI: 10.1007/s00.382-009-0640-6.

[25] C. Marzin, P. Braconnot, Variations of Indian and African monsoons induced by insolation changes at 6 and 9.5 kyr BP, Climate Dyn. 33 (2009) 215–231.

[26] G.A. Meehl, C. Covey, T. Delworth, M. Latif, B. McAvaney, J.F.B. Mitchell, R.J. Stouffer, K.E. Taylor, The WCRP CMIP3 multimodel dataset - A new era in climate change research, Bull. Amer. Meteor. Soc. 88 (9) (2007), 1383.

[27] R. Ohgaito, A. Abe-Ouchi, The role of ocean thermodynamics and dynamics in Asian summer monsoon changes during the Mid-Holocene, Climate Dyn. 29 (1) (2007) 39–50.

[28] S. Prasad, Y. Enzel, Holocene paleoclimates of India, Quatern. Res. 66 (3) (2006) 442–453.

[29] I.C. Prentice, T. Webb, BIOME 6000: reconstructing global mid-Holocene vegetation patterns from palaeoecological records, J. Biogeography 25 (6) (1998) 997–1005.

[30] M.J. Rodwell, B.J. Hoskins, Monsoons and the dynamics of deserts, Quart. J. Roy. Meteor. Soc. 122 (534) (1996) 1385–1404.

[31] S. Solomon, D. Qin, M. Manning, Z. Chen, M. Marquis, K.B. Averyt, M. Tignor, H.L. Miller (eds.) IPCC 2007: Climate Change 2007: The Physical Basis. Contribution of Working Group I to the Fourth Assessment Report of the Intergovernmental Panel on Climate Change, Cambridge University Press, Cambridge, United Kingdom and New York, NY, USA, 2007.

[32] L. Terray, E. Sevault, E. Guilyardi, O. Thual, The OASIS coupler user guide version 2.0, 1995.

[33] P.X. Wang, S. Clemens, L. Beaufort, P. Braconnot, G. Ganssen, Z.M. Jian, P. Kershaw, M. Sarnthein, Evolution and variability of the Asian monsoon system: state of the art and outstanding issues, Quatern. Sci. Rev. 24 (5–6) (2005) 595–629.

[34] H. Wright, J. Kutzbach, T. Webb III, W. Ruddiman, F. Street-Perrot, P. Bartlein (Eds.) Global Climates since the Last Glacial Maximum, University of Minnesota Press, 1993.

[35] Y. Zhao, P. Braconnot, O. Marti, S.P. Harrison, C. Hewitt, A. Kitoh, Z. Liu, U. Mikolajewicz, B. Otto-Bliesner, S.L. Weber, A multi-model analysis of the role of the ocean on the African and Indian monsoon during the Mid-Holocene, Climate Dyn. 25 (7–8) (2005) 777–800.

5.3 Influence du flux d'eau douce en Atlantique Nord et de la calotte de glace sur l'évolution des moussons à 9.5 ka

Impact of a meltwater flux and of the remnant ice sheet on monsoons at 9.5kyr BP

C. Marzin[1], P. Braconnot[1] and M. Kageyama[1]

The Northern Hemisphere summer monsoons are known to have been more intense than present day during the Early Holocene due to higher insolation during boreal summer. [*Marzin and Braconnot*, 2009a] have highlighted the differences of behaviour between the monsoon subsystems in response to the precession variation between Early and Mid-Holocene. Here, we conduct sensitivity experiments at 9.5kyr BP to the remnant ice sheet over North America and Europe at that time, and to a meltwater flux in the North Atlantic. These forcings affect the intensity of the Indian and African monsoons but do not alterate their relative amplifications between Early and Mid-Holocene. However, the East Asian monsoon is highly sensitive to the larger ice sheets. Our study highlights the complexity of the interaction between insolation, ice sheets, meltdowns and monsoons and shows that each monsoon system responds differently to these forcings.

1. Introduction

From the beginning to the Mid-Holocene, a humid period was established in the Tropics, emerging from the last glacial climate. The predominant climate forcing was the intensification of the seasonal cycle of insolation in the Northern Hemisphere (NH), due to the precession bringing the Earth closer to the Sun during boreal summer. The intensified land/ocean temperature contrast in the NH resulted in more intense monsoon systems as indicated by paleoclimatic evidences from West Africa, India and East Asia [*Wright et al.*, 1993]. Modeling past climates offers a possibility to shed light on the mechanisms of the climate changes and to evaluate the models.

A considerable effort has been realized by the paleoclimate community to compare results from models and paleorecords for the Mid-Holocene (6kyr BP) and the Last Glacial Maximum (LGM, 21kyr BP) periods [*Joussaume et al.*, 1999; *Braconnot et al.*, 2007]. However, in earlier studies, the analysis of monsoons in paleoclimate simulations were focused on the Early Holocene [*Kutzbach*, 1981; *Kutzbach and Ottobliesner*, 1982] when the summer insolation of the NH is at the maximum. Eventhough the precession is believed to be the predominant forcing during the Holocene, the presence of the remnant ice sheets over North America and northern Europe during the Early Holocene must have played a role on the monsoon changes. [*Renssen et al.*, 2009] have recently shown the sensitivity of the Early Holocene NH climate to the remnant Laurentide ice sheet. The relationship between weak monsoons and a cool high latitude climate and meltdowns has been highlighted in several modelling studies but is not fully understood [*Clement and Peterson*, 2008; *Cheng et al.*, 2009] due to the complexity of tropical-extratropical interactions [*Yang and Liu*, 2005; *Ding and Wang*, 2005].

Marzin and Braconnot [2009a] and *Marzin and Braconnot* [2009b] have analyzed the intensification of the Indian and Asian monsoons due to the changes in insolation seasonal cycle at 6 and 9.5kyr BP compared to present and have shown that the local responses can vary between the subsystems and that the effect of the precession on the seasonality is essential. The objective of this study is to provide sensitivity experiments to analyze separately the impact of a remnant ice sheet and of a meltwater flux in the North Atlantic on monsoon changes at 9.5kyr BP that were not included in the previous analyses. Finally the relative importance of these additional effects compared to the insolation change between 9.5kyr BP and the present climate is discussed.

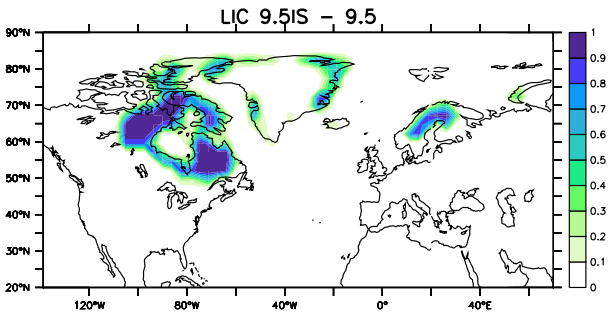

Figure 1. Differences in land ice grid-point fraction between 9.5IS and 9.5

2. Model and experiments

The experiments were conducted with the IPSL-CM4 ocean-atmosphere coupled model [*Marti et al.*, 2009], with the same version as for the PMIP [*Braconnot et al.*, 2007] and IPCC AR4 experiments [*Meehl et al.*, 2007]. We consider as a reference here a simulation of the 9.5kyr BP climate for which only the changes in orbital parameters (derived from *Berger* [1978]) are accounted for. A sensitivity experiment to a meltwater flux in the North Atlantic (9.5F) is set up using the land ice melting parametrization described in *Swingedouw et al.* [2006, 2009]. The meltwater resulting from this "calving" is distributed over a large area in the Arctic and North Atlantic and represents in this simulation a flux of 0.07Sv over 40°N. The sensitivity experiment to the remnant ice sheet at 9.5 kyr BP (9.5IS) is using the ICE-5G ice sheet reconstruction [*Peltier*, 2004] as boundary conditions. Fig.1 illustrates the differences in the Laurentide, Greenland and Fennoscandian ice sheet extensions between the 9.5IS and 9.5 simulations. The ice sheet representation used is coarse and should be viewed as a sensitivity experiment only. In particular, the coastlines are

[1]LSCE/IPSL, CEA-CNRS-UVSQ, Orme des Merisiers, Gif-sur-Yvette, France.

0094-8276/10/$5.00

kept the same. The experiments are respectively 600, 300 and 480 year long for 9.5, 9.5F and 9.5IS. The 100 years annual mean cycle is computed from the 100 (for 9.5F) to 250 (9.5 and 9.5IS) years of the simulations. The climatic changes are analyzed for June to September (JJAS) average in order to cover the whole summer monsoon season. Similar experiments as 9.5 and 9.5F have been conducted for the Mid-Holocene (6 and 6F), *Swingedouw et al.* [2009], and will only be discussed for analogy at the end of this study. More details on the coupled model simulations and on the evaluation of the representation of monsoon systems in IPSL-CM4 are given in *Marzin and Braconnot* [2009a].

3. Results

The meltwater flux in the North Atlantic and the larger ice sheets are both responsible for a large cooling of the Northern Hemisphere (Fig.2a and b). However this cooling differs in intensity and geographical distribution. For 9.5F, the meltwater flux results in a large cooling of the North Atlantic as well as a the well known bipolar seesaw pattern [*Vellinga and Wood*, 2002; *Stouffer et al.*, 2006] which consists of a cold tongue in the northern tropical Atlantic and a warmer SST to the south. The cooling of the North Atlantic is propagated throughout the Eurasian continent, extending to the north-western Pacific (Fig.2a). It induces an anomalous cyclonic circulation in the Atlantic and reduces the Tibetan Plateau heat low. The change in land/sea contrast leads to an eastward shift of the Islandic low. The effect of the ice sheet results in a more intense surface cooling that spreads downstream (Fig.2b). The Indian and Pacific oceans are colder as well as the tropical continents. The maximum cooling is depicted over North America, the Sahara and Eurasia with a strong high pressure anomaly and does not extend to the north-western Pacific in contrast to the effect of the meltwater flux. In addition the seesaw pattern in the Atlantic is not as developped as in 9.5F. This can be related to differences in the change in the Atlantic Ocean heat tranport. In both cases, the Atlantic heat transport is reduced in the Northern Hemisphere and enhanced south of the Equator. However the reduction is much larger (0.25 PW against 0.8PW) in 9.5F than in 9.5IS, leading to larger warming in 9.5F.

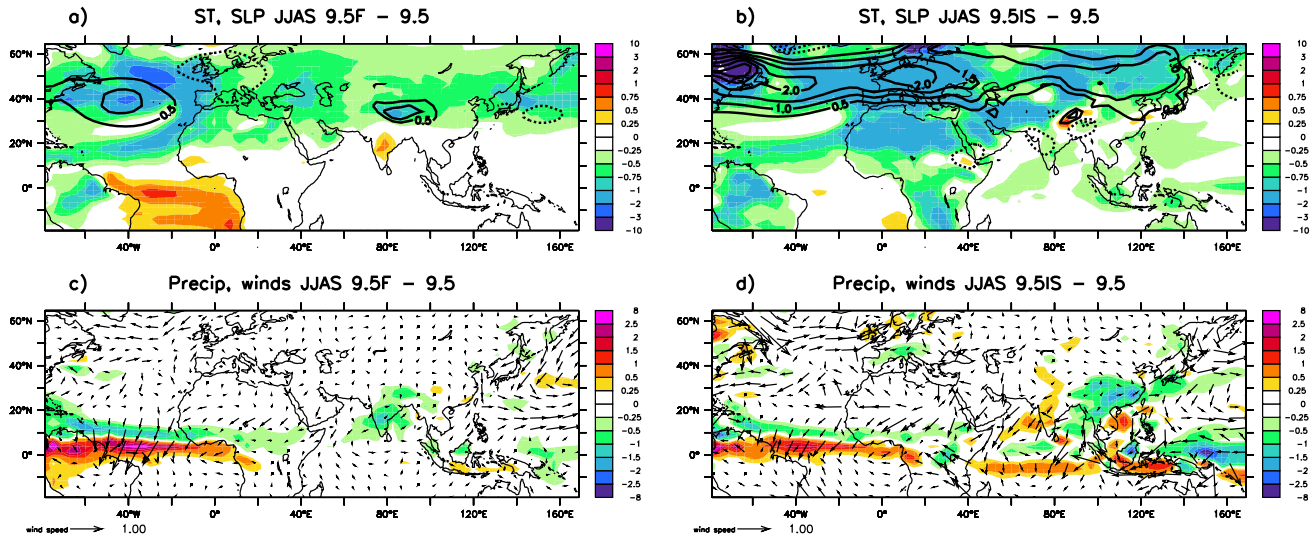

Figure 2. Differences in surface temperature (K) and sea level pressure (hPa) between a) 9.5F and 9.5, and b) 9.5IS and 9.5. Differences in precipitation (mm/day) and 10 meters winds (m/s) between c) 9.5F and 9.5, and d) 9.5IS and 9.5.

The ITCZ shifts southward in the tropical Atlantic in both sensitivity experiments, accompanied by a reduction of the precipitation over the Sahel and a weakening of the African monsoon flow (Fig.2c and d). The impact of the SST pattern in the northern tropical Atlantic in controlling the inland penetration of the African monsoon has been previously demonstrated [*Zhao et al.*, 2007; *Marzin and Braconnot*, 2009b].

On the contrary, the results for the Asian monsoon systems differ considerably. The meltwater flux impact induces very small SST changes over the Indian and Pacific Oceans. However the Indian monsoon is clearly diminished with negative anomalies of precipitation over the subcontinent and a weakening of the cross-equatorial flow (Fig.2c). The East Asian summer monsoon is not affected. The impact of the bigger ice sheet on the hydrology of the tropical Asian climate is much larger and much more complex (Fig.2d). The oceanic branch of the ITCZ is shifted southward over the Indian Ocean and over the Western Pacific. The East Asian monsoon rainfall is decreased by about 0.5 to 1mm/day,

but this anomaly is not monsoon-specific and is present throughout the year (Fig.4b). The weakening of the thermal low over north-east Asia and the weakening of the north-western Pacific high reduce the meridional and zonal gradients of surface pressure. However, the response of the Indian monsoon is counterintuitive as precipitation is enhanced to the western part of the Indian subcontinent but are reduced over the Bay of Bengal (actually reduced at the beginning of the monsoon season and enhanced later in the season, Fig.4b). The cross-equatorial flow is weakened but stronger south-westerly winds are observed locally. This local response of the Indian monsoon may be related to the lower sea level pressure just south of the Tibetan Plateau (Fig.2b).

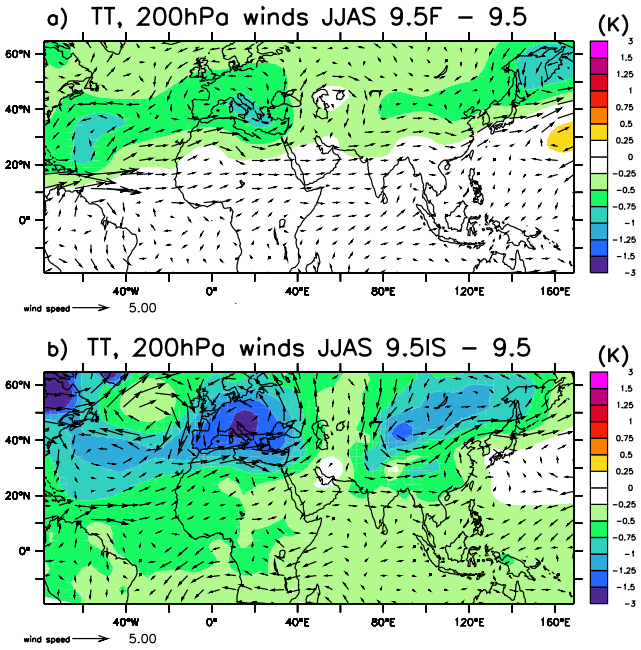

Figure 3. Differences in tropospheric temperature (averaged from 200 to 500hPa) and 200hPa winds between a) 9.5F and 9.5, and b) 9.5IS and 9.5.

The SST changes over the Indian Ocean and the western Pacific are small. This suggests that the Asian monsoon systems are affected by both forcings mostly through the atmospheric bridge over Eurasia. The cooling induced by the meltwaterflux or the topography and the albedo of the ice sheets alters the characteristics of the stationary waves downstream. The response of the troposphere is barotropic as the cooling of the tropospheric temperature (TT, averaged from 200 to 500hPa) presents the same patterns as at the surface (Fig.3a and b). The TT meridional and zonal gradients linked with the heating over the Tibetan Plateau are essential to the development of the Asian summer monsoon [*Yanai et al.*, 1992; *He et al.*, 2003]. They are significantly weakened for 9.5IS. The two forcings affect the same centres of perturbation of the westerly jet stream, over Europe, the Caspian Sea and north-east Asia. However the strength and extent of the perturbation over north-east Asia is larger in the 9.5IS experiment and may be responsible for the different responses of the Indian and East Asian monsoons between the two experiments. This hypothesis would need further analysis as the connection between the mid-latitude perturbations of the jet stream and monsoons is not yet fully understood [*Ding and Wang*, 2005].

4. Discussion

Marzin and Braconnot [2009a] have shown that the NH monsoon systems were enhanced at 9.5kyr BP compared to 6kyr BP (experiment 6) and the preindustrial time (experiment 0) in response to the intensified seasonal cycle of insolation, the NH summer occuring at the perihelion. They have highlighted the differences in response of the Indian and the African monsoons. The rainfall over India was significantly increased between 6 and 9.5kyr BP whereas it was of similar amplitude over the Sahel, mostly because of the seasonal effect of the precession. How does the influence of the land ice melting (also analyzed for 6kyr BP with the experiment 6F) and of the larger ice sheet affect these relative amplifications of monsoons during the Holocene? Fig.4 illustrates the annual cycle of continental rainfall differences from 0kyr BP for the three monsoon regions for all the experiments. The Indian monsoon intensity is reduced both at 9.5F and 6F compared to 9.5 and 6, and increased at 9.5IS. The African monsoon is weakened similarly between 9.5IS and 9.5, 9.5F and 9.5 and 6F and 6. Therefore, the conclusions on the relative amplifications for these two monsoon systems are not modified with these sensitivity experiments and show that their evolution is dominated by the annual cycle of insolation and that the timing of the insolation induced by precession is a key factor. The East Asian monsoon is not affected by the meltwater flux both at 6F and 9.5F, however, it is significantly weakened in 9.5IS and is even weaker than at 6kyr BP. The East Asian monsoon is the most sensitive to the remnant ice sheet at the Early Holocene and this counteracts the insolation impact.

The land ice melting experiments can be qualitatively compared to some extent to hosing experiments that are aiming to analyze the climatic response to a slowing down of the Atlantic meridional overturning circulation. Our results for the Early and Mid-Holocene are compatible with studies that show a reduction in monsoons intensity over India and Africa [*Chang et al.*, 2008; *Zhang and Delworth*, 2005; *Lu et al.*, 2008]. However, *Swingedouw et al.* [2009] have shown that the mean cli-

mate can alter the extent and the mechanisms of the remote impacts of this North Atlantic forcing.

Our results are different from the sensitivity to ice sheets during the last glacial maximum, when the NH cooling induced a large tropical drying [*Braconnot et al.*, 2007; *Yanase and Abe-Ouchi*, 2007]. The mean NH climate during the Early Holocene is dominated by the intense insolation annual cycle. *Yin et al.* [2008, 2009] have performed an extensive study to analyze the sensitivity of the East Asian summer monsoon to the size and location of ice sheets for the cool interglacial MIS-13 with a similar precession as 9.5kyr BP (at 506 kyr BP). Their experiments obtained with the LOVECLIM model of intermediate complexity reveals that the north American and Eurasian ice sheets significantly amplify the East Asian monsoon precipitation, however they show that similarly to our study they induce a decrease of the African monsoon and an amplification of the Indian monsoon for small ice sheets *Yin et al.* [2009]. *Masson et al.* [2000] have also shown that high insolation during boreal summer can generate stronger monsoons than at present day even under glacial conditions. This illustrates the complexity of the interaction between ice sheet, orbital parameters and monsoon evolutions.

The originality of this study relies on the differences in behaviour of the monsoon systems in response to diverse forcings such as the insolation, the land ice melting and the extension of ice sheets. The mechanisms of the combined influence of insolation and ice sheets on monsoons need further investigation and more model comparison experiments in order to better interprete the paleoclimatic reconstructions. It also questions the role of the Atlantic SST patterns in triggering the teleconnections from the north Atlantic to the different monsoon regions. This will shed light on the tropical climate transition from the last deglaciation to the building up of the Humid period during the Early Holocene.

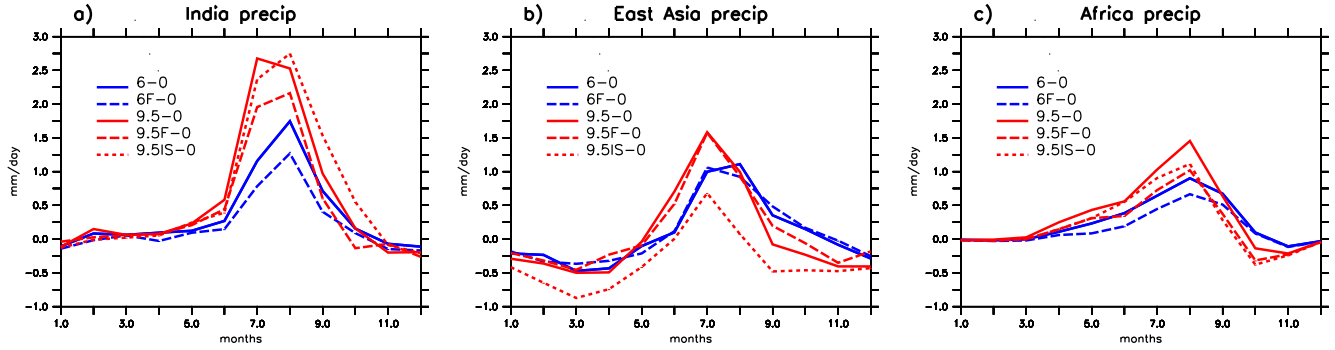

Figure 4. Seasonal cycle of continental rainfall (mm/day) difference with 0kyr BP for 6, 6F, 9.5, 9.5F, 9.5IS over a) India, b) East Asia, c) Africa

Acknowledgments. Charline Marzin is funded by a grant from the Commissariat a l'Energie Atomique. Computer time was provided by the Centre National de la Recherche Scientifique (IDRIS computing center) and the Commissariat a l'Energie Atomique (CCRT computing center). This work is a contribution to the French "ANR blanc" PICC project and to the "ANR Vulnerabilite Climat et Milieu" SAHELP project.

References

Berger, A. L. (1978), Long-Term Variations Of Daily Insolation And Quaternary Climatic Changes, *J. Atmos. Sci.*, *35*(12), 2362–2367.

Braconnot, P., et al. (2007), Results of PMIP2 coupled simulations of the Mid-Holocene and Last Glacial Maximum - Part 1: experiments and large-scale features, *Clim. Past*, *3*(2), 261–277.

Chang, P., R. Zhang, W. Hazeleger, C. Wen, X. Q. Wan, L. Ji, R. J. Haarsma, W. P. Breugem, and H. Seidel (2008), Oceanic link between abrupt changes in the north atlantic ocean and the african monsoon, *Nature Geoscience*, *1*(7), 444–448.

Cheng, H., R. L. Edwards, W. S. Broecker, G. H. Denton, X. G. Kong, Y. J. Wang, R. Zhang, and X. F. Wang (2009), Ice age terminations, *Science*, *326*(5950), 248–252.

Clement, A. C., and L. C. Peterson (2008), Mechanisms of abrupt climate change of the last glacial period, *Reviews Of Geophysics*, *46*(4), RG4002.

Ding, Q. H., and B. Wang (2005), Circtunglobal teleconnection in the northern hemisphere summer, *Journal Of Climate*, *18*(17), 3483–3505.

He, H. Y., C. H. Sui, M. Q. Jian, Z. P. Wen, and G. D. Lan (2003), The evolution of tropospheric temperature field and its relationship with the onset of asian summer monsoon, *Journal Of The Meteorological Society Of Japan*, *81*(5), 1201–1223.

Joussaume, S., et al. (1999), Monsoon changes for 6000 years ago: Results of 18 simulations from the Paleoclimate Modeling In-

tercomparison Project (PMIP), *Geophys. Res. Lett.*, *26*(7), 859–862.

Kutzbach, J. E. (1981), Monsoon climate of the early holocene - climate experiment with the earths orbital parameters for 9000 years ago, *Science*, *214*(4516), 59–61.

Kutzbach, J. E., and B. L. Ottobliesner (1982), The sensitivity of the african-asian monsoonal climate to orbital parameter changes for 9000 years bp in a low-resolution general-circulation model, *Journal Of The Atmospheric Sciences*, *39*(6), 1177–1188.

Lu, R. Y., W. Chen, and B. W. Dong (2008), How does a weakened atlantic thermohaline circulation lead to an intensification of the enso-south asian summer monsoon interaction?, *Geophysical Research Letters*, *35*(8), L08,706.

Marti, O., et al. (2009), Key features of the ipsl ocean atmosphere model and its sensitivity to atmospheric resolution, *Climate Dynamics*, pp. DOI 10.1007/s00,382–009–0640–6.

Marzin, C., and P. Braconnot (2009a), Variations of indian and african monsoons induced by insolation changes at 6 and 9.5 kyr bp, *Climate Dynamics*, *33*(2-3), 215–231.

Marzin, C., and P. Braconnot (2009b), The role of the ocean feedback on asian and african monsoon variations at 6 kyr and 9.5 kyr bp, *Comptes Rendus Geoscience*, *341*(8-9), 643–655.

Masson, V., P. Braconnot, J. Jouzel, N. de Noblet, R. Cheddadi, and O. Marchal (2000), Simulation of intense monsoons under glacial conditions, *Geophys. Res. Lett.*, *27*(12), 1747–1750.

Meehl, G. A., C. Covey, T. Delworth, M. Latif, B. McAvaney, J. F. B. Mitchell, R. J. Stouffer, and K. E. Taylor (2007), The WCRP CMIP3 multimodel dataset - A new era in climate change research, *Bull. Amer. Meteor. Soc.*, *88*(9), 1383–+.

Peltier, W. R. (2004), Global glacial isostasy and the surface of the ice-age earth: The ice-5g (vm2) model and grace, *Annual Review Of Earth And Planetary Sciences*, *32*, 111–149.

Renssen, H., H. Seppa, O. Heiri, D. M. Roche, H. Goosse, and T. Fichefet (2009), The spatial and temporal complexity of the holocene thermal maximum, *Nature Geoscience*, *2*(6), 410–413.

Stouffer, R. J., et al. (2006), Investigating the causes of the response of the thermohaline circulation to past and future climate changes, *Journal Of Climate*, *19*(8), 1365–1387.

Swingedouw, D., P. Braconnot, and O. Marti (2006), Sensitivity of the atlantic meridional overturning circulation to the melting from northern glaciers in climate change experiments, *Geophysical Research Letters*, *33*(7), L07,711.

Swingedouw, D., J. Mignot, P. Braconnot, E. Mosquet, M. Kageyama, and R. Alkama (2009), Impact of freshwater release in the north atlantic under different climate conditions in an oagcm, *Journal Of Climate*, *22*(23), 6377–6403.

Vellinga, M., and R. A. Wood (2002), Global climatic impacts of a collapse of the atlantic thermohaline circulation, *Climatic Change*, *54*(3), 251–267.

Wright, H., J. Kutzbach, T. Webb III, W. Ruddiman, F. Street-Perrot, and P. Bartlein (Eds.) (1993), *Global Climates since the Last Glacial Maximum*, University of Minnesota Press.

Yanai, M. H., C. F. Li, and Z. S. Song (1992), Seasonal Heating Of The Tibetan Plateau And Its Effects On The Evolution Of The Asian Summer Monsoon, *J. Meteor. Soc. Japan*, *70*(1B), 319–351.

Yanase, W., and A. Abe-Ouchi (2007), The lgm surface climate and atmospheric circulation over east asia and the north pacific in the pmip2 coupled model simulations, *Climate Of The Past*, *3*(3), 439–451.

Yang, H. J., and Z. Y. Liu (2005), Tropical-extratropical climate interaction as revealed in idealized coupled climate model experiments, *Climate Dynamics*, *24*(7-8), 863–879.

Yin, Q. Z., A. Berger, E. Driesschaert, H. Goosse, M. F. Loutre, and M. Crucifix (2008), The eurasian ice sheet reinforces the east asian summer monsoon during the interglacial 500 000 years ago, *Climate Of The Past*, *4*(2), 79–90.

Yin, Q. Z., A. Berger, and M. Crucifix (2009), Individual and combined effects of ice sheets and precession on mis-13 climate, *Climate Of The Past*, *5*(2), 229–243.

Zhang, R., and T. L. Delworth (2005), Simulated tropical response to a substantial weakening of the atlantic thermohaline circulation, *Journal Of Climate*, *18*(12), 1853–1860.

Zhao, Y., P. Braconnot, S. P. Harrison, P. Yiou, and O. Marti (2007), Simulated changes in the relationship between tropical ocean temperatures and the western African monsoon during the mid-Holocene, *Climate Dyn.*, *28*(5), 533–551.

P. Braconnot, LSCE/IPSL, CEA-CNRS-UVSQ, Orme des Merisiers, Gif-sur-Yvette, France. (pascale.braconnot@lsce.ipsl.fr)

M. Kageyama, LSCE/IPSL, CEA-CNRS-UVSQ, Orme des Merisiers, Gif-sur-Yvette, France. (masa.kageyama@lsce.ipsl.fr)

C. Marzin, LSCE/IPSL, CEA-CNRS-UVSQ, Orme des Merisiers, Gif-sur-Yvette, France. (charline.marzin@lsce.ipsl.fr)

5.4 Impact d'un évènement de type Heinrich sur les systèmes de mousson en climat glaciaire

5.4.1 Impact d'un évènement de type Heinrich sur la mousson indienne en climat glaciaire : comparaison modèle/données

Manuscript prepared for Clim. Past
with version 3.2 of the LaTeX class copernicus.cls.
Date: 12 January 2011

Impact of rapid events on the Indian monsoon under glacial conditions: a model/data comparison study

C. Marzin[1,*], N. Kallel[2], M. Kageyama[1], J.-C. Duplessy[1], and P. Braconnot[1]

[1]LSCE/IPSL, CEA-CNRS-UVSQ, Orme des Merisiers, Gif-sur-Yvette, France
[2]Faculté des Sciences de Sfax, Tunisia
[*]now at Met Office, Exeter, United Kingdom

Correspondence to: C. Marzin
(charline.marzin@metoffice.gov.uk)

Abstract. Several paleoclimate records like China loess sequence or upwelling indicators present large variations of the Asian monsoon system during the last glaciation. Here, a unique record in the Northern Andaman Sea is used to reconstruct the variations of the hydrological cycle of the Bay of Bengal. The high resolution salinity record of core MD77-176 displays large millennial scale oscillations over the period 40,000 to 11,000 yr BP that are synchronous with the Greenland ice core record of changes in polar air temperature during the last glaciation. Events of low and high salinity in the Bay of Bengal show that the Indian monsoon is extremely sensitive to abrupt climatic variations in the North Atlantic. A modelling experiment with the IPSL-CM4 model is used to represent such rapid event in the North Atlantic under glacial conditions by increasing the freshwater flux in the North Atlantic and reducing the intensity of the Atlantic meridional overturning circulation. This freshwater hosing results in a weakening of the Indian monsoon rainfall and circulation. The changes in the continental runoff and local hydrological cycle are responsible for the changes in salinity of the Bay of Bengal in the model. Additional sensitivity experiments are produced to analyse the teleconnection mechanisms between the North Atlantic and the Indian monsoon. The changes over the tropical Atlantic are shown to be essential in triggering perturbations of the subtropical jet over Eurasia that in turn affect the intensity of the Indian monsoon.

1 Introduction

During the last glaciation, the presence of large ice sheets and reduced atmospheric CO_2 concentration resulted in a drier climate and weaker monsoon systems over Asia observed in several paleo-

records. Yanase and Abe-Ouchi (2007) have shown that a reduction in moisture transport resulted in less precipitation over East Asia at the Last Glacial Maximum (LGM). The Paleoclimate Modeling Intercomparison Project 2 (PMIP2) indicates that the Indian monsoon rainfall was reduced in all models at the LGM (up to 1.7 mm/day, Braconnot et al. (2007)).

However, conditions prevailing during LGM are not representative of the whole glaciation. The climate of the last glaciation was characterized by rapid oscillations of air temperature over Greenland called Dansgaard/Oeschger (D/O) events and by Heinrich events (Bond et al., 1992; Broecker et al., 1992; Dansgaard et al., 1993; Grootes et al., 1993; Meese et al., 1997). Correlative climate changes have been identied in high resolution climate records from areas as distant as Santa Barbara Basin (Behl and Kennett, 1996), western and southern Europe (Thouveny et al., 1994; Allen et al., 1999), Socotra Island in the Arabian Sea (Burns et al., 2003), China (Wang et al., 2001). The Asian monsoon, which depends on orbitally-controlled changes of insolation in the 104 - 105 years frequency band (Xiao et al., 1999; Rousseau and Kukla, 2000) also responded to D/O events (Wang et al., 2001; Altabet et al., 2002). However, we still do not know the intensity of the response of the hydrological cycle to the rapid climate fluctuations in the North Atlantic. The Bay of Bengal, which receives the outow of the major rivers draining the Himalayan mountains and the Indian subcontinent, is therefore very sensitive to changes in the hydrological cycle and continental runoff in South Asia. Prell et al. (1980); Duplessy (1982). Here, we reconstruct surface water oxygen isotope composition/salinity variations recorded in a core raised from the southwest sector of the low surface salinity tongue of the northern Andaman Sea. This area directly receives the discharge of the Irrawady and Salween rivers and should reliably record their fluctuations.

Understanding the teleconnection between North Atlantic/Arctic climate and the Indian monsoon intensity is a challenge both for future and past climate changes (Khare, 2008). More generally, the tropical/extratropical teleconnection related to the abrupt climate changes of the last glacial period are not well understood, as reviewed by Clement and Peterson (2008). The teleconnection mechanisms explaining the correlative rapid climate variations between the North Atlantic and the Indian monsoon region in the past have been investigated through modelling experiments mostly under present day climate conditions (Vellinga and Wood, 2002; Zhang and Delworth, 2005; Lu and Dong, 2008). Zhang and Delworth (2005) have analyzed the tropical response to a weakened AMOC and suggest that the Indian monsoon is weakened due to a weakening of the Walker circulation in the southern tropical Pacific. Lu and Dong (2008) found that the atmospheric teleconnection in the eastern and central North Pacific and the atmosphere-ocean interaction in the tropical North Pacific play the most important role. Using a model of intermediate complexity, Jin et al. (2007) suggest that the Asian monsoon is weakened during Heinrich events of the last glacial age. In addition, several studies have analyzed the relationship between a warm phase of the North Atlantic Multidecadal

Oscillation (AMO) and a strong Indian monsoon (Zhang and Delworth, 2006; Goswami et al., 2006; Lu et al., 2006; Li and Harrison, 2008; Feng and Hu, 2008). Using observations, Goswami et al. (2006) and Feng and Hu (2008) propose a link between the North Atlantic surface temperature and the Indian monsoon intensity through a physical mechanism affecting the meridional gradient of upper tropospheric temperature between the Tibetan Plateau and the tropical Indian Ocean. This meridional gradient of temperature has been shown to be an indicator of the timing and intensity of the summer monsoon season (He et al., 2003; Goswami and Xavier, 2005).

Modelling experiments usually represent Heinrich events as fluctuation of the AMOC via freshwater discharges in the North Atlantic (review Clement and Peterson (2008); Kageyama et al. (2010)). Using the IPSL-CM4 ocean-atmosphere coupled model, we have shown that a collapse of the AMOC under glacial conditions also leads to a significant weakening of the Indian monsoon (Kageyama et al., 2009). This weakening is driven by the upper tropospheric cooling to the north of the Indian subcontinent, that is occurring simultaneously with the AMOC weakening. Following our previous study, we focus here the analysis of the modelling experiments on the impact of an Heinrich-type of event on the Indian monsoon and on the hydrological cycle of the Bay of Bengal. It is difficult to discern the teleconnection mechanisms between the North Atlantic and the Indian monsoon region because of interactions between the atmosphere and the ocean. The weakening of the AMOC affects sea surface temperatures (SST) of the North Atlantic and the tropical Atlantic that are key regions for the Indian monsoon. We performed additional sensitivity experiments in order to investigate which region of SST changes has the strongest impact on monsoon changes and what are the mechanisms for this North Atlantic/Indian monsoon teleconnection.

Section 2 discusses the method and the results of the North Andaman Sea record for the last 40,000 years. The modelling experiment of an Heinrich event and its impact on the Indian monsoon, are presented in section 3, as well as the sensitivity experiments. The study is discussed and concluded in section 4.

2 Indian monsoon variability in the 40,000 years record in the Bay of Bengal

2.1 Material and methods

Core MD77-176 (14°31N; 93°08E ; 1375 m water depth) has been selected to estimate surface salinity variations in the Bay of Bengal (Fig. 1). This core, which is located in the southwest sector of the present low surface salinity tongue of the northern Andaman Sea, also records the extreme dryness of the LGM Asian monsoon climate (Duplessy, 1982) and should be very sensitive to fluctuations of the hydrological cycle and continental runoff in the Irrawady-Salween drainage basin.

Oxygen isotope measurements ($\delta^{18}O$) were made on planktonic foraminifera Globigerinoides ruber (Fig. 2). The $\delta^{18}O$ values of planktonic foraminifera record changes in both the oxygen isotope composition of sea surface water δ_w and the isotopic fractionation between calcium carbonate and water, which depends upon the temperature at which foraminifera have formed their shell (Epstein et al., 1953; Shackleton, 1974).

In core MD77-176, sea surface temperature (SST) estimates were derived from foraminiferal counts, using the modern analogue technique (Hutson, 1979; Prentice, 1980; Overpeck et al., 1985). The squared chord distance dissimilarity coefcient was used to measure the mean degree of dissimilarity between each fossil assemblage and the modern analogues. It never exceeds 0.16 and the ten best modern analogues were selected to estimates past SST with a statistical error smaller than 1°C at 1 sigma (Fig. 2).

2.2 Results

The SST record exhibits no signicant changes from glacial period to Holocene (Fig. 2). These results are consistent with all SSTs reconstructed using planktonic foraminiferal assemblages (Cullen, 1981; Barrows and Juggins, 2005), but contrast with the 2 to 3°C cooling inferred from Mg/Ca and Uk-37 SST data in the same area (Rashid et al., 2007; Kudrass et al., 2001). In all cases, the SST changes from the glacial to interglacial conditions are small and the foraminiferal $\delta^{18}O$ record can be considered as a good approximation of the changes in the oxygen isotope composition of the surface water at the location of our core.

Sea water $\delta^{18}O$ variations directly reect those of surface water $\delta^{18}O$ due to both global ice volume changes (Emiliani, 1954) and local freshwater budget (Precipitation + Runoff - Evaporation) variations (Craig and Gordon, 1965; Delaygue et al., 2001). In order to subtract the global ice volume record (Waelbroeck et al., 2002) from the $\delta^{18}O$ record, we generated an absolute chronology using AMS radio-carbon dating on monospecic planktonic foraminiferal samples. For the last 20 ky, ^{14}C ages have been converted into calendar ages using the Calib 4.1 program (Stuiver and Reimer, 1993; Stuiver et al., 1998), which includes the correction for the ocean surface reservoir age (Broecker and Peng, 1982). This correction was assumed to be constant and equal to 400-yr because air-sea exchanges have always been high in tropical waters. The conversion of ^{14}C ages to calendar ages is less accurate before 20 ky ^{14}C BP, because the ^{14}C production rates in the upper atmosphere experienced major changes during the last glaciation (Laj et al., 1996; Volker et al., 1998; Bard, 1998; Hughen et al., 2004; van der Plicht et al., 2004; Fairbanks et al., 2005) and different calibration models provide age estimates, which differ by more than 2 ky.

The high resolution local δ_w record of core MD77-176 displays large millennial scale oscillations over the period 40,000 to 11,000 yr BP (Fig. 3). They closely correlate to the Greenland ice core record of changes in polar air temperature during the last glaciation. This correlation is in good agreement with previous observations of enhanced summer monsoon activity during D/O events (Wang et al., 2001; Burns et al., 2003). We have therefore developed a second age model for core MD77-176 assuming that local δ_w changes in the Northern Andaman Sea and GISP2 $\delta^{18}O$ are in phase and synchronous. Comparison of this new age model with the ages calibrated using the Fairbanks et al. (2005) model before 20 ^{14}C ky BP indicates that our assumption is realistic (Fig. 3). Between 13 and 10.5 ky BP, figure 3a displays a difference of about 1 to 1.5 ky between the age model based on calibrated ^{14}C ages and that obtained by correlation with GISP2 $\delta^{18}O$ record. During Younger Dryas for instance, the calibrated ^{14}C ages of the lowering of the Bay of Bengal δ_w is older than the cooling of the North Atlantic Younger Dryas by 1 to 1.5 kyr. This age anomaly is a local phenomenon as it is not observed in other cores, which are protected from the direct influence of rivers outflow (Rashid et al., 2007).

Core MD77-176 faithfully records the enhanced southwest monsoon rains over the Indian subcontinent at the beginning of the Holocene (Fontes et al., 1996; Gasse et al., 1996; VanCampo et al., 1996; COHMAP Members, 1988; VanCampo and Gasse, 1993). During the lower Holocene to about 4 ky BP, the surface water $\delta^{18}O$ (δ_w) was lower than today by about 0.2 to 0.8‰in the Bay of Bengal. Considering the δ_w/Salinity slope in the Northern Indian Ocean (0.25 to 0.37‰; Delaygue et al. (2001); Rostek et al. (1993), the corresponding surface salinity decrease is of about 0.5 to 2.5‰(Fig. 3b).

During the glaciation, the local sea water $\delta^{18}O$ record of core MD77-176 displays many periods during which the freshwater input exhibits significant variations (Fig. 3b). The highest surface salinities were reached during the Last Glacial Maximum. From 40 to 28 ky BP, surface salinity values were lower than those of the LGM but higher than today. These observations are in agreement with the loess deposits records in southern and southeastern Tibet and in western China (Porter and An, 1995; Xiao et al., 1995; Guo et al., 1996; Chen et al., 1997; An et al., 1991, 1993) and with the changes in the intensity of Somalian and Arabian upwelling (Sirocko et al., 1991; Zonneveld et al., 1997), which show that the Indian summer monsoon was generally weak during the glaciation and always weaker than today.

The general trend described above is complicated by large abrupt changes of millennial scale. During the LGM, three episodes of low surface salinity were centered at about 23, 20.5 and 19 ky BP (Fig. 3b). Also, during the upper part of the Marine Isotope Stage 3, 5 events of salinity decrease

are recorded in core MD77-176. They occurred at about 37.5, 35, 33.5, 32, and 27 ky BP. All these low salinity episodes observed in the Andaman Sea have equivalent warm episodes in the Greenland ice record (interstadials). During these events, summer monsoon was thus weaker than today and it resulted in significant rainfall over the Indian subcontinent.

Between the freshwater injection events into the Bay of Bengal, events of salinity increase reflecting extreme monsoon weakness are recorded. Four of them have been detected in China loess sequences (at around 39, 31, 24 and 16 ky BP), and are characterized by lower continental weathering intensity and coarser grain size peaks in the loess records (Porter and An, 1995; Xiao et al., 1995; Guo et al., 1996; Chen et al., 1997). Like the high salinity events in the Bay of Bengal, the Chinese dry/cold episodes are found to be synchronous with the last four North Atlantic Heinrich events. However, not all the periods of marked reduction in the continental runoff into the Bay of Bengal during the last 40,000 years correlate with Heinrich events and some cold stadial of the Greenland ice records are also correlated with extremely dry conditions over Asia.

The record of core MD77-176 displays a remarkable similarity with the oxygen isotope records of eastern China stalagmites (Wang et al., 2001; Cosford et al., 2008) and the nitrogen isotope ratio variations recorded in Arabian Sea sediment (Altabet et al., 2002). These records are also directly linked to the monsoon intensity. Eastern China stalagmites $\delta^{18}O$ values are controlled by the summer/winter precipitation ratio; summer precipitation $\delta^{18}O$ is about 10‰lower than that of winter. Warmer Greenland temperatures were found to correlate with periods of more intense summer East Asian Monsoon and then with more contribution of summer precipitation. In the Arabian Sea, $\delta^{15}N$ and thus denitrication were found to be high during the warm phases of the Dansgaard/Oeschger events and low during the cold phases of these events. High $\delta^{15}N$ values are interpreted as an indication of higher primary productivity and higher denitrication in the Arabian Sea which are largely the result more active upwelling and thus stronger summer monsoon winds (Altabet et al., 2002).

Therefore, warming in the North Atlantic area coincides with active glacial Indian summer monsoon circulation. Even within the last glacial maximum, which was not the coldest glacial period in the middle latitudes North Atlantic records (Duplessy et al., 1991), some short events of active summer monsoon circulation occurred in southeastern Asia. A similar relative strengthening of the Indian monsoon during the LGM was also inferred from the Somali and Arabian Sea upwelling records (Zonneveld et al., 1997; Sirocko et al., 1991). Nevertheless, our data demonstrate that the periods of Indian summer monsoon intensication during the last glaciation were not characterized by precipitation as intense as those of Holocene. Our data show that the hydrological cycle associated with the monsoon is highly sensitive and respond rapidly to abrupt climatic variations over the North Atlantic area.

3 Modelling study of the Indian monsoon response to a freshwater hosing under glacial conditions

3.1 Model and experiments

In order to better constrain the interpretation of the rapid variations of monsoon activity seen in the paleo-record presented above, two modelling experiments were analyzed to evaluate the impact of a freshwater hosing experiment on the Indian monsoon under glacial conditions. The model used in the present study is the coupled ocean-atmosphere IPSL-CM4 model (Marti et al., 2010). The atmospheric component of this coupled model is LMDZ.3.3 (Hourdin et al., 2006), with resolution 96x71x19 in longitudexlatitudexaltitude. The horizontal grid is regular, while the vertical levels are more numerous near the surface. This atmospheric component is coupled with the land surface scheme ORCHIDEE (Krinner et al., 2005) which includes a river routing scheme for the 50 largest river basins in order to close the water budget between land and ocean. The ocean component is ORCA2 (Madec et al., 1998), which uses an irregular horizontal grid of 182x149 points with a resolution of 2 degrees, refined over key regions such as the North Atlantic and near the Equator. This model has 31 depth levels. The sea-ice component is the Louvain Ice Model (LIM, Fichefet and Maqueda (1997)). The coupling of these components is performed using the OASIS (version 3) coupler (Terray et al., 1995).

The glacial conditions are representative of the Last Glacial Maximum (LGM) climate and are prescribed following the PMIP2 (Paleo-Modelling Intercomparison Project phase 2, Braconnot et al. (2007) protocol: we use the ICE-5G ice-sheet reconstruction (Peltier, 2004), atmospheric gas concentrations (Monnin et al., 2001; Dallenbach et al., 2000; Fluckiger et al., 1999) and orbital parameters (Berger, 1978) corresponding to the climate 21 ky BP. The control experiment is labeled LGMc (c for control) and presents an active AMOC (18 Sv). The second simulation is a ”hosing” experiment obtained by adding a 0.18 Sv freshwater input in the North Atlantic, resulting in a collapse of the AMOC (2 Sv after 250 years) and is labeled LGMh (h for hosing). This latter experiment is a highly idealized simulation of an Heinrich event under glacial conditions. The climatologies presented in this study are integrated over the years 200-250 for LGMc and 370-420 for LGMh. More details on the experimental set up and on the AMOC response to the freshwater input can be found in Kageyama et al. (2009).

The evaluation of the IPSL-CM4 coupled model is presented in Marti et al. (2010). In present day conditions, the model performs well in the tropical area. There is an underestimation of the amount of Indian monsoon rainfall over the land but the monsoon circulation is well depicted over

the Indian Ocean. The model results for the Mid-Holocene compare well with other models from the PMIP2 project (Braconnot et al., 2007). Using the same model, Marzin and Braconnot (2009) have shown that the Indian monsoon is sensitive to the precession changes between the Early Holocene, the Mid-Holocene and the preindustrial periods. These results indicate a gradual weakening of the Indian monsoon intensity throughout the Holocene and are consistent with the surface salinity evolution at the MD-77176 core site and with other paleo-records of monsoon intensity. Regarding the LGM experiment, the Indian monsoon is not very sensitive to the LGM conditions compared to other PMIP2 models (Braconnot et al., 2007). This is due to the fact that the AMOC is strong in this LGM control simulation and therefore it would correspond to a "warm" phase of a D/O event, with a monsoon not very different from today (Braconnot et al., 2007). However, the hosing experiment presents a much weaker AMOC and can be considered as representative of an Heinrich event.

3.2 Indian monsoon weakening due to the collapse of the AMOC

The results of the hosing experiment under LGM conditions are shown for the season averaged from June to September (JJAS) to encompass the whole boreal summer monsoon season. The main features discussed are significant at the 95% level based on the Student's t-test but the confidence intervals are not shown on the figures for more clarity. The freshwater input in the North Atlantic/Arctic region and the collapse of the AMOC between LGMh and LGMc results in a dipolar pattern of SST anomalies in the Atlantic, with a more than 3°C cooling in the North Atlantic and a more than 1°C warming in the South Atlantic (Fig. 4a). This typical cross-equatorial SST dipole is accompanied by a southward shift of the ITCZ in the Atlantic (Fig. 4b) that is consistent with previous studies (Stouffer et al., 2006; Timmermann et al., 2007; Wu and Kirtman, 2007; Chang et al., 2008). Significant remote impacts are also seen across the globe. The cooling of the North Atlantic extends across the whole Eurasian continent and the subtropical North-West Pacific, and an overall warming of the Southern Ocean. The North Atlantic forcing leads to significant precipitation and circulation changes in the Pacific Ocean. These features are discussed in details in Kageyama et al. (2009) and are shown to be more pronounced in the case of the LGM than for other climatic periods (Swingedouw et al., 2009).

The North Atlantic hosing experiment results in a statistically significant reduction of the Indian monsoon precipitation to the north-east and south-west of the subcontinent by about 10% (Fig. 4b). The reduction in precipitation coincides with the core regions of simulated monsoon precipitation. The monsoon cross-equatorial flow is weakened in the Indian Ocean, therefore reducing the moisture advection into the monsoon region. The strength of the southwesterly winds over the western Arabian Sea is reduced, this is consistent with paleo-records indicating changes in upwelling and productivity in this region coeval with North Atlantic changes (Schulz1998, Altabet2002, Gupta2003).

The weakening of the Indian monsoon due to the freshwater input in the North Atlantic is consistent with other modelling studies discussed in the introduction, but our experiments confirm that this teleconnection holds under glacial conditions.

The reduction of the Indian monsoon intensity induces an increase in salinity over the whole Bay of Bengal (Fig. 4c). The amplitude of the anomalies are from 0.6 to 2‰in the northern part of the Bay of Bengal, and are similar in amplitude to the large variations in the Northern Andaman sea surface salinity record presented in section 2.2. The fresh water content of the Bay of Bengal is under the influence of the fresh water input (precipitation minus evaporation and continental river runoff), as well as water transport from the South, this is reflected in the large variations of mixed layer thickness across the Bay of Bengal during the summer months (Varkey et al., 1996). The freshwater input is diagnosed from the model outputs and our hosing experiment shows that the river runoff in the north coastal region of the Bay of Bengal drops by 20% (by 0.02 to 0.06 10^-3 kg/m^2/s) and the local freshwater input (precipitation minus evaporation) is also reduced over the whole Bay of Bengal by approximately 10% (0.006 to 0.016 10^-3 kg/m^2/s) due to suppressed local precipitation over the ocean (Fig. 4a). Therefore, the model results show that the changes in salinity over the Bay of Bengal highlighted in the Northern Andaman Sea record as well as in the model outputs, are sensitive to the suppression of the hydrological cycle both over the land (reduction in river runoff) and over the ocean (reduction in local precipitation). As a result, this modelling study supports the hypothesis used for the age model of the core MD77-176 assuming that the local changes of the Andaman Sea are synchronous with the D/O events of the Greenland ice core records.

The large scale meridional gradient of upper tropospheric temperature over India has been shown to be an indicator of the monsoon seasonal evolution and intensity (He et al., 2003; Goswami and Xavier, 2005). This meridional gradient (tropospheric temperature averaged from 200 to 500 hPa) is considerably reduced in the hosing experiment (Fig. 4a) with the cooling anomaly over the Himalaya and is a direct indicator of the monsoon weakening. In our previous study, we have hypothesized that the predominant pathway from the North Atlantic perturbation to the Indian monsoon would be through the atmospheric circulation by affecting the large cooling of tropospheric temperature over the Eurasian continent. Moreover, we have shown that the JJAS tropospheric temperature and the JJAS Indian monsoon rainfall were decreasing synchronously with the strength of the AMOC throughout the simulation.

The underlying mechanisms of this North Atlantic/Indian monsoon teleconnection are still being investigated by the community. In order to refine these analyses and to better understand the teleconnection mechanisms, we have performed sensitivity experiments presented in the following section. We also test some of the hypotheses presented in the introduction.

3.3 Sensitivity experiments and the dominant role of the tropical Atlantic

To differentiate the impact of several key regions of SST changes on the Indian monsoon, we have performed several sensitivity experiments using the atmospheric component of the coupled model. We test the impact of SST changes due to the freshwater forcing in specific regions. The SST fields from the coupled experiments were used to force the atmospheric model. We applied the SSTs from the hosing experiment LGMh over the test region and the SSTs of the control experiment LGMc for the rest of the globe. To make sure that the atmospheric model replicates the results discussed above, we performed the control and the hosing experiments using the SSTs obtained from the coupled experiments over the whole globe (LGMcF and LGMhF). All the experiments are run for 50 years and use the same 50 years as on the previous subsection coupled simulations for the forcing SST fields. The SST fields used are monthly so that the interannual variability of the coupled experiments is passed on to the forced experiments. We describe each of the forced experiments performed:

- LGMcF: Simulation forced by the SST fields from the LGMc coupled control experiment over the whole globe.
- LGMhF: Simulation forced by the SST fields from the LGMh coupled hosing experiment over the whole globe.
- LGMhNA: Simulation forced by the SST fields from the LGMh simulation over the North Atlantic/Arctic region only (above 30°N), to analyze the impact of the North Atlantic cooling (Fig. 5b).
- LGMhTA: Simulation forced by the SST fields from the LGMh simulation over the tropical Atlantic region only (30°S to 30°N), to analyze the impact of the large dipolar SST anomaly (Fig. 5c).
- LGMhNTAC: Complementary simulation of LGMhNA and LGMhTA forced by the SST fields from the LGMh simulation over all the oceans except the North Atlantic/Arctic and tropical Atlantic regions that are forced by SSTs from the LGMc control experiment, to analyze the impact of the SST changes over the Indian and Pacific Oceans (Fig. 5d).

The results of these sensitivity experiments are presented in terms of surface and upper tropospheric temperature change (Fig. 5), precipitation and low level circulation change (Fig. 6), and 200 hPa geopotentiel and circulation change (Fig. 7). The atmospheric model, forced by the SSTs from the previous coupled experiments, is able to reciprocate the precipitation results presented in section 3.2 both in terms of precipitation change over the Indian region (Fig. 6a) and of upper tropospheric cooling over Eurasia (Fig. 5a). The first sensitivity experiment indicates that the North Atlantic

cooling has only a marginal impact on precipitation over the Indian region (Fig. 6b). Hence, our results demonstrate that the North Atlantic cooling associated with the freshwater input alone is not sufficient to explain the monsoon weakening. Even though the cooling over Eurasia is significant, the upper tropospheric temperature (TT) is decreased by only 0.25K over the Tibetan Plateau (Fig. 5b).

If only the SST perturbation over the tropical Atlantic is imposed (Fig. 5c), then the precipitation decrease seen in the coupled simulations over the south-west and north-east of India is fully recovered (Fig. 6c). The fact that only the bipolar SST structure across the equatorial Atlantic is able to trigger such a response over the Indian region is remarkable. The TT signature over the Tibetan Plateau in this sensitivity experiment is larger than in LGMhNA, even though the decrease in surface temperatures is not as extended over Eurasia (Fig. 5c). The weakening of the Indian monsoon intensity is associated with the reduction of the meridional gradient of upper tropospheric temperature in a consistent way with previous studies (Goswami et al., 2006; Lu and Dong, 2008). However, these studies suggest that the North Atlantic temperature changes directly impact the Eurasian continent, but we show that in our case it is more directly influenced by the tropical Atlantic bipolar SST anomaly and the associated southward shift of the ITCZ.

In addition to this hypothesis of predominant link between the North Atlantic and the Indian monsoon through Eurasian continent, Zhang and Delworth (2005) and Lu and Dong (2008) suggest that the Indian monsoon is mostly influenced by changes in the tropical Pacific in their coupled experiments. Indeed, several studies show that the Atlantic perturbation is propagated to the Pacific through the Central American region (Dong and Sutton, 2002; Zhang and Delworth, 2005). Here, to isolate the impact of the Pacific Ocean and Indian Ocean SST changes in our modelling experiments, we have performed the complementary simulation LGMhNTAC. The cooling over the equatorial Pacific and the north eastern Pacific warming (Fig. 5d) are consistent with the above studies. The anticyclonic anomaly over the subtropical eastern Pacific enhances precipitation. A warming over the southern equatorial Indian Ocean is associated with an amplification of convective rainfall (Fig. 5d and Fig. 6d), and a large anomaly of reduced precipitation appears over the subtropical western Pacific. More strikingly, this sensitive experiment shows that the SST changes in the Pacific and Indian Oceans actually amplify the monsoon rainfall over the south-west and the western part of the Bay of Bengal (Fig. 6d). This is associated with a positive anomaly of upper tropospheric temperature over the north-west of India. Indeed, it has been shown that the interannual variability of the Indian monsoon is very sensitive to the upper tropospheric warming over this region (Xavier et al., 2007).

Our sensitivity experiments show that the mechanisms that are suggested to be predominant in other studies are not sufficient to explain the impact of the AMOC weakening on the Indian monsoon rainfall. The North Atlantic SST changes cannot on their own directly produce a dampening of the monsoon activity. Moreover, the atmosphere and ocean interactions over the Pacific and Indian oceans actually result in an amplification of the Indian monsoon in our analysis. Therefore, using the sensitivity experiments, we isolate the impact of the tropical Atlantic SST changes associated with the large southward shift of the ITCZ as the predominant forcing. This bipolar SST anomaly is obtained both through atmospheric and oceanic pathways (Kageyama et al., 2009; Swingedouw et al., 2009), and we show with the atmosphere-only experiment LGMhTA that this anomaly is resulting in a weakening of the Indian monsoon through the Eurasian continent cooling.

The tropical Atlantic SST anomaly induces perturbations of the stationary waves in the northern extratropics seen in the TT. The wavetrain perturbations are propagated downstream from the North Atlantic to Eurasia as seen from the negative anomalies of 200 hPa geopotential (Fig. 7c). The cyclonic anomalies of 200 hPa winds and the acceleration of the subtropical westerly jet stream obtained in LGMhF (Fig. 7a) are also fully represented in the LGMhTA simulation (Fig. 7c). This atmospheric teleconnection could be explained through the mechanism suggested by Ding and Wang (2005, 2007) who showed that the Indian monsoon is interacting with a circumglobal teleconnection pattern with specific centers of perturbation in the mid-latitudes . In our LGMhTA experiment, the largest TT anomaly over the north-west Atlantic is associated with another center of upper tropospheric cooling over the eastern Mediterranean region and over the Tibetan Plateau. Ding and Wang (2005) suggest that if a wave train is excited at the jet exit of the North Atlantic, this influences the central Asian high and the Indian monsoon. Kucharski et al. (2008) use observation datasets to analyze the Atlantic component of the Indian monsoon interannual variability and show that by subtracting the ENSO-forced component, the strong Indian monsoon years are correlated with the cold south equatorial Atlantic SSTs. Kucharski et al. (2009); Losada et al. (2010) also highlight the teleconnection between the tropical Atlantic and the Indian monsoon circulation at shorther time scales. Therefore, the cold anomaly over the northern tropical Atlantic and the warm anomaly over the southern tropical Atlantic can both induce pathways to influence the reduction of the Indian monsoon circulation and precipitation.

Following the comment by Clement and Peterson (2008) that the contribution of the land surface snow cover and sensible heating over the Tibetan Plateau had not been investigated, we have verified that the Indian monsoon weakening is not driven by changes in the snow cover over the Tibetan Plateau as these are marginal in our experiments (not shown). The large scale deep upper tropospheric cooling over the Tibetan Plateau induced by the collapse of the AMOC is the main factor explaining the weakening of the Indian monsoon as suggested by Goswami et al. (2006). And

we have shown that this is most effectively caused by the tropical Atlantic influence than by the North Atlantic cooling itself, the anomaly over the tropical Atlantic being transported by the mid-westerlies. Our mechanism is also consistent with the hypothesis of a zonally symmetric adjustment discussed in Clement and Peterson (2008). Broccoli et al. (2006); Chiang and Bitz (2005) suggest that the North Atlantic forcing can trigger a high latitude cooling that is quickly propagated zonally via the westerly atmospheric flow and mixing and then influences the Tropics.

4 Conclusions

The Andaman Sea paleorecord shows very large salinity signature in the Bay of Bengal that are interpreted as Indian monsoon fluctuation by affecting the hydrological cycle of the Bay of Bengal. Warming in the North Atlantic area coincides with active glacial Indian summer monsoon circulation. Even within the last glacial maximum, some short events of active summer monsoon circulation occurred in southeastern Asia. A similar relative strengthening of the Indian monsoon during the LGM was also inferred from the Somali and Arabian Sea upwelling records (Zonneveld et al., 1997; Sirocko et al., 1991). Nevertheless, our data demonstrate that the periods of Indian summer monsoon intensication during the last glaciation were not characterized by precipitation as intense as those of Holocene. Our data show that the hydrological cycle associated with the monsoon is highly sensitive and respond rapidly to abrupt climatic variations over the North Atlantic area.

A modelling experiment of an Heinrich event under Last Glacial Maximum conditions is set up to test the interpretation of the paleorecord as Indian monsoon variations and the hypothesis of teleconnection between the North Atlantic abrupt events and the Bay of Bengal. We show that the coupled model reproduces the impact of a freshwater hosing in the North Atlantic on the weakening of the Indian monsoon rainfall and circulation. The increase in salinity in the Bay of Bengal is due to a decrease in continental runoff and in local precipitation minus evaporation. The monsoon weakening is associated with an upper tropospheric temperature cooling over the Tibetan Plateau.

A new teleconnection pathway is revealed in our sensitivity experiments. It is the dipole of SST anomalies obtained in the tropical Atlantic Ocean that impacts the most the Indian monsoon. These anomalies excite a wave train perturbation throughout the Eurasian continent with an associated acceleration of the subtropical westerly jet. The center of perturbation around the Tibetan Plateau directly affects the intensity of the monsoon through the reduction of the meridional tropospheric temperature gradient over India. We also show with these sensitivity tests that previously suggested mechanisms like the direct influence of the North Atlantic SST changes on the Indian monsoon and the ocean-atmosphere interactions in the Pacific are not sufficient to explain the changes obtained

over India. However, the patterns in the Pacific and Indian oceans vary between the different studies, but the SST and precipitation anomalies over the tropical Atlantic and the weakening of the Indian monsoon are always consistent. The mechanism suggested above could therefore be more robust, a detailed comparison analysis of hosing experiments, including sensitivity tests with several models would be of immense benefit to get more insight in this teleconnection.

A possible limitation of the modelling results is a bias in the representation of the Indian monsoon intensity and a bias in the westerly jet position that is too southward. The impact of variations of the North Atlantic climate is seen across the globe and at different time scales. The validity of this mechanism could also be tested under different climatic conditions, as a continuity of Swingedouw et al. (2009) who analyze the impact of freshwater hosing experiments for the present, the future, the Holocene, the LGM and the Eemian.

Our data/model comparison is successful in bringing the bigger picture resulting in the Bay of Bengal hydrology cycle changes. However, the fact that not all the low salinity events in the record are correlated with Heinrich events indicates that the complex variability of the Tropics during the last glaciation and its interaction with higher latitudes are not yet fully understood, and some studies suggest that the Tropics and high latitudes interactions should be approached as a more global and coupled feedback in order to explain the abrupt climate changes that happened around the globe (Tierney and Russell, 2007; Seager and Battisti, 2007; Clement and Peterson, 2008).

Acknowledgements. TEXT

References

Allen, J. R. M., Brandt, U., Brauer, A., Hubberten, H. W., Huntley, B., Keller, J., Kraml, M., Mackensen, A., Mingram, J., Negendank, J. F. W., Nowaczyk, N. R., Oberhansli, H., Watts, W. A., Wulf, S., and Zolitschka, B.: Rapid environmental changes in southern Europe during the last glacial period, Nature, 400, 740–743, 1999.

Altabet, M. A., Higginson, M. J., and Murray, D. W.: The effect of millennial-scale changes in Arabian Sea denitrification on atmospheric CO2, Nature, 415, 159–162, 2002.

An, Z. S., Wu, X. H., Wang, P. X., Wang, S. M., Dong, G. R., Sun, X. J., Zhang, D. E., Lu, Y. C., Zheng, S. H., and Zhao, S. L.: Paleomonsoons of China Over the Last 130,000 Years - Paleomonsoon Variation, Science In China Series B-chemistry Life Sciences & Earth Sciences, 34, 1016–1024, 1991.

An, Z. S., Porter, S. C., Zhou, W. J., Lu, Y. C., Donahue, D. J., Head, M. J., Wu, X. H., Ren, J. Z., and Zheng, H. B.: Episode of Strengthened Summer Monsoon Climate of Younger Dryas Age On the Loess Plateau of Central China, Quat. Res., 39, 45–54, 1993.

Bard, E.: Geochemical and geophysical implications of the radiocarbon calibration, Geochimica Et Cosmochimica Acta, 62, 2025–2038, 1998.

Barrows, T. and Juggins, S.: Sea-surface temperatures around the Australian margin and Indian Ocean during the Last Glacial Maximum, Quatern. Sci. Rev., 24, 1017–1047, 2005.

Behl, R. J. and Kennett, J. P.: Brief interstadial events in the Santa Barbara basin, NE Pacific, during the past 60 kyr, Nature, 379, 243–246, 1996.

Berger, A. L.: Long-Term Variations Of Daily Insolation And Quaternary Clim. Changes, J. Atmos. Sci., 35, 2362–2367, 1978.

Bond, G., Heinrich, ., Broecker, W., Labeyrie, L., McManus, J., Andrews, J., Huon, S., Jantschik, R., Clasen, S., Simet, C., Tedesco, K., Klas, M., Bonani, G., and Ivy, S.: Evidence for massive discharges of icebergs into the North Atlantic Ocean during the last glacial period, Nature, 360, 245–249, 1992.

Braconnot, P., Otto-Bliesner, B., Harrison, S., Joussaume, S., Peterchmitt, J. Y., Abe-Ouchi, A., Crucifix, M., Driesschaert, E., Fichefet, T., Hewitt, C. D., Kageyama, M., Kitoh, A., Laine, A., Loutre, M. F., Marti, O., Merkel, U., Ramstein, G., Valdes, P., Weber, S. L., Yu, Y., and Zhao, Y.: Results of PMIP2 coupled simulations of the Mid-Holocene and Last Glacial Maximum - Part 1: experiments and large-scale features, Clim. Past, 3, 261–277, 2007.

Broccoli, A. J., Dahl, K. A., and Stouffer, R. J.: Response of the ITCZ to Northern Hemisphere cooling, Geophys. Res. Lett., 33, L01 702, 2006.

Broecker, W. S. and Peng, T.-H.: Tracers in the Sea, Lamont-Doherty Geological Observatory, Palisades, N.Y., 1982.

Broecker, W. S., Bond, G., Klas, M., Clark, E., and McManus, J.: Origin of the northern Atlantic's Heinrich events, Climate Dyn., 6, 265–273, 1992.

Burns, S. J., Fleitmann, D., Matter, A., Kramers, J., and Al-Subbary, A. A.: Indian Ocean climate and an absolute chronology over Dansgaard/Oeschger events 9 to 13, Science, 301, 1365–1367, 2003.

Chang, P., Zhang, R., Hazeleger, W., Wen, C., Wan, X. Q., Ji, L., Haarsma, R. J., Breugem, W. P., and Seidel, H.: Oceanic link between abrupt changes in the North Atlantic Ocean and the African monsoon, Nature Geoscience, 1, 444–448, 2008.

Chen, F., Bloemendal, J., Wang, J., Li, J., Oldfield, F., and Ma, H.: High-resolution multi-proxy climate records from Chinese loess: evidence for rapid climatic changes between 70ka and 10ka, Paleogeography, Paleoclimatology Plalaeontology, 130, 323–335, 1997.

Chiang, J. C. H. and Bitz, C. M.: Influence of high latitude ice cover on the marine Intertropical Convergence Zone, Climate Dyn., 25, 477–496, 2005.

Clement, A. C. and Peterson, L. C.: Mechanisms of abrupt climate change of the last glacial period, Rev. Geophys., 46, RG4002, 2008.

COHMAP Members, .: Clim. Changes of the Last 18,000 Years: Observations and Model Simulations, Science, 241, 1043–1052, 1988.

Cosford, J., Qing, H. R., Yuan, D. X., Zhang, M. L., Holmden, C., Patterson, W., and Hai, C.: Millennial-scale variability in the Asian monsoon: Evidence from oxygen isotope records from stalagmites in Southeastern China, Palaeogeography Palaeoclimatology Palaeoecology, 266, 3–12, doi:10.1016/j.palaeo.2008.03.029, 2008.

Craig, H. and Gordon, L. I.: Deuterium and oxygen 18 variations in the ocean and the marine atmosphere, Marine Geochemistry, Narragansett Marine Laboratory, University of Rhode Island, 3, 277–374, 1965.

Cullen, J. L.: Microfossil Evidence For Changing Salinity Patterns In the Bay of Bengal Over the Last 20000 Years, Palaeogeography Palaeoclimatology Palaeoecology, 35, 315–356, 1981.

Dallenbach, A., Blunier, T., Fluckiger, J., Stauffer, B., Chappellaz, J., and Raynaud, D.: Changes in the atmospheric CH4 gradient between Greenland and Antarctica during the Last Glacial and the transition to the Holocene, Geophys. Res. Lett., 27, 1005–1008, 2000.

Dansgaard, W., Johnsen, S. J., Clausen, H. B., Dahljensen, D., Gundestrup, N. S., Hammer, C. U., Hvidberg, C. S., Steffensen, J. P., Sveinbjornsdottir, A. E., Jouzel, J., and Bond, G.: Evidence For General Instability Of Past Climate From A 250-Kyr Ice-Core Record, Nature, 364, 218–220, 1993.

Delaygue, G., Bard, E., Rollion, C., Jouzel, J., Stievenard, M., Duplessy, J. C., and Ganssen, G.: Oxygen isotope/salinity relationship in the northern Indian Ocean, J. Geophys. Res.-oceans, 106, 4565–4574, 2001.

Ding, Q. H. and Wang, B.: Circtunglobal teleconnection in the Northern Hemisphere summer, J. Climate, 18, 3483–3505, 2005.

Ding, Q. H. and Wang, B.: Intraseasonal teleconnection between the summer Eurasian wave train and the Indian monsoon, J. Climate, 20, 3751–3767, 2007.

Dong, B. W. and Sutton, R. T.: Adjustment of the coupled ocean-atmosphere system to a sudden change in the Thermohaline Circulation, Geophys. Res. Lett., 29, 1728, 2002.

Duplessy, J. C.: Glacial to interglacial contrasts in the northern Indian Ocean, Nature, 295, 494–498, http://dx.doi.org/10.1038/295494a0, 1982.

Duplessy, J. C., Labeyrie, L., Juilletleclerc, A., Maitre, F., Duprat, J., and Sarnthein, M.: Surface Salinity Reconstruction of the North-atlantic Ocean During the Last Glacial Maximum, Oceanologica Acta, 14, 311–324, 1991.

Emiliani, D.: Depth habitats of some species of pelagic foraminifera as indicated by oxygen isotope ratios, Am. J. Sci., 252, 149–158, 1954.

Epstein, S. R., Buchsbaum, R., Lowenstam, H. A., and Urey, H. C.: Revised carbonate-water isotopic temperature scale, Geol. Soc. Am. Bull., 64, 1315–1325, 1953.

Fairbanks, R. G., Mortlock, R. A., Chiu, T. C., Cao, L., Kaplan, A., Guilderson, T. P., Fairbanks, T. W., Bloom, A. L., Grootes, P. M., and Nadeau, M. J.: Radiocarbon calibration curve spanning 0 to 50,000 years BP based on paired Th-230/U-234/U-238 and C-14 dates on pristine corals, Quatern. Sci. Rev., 24, 1781–1796, doi:10.1016/j.quascirev.2005.04.007, 2005.

Feng, S. and Hu, Q.: How the North Atlantic Multidecadal Oscillation may have influenced the Indian summer monsoon during the past two millennia, Geophys. Res. Lett., 35, L01 707, 2008.

Fichefet, T. and Maqueda, M. A. M.: Sensitivity of a global sea ice model to the treatment of ice thermodynamics and dynamics, J. Geophys. Res., 102, 12 609–12 646, 1997.

Fluckiger, J., Dallenbach, A., Blunier, T., Stauffer, B., Stocker, T. F., Raynaud, D., and Barnola, J. M.: Variations in atmospheric N2O concentration during abrupt climatic changes, Science, 285, 227–230, 1999.

Fontes, J. C., Gasse, F., and Gibert, E.: Holocene environmental changes in Lake Bangong basin (western Tibet) .1. Chronology and stable isotopes of carbonates of a Holocene lacustrine core, Palaeogeography Palaeoclimatology Palaeoecology, 120, 25–47, 1996.

Gasse, F., Fontes, J. C., VanCampo, E., and Wei, K.: Holocene environmental changes in Bangong Co basin (western Tibet) .4. Discussion and conclusions, Palaeogeography Palaeoclimatology Palaeoecology, 120, 79–92, 1996.

Goswami, B. N. and Xavier, P. K.: ENSO control on the south Asian monsoon through the length of the rainy season, Geophys. Res. Lett., 32, L18 717, 2005.

Goswami, B. N., Madhusoodanan, M. S., Neema, C. P., and Sengupta, D.: A physical mechanism for North Atlantic SST influence on the Indian summer monsoon, Geophys. Res. Lett., 33, L02 706, 2006.

Grootes, P. M., Stuiver, M., White, J. W. C., Johnsen, S., and Jouzel, J.: Comparison Of Oxygen-Isotope Records From The Gisp2 And Grip Greenland Ice Cores, Nature, 366, 552–554, 1993.

Guo, Z., Liu, T., Guiot, J., Wu, N., Lu, H., Han, J., Liu, J., and Gu, Z.: High frequency pulses of East Asian monsoon climate in the last two glaciations: Link with the North Atlantic, Climate Dyn., 12, 701–709, 1996.

He, H. Y., Sui, C. H., Jian, M. Q., Wen, Z. P., and Lan, G. D.: The evolution of tropospheric temperature field and its relationship with the onset of Asian summer monsoon, J. Meteor. Soc. Japan, 81, 1201–1223, 2003.

Hourdin, F., Musat, I., Bony, S., Braconnot, P., Codron, F., Dufresne, J. L., Fairhead, L., Filiberti, M. A., Friedlingstein, P., Grandpeix, J. Y., Krinner, G., Levan, P., Li, Z. X., and Lott, F.: The LMDZ4 general circulation model: climate performance and sensitivity to parametrized physics with emphasis on tropical convection, Climate Dyn., 27, 787–813, 2006.

Hughen, K., Lehman, S., Southon, J., Overpeck, J., Marchal, O., Herring, C., and Turnbull, J.: C-14 activity and global carbon cycle changes over the past 50,000 years, Science, 303, 202–207, 2004.

Hutson, W.: The Agulhas Current during the Late Pleistocene: Analysis of modern faunal analogs, Science, 207, 64–66, 1979.

Jin, L., Chen, F., Ganopolski, A., and Claussen, M.: Response of East Asian climate to Dansgaard/Oeschger and Heinrich events in a coupled model of intermediate complexity, J. Geophys. Res.-Atmospheres, 112, D06 117, 2007.

Kageyama, M., Mignot, J., Swingedouw, D., Marzin, C., Alkama, R., and Marti, O.: Glacial climate sensitivity to different states of the Atlantic Meridional Overturning Circulation: results from the IPSL model, Clim. Past, 5, 551–570, 2009.

Kageyama, M., Paul, A., Roche, D. M., and Meerbeeck, C. J. V.: Modelling glacial climatic millennial-scale variability related to changes in the Atlantic meridional overturning circulation: a review, Quaternary Science Reviews, 29, 2931 – 2956, doi:DOI:10.1016/j.quascirev.2010.05.029, http://www.sciencedirect.com/science/article/B6VBC-50KVGDK-3/2/fa9878b46900b3182c5fc8a03333da7f, vegetation Response to Millennial-scale Variability during the Last Glacial, 2010.

Khare, N.: Climatically sensitive 'Arctic': Another scientific frontier for India, Current Science, 94, 176–178, 2008.

Krinner, G., Viovy, N., de Noblet-Ducoudre, N., Ogee, J., Polcher, J., Friedlingstein, P., Ciais, P., Sitch, S., and Prentice, I. C.: A dynamic global vegetation model for studies of the coupled atmosphere-biosphere system, Global Biogeochemical Cycles, 19, GB1015, 2005.

Kucharski, F., Bracco, A., Yoo, J. H., and Molteni, F.: Atlantic forced component of the Indian monsoon interannual variability, Geophys. Res. Lett., 35, L04 706, 2008.

Kucharski, F., Bracco, A., Yoo, J. H., Tompkins, A. M., Feudale, L., Ruti, P., and Dell'Aquila, A.: A Gill-Matsuno-type mechanism explains the tropical Atlantic influence on African and Indian monsoon rainfall, Quarterly Journal Of The Royal Meteorological Society, 135, 569–579, 2009.

Kudrass, H. R., Hofmann, A., Doose, H., Emeis, K., and Erlenkeuser, H.: Modulation and amplification of climatic changes in the Northern Hemisphere by the Indian summer monsoon during the past 80 k.y., Geology, 29, 63–66, 2001.

Laj, C., Mazaud, A., and Duplessy, J. C.: Geomagnetic intensity and C-14 abundance in the atmosphere and ocean during the past 50kyr, Geophys. Res. Lett., 23, 2045–2048, 1996.

Li, Y. F. and Harrison, S. P.: Simulations of the impact of orbital forcing and ocean on the Asian summer monsoon during the Holocene, Global And Planetary Change, 60, 505–522, 2008.

Losada, T., Rodriguez-Fonseca, B., Polo, I., Janicot, S., Gervois, S., Chauvin, F., and Ruti, P.: Tropical response to the Atlantic Equatorial mode: AGCM multimodel approach, Climate Dyn., 35, 45–52, 2010.

Lu, R. Y. and Dong, B. W.: Response of the Asian Summer Monsoon to Weakening of Atlantic Thermohaline Circulation, Advances In Atmospheric Sciences, 25, 723–736, 2008.

Lu, R. Y., Dong, B. W., and Ding, H.: Impact of the Atlantic multidecadal oscillation on the Asian summer monsoon, Geophys. Res. Lett., 33, L24 701, 2006.

Madec, G., Delecluse, P., Imbard, M., and Levy, C.: OPA version 8.1 ocean general circulation model reference manual, LODYC/IPSL, Paris, France, 11, 1998.

Marti, O., Braconnot, P., Dufresne, J-L. Bellier, J., Benshila, R., Bony, S., Brockmann, P., Cadule, P., Caubel, A., Codron, F., Denvil, S., Fairhead, L., Fichefet, T., Foujols, M. A., Friedlingstein, P., Goosse, H., Grandpeix, J. Y., Guilyardi, E., Hourdin, F., Idelkadi, A., Kageyama, M., Krinner, G., Levy, C., Madec, G., Musat, I., Swingedouw, D., and Talandier, C.: Key features of the IPSL ocean atmosphere model and its sensitivity to atmospheric resolution, Climate Dyn., pp. DOI 10.1007/s00 382–009–0640–6, 2010.

Marzin, C. and Braconnot, P.: Variations of Indian and African monsoons induced by insolation changes at 6 and 9.5 kyr BP, Climate Dyn., 33, 215–231, 2009.

Meese, D. A., Gow, A. J., Alley, R. B., Zielinski, G. A., Grootes, P. M., Ram, M., Taylor, K. C., Mayewski, P. A., and Bolzan, J. F.: The Greenland Ice Sheet Project 2 depth-age scale: Methods and results, J. Geophys. Res.-Oceans, 102, 26 411–26 423, 1997.

Monnin, E., Indermuhle, A., Dallenbach, A., Fluckiger, J., Stauffer, B., Stocker, T. F., Raynaud, D., and Barnola, J. M.: Atmospheric CO2 concentrations over the last glacial termination, Science, 291, 112–114, 2001.

Overpeck, J. T., Webb, T., and Prentice, I. C.: Quantitative Interpretation of Fossil Pollen Spectra - Dissimilarity Coefficients and the Method of Modern Analogs, Quat. Res., 23, 87–108, 1985.

Peltier, W. R.: Global glacial isostasy and the surface of the ice-age earth: The ice-5G (VM2) model and grace, Annual Review Of Earth And Planetary Sciences, 32, 111–149, 2004.

Porter, S. C. and An, Z. S.: Correlation Between Climate Events In The North-Atlantic And China During Last Glaciation, Nature, 375, 305–308, 1995.

Prell, W. L., Hutson, W. H., Williams, D. F., Be, A. W. H., Geitzenauer, K., and Molfino, B.: Surface Circulation of the Indian-ocean During the Last Glacial Maximum, Approximately 18,000 Yr Bp, Quat. Res., 14, 309–336, 1980.

Prentice, I. C.: Multidimensional-scaling As A Research Tool In Quaternary Palynology - A Review of Theory and Methods, Review of Palaeobotany and Palynology, 31, 71–104, 1980.

Rashid, H., Flower, B. P., Poore, R. Z., and Quinn, T. M.: A similar to 25 ka Indian Ocean monsoon variability record from the Andaman Sea, Quatern. Sci. Rev., 26, 2586–2597, 2007.

Rostek, F., Ruhland, G., Bassinot, F. C., Muller, P. J., Labeyrie, L. D., Lancelot, Y., and Bard, E.: Reconstructing Sea-surface Temperature and Salinity Using Delta-o-18 and Alkenone Records, Nature, 364, 319–321, 1993.

Rousseau, D. D. and Kukla, G.: Abrupt retreat of summer monsoon at the S1/L1 boundary in China, Global and Planetary Change, 26, 189–198, 2000.

Seager, R. and Battisti, D. S.: The General Circulation of the Atmosphere, chap. Challenges to our understanding of the general circulation: Abrupt climate change, pp. 331–371, Princeton University Press, 2007.

Shackleton, N. J.: Attainment of isotopic equilibrium between ocean water and benthonic foraminifera genus Uvigerina: Isotopic changes in the ocean during the last glacial, Colloq. Int. C.N.R.S., 219, 203–209, 1974.

Sirocko, F., Sarnthein, M., Lange, H., and Erlenkeuser, H.: Atmospheric Summer Circulation and Coastal Upwelling In the Arabian Sea During the Holocene and the Last Glaciation, Quat. Res., 36, 72–93, 1991.

Stouffer, R. J., Yin, J., Gregory, J. M., Dixon, K. W., Spelman, M. J., Hurlin, W., Weaver, A. J., Eby, M., Flato, G. M., Hasumi, H., Hu, A., Jungclaus, J. H., Kamenkovich, I. V., Levermann, A., Montoya, M., Murakami, S., Nawrath, S., Oka, A., Peltier, W. R., Robitaille, D. Y., Sokolov, A., Vettoretti, G., and Weber, S. L.: Investigating the causes of the response of the thermohaline circulation to past and future climate changes, J. Climate, 19, 1365–1387, 2006.

Stuiver, M. and Reimer, P. J.: Extended C-14 Data-base and Revised Calib 3.0 C-14 Age Calibration Program, Radiocarbon, 35, 215–230, 1993.

Stuiver, M., Reimer, P. J., and Braziunas, T. F.: High-precision radiocarbon age calibration for terrestrial and marine samples, Radiocarbon, 40, 1127–1151, 1998.

Swingedouw, D., Mignot, J., Braconnot, P., Mosquet, E., Kageyama, M., and Alkama, R.: Impact of Freshwater Release in the North Atlantic under Different Climate Conditions in an OAGCM, J. Climate, 22, 6377–6403, 2009.

Terray, L., Sevault, E., Guilyardi, E., and Thual, O.: The OASIS coupler user guide version 2.0., 1995.

Thouveny, N., Debeaulieu, J. L., Bonifay, E., Creer, K. M., Guiot, J., Icole, M., Johnsen, S., Jouzel, J., Reille, M., Williams, T., and Williamson, D.: Climate Variations In Europe Over The Past 140-Kyr Deduced From

Rock Magnetism, Nature, 371, 503–506, 1994.

Tierney, J. E. and Russell, J. M.: Abrupt climate change in southeast tropical Africa influenced by Indian monsoon variability and ITCZ migration, Geophys. Res. Lett., 34, L15 709, 2007.

Timmermann, A., Okumura, Y., An, S. I., Clement, A., Dong, B., Guilyardi, E., Hu, A., Jungclaus, J. H., Renold, M., Stocker, T. F., Stouffer, R. J., Sutton, R., Xie, S. P., and Yin, J.: The influence of a weakening of the Atlantic meridional overturning circulation on ENSO, J. Climate, 20, 4899–4919, 2007.

van der Plicht, J., Beck, J. W., Bard, E., Baillie, M. G. L., Blackwell, P. G., Buck, C. E., Friedrich, M., Guilderson, T. P., Hughen, K. A., Kromer, B., McCormac, F. G., Ramsey, C. B., Reimer, P. J., Reimer, R. W., Remmele, S., Richards, D. A., Southon, J. R., Stuiver, M., and Weyhenmeyer, C. E.: NotCal04 - Comparison/calibration C-14 records 26-50 cal kyr BP, Radiocarbon, 46, 1225–1238, 2004.

VanCampo, E. and Gasse, F.: Pollen-inferred and Diatom-inferred Climatic and Hydrological Changes In Sumxi Co Basin (western Tibet) Since 13,000 Yr Bp, Quat. Res., 39, 300–313, 1993.

VanCampo, E., Cour, P., and Hang, S. X.: Holocene environmental changes in Bangong Co basin (western Tibet) .2. The pollen record, Palaeogeography Palaeoclimatology Palaeoecology, 120, 49–63, 1996.

Varkey, M. J., Murty, V. S. N., and Suryanarayana, A.: Oceanography and Marine Biology: an Annual Review, chap. Physical oceanography of the Bay of Bengal and Andaman Sea, pp. 1–70, UCL Press, 1996.

Vellinga, M. and Wood, R. A.: Global climatic impacts of a collapse of the Atlantic thermohaline circulation, Clim. Change, 54, 251–267, 2002.

Volker, A., Sarnthein, M., Grootes, P., Erlenkeuser, H., Laj, C., Mazaud, A., Nadeau, M.-J., and Schleicher, M.: Correlation of marine 14C ages from the Nordic Sea with the GISP2 isotope record: Iimplications for 14C calibration beyond 25 ka BP, Radiocarbon, 40, 517–534, 1998.

Waelbroeck, C., Labeyrie, L., Michel, E., Duplessy, J. C., McManus, J. F., Lambeck, K., Balbon, E., and Labracherie, M.: Sea-level and deep water temperature changes derived from benthic foraminifera isotopic records, Quatern. Sci. Rev., 21, 295–305, 2002.

Wang, B., Wu, R. G., and Lau, K. M.: Interannual variability of the Asian summer monsoon: Contrasts between the Indian and the western North Pacific-east Asian monsoons, J. Climate, 14, 4073–4090, 2001.

Wu, R. G. and Kirtman, B. P.: Observed relationship of spring and summer East Asian rainfall with winter and spring Eurasian snow, J. Climate, 20, 1285–1304, 2007.

Xavier, P. K., Marzin, C., and Goswami, B. N.: An objective definition of the Indian summer monsoon season and a new perspective on the ENSO-monsoon relationship, Quart. J. Roy. Meteor. Soc., 133, 749–764, 2007.

Xiao, J., Porter, S. C., An, Z. S., Kumai, H., and Yoshikawa, S.: Grain-size of Quartz As An Indicator of Winter Monsoon Strength On the Loess Plateau of Central China During the Last 130,000-yr, Quat. Res., 43, 22–29, 1995.

Xiao, J. L., An, Z. S., Liu, T. S., Inouchi, Y., Kumai, H., Yoshikawa, S., and Kondo, Y.: East Asian monsoon variation during the last 130,000 Years: evidence from the Loess Plateau of central China and Lake Biwa of Japan, Quatern. Sci. Rev., 18, 147–157, 1999.

Yanase, W. and Abe-Ouchi, A.: The LGM surface climate and atmospheric circulation over East Asia and the North Pacific in the PMIP2 coupled model simulations, Clim. Past, 3, 439–451, 2007.

Zhang, R. and Delworth, T. L.: Simulated tropical response to a substantial weakening of the Atlantic thermohaline circulation, J. Climate, 18, 1853–1860, 2005.

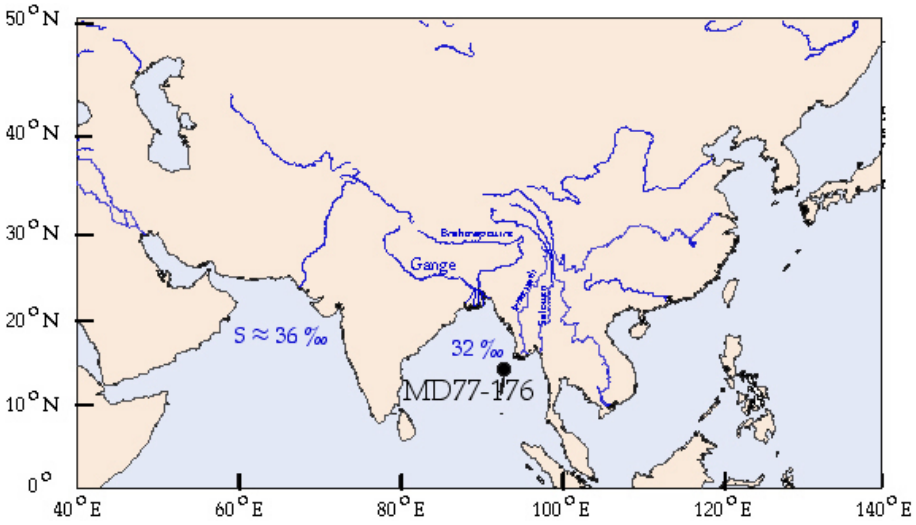

Fig. 1. Location map of the sediment core MD77-176 in the Bay of Bengal: 14°31N; 93°08E ; 1375 m water depth

Zhang, R. and Delworth, T. L.: Impact of Atlantic multidecadal oscillations on India/Sahel rainfall and Atlantic hurricanes, Geophys. Res. Lett., 33, L17 712, 2006.

Zonneveld, K. A. F., Ganssen, G., Troelstra, S., Versteegh, G. J. M., and Visscher, H.: Mechanisms forcing abrupt fluctuations of the Indian Ocean summer monsoon during the last deglaciation, Quatern. Sci. Rev., 16, 187–201, 1997.

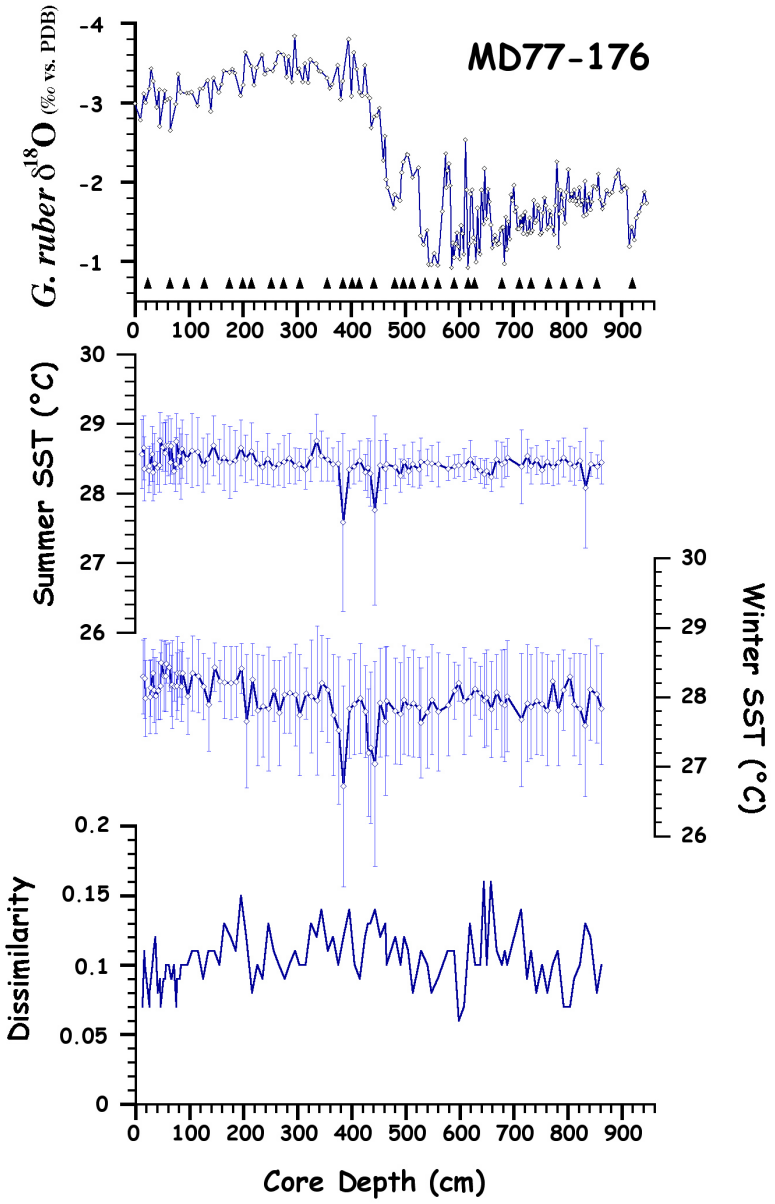

Fig. 2. Depth-age plots for core MD77-176. From top to bottom: $\delta^{18}O$ of G. ruber, reconstructions of summer SST and winter SST with error bars and dissimilarity coefficients between fossil assemblages and the modern analogues.

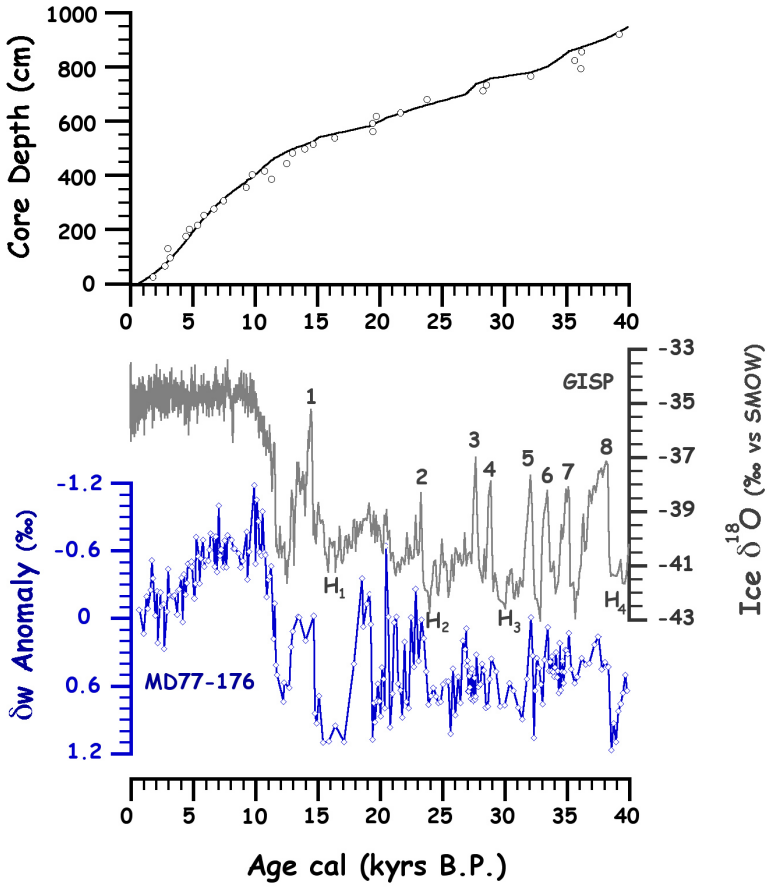

Fig. 3. From top to bottom: MD77-176 core depth versus age, Greenland ice core record GISP2 ice $\delta^{18}O$ versus age and MD77-176 core δ_w anomaly versus age.

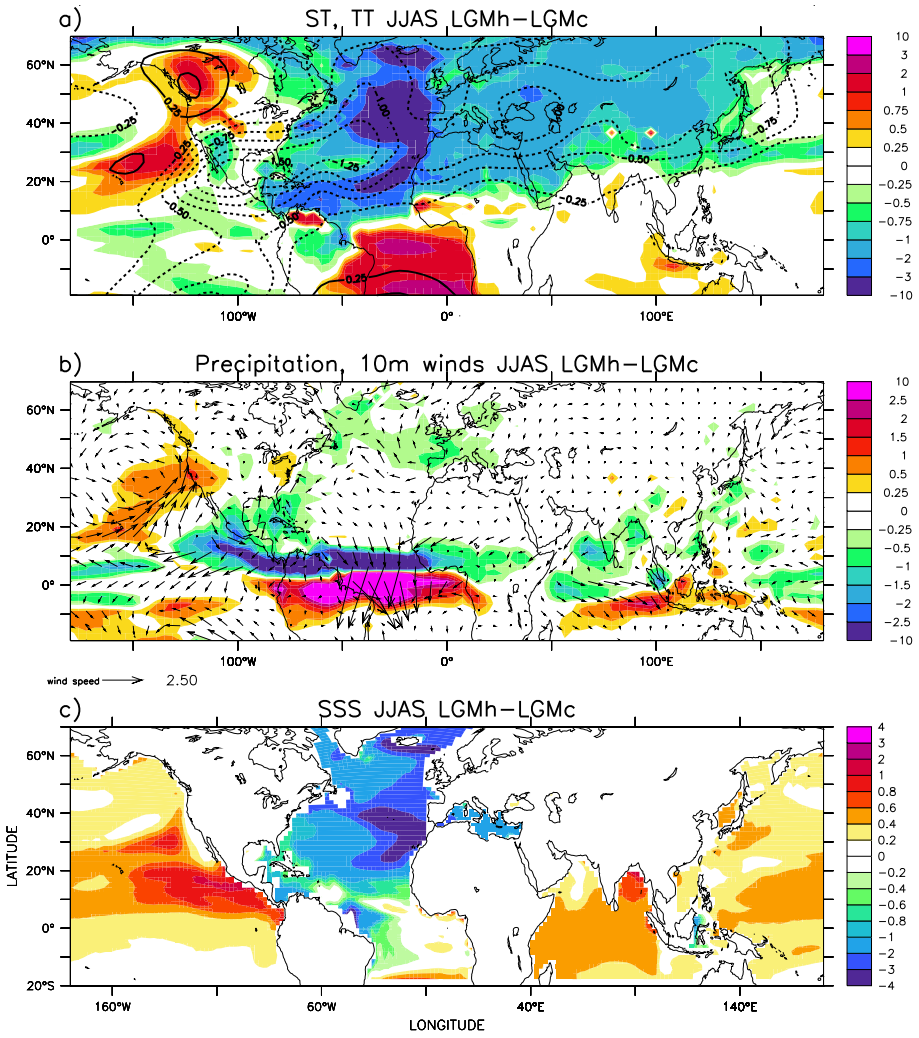

Fig. 4. Differences between LGMh and LGMc of (a) JJAS surface temperature (shaded) and tropospheric temperature averaged from 200 to 500 hPa (contours), (b) precipitation and 10 m winds, (c) sea surface salinity

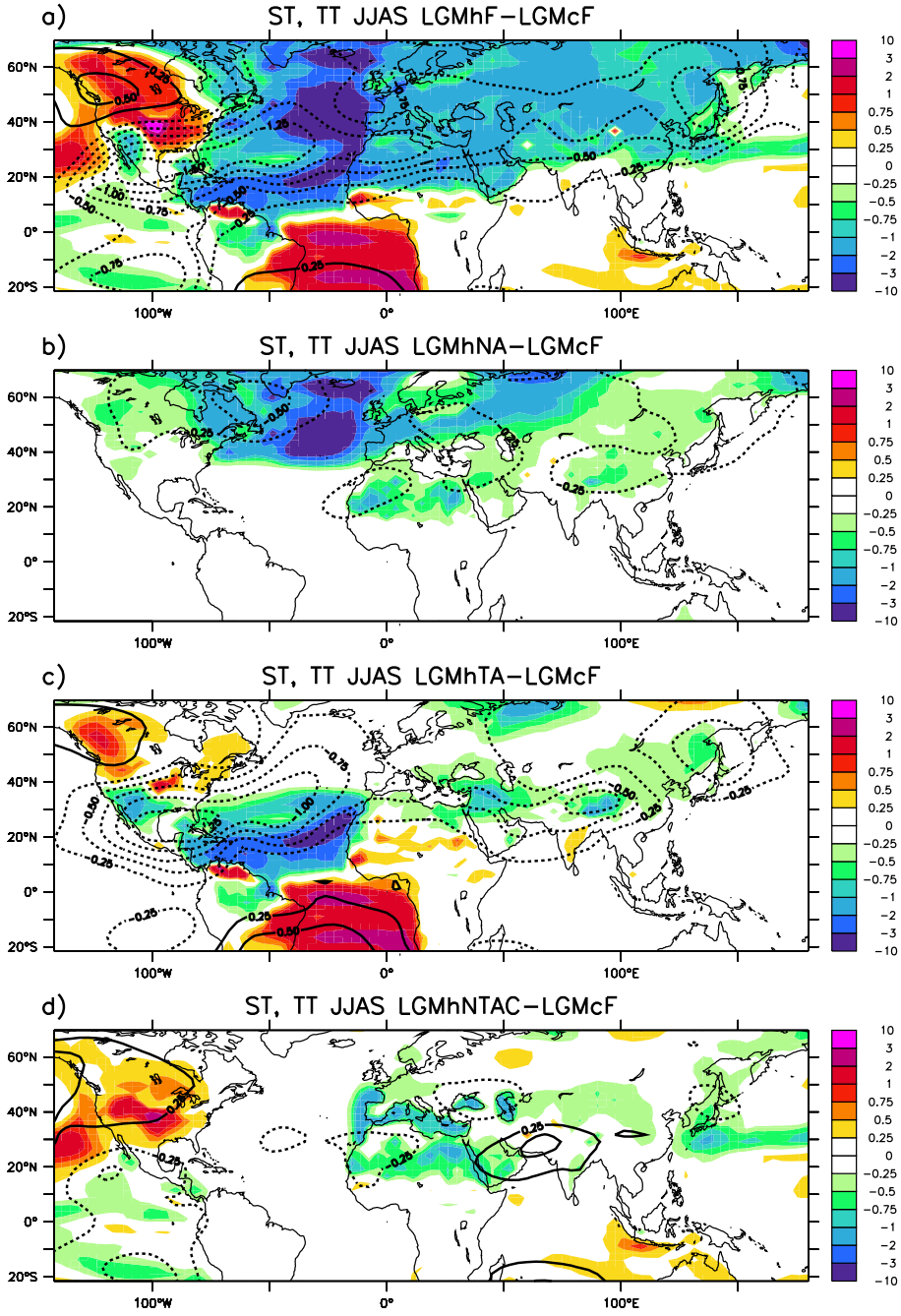

Fig. 5. Differences of JJAS surface temperature (shaded) and tropospheric temperature averaged from 200 to 500 hPa (contours) between (a) LGMhF and LGMcF, (b) LGMhNA and LGMcF, (c) LGMhTA and LGMcF, (d) LGMhTAC and LGMcF.

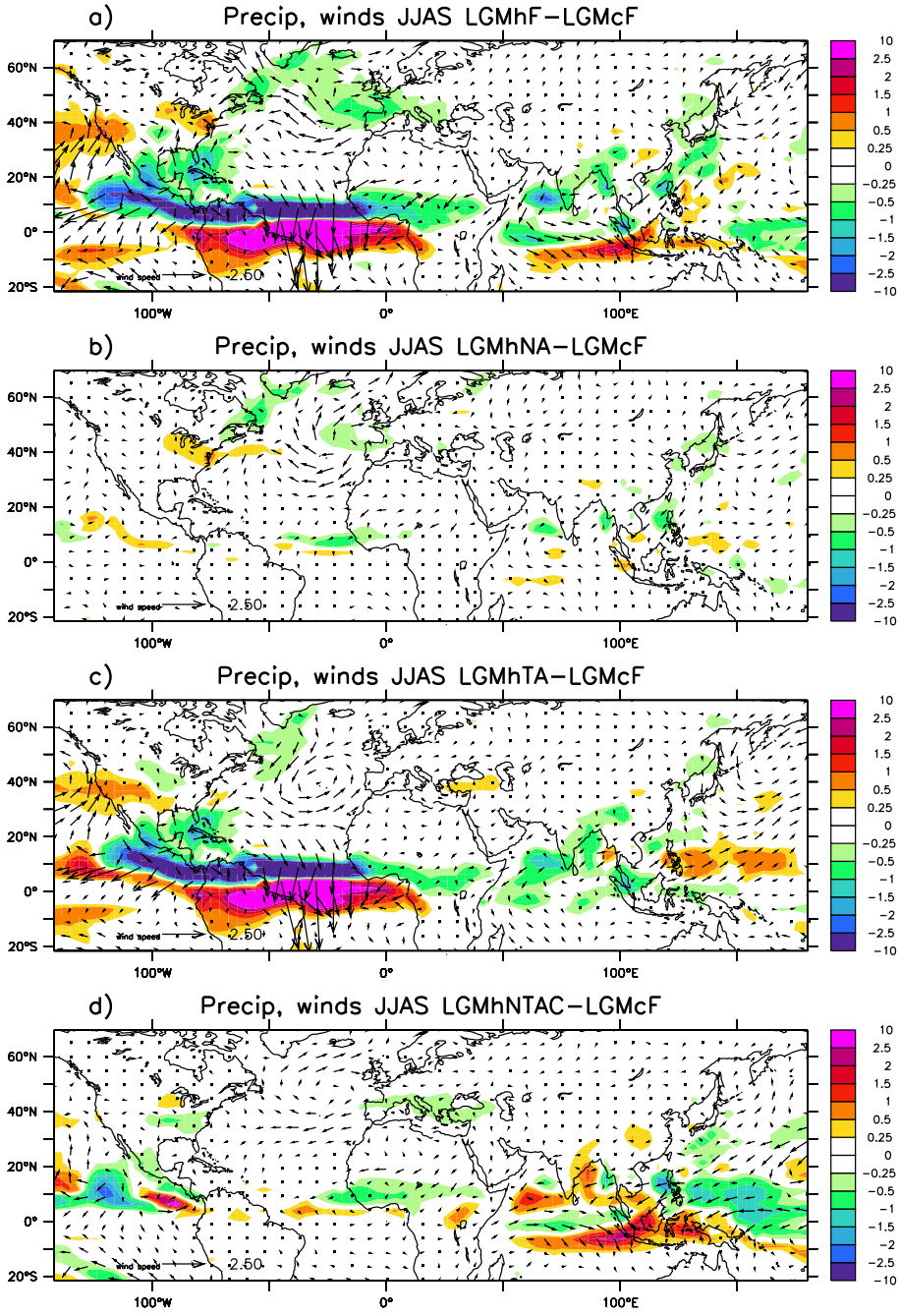

Fig. 6. Differences of JJAS precipitation and 10 m winds between (a) LGMhF and LGMcF, (b) LGMhNA and LGMcF, (c) LGMhTA and LGMcF, (d) LGMhTAC and LGMcF.

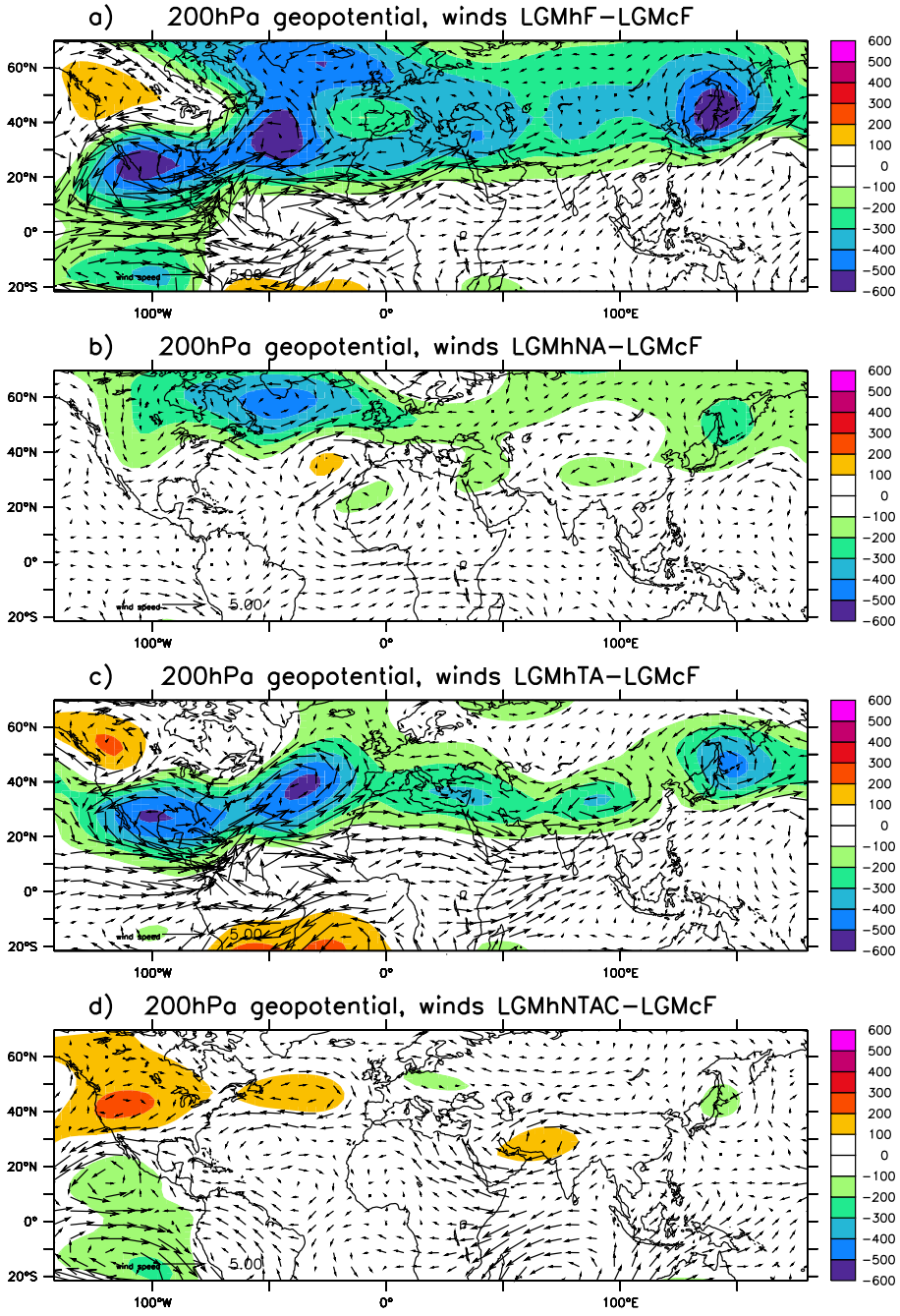

Fig. 7. Differences of 200 hPa geopotential and winds between (a) LGMhF and LGMcF, (b) LGMhNA and LGMcF, (c) LGMhTA and LGMcF, (d) LGMhTAC and LGMcF.

5.4.2 Compléments d'étude

Des expériences supplémentaires à celles présentées dans la partie 5.4.1 ont été réalisées en collaboration avec Masa Kageyama. De façon à mieux comprendre la téléconnection entre les moussons et le signal de SST en Atlantique Nord, j'ai souhaité isoler l'impact de plusieurs zones de changements de SSTs. Les tests sur les zones de changements de SST ont tous été réalisés deux fois, une fois en imposant la climatologie sur 50 ans des SSTs de l'expérience couplée de flux d'eau douce, une autre fois en imposant ces conditions aux limites en incluant la variabilité interannuelle. Voici une description de l'ensemble des expériences forcées qui ont été réalisées par Masa Kageyama mais que j'ai suggérées et analysées :

- LGMcF : expérience forcée par les SSTs du contrôle LGMc.
- LGMhF : expérience forcée par les SSTs de LGMh (climatologie), expérience de flux d'eau douce.
- LGMhNA : expérience forcée par les SSTs de LGMh (climatologie) dans l'Atlantique Nord (au-delà de 30°N) et de LGMc par ailleurs.
- LGMhNAv : similaire à LGMhNA en incluant la variabilité interannuelle des variations de SSTs pour les conditions aux limites.
- LGMhTA : expérience forcée par les SSTs de LGMh (climatologie) dans l'Atlantique tropical (de 30°S à 30°N) et de LGMc par ailleurs.
- LGMhTAv : similaire à LGMhTA en incluant la variabilité interannuelle des variations de SSTs pour les conditions aux limites.
- LGMhTACv : complémentaire de l'expérience LGMhTAv, SSTs de LGMh imposées partout sauf dans l'Atlantique tropical.
- LGMhTNA : expérience forcée par les SSTs de LGMh (climatologie) dans l'Atlantique Nord et tropical et de LGMc par ailleurs.
- LGMhTNAv : similaire à LGMhTNA en incluant la variabilité interannuelle des variations de SSTs pour les conditions aux limites.
- LGMhTNACv : complémentaire de l'expérience LGMhTNAv, SSTs de LGMh imposées partout sauf dans l'Atlantique Nord et tropical.

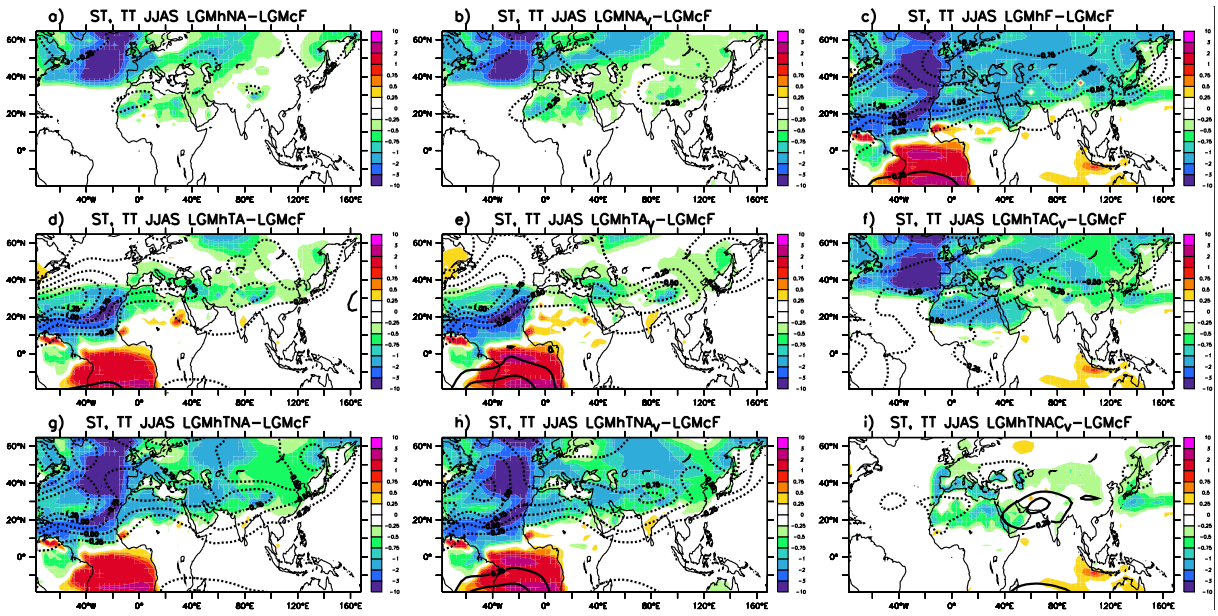

FIGURE 5.1: Différences de température de surface (couleurs) et de température troposphérique JJAS (moyennées de 500 à 200 hPa, contours) entre les expériences de sensibilité au flux d'eau et l'expérience de contrôle LGMcF.

La figure 5.1 permet de visualiser les zones de changements de SSTs testées dans chaque expérience par rapport au contrôle LGMhC. Ces tests supplémentaires confirment le rôle principal que joue le dipôle d'anomalies de SST de l'Atlantique tropical sur l'atténuation de la mousson indienne. L'introduction de la variabilité interannuelle du forçage ne faisant que renforcer l'assèchement du sous-continent indien (Fig. 5.2 d et e). Les conditions aux limites entre les expériences LGMhTA et LGMhTAv ne sont que légèrement différentes, mais elles illustrent à nouveau le lien entre la diminution des précipitations en Inde, le refroidissement de la couche troposphérique au niveau du Plateau Tibétain (Fig. 5.1 d et e) et l'anomalie de géopotentiel à 200 hPa accompagnée de l'accélération de la partie sud du jet d'ouest (Fig. 5.3 d et e). L'expérience LGMhTNAv montre que l'on peut recréer intégralement l'anomalie de précipitation sur le continent indien ainsi que la diminution du flux de mousson en imposant seulement le forçage en Atlantique nord et tropical (Fig. 5.2 h et c). Cependant, les anomalies de précipitation à l'est de l'Océan Indien équatorial sont expliquées par l'interaction avec les anomalies positives de SST au sud de l'Indonésie (Fig. 5.1 i et c).

Ces expériences nous permettent aussi d'explorer la réponse d'autres systèmes de mousson à un flux d'eau douce dans l'Atlantique nord en conditions glaciaires. La mousson africaine

est elle aussi affaiblie dans l'expérience d'évènement Heinrich idéalisée. Les précipitations de mousson sont diminuées sur le continent du Sahel à l'est de l'Afrique, et augmentées sur le Golfe de Guinée (Fig. 5.2 c), ce qui correspond à un déplacement vers le sud de la ZCIT. Le flux de mousson est diminué et on observe aussi une anomalie nord-est des vents de surface au niveau de la limite de la convergence au nord du Sahel (Fig. 5.2 c). Chang et al. (2008) ont analysé la réponse de la mousson africaine à un affaiblissement de la circulation thermohaline, et conclue que l'intensité de la mousson est particulièrement affectée par le réchauffement du Golfe de Guinée.

Contrairement à la mousson indienne, aucune des expériences de sensibilité ne permet de reconstruire entièrement les variations de précipitation sur le Sahel (Fig. 5.2). Une partie de la réponse sur l'Afrique apparaît dans l'expérience LGMhTAv pour la partie sud de l'anomalie sur le continent (Fig. 5.2 e). Cette diminution correspond à l'explication souvent apportée, comme quoi le dipôle d'anomalie de SSTs sur l'Atlantique tropical (Fig. 5.1 e) induit un shift de la ZCIT qui se prolonge sur le continent et affecte l'intensité de la mousson africaine. Cependant, les expériences LGMhTACv et LGMhTNACv présentent aussi un signal de diminution des précipitations sur la partie nord de la mousson africaine (Fig. 5.2 f et i). Le fait que la diminution de la mousson africaine n'est pas essentiellement influencée par le dipôle de SST dans l'Atlantique tropical est surprenant. Ceci implique une contribution importante du refroidissement sur la Méditerranée (Fig. 5.1 i). Dans l'expérience LGMhTACv, le Sahara est ainsi refroidi et l'anomalie de vent du nord-est apparaît au nord du Sahel. Bien que d'autres études montrent l'impact de l'affaiblissement de la circulation thermohaline sur l'affaiblissement de la mousson africaine, aucune ne teste les zones d'influence principales qu'engendre un tel forçage. Nous montrons ici que la mousson africaine est aussi bien influencée par le dipôle d'anomalies de SSTs dans l'Atlantique tropical que par le refroidissement autour de la Méditerranée. Les résultats de ces tests pourraient être analysés plus détail, la significativité des résultats limite leur interprétation. Par exemple, le signal d'affaiblissement des précipitations de mousson africaine ne se retrouve pas dans l'expérience LGMhTA mais est bien présent dans l'expérience ou la variabilité interannuelle du forçage est incluse, LGMhTAv.

En ce qui concerne la mousson d'Asie du sud-est, l'intensité des précipitations n'est pas affectée sur le continent, seule une diminution des pluies est obtenue sur le nord-ouest du Pacifique (Fig. 5.2 c). Ce système de mousson est influencé par le gradient méridional et longitudinal de température troposphérique entre le continent asiatique et le Pacifique ouest. Dans nos simulations, le forçage en Atlantique nord engendre un refroidissement de la troposphère aussi bien sur le continent que sur le Pacifique ouest (Fig. 5.1 c). Le contraste longitudinal n'est pas diminué, le flux de mousson est ainsi peu perturbé. Les tests de sensibilité montrent que le refroidissement sur cette région a deux contributions : l'une provient du mécanisme de refroidissement de l'Eurasie en lien avec les changements de SST en Atlantique tropical et les perturbations du jet d'ouest (Fig. 5.1 h), l'autre provient des changements de SST dans le Pacifique (Fig. 5.1 i)

.

Ces tests de sensibilité permettent de mettre en évidence les mécanismes de réponse des systèmes de mousson à un flux d'eau douce en Atlantique Nord. Nos expériences montrent la sensibilité des moussons africaines et indienne à ce type de forçage, tandis que le signal sur l'Asie de l'est n'est pas concluant. Bien que l'affaiblissement des moussons africaine et indienne soient en accord avec d'autres études de modélisation, les tests de sensibilité ont permis de tester les hypothèses de mécanismes préalablement avancées et suggèrent de nouveaux mécanismes de téléconnection. La mousson indienne est influencée par le dipôle de SST et le shift de la ZCIT vers le sud dans l'Atlantique tropical via des perturbations du jet d'ouest qui refroidissent l'Eurasie et le Plateau Tibétain, ce qui engendre une diminution du flux de mousson sur l'Inde. La mousson africaine est quant à elle dans ces expériences de flux d'eau, influencée par ce dipôle d'anomalies de SST dans l'Atlantique tropical, mais aussi par un refroidissement sur la Méditerranée. Ces résultats sont cohérents avec les études récentes de Kucharski et al. (2009); Losada et al. (2010) sur l'influence du mode de variabilité de l'Atlantique tropical sur les moussons africaine et indienne à l'échelle interannuelle. Une étude de comparaison de résultats de tests similaires avec d'autres modèles permettraient de déterminer si ces mécanismes sont prédominants et s'ils pourraient apporter une explication robuste aux variations abruptes observées dans les enregistrements paléoclimatiques des régions de mousson.

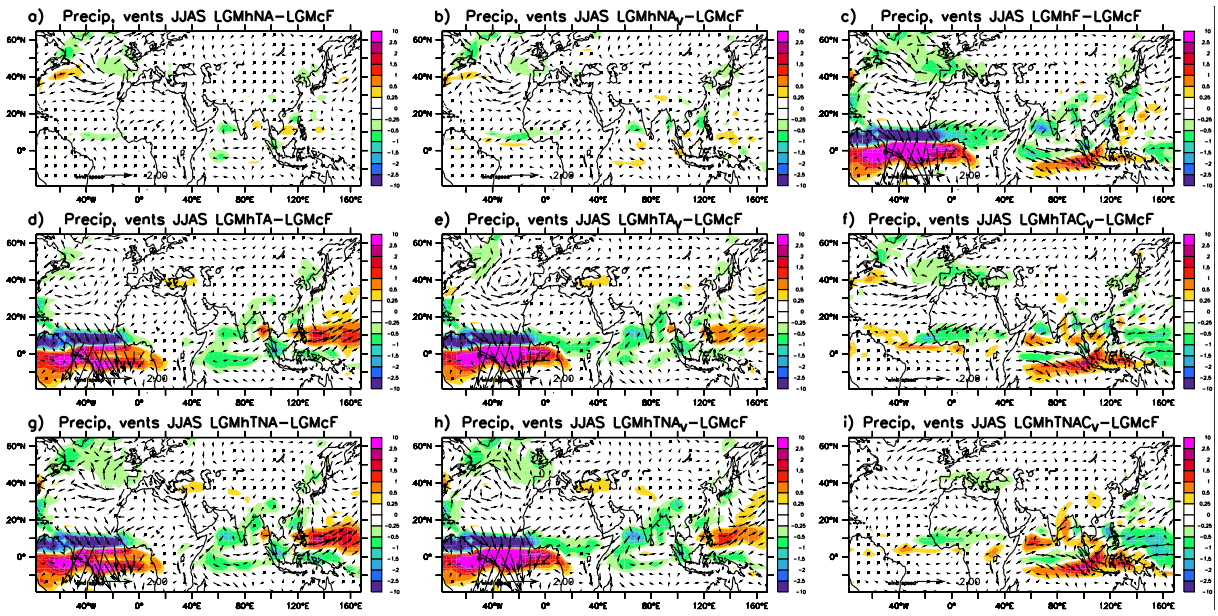

FIGURE 5.2: Différences de précipitations et de vents de surface JJAS entre les expériences de sensibilité au flux d'eau et l'expérience de contrôle LGMcF.

5.5 Comparaison de la téléconnection entre Atlantique Nord et systèmes de mousson pour différentes conditions climatiques

La téléconnection entre les évènements abrupts des hautes latitudes et les tropiques a principalement été mise en évidence dans les paléoenregistrements de la période glaciaire et de déglaciation. Cependant, des enregistrements montrent que de tels évènements ont aussi lieu pendant les périodes interglaciaires, et l'impact du ralentissement de la circulation thermohaline dans les projections climatiques futures représente un véritable enjeu pour ces régions tropicales. Swingedouw et al. (2009) ont analysé l'impact d'un flux d'eau douce en Atlantique Nord sous différentes conditions climatiques (interglaciaire Eémien, Dernier Maximum Glaciaire, Holocène moyen, préindustriel et futur (2xCO2)) de manière à évaluer le rôle de la climatologie sur les mécanismes de réponse à ce forçage. Pour ce faire, des paires de simulations sont analysées, à chaque climat correspond une expérience de contrôle et une expérience de flux d'eau douce interactif. Dans leur étude, toutes les expériences présentent un refroidissement de l'hémisphère nord ainsi qu'un shift de la ZCIT vers le sud. L'intensité du forçage de flux d'eau

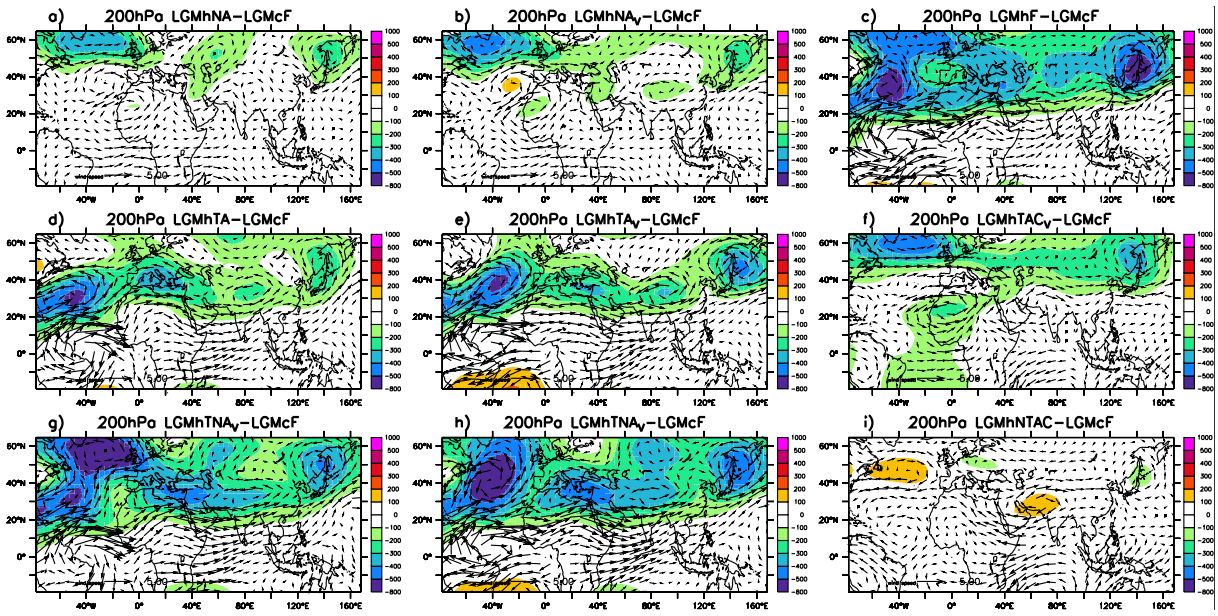

FIGURE 5.3: Différences de géopotentiel et de vents à 200 hPa entre les expériences de sensibilité au flux d'eau et l'expérience de contrôle LGMcF.

douce est dépendant de l'insolation (il est plus fort à l'Eémien). Cependant, la non-linéarité de la réponse de la circulation thermohaline au forçage en Atlantique nord est mise en évidence. Il est montré en particulier que le climat du Dernier Maximum Glaciaire présente une plus grande sensibilité de la circulation thermohaline au flux d'eau douce en Atlantique nord.

J'ai repris l'analyse de ces simulations pour étudier la sensibilité de la réponse des systèmes de mousson au forçage de flux d'eau douce dans différentes conditions climatiques. Les mêmes périodes que Swingedouw et al. (2009) sont considérées, en ajoutant l'expérience réalisée pour le début de l'Holocène. Le jeu de simulations représente ainsi l'interglaciaire Eémien à 126 ka BP (LIGc et LICh), le Dernier Maximum Glaciaire (LGMc et LGMh), le début de l'Holocène (EHOLc et EHOLh), l'Holocène Moyen (MHOLc et MHOLh), le préindustriel (PREc et PREh) et le futur à 2xCO2 (FUTc et FUTh). Les simulations ainsi que les résultats pour la circulation thermohaline sont détaillées dans Swingedouw et al. (2009). Les figures Fig. 5.4 et Fig. 5.5 montrent les différences entre les expériences de flux d'eau et les contrôles pour ces différents climats en terme de température de surface et de températures troposphériques, ainsi qu'en terme de précipitation et de circulation de surface pour la saison de mousson boréale. La figure 5.4 montre que toutes les expériences représentent un refroidissement de l'hémisphère nord au

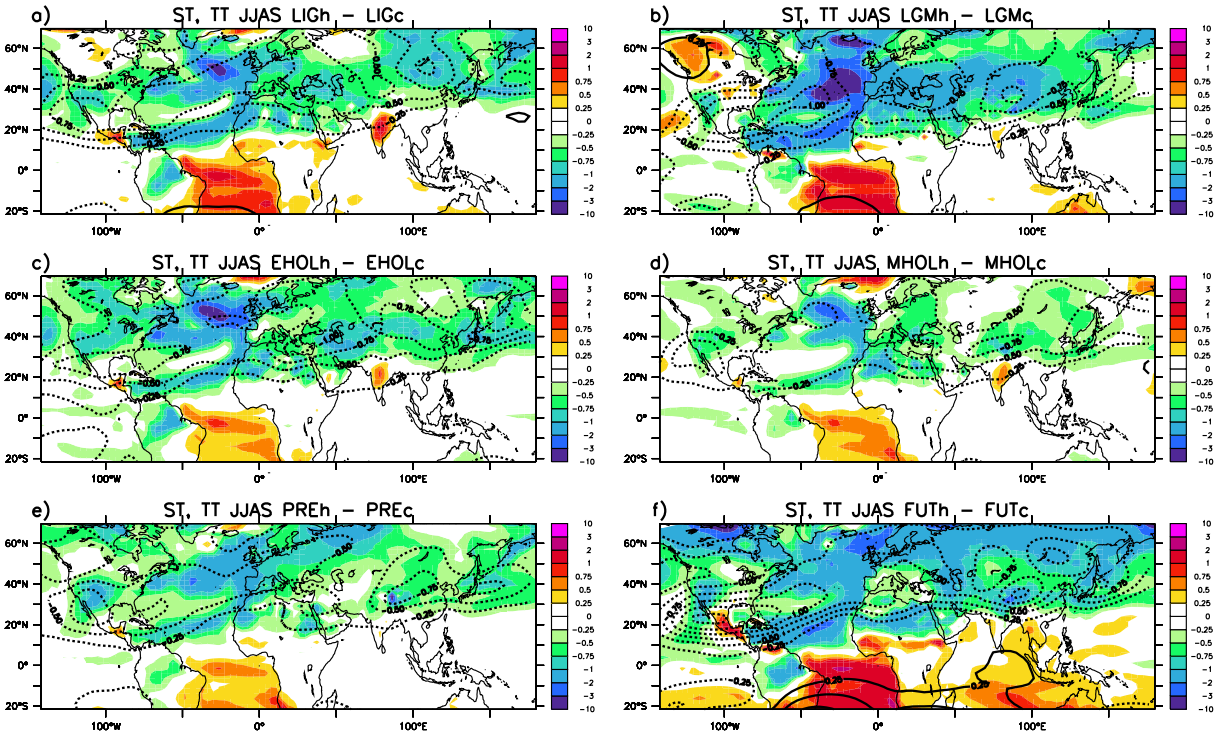

FIGURE 5.4: Différences de températures de surface (couleurs) et de températures troposphériques JJAS (moyennées de 500 à 200 hPa, contours) entre chaque expérience de sensibilité au flux d'eau et chaque expérience de contrôle.

niveau de la surface et pour la partie supérieure de la troposphère (TT) (Fig. 5.4). Le dipôle d'anomalies de SST en Atlantique est aussi présent avec une intensité variable d'un climat à l'autre.

Toutes les expériences représentent en général un affaiblissement des moussons indienne et africaine, mais pas d'impact sur la mousson d'Asie du sud-est, en accord avec l'étude précédente sur le Dernier Maximum Glaciaire. Cependant, des différences significatives sont à noter. En tenant compte seulement des expériences qui diffèrent en terme d'insolation, PRE, MHOL, EHOL et LIG, la réponse des moussons africaine et indienne est proportionnelle à l'étendue de la mousson sur le Sahel et sur le sous-continent indien dans les simulations de référence sans flux d'eau. La superposition des anomalies de précipitation en couleur et des contours à 3 mm/jour et 5 mm/jour permettent de rendre compte de ce résultat sur les Fig. 5.5 a, c, d et e. Plus les pluies de mousson sont importantes sur le continent, plus ces zones sont sensibles au forçage

en Atlantique nord. Le gradient méridional d'insolation qui est modulé par les paramètres orbitaux a ainsi un rôle amplificateur d'évènements abrupts pour ces périodes interglaciaires.

Ceci n'est par contre pas vérifié au LGM et pour le futur (Fig. 5.5 b et f). Swingedouw et al. (2009) ont montré que la circulation thermohaline est plus sensible au forçage d'eau douce en climat glaciaire, ceci induit une large perturbation des conditions de surface en Atlantique (Fig. 5.4 b et f) qui interagit avec les systèmes de mousson comme nous l'avons démontré dans la partie précédente. Ainsi, nous montrons que de la même manière les moussons indienne et africaine sont plus sensibles au forçage de flux d'eau douce au LGM dans nos expériences (Fig. 5.5 b).

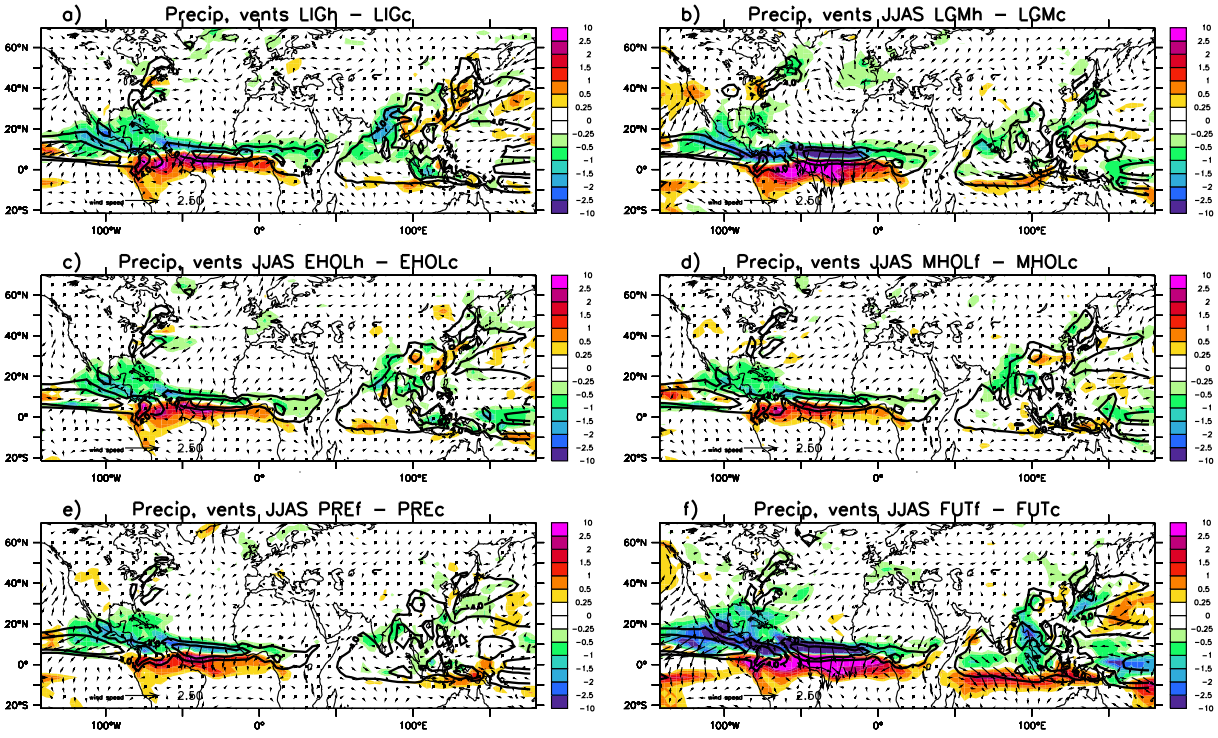

FIGURE 5.5: Différences de précipitation et de vents de surface JJAS entre chaque expérience de sensibilité au flux d'eau et chaque expérience de contrôle.

La figure 5.5 f indique une réponse différente des moussons en conditions de réchauffement climatique. Bien que le shift de la ZCIT et les anomalies de SST en Atlantique soient maximum entre les expériences FUTh et FUTc, la réduction des précipitations sur le Sahel n'est pas aussi importante qu'au LGM. Nous avons montré précédemment que le refroidissement de la

Méditerranée peut aussi contribuer à l'affaiblissement de la mousson africaine, et ce refroidissement n'est pas aussi marqué dans l'expérience de flux d'eau douce dans le futur qu'au LGM. Ceci expliquerait en partie la réponse atténuée sur le Sahel.

Les réponses de ces systèmes de mousson ne sont pas linéaires au déplacement de la ZCIT sur l'Atlantique tropical (Fig. 5.5). Bien que celui-ci soit maximum dans l'expérience FUTh (voir aussi figure 12 dans Swingedouw et al. (2009)), les précipitations ne sont pas diminuées sur le continent indien et l'anomalie sur le Sahel n'est pas étendue bien qu'elle soit importante sur la côte (2mm/jour). La réponse de l'océan indien au flux d'eau douce est très différente dans le cas du climat futur par rapport aux autres (Fig. 5.5 f). En effet, on observe une importante diminution des précipitations sur la Baie du Bengal, là où le contrôle présente un maximum de pluie, mais pas de changement sur le sous-continent. De plus, cette simulation présente un déplacement important des précipitations de l'océan Indien équatorial nord à l'Océan Indien équatorial sud. Ceci s'explique par une redistribution des précipitations sur l'océan plus chaud. La figure 5.4 f indique ce réchauffement de l'Océan Indien induit par le flux d'eau douce en Atlantique nord. De plus, les anomalies de SST et de précipitation sont plus prononcées dans le Pacifique pour FUTh.

De la même manière, les réponses au flux d'eau douce en climat futur sont très différentes des autres simulations en terme de changement de température de surface et de la partie supérieure de la troposphère (TT). Le refroidissement en surface de l'hémisphère nord est plus étendu vers les hautes latitudes, et c'est la seule simulation où un réchauffement des océans de l'hémisphère sud autre que l'Atlantique est clairement observé. Bien que les anomalies négatives de température troposphérique soient maximum sur l'hémisphère nord dans cette simulation, elles sont situées plus au nord et sont accompagnées par un réchauffement de la troposphère dans le sud des tropiques. Ces résultats montrent la plus sensibilité du climat tropical à une expérience de flux d'eau douce en conditions de réchauffement climatique, bien que la réponse de la circulation thermohaline ne soit pas la plus forte pour ce climat (Swingedouw et al., 2009).

Cette étude démontre l'importance de tenir compte des conditions climatiques (paramètres orbitaux, représentation des calottes de glaces, et concentration des gaz à effet de serre) pour

analyser l'impact d'évènements abrupts dans l'Atlantique nord et l'Arctique sur le climat tropical. Il faudrait approfondir ces analyses de façon à mieux comprendre les influences de grande échelle sur les systèmes de mousson, nous n'avons pas ici vérifié l'impact des variations de climat dans le Pacifique et l'hémisphère sud sur les moussons, alors qu'il pourrait être déterminant. Cette partie d'ouverture permet de poser la question jusqu'où peut-on utiliser la modélisation des climats passés pour prévoir et comprendre les variations climatiques futures. Les différences de forçages activent différents types de mécanismes de réponse et sont la plupart du temps incomparables (changements de paramètres orbitaux, de concentration en gaz à effet de serre...). Mais notre étude va plus loin et montre que même en réalisant le même type d'expérience de flux d'eau douce en Atlantique nord, les réponses climatiques bien que similaires peuvent présenter des différentes locales non négligeables.

6

Conclusions et perspectives

6.1 Synthèse

La principale question autour de laquelle ces résultats se sont construits était la suivante : les sous-systèmes de mousson varient-t-ils de façon synchrone en réponse aux changements de saisonnalité du forçage solaire ou présentent-ils des particularités régionales ? Pour ce faire, la modélisation de périodes climatiques présentant des différences du cycle saisonnier d'insolation ont été utilisées pour analyser le lien entre l'insolation et les moussons en Afrique, en Inde et en Asie. Ces simulations principales ont été complétées par des tests de sensibilité pour tester comment certaines rétroactions et d'autres forçages climatiques affectent ce lien entre l'insolation et les moussons. De plus, d'autres tests ont permis d'étudier plus en détail les mécanismes de téléconnection entre systèmes de mousson et entre des perturbations de l'Atlantique Nord et des moussons. L'ensemble de ces expériences est synthétisé dans le tableau suivant :

Période	Paramètres orbitaux	Tests atm	Tests OA flux d'eau	Test OA calotte
0 ka	X	X (SSTs ctrl)	X	
6 ka	X	X (SSTs ctrl)	X	
9.5 ka	X	X (SSTs ctrl)	X	X
21 ka	X (+autres conditions aux limites glaciaires)	X (tests distribution SSTs)	X	
115 ka	X			
122 ka	X			
126 ka	X		X	
Futur			X	

TABLE 6.1: Tableau synthétique des simulations analysées dans cette thèse. Les périodes principales analysées sont indiquées en gras. "Tests atm" se réfère aux tests réalisés avec le modèle atmosphérique forcé par des SSTs provenant de simulations couplées. "Tests OA" se réfère aux tests réalisés à l'aide du modèle couplé Océan-Atmosphère. "Ctrl" se réfère à la simulation couplée de référence 0 ka.

L'objectif principal de ce travail était premièrement d'analyser l'effet des variations d'insolation à l'Holocène sur les systèmes de mousson en Asie et en Afrique entre 0, 6 et 9.5 ka. La partie 3.2 (Marzin and Braconnot, 2009b) montre que l'intensification des moussons indienne et africaine suit au premier ordre les variations du cycle saisonnier de l'insolation. Les précipitations sont augmentées sur les continents principalement par plus d'advection d'humidité par les flux de mousson à 6 et 9.5 ka par rapport à 0 ka, et d'autre part par un recyclage de l'évaporation locale. Les variations de la mousson indienne sont associées au large renforcement du gradient de température troposphérique entre le Plateau Tibétain et l'Océan Indien de la fin du printemps au début de l'automne. Le rôle de la précession des équinoxes sur le cycle saisonnier des précipitations est mis en avant dans ces simulations à l'aide de climatologies journalières, pour analyser le déroulement du phénomène au-delà de limites mensuelles fixes. Celles-ci présentent un décalage de la saison des pluies entre 6 et 9.5 ka et un allongement de la longueur totale de la saison de mousson à 6 et 9.5 ka par rapport à la simulation de référence. L'amplification relative des moussons entre ces trois périodes est différente pour l'Inde et l'Afrique. La mousson africaine est peu modifiée entre 6 et 9.5 ka, alors que des différences marquées sont simulées

entre ces 2 périodes pour la mousson indienne. Les données de niveau des lacs, de pollens et de productivité marine suggèrent aussi que la diminution de l'intensité des moussons au cours de l'Holocène s'est faite plus lentement en Afrique qu'en Inde. Cette différence est expliquée par le biais de plusieurs hypothèses. La saisonnalité du forçage par l'insolation favorise relativement la mousson indienne à 9.5 ka tandis que c'est la mousson africaine qui est favorisée à 6 ka de par un phénomène de résonance entre la saisonnalité du forçage et des systèmes de mousson. De plus, la fonte rapide de la couverture de neige sur le Plateau Tibétain au printemps à 9.5 ka par rapport à 0 et 6 ka induit une rétroaction positive sur le déclenchement et l'intensité de la mousson indienne. L'effet de la précession sur l'amplification relative des systèmes de mousson a été confirmé à l'aide d'un jeu de simulations pendant l'Eémien présentant des changements de précession similaire (Braconnot et al. (2008), annexe A.1). Les mêmes déphasages et amplifications de mousson sont observés, mais de façon exacerbée, l'excentricité étant plus grande à cette période.

En plus de la climatologie des sytèmes de mousson, leur variabilité est aussi affectée par les changements de climat à l'Holocène. Les résultats de la partie 3.3 indiquent que la variabilité des moussons en Inde, en Asie du Sud-Est et en Afrique est intensifiée aussi bien à l'échelle intra-saisonnière qu'à l'échelle interannuelle à 6 et 9.5 ka par rapport à 0 ka, tandis que la variabilité d'ENSO est elle diminuée. A plus courte échelle, l'amplification de la mousson sur la saison JJAS est due à de plus nombreux évènements fortement précipitants. Les différences relatives d'intensité et de nombre d'évènements précipitants suivent les amplifications de la saison de mousson. Ainsi, les différences entre 6 et 9.5 ka sont faibles pour la mousson africaine et d'Asie du sud-est par rapport à la mousson indienne.

Les résultats de ces simulations à l'Holocène ont été comparés à des enregistrements océaniques dans l'Océan Indien (partie 3.4). Ils ont permis d'aider à interpréter les variations des upwellings observées le long de la marge d'Oman, et à la pointe sud de l'Inde. La diminution au cours de l'Holocène de la productivité dans la Mer d'Arabie et l'augmentation de la productivité à la pointe sud de l'Inde sont en accord avec les différences de vents de surface représentées dans les simulations et indiquent un déplacement vers le nord de la circulation de mousson indienne. L'évolution des gradients de salinité est-ouest et nord-sud sont plus difficiles à comparer

aux indicateurs paléoclimatiques à cause d'une mauvaise distribution des précipitations sur le continent affectant l'écoulement des rivières dans le modèle.

La question s'est ensuite posée de savoir si des téléconnections à distance entre les systèmes de mousson peuvent influencer les variations relatives des moussons pendant l'Holocène, en plus du forçage climatique local par l'insolation. Le chapitre 4 discute la possible téléconnection entre la mousson indienne, la Méditerranée et l'Afrique du nord. Il est montré que l'intensification des systèmes de mousson au début de l'Holocène sont accompagnées par une intensification de la subsidence autour de la Méditerranée. Ceci concorde avec plusieurs jeux de données paléoclimatiques qui indiquent un climat estival plus aride au début de l'Holocène sur l'est de la Méditerrannée. Les corrélations entre la mousson indienne, la Méditerranée et la mousson africaine ont été étudiées à plusieurs échelles de temps dans la bibliographie. Le lien entre la mousson indienne et la Méditerranée est aussi présent dans ces simulations à l'échelle interannuelle. Cependant le lien avec la mousson africaine est biaisé par une mauvaise représentation de sa variabilité interannuelle dans le modèle. Le mécanisme de Rodwell and Hoskins (1996) permet en partie d'expliquer cette téléconnection. Le déclenchement d'ondes de Rossby par la convection sur l'Inde et l'intéraction avec le jet d'ouest pour résulter en une subsidence renforcée sur l'est de la Méditerranée et la mer d'Aral interagissant avec le relief local. Il est difficile de conclure sur la possible influence de la subsidence de la Méditerranée sur les différences observées de structures dynamiques de la mousson africaine dans les simulations couplées. Un protocole expérimental a été mis en place de façon à isoler l'impact de la convection sur l'Inde sur la Méditerranée et le Sahel à l'aide du modèle atmosphérique. Malheureusement, ces tests de sensibilité n'ont pu aboutir dans le temps imparti à la thèse. L'analyse de ces téléconnections est cependant prometteuse et d'autres méthodologies seront testées à la suite de ce travail.

Le rôle de l'océan sur les variations des moussons à l'Holocène moyen a été analysé dans différentes publications, mais ces études antérieures n'ont pas considéré les possibles différences entre le début de l'Holocène et l'Holocène Moyen. Ce thème a été abordé dans le chapitre 5.2 (Marzin and Braconnot, 2009a). L'effet de la rétroaction de l'océan sur les variations de précipitations de mousson a pu être isolé à l'aide d'expériences réalisées avec le modèle atmosphérique

forcé par les SSTs de la simulation couplée de référence à 0, 6 et 9.5 ka. Les différences entre ces deux ensembles de simulations montrent que la rétroaction de l'océan est légèrement positive sur la mousson africaine et négative sur les moussons asiatiques, en accord avec les études précédentes pour le milieu de l'Holocène. Sur la partie nord de l'Océan Indien, l'effet de l'évaporation dû aux vents et l'amincissement de la couche de mélange contribuent à un réchauffement de la température de surface vers la fin de la période de mousson, attirant plus de précipitataions vers le sud. Les changements du cycle saisonnier des températures de surface de l'océan ne sont pas une réponse linéaire aux changements d'insolation, et varient localement. L'anomalie froide de SST sur le Golfe de Guinée à la fin du printemps explique le démarrage précoce de la mousson africaine à 6 et 9.5 ka. Le cycle saisonnier du dipôle d'anomalies de SST sur l'Atlantique tropical n'est pas amplifié entre 6 et 9.5 ka, dû à une compensation du réchauffement de la partie nord de l'Atlantique tropical par le réchauffement de la bande équatoriale provenant de l'affaiblissement de l'upwelling équatorial à 9.5 ka. Ceci apporte une explication de plus aux faibles variations de la mousson africaine entre 6 et 9.5 ka dans les simulations couplées.

La partie 5.3 a présenté l'analyse de l'impact de la calotte réminiscente sur la Laurentide et la Fennoscandie à 9.5 ka à la fin de la déglaciation, ainsi que celui de la fonte des calottes de glace sur les variations des moussons du début au milieu de l'Holocène. La fonte des icebergs induit un refroidissement de l'Atlantique Nord et un réchauffement de l'Atlantique sud tropical et a pour effet de diminuer les précipitations de mousson en Inde et au Sahel, mais pas en Asie du sud-est. La présence de plus larges calottes de glace à 9.5 ka induit un refroidissement global de l'hémisphère nord. La mousson d'Asie du sud-est est affaiblie, tandis que la mousson africaine l'est seulement légèrement. La réponse de la mousson indienne à ces calottes est plus ambiguë, car elle est diminuée en début de saison et amplifiée par la suite. En Asie du sud-est, les précipitations sont considérablement diminuées tout au long de l'année. Les deux forçages introduisent des perturbations importantes du jet d'ouest. Les changements des moussons asiatiques reflètent l'extension des centres de refroidissement de la couche troposphérique au niveau des moyennes latitudes. Ces expériences de sensibilité montrent que les systèmes de mousson sont affectés différemment par ces forçages climatiques.

L'impact d'un flux d'eau douce en Atlantique Nord sur les systèmes de mousson a aussi été analysé au dernier maximum glaciaire (partie 5.4). Les simulations réalisées ont permis de confirmer le lien entre les variations abruptes en Atlantique Nord et celles observées dans un enregistrement marin de la mer d'Andaman, celui-ci étant utile à la datation de ces enregistrements. De plus, des tests de sensibilité à la répartition des variations de température de surface de l'océan engendrées par ce flux d'eau douce ont mis en évidence des mécanismes de téléconnection entre l'Atlantique et les systèmes de mousson. Le forçage de flux d'eau douce induit un refroidissement de l'Atlantique Nord ainsi qu'un déplacement de la ZCIT vers le sud accompagné d'un dipôle de température de surface sur l'Océan Atlantique tropical. Ce sont ces différences sur l'Atlantique tropical plus que celles directement sur l'Atlantique Nord qui sont responsables de l'effet sur les moussons africaine et indienne. La téléconnection avec la mousson indienne se fait par le biais de perturbations du jet d'ouest subtropical sur l'Eurasie qui engendrent une diminution du gradient méridional de température troposhérique entre le Plateau Tibétain et l'Océan Indien. Ce tests de sensibilité permettent d'apporter un nouveau mécanisme de téléconnection suppléant les hypothèses énoncées mais non testées dans des études précédentes et qui ne sont pas vérifiées dans ces expériences (influence directe de l'Atlantique Nord et influence du Pacifique ouest).

La corrélation entre les systèmes de mousson et les évènements abrupts de l'Atlantique Nord est très régulièrement invoquée pour expliquer les variations dans les enregistrements paléoclimatiques, que ce soit en période glaciaire ou interglaciaire. La partie 5.5 s'est intéressée à démontrer si la nature de ce lien dépend de la période climatique considérée. Des tests de sensibilité à un flux d'eau douce en Atlantique Nord ont été analysés pour l'Eémien, le Dernier Maximum Glaciaire, le début de l'Holocène, le milieu de l'Holocène, la période préindustrielle et pour un scénario de doublement du taux de CO_2. Toutes les simulations ont en commun un affaiblissement des moussons africaine et indienne associées au refroidissement de l'hémisphère nord et au dipôle de SST dans l'Atlantique tropical, mais celles-ci ne sont pas linéaires au flux d'eau douce, ni à la diminution de l'intensité de la circulation thermohaline, sauf dans le cas de la seule variation des paramètres orbitaux (0 ka, 6 ka, 9.5 ka et 126 ka). En effet, plus l'insolation est forte en été, plus l'effet du flux d'eau douce est important sur l'Atlantique tropical et sur les systèmes de mousson en Inde et en Afrique. Cependant, bien que l'Atlantique

tropical soit fortement perturbé dans les expériences au DMG et dans le futur, les changements de précipitations sur l'Inde sont très différentes, les résultats suggérant une diminution des précipitations plus à l'est dans le futur mais pas sur le continent indien. Ainsi, un forçage similaire peut ne pas avoir les mêmes conséquences localement suivant les conditions climatiques préalables. Ces résultats montrent l'importance de tester les mécanismes que l'on souhaite mettre en évidence dans des paramètres correspondant au plus près à la période climatique étudiée.

En conclusion, ce travail a montré que les réponses relatives des sous-systèmes de mousson au cours de l'Holocène sont principalement pilotées par la saisonnalité du forçage par l'insolation. D'autres forçages climatiques comme une plus large calotte de glace ou un flux d'eau douce en Atlantique Nord ont également un impact différent suivant le système de mousson considéré. Même en tenant compte de ces forçages climatiques supplémentaires, les conclusions sur les amplifications relatives des moussons entre 0, 6 et 9.5 ka ne sont pas affectées pour les moussons indienne et africaine, cependant la présence d'une plus large calotte de glace affecte considérablement la mousson d'Asie du sud-est dans ce modèle. L'étude sur la rétroaction de l'océan a à nouveau montré que les systèmes de mousson répondent de manière différente à l'insolation, par le biais de la rétroactions avec les variations de température de surface de l'océan. Cependant, les amplifications relatives des systèmes de mousson entre les trois périodes de l'Holocène sont similaires entre les simulations couplées et forcées, la rétroaction de l'océan ne permet donc pas d'apporter d'explication supplémentaire aux différences de comportement observées pour 6 et 9.5 ka entre la mousson indienne, africaine et d'Asie du sud-est. Des mécanismes de transmission du signal des perturbations sur l'Atlantique Nord aux systèmes de mousson ont ensuite été mis en évidence. Les collaborations avec des équipes de données paléoclimatologiques présentées ici sont focalisées sur l'Océan Indien et ont permis de valider les variations simulées et de mieux interpréter les variations des indicateurs paléoclimatiques.

6.2 Perspectives

"Essentially, all models are wrong, but some are useful."
Box and Draper (1987)

Sans aucun doute la plus grande limitation de cette étude réside dans les biais importants de précipitation sur les régions de mousson indienne et africaine dans le modèle IPSL-CM4. Peut-être que les variations mises en évidence sont sous-estimées à cause de ce déficit de pluies dans la simulation de référence ou bien l'amplitude des variations est surestimée dans certains cas, le forçage par l'insolation permettant peut-être de passer un seuil pour augmenter les précipitations de mousson dans le modèle. Une comparaison multi-modèles serait indispensable pour vérifier la robustesse des mécanismes mis en évidence dans cette thèse. La prochaine étape du projet d'intercomparaison PMIP3 sera toujours focalisée principalement sur 6 et 21 ka et pas sur le début de l'Holocène, mais certains centres ont l'intention de réaliser ces simulations, il y a ainsi une opportunité dans les prochaines années d'évaluer l'effet de la précession et de la saisonnalité sur les moussons entre le début et le milieu de l'Holocène dans plusieurs modèles. Ce travail de thèse représentera une base de référence quand un ensemble multi-modèles de simulations pour analyser l'effet de la précession sera disponible. De plus, les expériences de flux d'eau à 8.2 ka (pour représenter l'évènement abrupt global observé à cette période suite au déversement d'eaux de fonte de la Laurentide) réalisées par un groupe secondaire pour PMIP3 permettront d'approfondir la compréhension des téléconnections Atlantique Nord-moussons.

Les composantes du système Terre sont de mieux en mieux représentées dans les derniers développements des modèles climatiques. L'impact des interactions entre l'atmosphère, l'océan, la végétation, le cycle du carbone, les calottes de glace et la biogéochimie marine sur les variations paléoclimatiques pourront bientôt être analysées en parallèle, pour une compréhension plus complète des variations climatiques passées. La rétroaction de la végétation n'est pas considérée dans les simulations présentées dans ce travail. Or celle-ci est essentielle, en particulier pour la mousson africaine qui est très sensible à la répartition de l'albédo de surface sur l'Afrique de l'ouest. Des études précédentes ont montré le rôle des changements de végétation à l'Holocène sur le recyclage local et les modifications du cycle saisonnier des précipitations de la mousson africaine (Texier et al., 1997; Tuenter et al., 2005). Liu et al. (2007) analyse cette rétroaction pour mieux comprendre la fin de la période humide en Afrique à la fin de l'Holocène. Cependant, même en intégrant cette interaction comme dans certaines expériences du projet PMIP2 à 6 ka, les modèles climatiques ne sont pas à même d'atteindre l'ordre de grandeur d'amplification et d'extension de la mousson africaine suggéré par les données. Les

simulations prévues pour PMIP3/CMIP5 avec le modèle de l'IPSL devraient permettre d'affiner les résultats de cette thèse en tenant compte de la végétation interactive.

Les tests de sensibilité aux zones de variations de température de surface de l'océan Atlantique ont permis de mettre en évidence un nouveau mécanisme de téléconnection entre l'Atlantique Nord et la mousson indienne. J'espère que ces résultats encourageront d'autres études à effectuer des tests de sensibilité pour prouver les mécanismes évoqués dans la bibliographie. Nous aurions nous-même souhaité étendre ces tests aux autres périodes climatiques étudiées, ceci sera peut-être réalisé dans un futur proche. Les téléconnections entre systèmes de mousson et entre les moussons et les moyennes latitudes sont d'une importance capitale pour pouvoir améliorer la prévision à diverses échelles de temps des pluies de mousson. Des expériences de sensibilité supplémentaires seront nécessaires pour étudier ces téléconnections aux échelles de temps climatiques, interannuelle et intra-saisonnière.

Deux aspects de cette thèse rapidement évoqués pourront être poursuivis. Premièrement, j'aurais souhaité découpler l'effet de l'obliquité de celui de la précession à 9.5 ka sur les variations des moussons. Les simulations ont été réalisées par Pascale Braconnot mais je n'ai pas pu les analyser dans le temps imparti à la thèse. De même, l'analyse des changements de variabilité interannuelle au début de l'Holocène doit être approfondie. Ceci sera certainement poursuivi dans le cadre du projet ANR ELPASO qui vise à étudier les variations de la variabilité d'ENSO et de ses téléconnections dans le passé avec une approche de comparaison modèle-données.

Ce travail d'analyse des variations passées des systèmes de moussons pendant l'Holocène aide à une meilleure compréhension de ces phénomènes climatiques. Cette information est utile à l'amélioration de la représentation des moussons dans les modèles et à une meilleure compréhension des variations des moussons dans le futur. Cependant, il faut être extrêmement vigilant pour interpréter les variations futures d'après les changements passés observés ou simulés. D'une part, la nature et l'effet climatique du forçage peuvent être très différents (par exemple insolation et variations des gaz a effets de serre), bien que certaines caractéristiques peuvent être similaires (il fait plus chaud en été dans l'hémisphère nord dans les deux cas). D'autre part, même en considérant un forçage similaire comme un flux d'eau douce dans l'Atlantique Nord,

les résultats de cette thèse montrent que l'impact sur un phénomène climatique local comme la mousson peut varier en fonction de la période climatique considérée.

Pour finir, les deux études de comparaison modèle-données sont le résultat de collaborations fructueuses et ont apporté un véritable enrichissement mutuel de deux équipes scientifiques par rapport à une simple analyse bibliographique. J'espère que ces deux exemples contribueront à encourager beaucoup d'autres étroites collaborations de ce type, nécessaires à l'évaluation des modèles et à l'interprétation des variations des indicateurs paléoclimatiques.

A

Annexes

A.1 Réponse des moussons aux changements de paramètres orbitaux : comparaison entre les simulations de l'Eémien et de l'Holocène

Clim. Past, 4, 281–294, 2008
www.clim-past.net/4/281/2008/

Climate of the Past

Monsoon response to changes in Earth's orbital parameters: comparisons between simulations of the Eemian and of the Holocene

P. Braconnot[1], **C. Marzin**[1], **L. Grégoire**[2], **E. Mosquet**[1], **and O. Marti**[1]

[1]Laboratoire des Sciences du Climat et de l'Environnement, Unité mixte CEA-CNRS-UVSQ, Orme des Merisiers, bât. 712, 91191 Gif-sur-Yvette Cedex, France
[2]School of Geographical Sciences, University of Bristol, University Road, Bristol, BS8 1SS, UK

Received: 1 February 2008 – Published in Clim. Past Discuss.: 21 April 2008
Revised: 22 September 2008 – Accepted: 7 October 2008 – Published: 24 November 2008

Abstract. Monsoon is the major manifestation of the seasonal cycle in the tropical regions, and there is a wide range of evidence from marine and terrestrial data that monsoon characteristics are affected by changes in the Earth's orbital parameters. We consider 3 periods in the Eemian and 3 in the Holocene that present some analogy in the Earth's orbital configuration in terms of obliquity and precession. Simulations with the IPSL_CM4 ocean-atmosphere coupled model allow us to discuss the response of the Indian and African monsoon in terms of amplitude and response to the insolation forcing. Results show that precession plays a large role in shaping the seasonal timing of the monsoon system. Differences are found in the response of the two sub-systems. They result from the phase relationship between the insolation forcing and the seasonal characteristics of each subsystem. Also the response of the Indian Ocean is very different in terms of temperature and salinity when the change in insolation occurs at the summer solstice or later in the year. Monsoon has a large contribution to heat and water transports. It is shown that the relative importance of monsoon on the change in the energetic of the tropical regions also vary with precession.

1 Introduction

Since the 80's, changes in the Earths orbital parameters have been recognized as the pacemaker of the climate system (i.e. Berger, 1988). There is now a wide range of evidences from different environmental indicators over land, ice and ocean that the Asian monsoon varies depending on the insolation forcing (Wang et al., 2005). Several modeling studies have tested the impact of insolation on the response of monsoon. For example Prell and Kutzbach (1987) clearly establish a quasi-linear relation between monsoon precipitation in West Africa and in India and the summer insolation integrated over the Northern Hemisphere (NH). Several feedbacks have also been identified to trigger the response of the system to the initial insolation signal, such as the response of the ocean and of the vegetation (Braconnot, 2004; Braconnot et al., 2004; Cane et al., 2006).

In most studies the monsoon has been considered as one phenomenon affecting a tropical belt from Africa, India to South East and East Asia. Little attention has been put on possible differences in the response of the different monsoon sub-systems to the changes in the intensity and in the seasonal timing of the insolation forcing. However regional dissimilarities have been identified when comparing the role of the ocean feedback on the African and the Indian monsoons. Braconnot et al. (2007b) for example have shown from the most recent set of coupled simulations of the mid-Holocene that the feedbacks from the ocean tend to amplify the strengthening of the African monsoon induced by insolation, whereas in India they tend to reduce it. The reason is that an interhemispheric gradient is created in the Atlantic Ocean, which favors the inland advection of moist air into the continent (Kutzbach and Liu, 1997; Braconnot et al., 2000; Zhao et al., 2005). In the Indian and Asian sector, on the contrary, the ocean surface warming during summer, favors the development of deep convection over the ocean at the expense of the continent (Liu et al., 2004; Braconnot et al., 2007b).

Correspondence to: P. Braconnot
(pascale.braconnot@cea.fr)

Published by Copernicus Publications on behalf of the European Geosciences Union.

Table 1. Orbital characteristics for the 6 simulations considered in this study.

Period	Eccentricity (°)	Obliquity (°)	Precession o(ω–180°)	Length of the seasons	
				VE to AE (days)	AE to VE (days)
126 ka	0.0397	23.9	201	192	168
122 ka	0.0407	23.2	356	186	174
115 ka	0.0414	22.4	111	175	185
9.5 ka	0.0194	24.2	303	188	172
6 ka	0.0187	24.1	1	184	176
0 ka (ctrl)	0.0167	23.4	102	180	180

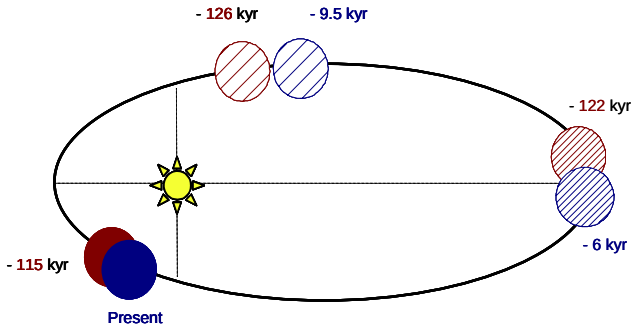

Fig. 1. Location of the vernal equinox on the Earth's orbit around the Sun for the 6 simulations considered in this study.

Other effects need to be accounted for when analyzing the response of monsoons to the insolation forcing. Precession plays a large role in modulating the length of the season. Braconnot and Marti (2003) have shown that the response of the Indian ocean is very different whether the change in insolation occurs in early or late summer. In the first case the mixed layer depth in the Indian Ocean is shallower than in the control simulation and the ocean responds in phase with the insolation forcing. In the second case, the mixed layer depth remains deeper during a large part of the year and the ocean responds with a larger delay (one to two months) to the insolation forcing. The changes in the mixed layer depth are a function of the winter mixing and of the change in local precipitation and river runoff that favor the development of the halocline in the Indian Ocean.

The change in the timing of the insolation forcing relative to the equinoxes and solstices also has implications on the development and the response of the different monsoon subsystems. Prell and Kutzbach (1987) found different regression parameters between insolation and precipitation for India and Africa. Furthermore Marzin and Braconnot (in revision, 2008) report that the decrease of the African monsoon between the Early Holocene and the mid-Holocene was relatively smaller than for the Indian monsoon. They argued that the reason is a resonant response of the Indian monsoon to the insolation forcing when the maximum change in insolation occurs near the summer solstice and a resonant response of the African monsoon when the maximum insolation change is delayed after the summer solstice.

In this manuscript we investigate this effect using a large set of simulations covering different periods in the Holocene and the last interglacial period (Eemian, LIG) that present analogies in the orbital configurations. Earth's orbital parameters were chosen in order to represent different seasonal timing compared to the modern insolation. Since the effect of precession is larger when the eccentricity is large, we also expect to have a larger impact of the seasonal shift in the simulations of the LIG. We investigate the response of the monsoon system and the amplification of the African and Indian monsoon. We also consider how the changes in the seasonal cycle affect the characteristics of the upper ocean in the Indian Ocean, by analyzing the changes in temperature and salinity and the link with the seasonal evolution of the mixed layer depth.

Monsoon is also part of the global energetics and participates to the redistribution of heat and water across the two hemispheres and between land and ocean. Braconnot et al. (2000) reported that for the mid-Holocene the role of the ocean in redistributing heat is equivalent between ocean and atmosphere in the tropical regions. However they considered only one period and didn't show the role of monsoon in the energy redistribution. Here we go one step further by quantifying the role of monsoon in the system and by investigating if the changes of seasonality between the different periods have an impact on the role of monsoon in the system.

In part 2 we present the experimental design and the insolation characteristics of the different periods. Part 3 considers the large scale climatic changes and the impact on the Indian and African monsoons. The role of monsoon in the energetics of the tropical regions is discussed in part 4, and part 5 highlights the major conclusions.

2 Experimental design

A set of 6 simulations was performed for the Eemian and the Holocene, to account for different orbital configurations across these two interglacial periods (Table 1), using the

IPSL_CM4 coupled model (Marti et al., 2005). The choice of the periods results from a compromise between a strict analogy in precession between different periods in the Eemian and the Holocene and the expertise developed at LSCE for the last interglacial (126 ka – Joussaume and Braconnot, 1997; Khodri et al., 2003), the last glacial inception (115 ka – de Noblet et al., 1996; Khodri et al., 2001), or the mid Holocene (6 ka – Braconnot et al., 1999; Braconnot et al., 2000). The orbital parameters corresponding to these simulations are listed in Table 1. They were computed following Berger (1978).

2.1 Model description and experiments

The simulations were performed with the same version of the IPSL model than the one used for future climate projections (Dufresne et al., 2005; Marti et al., 2005) and for the simulations of the second phase of the Paleoclimate Modelling Intercomparison Project (Braconnot et al., 2007a). IPSL_CM4 couples the grid point atmospheric general circulation model LMDZ (Hourdin et al., 2006) developed at Laboratoire de Météorologie Dynamique (LMD, France) to the oceanic general circulation model (Madec et al., 1998) developed at the Laboratoire d'Océanographie et du Climat (LOCEAN, ex LODYC, France). On the continent, the land surface scheme ORCHIDEE (Krinner et al., 2005) is coupled to the atmospheric model. Only the thermodynamic component of ORCHIDEE is active in the simulations presented here. The closure of the water budget with the ocean is achieved thanks to a river routing scheme implemented in the land surface model. A sea-ice model (Fichefet and Morales Maqueda, 1997), which computes ice thermodynamics and dynamics, is included in the ocean model. The ocean and atmospheric models exchange surface temperature, sea-ice cover, momentum, heat and fresh water fluxes once a day, using the OASIS coupler (Terray et al., 1995) developed at CERFACS (France). None of these fluxes are corrected.

In its present configuration, the model is run at medium resolution. The atmospheric grid is regular, with a resolution of 3.75° in longitude, 2.5° in latitude, and 19 levels in the vertical. The ocean model grid has approximately 2 degrees resolution (0.5 degrees near the equator) with 182 points in longitude, 149 points in latitude and 31 1evels in the ocean.

For all the simulations the model is integrated from an ocean at rest with temperature and salinity prescribed to the Levitus's (1982) climatology. In all simulations the date of the vernal equinox is fixed to March 21 at noon. Trace gases are prescribed to the preindustrial values, so that only the changes in the orbital parameters are accounted for. The initial state for the atmosphere corresponds to a 1st January representative of present day climate. The model is then run long enough, so that the surface and middle ocean are equilibrated with the forcing. The lengths of the simulations range from 300 to 700 years. In some of the shorter simulations the deep ocean still drifts by a small amount. However, this drift doesn't affect the characteristics of the monsoon we analyse here. The analyses are performed considering mean annual cycles that were computed from the last 100 years of each simulation. Note that, for all the simulations, we use the present day calendar to compute the monthly means rather that a "celestial calendar" based on the time spent between equinoxes and solstices that would be more appropriate (see Joussaume and Braconnot, 1997). The leads and lags between the different simulations should thus be interpreted with caution around the autumnal equinox, when the difference between the two calendars is the largest.

2.2 Insolation for key periods of the Eemian and of the Holocene

The major differences between the simulations come from the insolation forcing (Table 1). The time periods were chosen to allow similar changes in precession and thus in seasonality across the Eemian and the Holocene. Indeed precession is the key parameter that determines at which time in the year insolation is maximum or minimum, as well as the length of the seasons (see Berger, 1988). Compared to present day, 126 ka and 9.5 ka are two periods for which the equinoxes and solstices are rotated by 180° along the Earth's orbit. Therefore, for these two periods, the seasonal cycle of insolation is enhanced in the Northern Hemisphere and damped in the Southern Hemisphere (SH). The major changes in insolation occur at the solstices. Following Kepler's laws boreal winter is also longer and boreal summer shorter (Table 1). Here we define these two seasons by the time spent between the equinoxes. Note that 9.5 ka was chosen so as to be consistent with the simulation of the Early Holocene proposed as part of the PMIP working group on the Holocene of PMIP2 (Crucifix et al., 2005).

The mid-Holocene (6 ka) is also a key period of interest for the Palaeoclimate Modeling Intercomparison Project (Joussaume et al., 1999, Braconnot et al., 2007b) for which the seasonal cycle of insolation is also enhanced in the NH and damp in the SH. In that case, solstices and equinoxes are rotated by about 90° compared to present day. The maximum changes in insolation with present day do not occur at the solstices but later in the summer season. We added a corresponding period in the Eemian with a simulation of 122 ka. The latter was chosen so that the precession is as close as possible to the precession of 6 ka and of the simulation VE11 discussed by Braconnot and Marti (2003) to allow for possible comparisons with earlier studies on the seasonality in the tropical regions.

For the last two periods considered, the precession is similar to present day. The pre-industrial is the reference for the reminder of this study. This simulation is the same as the one used for future climate projections (Dufresne et al., 2005; Swingedouw et al., 2006). In the Eemian we consider for analogy the last glacial inception at 115 ka. The differences between 115 ka and the preindustrial are thus mainly due to

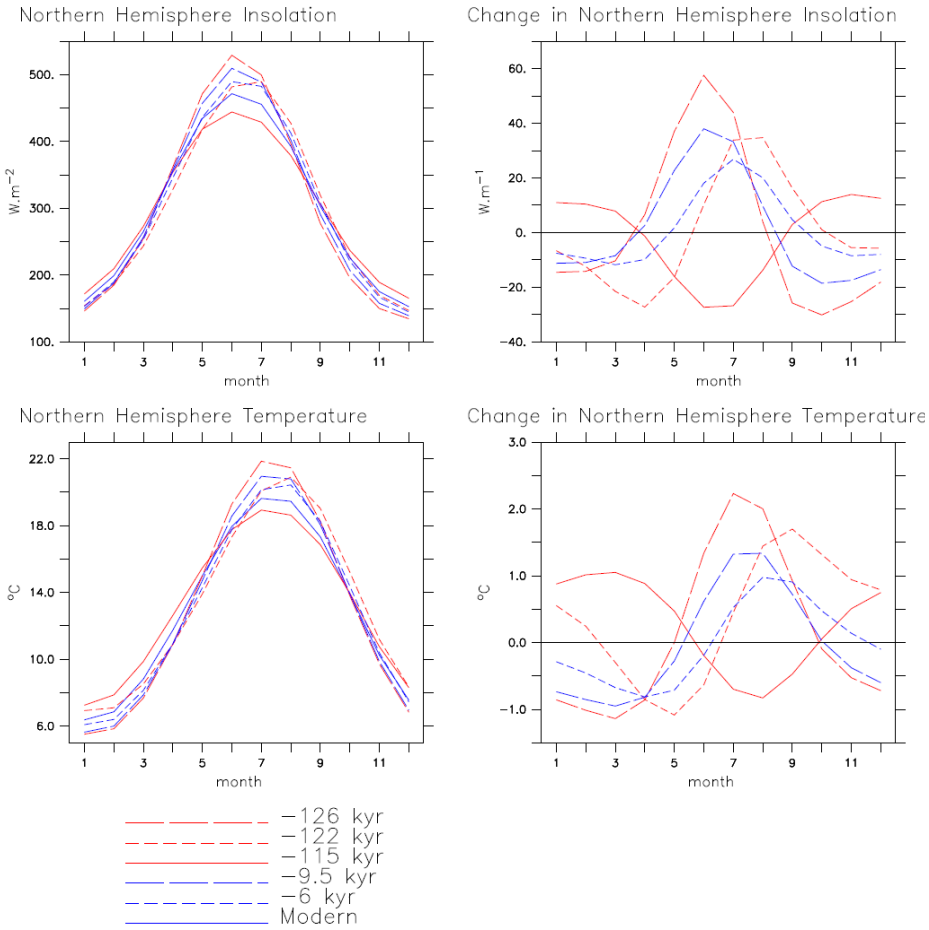

Fig. 2. **(a)** Insolation (W/m^2) and **(b)** surface air temperature (°C) averaged over the Northern Hemisphere and plotted as a function of months. **(c)** and **(d)** same as (a) and (b), but for the differences with 0 ka. In all the figures, periods in the last interglacial are represented with red lines and periods in the Holocene with blue lines. Periods with similar precession are represented with lines of the same type.

eccentricity. Indeed, the effect of precession on the insolation forcing is modulated by eccentricity (Berger, 1988). It is larger when eccentricity is larger. The effect of eccentricity also explains why the changes in the length of the seasons are larger for the Eemian than for the Holocene for similar precession parameters (Table 1).

The combination of the different parameters leads to the insolation provided in Fig. 2 for the NH. As expected from the orbital parameters the seasonal cycle of insolation in the Northern Hemisphere increases when the perihelion occurs near the summer solstice and eccentricity is large. Therefore the amplitude of the insolation seasonal cycle is minimum at 115 ka, and increases respectively for 0 ka, 6 ka, 122 ka, 9.5 ka to reach the maximum at 126 ka (Fig. 2). The maximum differences between the simulations occur during boreal summer where it reaches up to 50W/m^2 for 126 ka (Fig. 2). Figure 2 also clearly shows the different seasonal phasing of the change in insolation. The maximum differences are in phase with the modern insolation for 126 ka, 9.5 ka and 115 ka, and are thus maximum in December–January and June–July, near the time of the solstices. For 6 ka and 122 ka, the differences are shifted in time by about 1 month. The maximum shift is seen for 122 ka (Fig. 2).

Insolation at mid and high latitude is affected by the changes in precession and eccentricity, but the impact of these two parameters is emphasised in these regions when the obliquity is large. The decrease in obliquity across the interglacial is also a common feature between the Eemian and the Holocene. This means that high latitudes received less insolation with time from 126 ka to 115 ka or from 9.5 ka to 0 ka and that the tropical and the equatorial regions received more insolation. However the changes in obliquity are larger (1.5°) and more gradual across the Eemian than across the Holocene (0.8°), for which there is nearly no change between 9.5 ka and 6 ka.

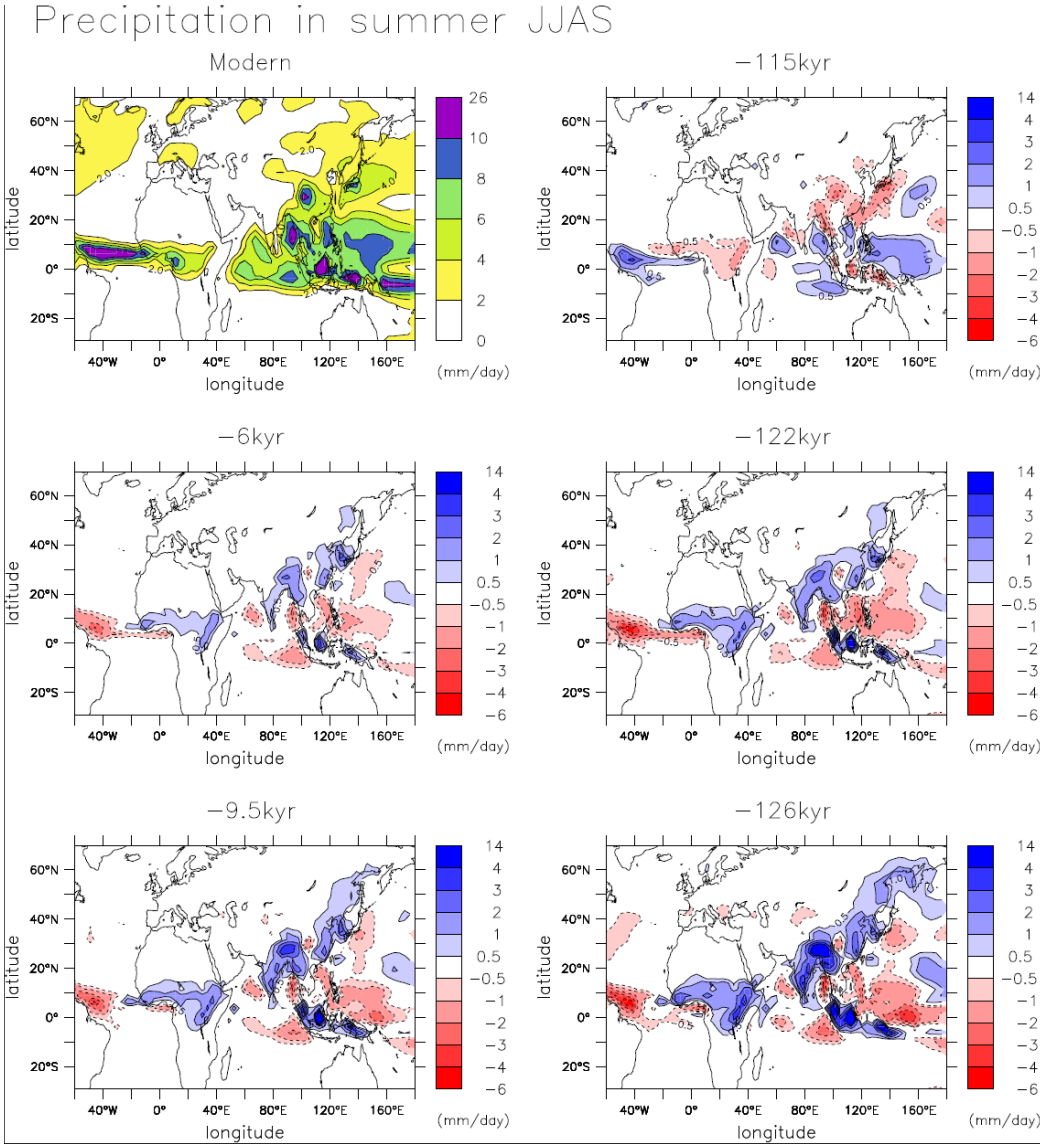

Fig. 3. 0 ka precipitation over Asia (mm/d) and differences with 0 ka precipitation over Asia (mm/d) for the different periods analysed here.

3 Characteristics of the Asian monsoon for the different time periods

3.1 Large scale features

The NH warming increases from 115 ka, 0 ka, 6 ka, 9.5 ka, 122 ka to 126 ka (Fig. 2). The response of the surface air temperature follows quite well the insolation forcing with about one month delay. As discussed is several publications, this delay is mostly induced by the response of the ocean (Braconnot et al., 2000; Liu et al., 2003a). The difference reaches about 2°C between 126 ka and 0 ka in July–August averaged over the NH (Fig. 2). However, the temperature change over the NH is not a true linear response to the insolation forcing. As an example, the spring temperature change is relatively more pronounced in all simulations than the summer one. Also the summer warming at 122 ka is larger than at 9.5 ka, whereas the NH insolation has a similar magnitude. These differences come from the latitudinal distribution of the insolation forcing that differs from one period to the other. Therefore, the hemispheric averages mask differences in the insolation for different latitude bands that also controls large scale temperature, pressure gradients, and non-linear hydrological feedbacks.

All the simulations share similar gross features compared to 0 k. The warming is larger over land than over the ocean and the pattern resembles the pattern found for 6 ka for the PMIP2 simulations (Braconnot et al., 2007a). This increased warming from 115 ka, 0 ka, 6 ka, 122 ka, 9.5 ka to 126 ka

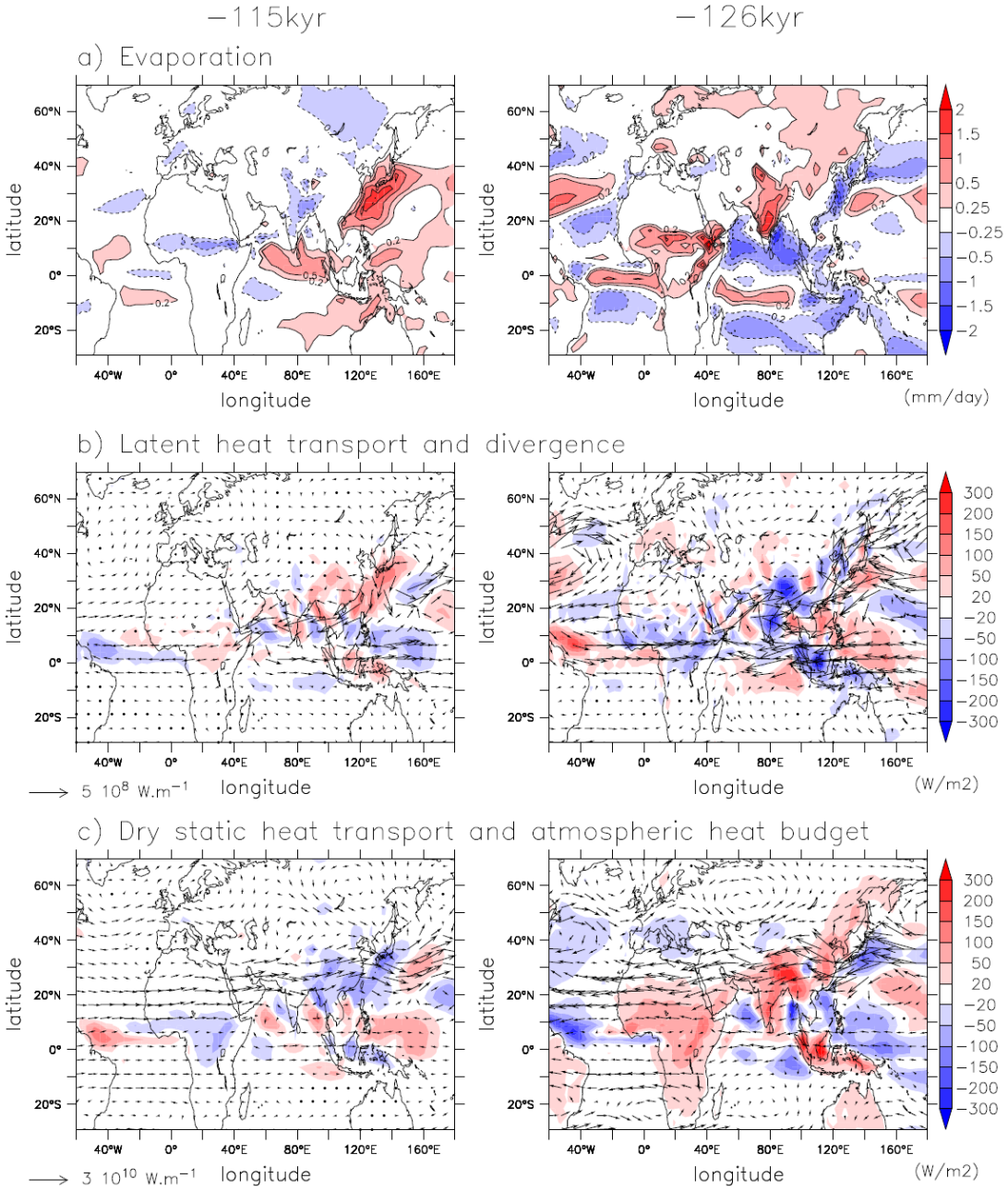

Fig. 4. 126 ka and 115 ka differences with 0 ka for **(a)** evaporation (mm/day), **(b)** the transport of latent heat integrated over the atmospheric column (arrows, W/m) and its divergence (shading, W/m^2) (b) the transport of dry static energy integrated over the atmospheric column (arrows, W/m) and the net heat budget for the dry atmosphere (shading, W/m^2).

enhances the interhemispheric temperature contrast in summer as well as the land-sea temperature contrast and contributes to enhance the monsoon flow (Fig. 3).

Compared to the pre-industrial (0 ka) period, precipitations are increased over India, southwest Asia and Africa for 126 ka, 9.5 ka, 122 ka and 6 ka following the increased contrast in temperature between land and ocean, and reduced for 115 ka (Fig. 3). The changes in precipitation have opposite sign over the warm pool, the Arabian Sea and the Bay of Bengal. Note that the change in precipitation over land and the meridional shift of the Intertropical Convergence Zone (ITCZ) may be underestimated in our results because monsoon intensity is underestimated in the northern part of the ITCZ in the version of the IPSL model we use (Fig. 3a).

The change in precipitation over land is a combination of change in the large scale advection of water vapour and local recycling. We illustrate these two terms for 126 ka and 115 ka in Fig. 4. At 126 ka, evaporation is reduced over the ocean compared to the control simulation. This results from a combination of a cooler ocean, which imposes a large stability over the ocean and from reduced wind speed. Over land, evaporation increases where precipitation increases in the monsoon regions. However, the increase in the local recycling is not the dominant source of precipitation. The large scale dynamics plays a dominant role. The strengthening of the interhemispheric gradient and the increased land-sea contrast with large increase of tropospheric warming over the Tibetan plateau, favours the advection of moist air from the ocean into the monsoon regions. Figure 4b shows the strengthening of the monsoon flow at 126 ka, the increased moisture divergence over the ocean and increased moisture convergence over land. Even though evaporation is reduced over the ocean, the change in the atmospheric circulation is such that moisture is depleted over the ocean at the expense of the continent. Regions that most contribute to the water advections over land are the Pacific warm pool, the southern tropical Indian Ocean, and the tropical Atlantic north of the Equator. At 115 ka, the situation is reversed and the regions acting as an additional source for 126 ka are convergence zones (Fig. 4). The monsoon flow is reduced and so is the local recycling over land. The local recycling over land is therefore strongly coupled to the intensity of the monsoon, and also results from the changes in large scale circulation. Note that changes extend also to mid latitudes at 126 ka, whereas they are more limited to the Tropics at 115 ka. This may be due to the low obliquity at 115 ka. The other periods present similarities with 126 ka, even though the magnitude of the changes is smaller. Also mid-Holocene simulations (9.5 ka and 6 ka) do not show strong signal in mid-latitudes. The 122 ka also shows large changes in the mid-latitudes in the North Atlantic and the North Pacific (Fig. 3).

3.2 Changes in seasonality over India and Africa

Changes in insolation have a large impact on African and Indian monsoon precipitation. Figure 5 shows the precipitation averaged over these two regions for the different simulations compared to pre industrial. In each region the change in precipitation follows well the change in insolation and in temperature averaged over the NH (Fig. 2). The smaller precipitation is found for 115 ka, where the monsoon is damped compared to present, and the maximum precipitation is found for 126 ka. It is however interesting to note some differences in the timing of the precipitation change compared to insolation and temperature averaged over the NH.

The precipitation in India is stronger from May to July at 126 ka compared to present. Consistently with the insolation forcing, the maximum change is reach in August at 122 ka and extends to the late summer season (Fig. 5), whereas

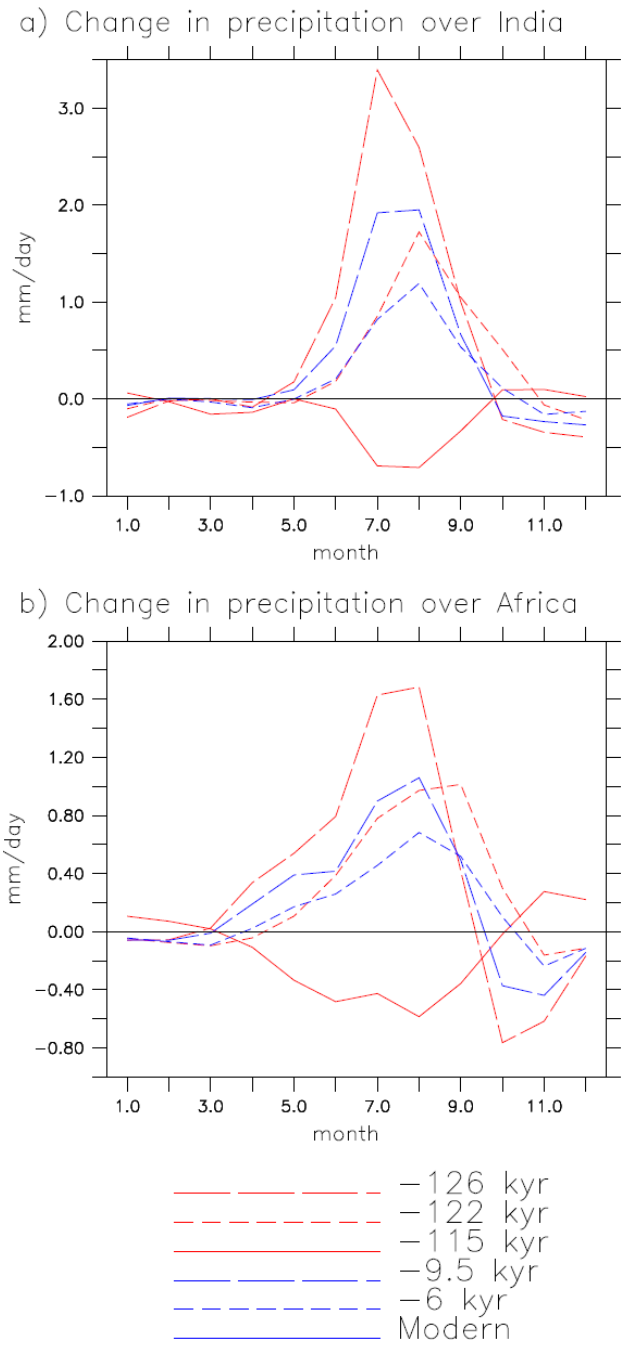

Fig. 5. Precipitation (mm/day) averaged over West Africa (17° W–30° E; 8° N–18° N) and north of India (70° E–100° E; 25° N–40° N) in the northern flank of the ITCZ.

the reduced precipitation simulated for 115 ka varies seasonally in phase with 126 ka. The shape of the changes in the seasonal cycle at 9.5 ka has similar shape to the one found for 126 ka due to similar precession. Also since 126 ka and 9.5 ka have similar obliquity the insolation forcing acts similarly as a function of latitude and the major differences in the magnitude of the change are due to the magnitude of the

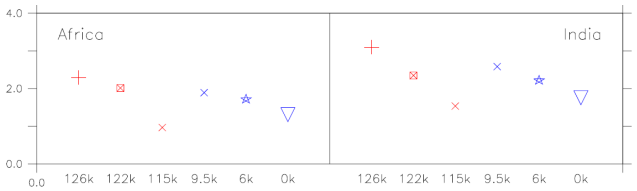

Fig. 6. Mean change of precipitation (mm/day) averaged from June to September in North India (70° E–100° E; 25° N–40° N) and Africa (17° W–30° E; 8° N–18° N) for the different periods considered in this study.

insolation. Similarly, the timing of the change of the seasonal cycle of precipitation at 6 ka shares lots of analogy with 122 ka. However, the shape of the insolation forcing suggests that the change in precipitation at 122 ka should lag those of 6 ka. The similarity in precipitation between those two periods results from changes in the latitudinal gradient of the insolation forcing and of the temperature response. At 6 ka the maximum change in insolation is located rather north in spring, because of the larger obliquity. At 122 ka the maximum change in spring and early summer insolation is located in mid-latitudes, because of reduced obliquity. Therefore the heating of the Tibetan plateau is equivalent for these two periods and so is the amplification of the Indian monsoon. Then the larger insolation at 122 ka compared to 6 ka drives stronger Indian and African monsoons. It is not possible to discuss the timing of the withdrawal of the monsoon from these figures, since the calendar we use introduces artificial biases in the analyses (see Sect. 2.2).

Figure 5 also suggests that the Indian and the African monsoons have specific regional responses. In particular the relative magnitude of the two monsoon systems seems to depend on the insolation forcing. This is better highlighted in Fig. 6 which presents the average precipitation over the whole monsoon season (JJAS) for these two regions. Interestingly the Indian monsoon intensity decreases gradually across the Eemian and across the Holocene, whereas in Africa the decrease between 126 and 122 k or between 9.5 k and 6 ka is smaller than the decrease between 122 ka and 115 ka or between 6 ka and 0 ka. This result is discussed in Marzin and Braconnot (in revison, 2008) for the Holocene. It involves a resonant response of the monsoon to the insolation forcing, which is therefore maximum when the forcing is in phase with the development of the monsoon. Since the Indian monsoon is quite strong in July, the changes are more efficient with the 126 ka and the 9.5 ka insolation. The African monsoon is fully developed in August. Therefore it is more affected when the change in insolation is maximum in August, which is the case at 122 ka and 6 ka. The similarities we find between the Eemian and the Holocene in the relative variations of the Indian and African monsoons confirms the relationship between the insolation and the monsoon response, and the strong role of the precession in modulating

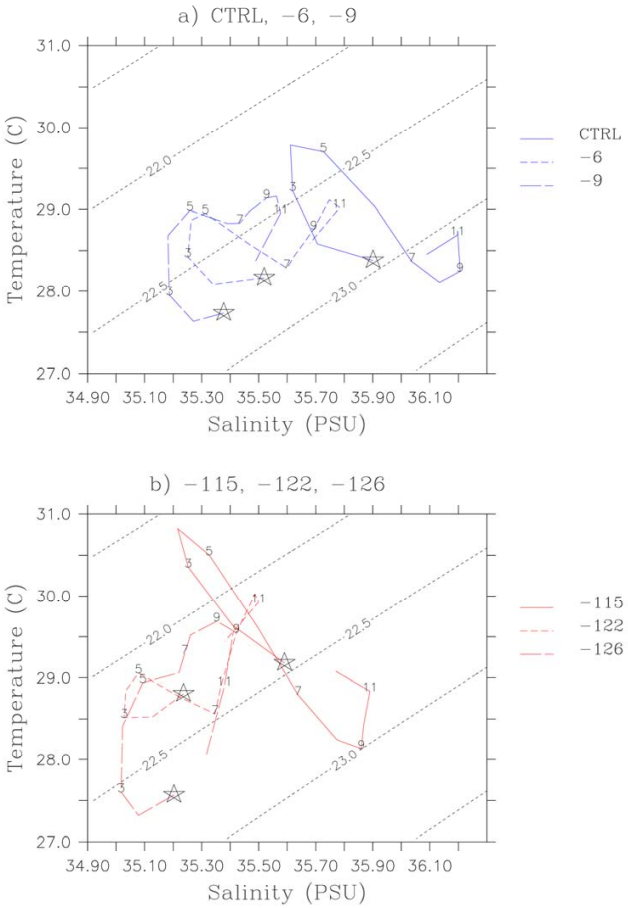

Fig. 7. T/S diagram for a box located between the Equator and the tip of India in the Indian Ocean (65° E–95° E; 0° N–8° N) for **(a)** the Holocene simulations and **(b)** Eemian simulations. The different points on the curves represent the months and the star stands for January. The dotted lines are the lines of equal density in the T/S diagram.

the timing of the seasonal cycle. The interesting aspect is that the modulation does not have the same impact on different subsystems, and that similarities are found between periods of similar precession.

3.3 3.3. Change in seasonality over the Indian Ocean

Braconnot and Marti (2003) found a strong link between precession, temperature and salinity in the Indian Ocean. Figure 7 presents the surface T/S diagram for a box located between the Equator and the tip of India (65° E–95° E; 0° N–8° N). The control simulation shares most of the feature we know for present day climate. The SST maximum occurs between the equator and the tip of India in April, prior to the onset of the summer monsoon (Fig. 7) (Rao and Sivakumar, 1999). It corresponds also to the season where the mixed layer depth is quite deep and shoals northward in the Arabian Sea (Rao et al., 1989). Temperature then decreases until

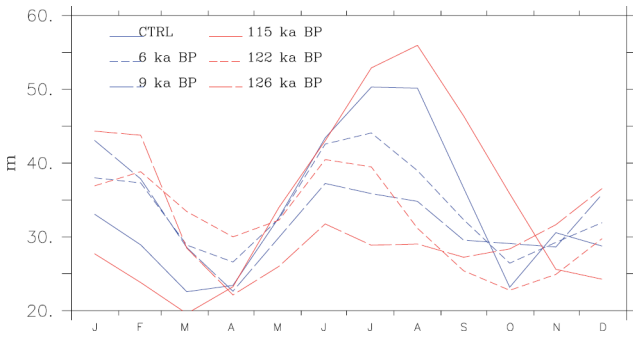

Fig. 8. Annual mean evolution of the mixed layer depth (m) for the different simulations for the same box as in Fig. 7.

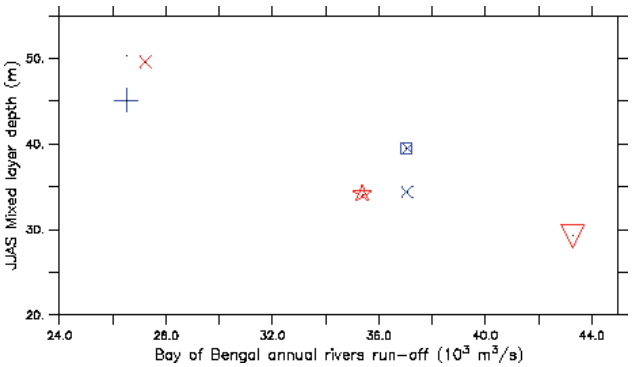

Fig. 9. Relationship between the mixed layer depth in the ocean box located south of the tip of India (65° E–95° E; 0° N–8° N) and the annual mean continental runoff in the Bay of Bengal. Each simulation is represented by the same symbol as in Fig. 6.

Autumn (Fig. 7). In this box salinity is lower during the first half of the year and then increases. The seasonal evolution of salinity is modulated by local precipitation and evaporation and by the advection of fresh water from the Bay of Bengal along the tip of India during winter. In addition, the seasonal evolution of the mixed layer depth is a response to the large scale circulation and to the reversal of the wind between the continent and the ocean. This reversal of wind is associated with the reversal of the monsoon flow that favours upwelling conditions in winter and downwelling conditions during summer (Fig. 8).

During the Holocene, the model produces a reduction of the magnitude of the seasonal cycle of temperature at 9.5 ka and a mean freshening of the surface (Fig. 7). The latter is related to the increase runoff in the Bay of Bengal induced by the strengthening of monsoon rain over the continent, which creates a halocline at the surface (Fig. 3). The SST exhibits warmer than present water throughout summer and a second peak in autumn (Fig. 7a). Similar features are found for 6 ka, except that the summer cooling is still present and that a double peak is also created in autumn. The change in surface salinity is slightly smaller, which is consistent with the smaller monsoon amplification relative to the early Holocene. From Fig. 7 we can see that the surface density is smaller during summer. It is associated to a shallower mixed layer depth (Fig. 8). The change of the mixed layer depth reaches approximately 15 m (about two model vertical levels) at 9.5 ka. As discussed in Zhao et al. (2005) and in Braconnot and Marti (2003), it reduces the thermal inertia of the surface ocean, which explains partly the response to the insolation forcing in autumn. Interestingly, compared to 0 ka, the shoaling occurs as early as April at 9.5 ka, whereas is becomes effective only in July–August at 6 ka (Fig. 8). The difference in the behaviour of the mixed layer depth between the simulations is consistent with the difference in the summer warming between the two simulations. The simulation with the shallower mixed layer depth throughout a longer period responds in phase to the insolation forcing, whereas the other one responds with a delay of one to two months to the insolation forcing (Fig. 7).

The seasonal evolution of SST and salinity across the Eemian shows lots of similarities with the evolution across the Holocene, even though the changes are of larger magnitude (Fig. 7b). In particular, the second peak of SST in autumn is also larger at 126 ka and 122 ka, whereas it is not there at 115 ka. Also the increased river runoff induces a shift in the mean salinity at 126 ka and 122 ka compared to 115 ka. As a result, the thermocline is quite shallow at 126 ka (30 m less than at present day) and responds in phase to the insolation forcing. Figure 9 further assesses the role of the continental runoff in the Bay of Bengal by constraining the surface halocline and therefore the mixed layer depth. Indeed the larger the runoff the shallower the mixed layer is. The remainder of the variations is due to the slight northward shift of the monsoon flow that slightly reduces the Ekman pumping over the tip of India.

This analogy between the changes across the Eemian and the Holocene, for similar orbital configurations, confirms that the timing of the insolation change in spring has a large impact on the development of the mixed layer depth, and that local changes in the mixed layer are coupled to the monsoon activity through local dynamics over the Indian Ocean. The changes in the hydrological cycle and enhanced precipitation over the continent have a remote effect on the ocean mixed layer depth through the river runoff in the Bay of Bengal and the advection of low salinity to the tip of India by the ocean circulation. The difference in the timing of the mixed layer depth and of the surface ocean amongst the simulations is not a simple relationship to the insolation forcing. This certainly needs to be considered when analysing marine proxy that depends on the evolution of the mixed layer depth.

4 Monsoon and tropical energetics

Monsoon circulation contributes to redistribute heat and moisture between the hemisphere and across the tropical regions and acts as a major driver of the change in the

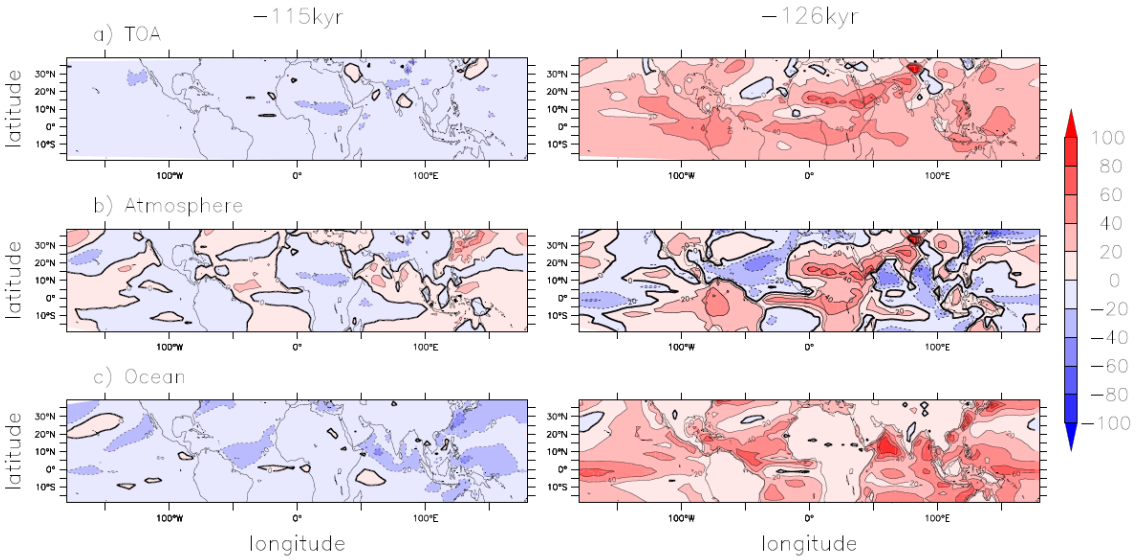

Fig. 10. Characteristics of the change in the ocean-atmosphere heat budget for 115 ka (left and 126 ka (right) and **(a)** Change in the net heat flux at the top of the atmosphere (W/m^2) computed as the budget between shortwave and longwave radiation (positive downward), **(b)** the change in the total heat budget of the atmosphere (W/m^2), considering a humid atmosphere, and **(c)** the change in the heat fluxes (positive downward) at the ocean surface (W/m^2).

atmospheric heat transport and of the large scale circulation between land and ocean. Figure 4c shows that, in the monsoon region, the atmosphere has excess energy compared to pre-industrial for 126 ka and reduced energy for 115 ka during boreal summer. This excess is then advected to regions where energy is depleted, such as the surrounding tropical oceans (Fig. 4c). It is thus interesting to analyse if the differences found and the seasonal evolution of the African and Indian monsoons have an impact on the contribution of monsoon in the global energetics of the tropical regions.

4.1 Changes in the tropical heat budget for 115 and 126 ka

The total change in the energetics involves both the response of the ocean and of the atmosphere. Changes in the global energetics of the whole system are well depicted by changes in *radTOA*, the net heat flux at the top of the atmosphere (Fig. 10a). Changes in *radTOA* results from changes in the ocean heat gain and in the atmospheric heat budget. The ocean heat budget is provided by the surface heat budget (Qsurf):

Qsurf=*radsurf*−Hs−Hl

where *radsurf* stand for the radiative heat flux (short wave minus long wave) at the surface. The atmospheric heat budget in that case is computed as the difference between the heat budget at the top of the atmosphere and the heat budget at the ocean surface. Therefore evaporation contributes to the budget which implies that we consider a moist atmosphere. This is needed to analyse in a consistent way the global energetics.

For 126 ka and 115 ka the largest changes in *radTOA* are found in Africa and in Asia, where monsoon is most affected by the insolation change. Excess energy is also found along the Equator over Africa, the Atlantic Ocean and the East Pacific at 126 ka (Fig. 10a, right). A region of reduced energy also appears for 115 ka in the Atlantic between the Equator and 10° N, but is not well defined. The comparison of the two periods shows that, except over the Afro-Asian monsoon region, the response of the system is not symmetrical in summer between a period where insolation is in excess and a period where insolation is depleted. Part of the reason comes from a different response of the ocean between the two types of period. Figure 10c shows that the ocean gains more energy at the surface in the Western Pacific at 126 ka, whereas nearly no change in the surface heat budget is found for 115 ka. Similarly large changes are found south of the equator in the Atlantic and in the Indian ocean at 126 ka that have no counterpart in the 115 ka simulation. On the other hand several regions show a more symmetrical behaviour. This is the case for the Atlantic between 0 and 10° N, the northern part of the Indian Ocean in the Arabian Sea and the Bay of Bengal, the warm pool and the subtropical high in the West Pacific. All these regions show excess heating at 126 ka and reduced heating at 115 ka. They are closely related to a change of opposite sign in the atmospheric heat budget (Fig. 10b). These regions of opposite sign between the ocean and the atmosphere reflects the large scale redistribution of heat between monsoon regions where energy is in excess to ocean regions where ocean seems to pump the energy to the atmosphere. In the East Pacific it is interesting to

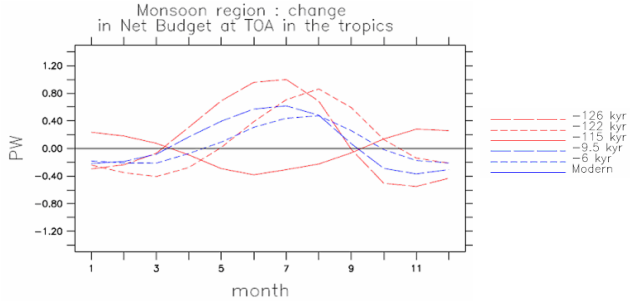

Fig. 11. Change in the top of the atmosphere heat budget (PW) integrated over a box covering the regions affected by the African and the Indian monsoon (17° W–100° E; 5° N–35° N) for the different simulations plotted as a function of month.

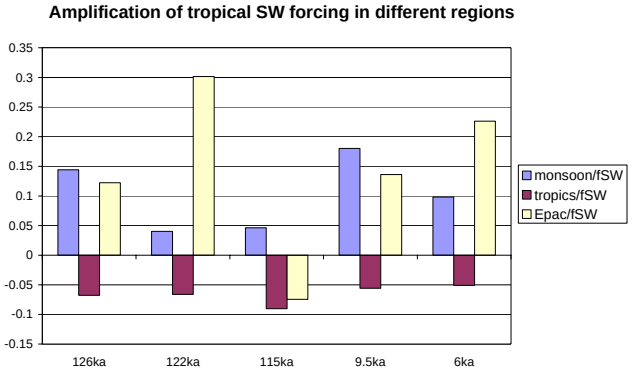

Fig. 12. Amplification of the insolation forcing (fSW; see text for the definition) in different regions of the Tropics and the different simulations. Only the departures to 1 are considered to better highlight the amplification.

note that both the atmosphere and the ocean contribute to the excess energy at the top of the atmosphere at 126 ka, and that this region has a non negligible contribution to the change in the tropical energetics.

4.2 Contribution of monsoon to the tropical heat budget for the different periods

In order to evaluate the role of monsoon in the global energetics of the tropical regions we integrated the changes found over the continent from 17° W to 100° E and from the Equator to 35° N (Fig. 11). It corresponds to the whole region where the monsoon has a signature at the top of the atmosphere in all the simulations (Fig. 10a). As it is expected from the analysis of monsoon precipitation, the changes over the monsoon region follow the insolation forcing and the changes in precipitation in the African and Indian boxes. It is however difficult from this diagram to tell if the changes only reflect the changes in the insolation or if the monsoon has a larger contribution in some periods compared to others.

In order to better quantify the role of monsoon we compare the mean change in radiative fluxes at TOA averaged over the monsoon season in all the simulation by considering the average value of the positive part of the curves in Fig. 11 for 126 ka, 122 ka, 9.5 ka, and 6 ka, and the negative part of the curve for 115 ka. Then we compare the effect of monsoon to similar values obtained for the whole tropics and the east Pacific (130° W–80° W; 10° S–20° S) which also has a large signature at TOA (Fig. 12). The comparison in Fig. 12 is done by normalizing each value by the insolation forcing of the period to provide a common metrics independent of the magnitude of the incoming insolation. Following Hewitt and Mitchell (1996), the forcing is the net change in solar radiation at the top of the atmosphere with the assumption that the planetary albedo is that of the control simulation (α_0). Therefore:

$$fSW = (1-\alpha_0)\Delta SW_i,$$

where ΔSW_i represents the change in insolation.

When the whole Tropics are considered the net change in heat fluxes at TOA is smaller than the forcing and represents about 93% of the forcing whatever the period (Fig. 10). This simply reflects that the different feedbacks, involving changes in shortwave radiation and longwave radiations, damp the insolation forcing. It is however not surprising that the net change at the top of the atmosphere is nearly the insolation forcing since the climate equilibrates to a new state controlled by the change in insolation. Interestingly, this is not the case for the different phenomena (monsoon or mean and variability in the East Pacific). They have a different contribution to this global energetic depending on the period considered (Fig. 12). In all cases the monsoon is a dominant feature of the Tropics and controls part of the response to the insolation forcing. The larger amplification in the monsoon region of 15% (126 ka) or 18% (9.5 ka) is found for periods for which the solar forcing is at a maximum at the summer solstice. This figure also shows that, in some periods, the changes are dominated by the East Pacific. The maximum contribution of the Pacific is for periods where the shift in the seasonal changes of insolation relative to the summer solstice is maximum (122 ka and 6 ka). This comparison confirms that the new equilibrium of the tropical region is dominated by the insolation forcing, but that depending on the seasonal phasing between the insolation and different climate phenomena, the relative impact of the different regions is different from one climate to the other (Fig. 12). It is however beyond the scope of this paper to analyse the reason of the relative impact of the monsoon and the East Pacific region.

5 Conclusions

We made use of a set of simulations of the Eemian and of the Holocene to analyse the role of the Earth's orbital parameters in shaping the response of the Indian and African monsoon. Our results confirm the strong relationship between increased seasonality of the insolation in the Northern Hemisphere and monsoon amplification. This relationship between monsoon and insolation has been widely discussed in the literature (Prell and Kutzbach, 1987; Liu et al., 2003b) and indicates that the larger the insolation, the larger the monsoon response. To first order it is quasi linear. However we highlight some nonlinear response between the change in insolation averaged over the NH, the temperature response and the precipitation response, which reflects that changes in the latitudinal gradients of insolation and in seasonality have an impact on the response in shaping the latitudinal change in temperature, and trigger or not some of the hydrological feedbacks. The illustration is provided by the intensity of the change in precipitation and in the energetics between the tropical regions and the mid-latitudes.

Our analyses go one step further by considering the relative changes between the Indian and the African monsoon across the Eemian and the Holocene. Our results confirm that the precession has a major contribution to shape the changes in the seasonal cycle, and that the relationship between the seasonal timing of the changes in insolation and the seasonal development of climate phenomena is critical. Indeed we show that it is at the origin of differences between different subsystems, such as the Indian or the African monsoon. It involves resonant interaction between the insolation forcing and the climate response. In particular, increased insolation in the NH in phase with the summer solstice has a larger impact on the Indian monsoon than on the African monsoon. The African monsoon is more affected when the increased summer insolation occurs in late summer. These resonant responses with the forcing could explain some of the lead and lags between different regions when compared to a particular insolation forcing. They should be considered more carefully when discussing regional changes through time.

This is also the case for the changes in the ocean circulation. We show that when the maximum change in insolation occurs near the summer solstice, the ocean responds nearly in phase with the insolation forcing, whereas when the change in insolation is slightly delayed in summer, the ocean has a larger inertia and respond with a one or two month delay to the insolation forcing. The response of the surface ocean to the insolation forcing has thus implications both on the characteristics of the mixed layer depth and on the timing of its shoaling and deepening. These changes in the seasonal evolution of the mixed layer are linked to the seasonal evolution of precipitation over the continent through the large scale circulation and the river runoff. The reason is that the shallower mixed layer in that case mainly results from the increase fresh water forcing induced by the increased precipitation over land. The shoaling of the mixed layer is still effective when the monsoon retreats from its summer location onto the continent to its winter position over the ocean. The changes in monsoon intensity over land and in the seasonal evolution of the mixed layer do not necessarily cover the same seasons. The change in seasonality of the upper ocean should be considered to analyse multi-proxy records for which each proxy may be representative of a different periods in the seasonal cycle (see Wang et al., 2005). The relative abundance of the different proxies may reflect a different sensitivity to the seasonal cycle. These results reinforced the conclusion of Braconnot and Marti (2003) with an earlier version of the IPSL coupled model. It would be worth complementing this analysis with a simulation of the ocean biology to better infer the role of the change of the mixed layer depth on productivity and on the major characteristics of the ocean ecosystems.

The role of precession in shaping the response of the monsoon and of the coupling between ocean and land also affects the relative role of monsoon in the changes of the energetics of the tropics. Consistent with the dominant role of the summer monsoon in the large scale tropical circulation at the seasonal time scale, the changes in monsoon have a dominant impact on the change in the tropical energetic. We show however that the relative role of monsoon varies from one period to the other, as a function of precession. Again, in our simulations the role of monsoon is dominant when the summer solstice is at the perihelion, which stresses that the role of monsoon is not a simple relationship with insolation forcing in the Tropics. Interestingly the East tropical Pacific also plays a large role when the maximum insolation occurs in late summer. This should be analysed in more depth in future studies. It may reflect large changes in the seasonal evolution of the equatorial upwelling or a signature of the changes of the interannual variability of the El-Nino phenomenon. Several studies indeed show that El-Nino is reduced during the Early and mid-Holocene (Clement et al., 2000), and that this feature is consistent in different simulations (Cane et al., 2006; Zheng et al., 2007). Our results suggest that monsoon and the east Pacific, both contribute to the redistribution of energy and that their relative contribution is controlled by precession. Therefore changes in monsoon do not dominate the changes in the tropical energetics in summer in all the periods. Additional models and model-data comparisons will be needed to fully assess this point and define the role of the changes in the mean position of the ITCZ and clouds compared to changes in climate variability.

Acknowledgements. Computer time was provided by the Centre National de la Recherche Scientifique (IDRIS computing center) and the Commissariat à l'Energie Atomique (CCRT computing center). This work is a contribution to the French ANR blanc " PICC" and ANR Vulnérabilité climat et milieu "Sahelp".

Edited by: A. L. Berger

References

Berger, A.: Long-Term Variations of Caloric Solar Radiation Resulting from the Earth's Orbital Elements, Quaternary Res., 9, 139–167, 1978.

Berger, A.: Milankovitch Theory and Climate, Rev. Geophysics, 26, 624–657, 1988.

Braconnot, P., Joussaume, S., Marti, O., and de Noblet, N.: Synergistic Feedbacks from Ocean and Vegetation on the African Monsoon Response to Mid-Holocene Insolation, Geophys. Res. Lett., 26, 2481–2484, 1999.

Braconnot, P., Marti, O., Joussaume, S., and Leclainche, Y.: Ocean Feedback in Response to 6 Kyr BP Insolation, J. Clim., 13, 1537–1553, 2000.

Braconnot, P. and Marti, O.: Impact of Precession on Monsoon Characteristics from Coupled Ocean Atmosphere Experiments: Changes in Indian Monsoon and Indian Ocean Climatology, Mar. Geol., 201, 23–34, 2003.

Braconnot, P.: Modeling the Last Glacial Maximum and Mid-Holocene, C. R. Geosci.e, 336, 711–719, 2004.

Braconnot, P., Harrison, S., Joussaume, J., Hewitt, C., Kitoh, A., Kutzbach, J., Liu, Z., Otto-Bleisner, B. L., Syktus, J., and Weber, S. L.: Evaluation of Coupled Ocean-Atmosphere Simulations of the Mid-Holocene, in: Past Climate Variability through Europe and Africa, edited by: Bartabee, R. W., Gasse, F., and Stieckley, C. E., Kluwer Academic publisher, 515–533, 2004.

Braconnot, P., Otto-Bliesner, B., Harrison, S., Joussaume, S., Peterchmitt, J. Y., Abe-Ouchi, A., Crucifix, M., Driesschaert, E., Fichefet, T., Hewitt, C. D., Kageyama, M., Kitoh, A., Laine, A., Loutre, M. F., Marti, O., Merkel, U., Ramstein, G., Valdes, P., Weber, S. L., Yu, Y., and Zhao, Y.: Results of PMIP2 Coupled Simulations of the Mid-Holocene and Last Glacial Maximum – Part 1: Experiments and Large-Scale Features, Clim. Past, 3, 261–277, 2007a, http://www.clim-past.net/3/261/2007/.

Braconnot, P., Otto-Bliesner, B., Harrison, S., Joussaume, S., Peterchmitt, J. Y., Abe-Ouchi, A., Crucifix, M., Driesschaert, E., Fichefet, T., Hewitt, C. D., Kageyama, M., Kitoh, A., Loutre, M. F., Marti, O., Merkel, U., Ramstein, G., Valdes, P., Weber, L., Yu, Y., and Zhao, Y.: Results of Pmip2 Coupled Simulations of the Mid-Holocene and Last Glacial Maximum – Part 2: Feedbacks with Emphasis on the Location of the Itcz and Mid- and High Latitudes Heat Budget, Clim. Past, 3, 279–296, 2007b, http://www.clim-past.net/3/279/2007/.

Cane, M. A., Braconnot, P., Clement, A., Gildor, H., Joussaume, S., Kageyama, M., Khodri, M., Paillard, D., Tett, S., and Zorita, E.: Progress in Paleoclimate Modeling, J. Clim., 19, 5031–5057, 2006.

Clement, A. C., Seager, R., and Cane, M. A.: Suppression of El Nino During the Mid-Holocene by Changes in the Earth's Orbit, Paleoceanography, 15, 731–737, 2000.

Crucifix, M., Braconnot, P., and Otto-Bleisner, B. L.: New Targets for the Paleo Modeling Intercomparison Project, EOS, 86, 264–265, 2005.

de Noblet, N., Prentice, I. C., Joussaume, S., Texier, D., Botta, A., and Haxeltine, A.: Possible Role of Atmosphere-Biosphere Interactions in Triggering the Last Glaciation, Geophys. Res. Lett., 23, 3191–3194, 1996.

Dufresne, J., Quaas, J., Boucher, O., Denvil, S., and Fairhead, L.: Contrasts in the Effects on Climate of Anthropogenic Sulfate Aerosols between the 20th and the 21st Century, Geophys. Res. Lett., 32, 21, L21703, doi:10.1029/2005GLO23619, 2005.

Fichefet, T. and Morales Maqueda, M. A.: Sensitivity of a Global Sea Ice Model to the Treatment of Ice Thermodynamics and Dynamics, J. Geophys. Res., 102(C6), 12 609–12 646, 1997.

Hewitt, C. D. and Mitchell, J. F. B.: GCM Simulations of the Climate of 6 Kyr BP: Mean Changes and Interdecadal Variability, J. Clim., 9, 3505–3529, 1996.

Hourdin, F., Musat, I., Bony, S., Braconnot, P., Codron, F., Dufresne, J. L., Fairhead, L., Filiberti, M. A., Friedlingstein, P., Grandpeix, J. Y., Krinner, G., Levan, P., Li, Z. X., and Lott, F.: The Lmdz4 General Circulation Model: Climate Performance and Sensitivity to Parametrized Physics with Emphasis on Tropical Convection, Clim. Dyn., 27, 787–813, 2006.

Joussaume, S. and Braconnot, P.: Sensitivity of Paleoclimate Simulation Results to Season Definitions, J. Geophys. Res., 102, 1943–1956, 1997.

Joussaume, S., Taylor, K. E., Braconnot, P., Mitchell, J. F. B., Kutzbach, J. E., Harrison, S. P., Prentice, I. C., Broccoli, A. J., Abe-Ouchi, A., Bartlein, P. J., Bonfils, C., Dong, B., Guiot, J., Herterich, K., Hewitt, C. D., Jolly, D., Kim, J. W., Kislov, A., Kitoh, A., Loutre, M. F., Masson, V., McAvaney, B., McFarlane, N., de Noblet, N., Peltier, W. R., Peterschmitt, J. Y., Pollard, D., Rind, D., Royer, J. F., Schlesinger, M. E., Syktus, J., Thompson, S., Valdes, P., Vettoretti, G., Webb, R. S., and Wyputta, U.: Monsoon Changes for 6000 Years Ago: Results of 18 Simulations from the Paleoclimate Modeling Intercomparison Project (PMIP), Geophys. Res. Lett., 26, 859–862, 1999.

Khodri, M., Leclainche, Y., Ramstein, G., Braconnot, P., Marti, O., and Cortijo, E.: Simulating the Amplification of Orbital Forcing by Ocean Feedbacks in the Last Glaciation, Nature, 410, 570–574, 2001.

Khodri, M., Ramstein, G., de Noblet-Ducoudre, N., and Kageyama, M.: Sensitivity of the Northern Extratropics Hydrological Cycle to the Changing Insolation Forcing at 126 and 115 Ky BP, Clim. Dyn., 21, 273–287, 2003.

Krinner, G., Viovy, N., de Noblet-Ducoudre, N., Ogee, J., Polcher, J., Friedlingstein, P., Ciais, P., Sitch, S., and Prentice, I. C.: A Dynamic Global Vegetation Model for Studies of the Coupled Atmosphere-Biosphere System, Global Biogeochem. Cy., 19, GB1015, doi:10.1029/2003GB002199, 2005.

Kutzbach, J. E. and Liu, Z.: Response of the African Monsoon to Orbital Forcing and Ocean Feedbacks in the Middle Holocene, Science, 278, 440–443, 1997.

Levitus, S.: Climatological Atlas of the World Ocean, NOAA/ERL GFDL professional paper 13, Princeton, New Jersey, USA, 276 pp., 1982.

Liu, Z., Brady, E. C., and Lynch-Stieglitz: Global Ocean Response to Orbital Foring in the Holocene, Paleoceanography, 18, 1041, 2003a.

Liu, Z., Otto-Bliesner, B., Kutzbach, J., Li, L., and Shields, C.: Coupled Climate Simulation of the Evolution of Global Monsoons in the Holocene, J. Clim., 16, 2472–2490, 2003b.

Liu, Z., Harrison, S. P., Kutzbach, J., and Otto-Bliesner, B.: Global Monsoons in the Mid-Holocene and Oceanic Feedback, Clim. Dyn., 22, 157–182, 2004.

Madec, G., Delecluse, P., Imbart, M., and Levy, C.: Opa 8.1 Ocean General Circulation Model Reference Manual., Note du Pôle de modélisation, Institut Pierre-Simon Laplace, 11, 94 pp., 1998.

Marti, O., Braconnot, P., Bellier, J., Benshila, R., Bony, S., Brock-

mann, P., Cadule, P., Caubel, A., Denvil, S., Dufresne, J. L., Fairhead, L., Filiberti, M. A., Foujols, M.-A., Fichefet, T., Friedlingstein, P., Goosse, H., Grandpeix, J. Y., Hourdin, F., Krinner, G., Lévy, C., Madec, G., Musat, I., deNoblet, N., Polcher, J., and Talandier, C.: The New IPSL Climate System Model: IPSL-CM4, Note du Pôle de Modélisation, no. 26, ISSN 1288–1619, 2005.

Marzin, C. and Braconnot, P.: Variations of Indian and African monsoons induced by insolation changes at 6 Kyr BP and 9.5 Kyr BP, Clim Dynam., in revision, 2008.

Prell, W. L. and Kutzbach, J. E.: Monsoon Variability over the Past 150,000 Years, J. Geophys. Res., 92, 8411–8425, 1987.

Rao, R. R., Molinari, R. L., and Festa, J. F.: Evolution of the Climatological near-Surface Thermal Structure of the Tropical Indian Ocean.1. Description of Mean Monthly Mixed Layer Depth, and Sea Surface Temperature, Surface Current, and Surface Meteorological Fields, J. Geophys. Res., 94, 10 801–10 815, 1989.

Rao, R. R. and Sivakumar, R.: On the Possible Mechanisms of the Evolution of a Mini-Warm Pool During the Pre-Summer Monsoon Season and the Genesis of Onset Vortex in the South-Eastern Arabian Sea, Q. J. R. Meteor. Soc., 125, 787–809, 1999.

Swingedouw, D., Braconnot, P., and Marti, O.: Sensitivity of the Atlantic Meridional Overturning Circulation to the Melting from Northern Glaciers in Climate Change Experiments, Geophys. Res. Lett., 33, LO7711, doi:10.1029/2006GLO25765, 2006.

Terray, L., Sevault, E., Guilyardi, E., and Thual, O.: The Oasis Coupler User Guide Version 2.0, Cerfacs technical report TR/CMGC, 95–46, 1995.

Wang, P. X., Clemens, S., Beaufort, L., Braconnot, P., Ganssen, G., Jian, Z. M., Kershaw, P., and Sarnthein, M.: Evolution and Variability of the Asian Monsoon System: State of the Art and Outstanding Issues, Quat. Sci. Rev., 24, 595–629, 2005.

Zhao, Y., Braconnot, P., Marti, O., Harrison, S. P., Hewitt, C., Kitoh, A., Liu, Z., Mikolajewicz, U., Otto-Bliesner, B., and Weber, S. L.: A Multi-Model Analysis of the Role of the Ocean on the African and Indian Monsoon During the Mid-Holocene, Clim. Dyn., 25, 777–800, 2005.

Zheng, W., Braconnot, P., Guilyardi, E., Merkel, U., and Yu, Y.: Enso at 6 ka and 21 ka from Ocean-Atmosphere Coupled Model Simulations, Clim. Dyn., 30, 7–8, 745–762, doi:10.1997/s00382-007-0320-3, 2007.

A.2 Evolution des vents d'été et de la productivité marine dans l'Océan Indien tropical en réponse aux variations d'insolation à l'Holocène : comparaison modèle-données

Holocene evolution of summer winds and marine productivity in the tropical Indian Ocean in response to insolation forcing: data-model comparison.

Bassinot, F.C.[1], Marzin, C.[1,2], Braconnot, P.[3], Marti, O.[3], Mathien-Blard, E.[1], Lombard, F.[4], and Bopp, L.[3]

[1] LSCE/IPSL (laboratoire CEA/CNRS/UVSQ), Domaine du CNRS, bâtiment 12, 91198 Gif-sur-Yvette, France.
[2] Met Office Hadley Centre, FitzRoy Road, Exeter EX1 3PB, United Kingdom
[3] LSCE/IPSL (laboratoire CEA/CNRS/UVSQ), Centre CEA-Saclay, Orme-les-Merisiers, 91190 Gif-sur-Yvette
[4] Université de la Méditerranée, CNRS, Laboratoire d'Océanographie Physique et Biogéochimique, LOPB - UMR 6535 Campus de Luminy, Case 901, F-13288 MARSEILLE Cedex 9, France

Abstract

The relative abundance of *Globigerinoides bulloides* was used to infer Holocene paleo-productivity changes at ODP Site 723 (19°03N, 57°37E; Oman Margin) and core MD77-191 (07°30'N, 76°43'E; Southern tip of India). Today, the primary productivity at both sites peaks during the summer season, when monsoon winds result in local Eckman pumping, which brings more nutrients to the surface. On a millennium time-scale, however, the %*G. bulloides* records indicate an opposite evolution of paleo-productivity at these sites through the Holocene. The Oman Margin productivity was maximal at ~9 ka (boreal summer insolation maximum) and decreased since then, suggesting a direct response to insolation forcing. On the opposite, the productivity at the southern tip of India was minimum at ~ 9 ka, and strengthened towards the present.

Paleo-reconstructions of wind patterns, marine productivity and foraminifera assemblages were obtained using the IPSL-CM4 climate model coupled to the PISCES marine biogeochemical model and the FORAMCLIM ecophysiological model. These reconstructions are fully coherent with the marine core data. They confirm that the evolution of particulate export production and foraminifera assemblages at our two sites have been directly linked with the strength of the upwelling. Model simulations at 9 ka and 6 ka BP show that the relative evolution between the two sites since the early Holocene can be explained by the weakening but also the southward shift of monsoon winds over the Arabian sea during boreal summer.

1. Introduction

The northern tropical Indian Ocean and the surrounding lands are the location of a strong monsoon system, which has a profound impact on the socio-economy of one of the most densely populated areas of the world (Saha et al., 1979; Mooley et al., 1981; Mall et al., 2006). During the southwest (summer) monsoon, warm, moist air prevails, and a strong south-westerly wind jet runs diagonally across the Arabian Sea (Figure 1A ; Lee et al., 2000 ; Schott and McCreary, 2001). Reputedly, the southwest monsoon produces the strongest sustained oceanic winds outside the Southern Ocean. Winds during this period remain remarkably unidirectional, though magnitudes vary somewhat with time and space. This wind forcing contributes to the development of a clockwise upper ocean circulation pattern, with the South Equatorial Current and the East African Coast Current both supplying the northward flowing Somali Current, in the western part of the Arabian Sea (Schott and McCreary, 2001). This Arabian Sea surface circulation reverses somewhat to an anti-clockwise pattern during the northeast (winter) monsoon, when sustained, but weaker, winds blow to the southwest (Figure 1B).

The circulation at the tip of India is also affected by fresh water current from the Bay of Bengal (e.g., Durand et al., 2007). The fresh water is advected in winter by the westward flowing, North Equatorial Current (NEC). During the boreal summer, in response to the monsoon wind reversal, the flow in the NEC reverses and combines with a weakened Equatorial Counter-Current to form the South-West Monsoon Current. The maximum surface temperature occurs in spring between the equator and the tip of India, prior to the monsoon onset (Rao and Sivakumar, 1999). These changes result either from local adjustments or from wave propagation. In March, the mixed layer depth is also deeper on both side of the tip of India (Rao et al., 1989). Climate simulations indicate that the salinity has a strong impact on the local stratification and surface warming and is likely to govern the date of onset of the summer monsoon (Masson et al., 2005).

In these Indian regions, climate modelling and forecasting are notoriously difficult. The Indian Monsoon is a particularly complex system, affected by a large array of periodic to semi-periodic forcings, regional to global in extent, with timescales ranging from inter-annual variations (i.e. El Niño-Southern Oscillation-ENSO) to long-term (10^4 to 10^5 yr) orbital modulation of the solar insolation (i.e. Clemens et al., 1991; Prell and Kutzbach, 1992; Camberlin, 1997; Ashok et al., 2004; Kumar et al., 2006; Zhang et al., 2006; Ihara et al., 2007; Braconnot et al., 2008). In order to address and unravel this complexity, meteorological and oceanographic instrumental records are too short, and one has to look for long, paleo-climatic records - such as those provided by marine sedimentary cores - to better understand the natural (*pre-anthropic*) variability of the Indian Monsoon system over a few thousand years. These data can be compared with model outputs for model benchmarking or, alternatively, to help addressing the complexity of paleo-data interpretation by identifying the potential climatic features at play (i.e. Overpeck et al., 1996; An et al., 2000; Liu et al., 2003; Braconnot et al., 2007a-b).

In this paper, we consider the monsoon evolution throughout the Holocene. Several studies combining proxy data and climate model simulations have shown that changes in insolation induced by the slow variation of the Earth's orbital parameters, and mainly precession, have been the major driver of the Holocene afro-asian monsoon evolution (COHMAP 1988; Prell and Kutzbach, 1987; Joussaume et al. 1999; Liu et al. 2003). The orbital configuration that prevailed during the first half of the Holocene enhanced (reduced) seasonality in the northern (southern) hemisphere. During boreal summer, the corresponding increase in the inter-hemispheric and the land-ocean temperature contrasts triggered the summer thermal lows over

the Tibetan plateau and in the Sahara, which enhanced the monsoon flow from the moist tropical ocean into land. Regional patterns are, of course, superimposed on this large-scale scheme. These complex, regional changes result from the relative response of the different monsoon sub-systems to the insolation forcing, which include various feedbacks mechanisms and the important role played by water column stratification on monsoon inception and intensity (Braconnot and Marti, 2003; Zhao et al., 2005; Ohgaito and Abe-Ouchi, 2007; Braconnot et al., 2008; Marzin and Braconnot, 2009). There is a clear need to conduct data-model comparisons in order to better understand and simulate the relationship between the large-scale variations in the monsoon flow and the characteristics of the water column in different areas of the Indian Ocean.

Seasonal upwellings that develop in various parts of the Indian Ocean provide key locations in which sedimentary records can provide estimates of wind forcing changes (i.e. Clemens et al., 1991 ; Anderson and Prell, 1993; Emeis et al., 1995; Naidu and Malmgren, 1996; Clemens and Prell, 2003) that can be compared to model simulations. In this paper, we selected two zones: the upwelling area over the Oman Margin, and the upwelling area at the southern tip of India. Because of the different contexts in which these summer upwellings develop, the comparison of their respective paleo-productivity records has the potential to bring significant pieces of information about past changes in wind patterns over the northern Indian Ocean.

The aims of this paper are:

- 1/ to compare the temporal evolution over the Holocene of monsoon-driven upwellings from the Oman margin and the southern tip of India based on sedimentary records of productivity changes;
- 2/ to understand the relationship between the change in the ocean dynamics, marine biogeochemistry, foraminifera assemblages and monsoon, in order to refine the interpretation of the different ocean proxy records and produce key target points that can be used to evaluate the ability of climate models to reproduce monsoon fluctuations.

The paleo-reconstructions and the model simulations will be described in section 2. The, section 3 will look at the intimate relationship between productivity changes and monsoon evolution based on a thorough data-model comparison. In order to unravel properly the climatic signal embedded in our sedimentary records, the first part of this section 3 will be devoted to study the coherency between model simulations and our sedimentary records. This will be done by analyzing outputs of the PISCES ocean biogeochemical model (Aumont and Bopp, 2006; Gehlen et al., 2007) forced with the mid-Holocene and the pre-industrial simulations obtained with the IPSL-CM4 climate model (Braconnot et al.; 2008; Marzin et al., 2009). Then, using the IPSL-CM4 and PISCES outputs, we will force a new eco-physiological model reproducing the growth of height foraminifera species (FORAMCLIM model; Lombard et al, submitted) in order to better address model-data coherency. In the final part of this paper, we will combine data and model over the whole Holocene period to explore climatic implications of environmental changes recorded at the two sites studied.

2. Data and model

2.1 Paleo-reconstructions from sedimentary records

2.1.1 Core locations

In the Arabian sea, monsoon-driven vertical mixing, and coastal and open ocean upwellings show an important basin-wide spatio-temporal variability resulting in a large variety of phytoplankton blooms (Levy et al., 2007). On the western side of the Arabian Sea, strong upwelling cells develop along the Somalian and Arabian coasts during the summer monsoon, when the winds blow from the SW, parallel to the coast (Figure 1A), resulting in a massive Eckman pumping. These upwellings can be clearly identified through satellite imaging of chlorophyll abundance (Figure 2A). They weaken and stop during the winter season (Figure 2B), when the winds reverse direction (Figures 1B). On the opposite side of the Arabian Sea, off the Indian margin, prevailing winds blow to the east during the summer season (Figure 1A). The summer productivity increase along the western coast of India (Figure 2A) is associated to a complex interplay of lateral advection, mixed-layer deepening and upwellings (i.e. Sharma, 1978; Shetye et al., 1990). At the southern tip of India, however, the summer increase in productivity is chiefly associated to the development of a seasonal upwelling (Levy et al., 2007).

In order to reconstruct paleo-productivity variations and address past changes in summer monsoon wind patterns and intensity over the Holocene, we selected two cores from these areas: Ocean Drilling Program (ODP) Site 723 (19°03N, 57°37E, 808 m water depth) retrieved from the Oman margin, and core MD77-191 (07°30'N, 76°43'E, 1254 m water depth) located at the southern tip of India (Table 1 ; Figure 3). The bioturbation smoothing is likely minimal at these sites, owing to the strong oxygen-minimum zone that develops at these water depths on the margins of the Arabian Sea. ODP Site 723 sedimentary record has been used in several studies devoted to reconstruct monsoon dynamics at millennial to orbital timescales (i.e. Anderson and Prell, 1993; Emeis et al., 1995; Naidu and Malgrem, 1995, 1996; Gupta et al., 2003). On orbital timescales, productivity records obtained in these studies clearly indicate that the strongest summer winds occurred in interglacial times, when perihelion was aligned with the summer solstice. Within the Holocene, the SW monsoon reached a peak between ~10 and 8 ka (Naidu and Malgrem, 1995, 1996; Gupta et al., 2003), in good accordance with independent paleo-monsoon records such as the speleothem oxygen series from the Qunf and Hoti caves, in Oman (Fleitmann et al., 2003).

2.1.2 G. bulloides abundance - productivity proxy

In order to reconstruct past changes in wind-driven, upwelling intensity from our sediment records, we need first to choose a sensitive paleo-productivity index. Upwellings activity has a strong signature in the fluxes and composition of planktonic foraminifera assemblages (Cullen et al., 1984; Curry et al., 1992; Conan and Brummer, 2000). Within these assemblages, *G. bulloides*, which is a common mid-latitude and subpolar species, is particularly abundant in eutrophic waters with high phytoplankton productivity (Sautter and Thunell, 1989; Ortiz et al., 1995; Watkins and Mix, 1998 ; Zaric et al., 2005), explaining its abundance in upwelling cells that develop at various locations around the Arabian Sea, such as on the Oman Margin or on the western side of India (Prell and Curry, 1981; Naidu, 1990, 1993). In the northern Indian Ocean, *G. bulloides* relative abundance (Prell and Curry, 1981; Naidu and Malmgren, 1995; Gupta et al., 2003; Anderson et al., 2010) and *G. bulloides* flux (Conan and Brummer, 2000; Naidu and Malmgren, 1996) have been successfully used to reconstruct past changes in the intensity of monsoon-driven upwellings.

The planktonic foraminifera counts of core MD77-191 were obtained by Mléneck-Vautravers during her PhD thesis (Mléneck-Vautravers, 1997). Since the dry-bulk densities of core MD77-191 were not measured, *G. bulloides* fluxes could not be accurately computed at this site. Thus, in the present paper, we will only consider the relative abundance of *G. bulloides* (%) as our paleo-productivity index. The high-resolution record of *G. bulloides*

abundance in ODP Site 723 was published by Gupta et al. (2003). *G. bulloides* counts on both the MD77-191 core and at ODP Site 723 were obtained on the >150 μm fraction.

Gupta et al's % *G. bulloides* record at ODP Site 723 shows lower percentages compared to similar records obtained in the same area (Anderson and Prell, 1993; Naidu and Malgrem, 1995, 1996). Anderson et al., (2010) suggested that this might be due to 1/ differences in sample washing, which altered the preservation of *G. bulloides*, and/or 2/ differences in taxonomic recognition (Gupta et al. being less inclusive in their classification of small, difficult to recognize juvenile forms). Within the present paper, Gupta et al. (2003)'s data were re-scaled following the procedure developed by Anderson et al., (2010) (rescaled *%bulloides* = *%bulloides* x 1.33 + 12).

2.1.3/ Age model, ^{14}C dating

On core MD77-191, the age model was developed based on nine accelerated mass spectrometry (AMS) ^{14}C dates obtained on monospecific *G. bulloides* samples, and a ^{14}C date obtained on pteropods (Mléneck Vautravers, 1997; Table 1). ODP Site 723 record spans the time interval 0.7-10.7 ka and is chronographically constrained by eleven ^{14}C dates obtained on *G. bulloides* or planktonic foraminifera mixes (Gupta et al., 2003). The ^{14}C ages were converted to calendar ages using the CALIB Rev 5.1 beta software (Stuiver and Braziunas, 1993), the marine calibration curve (Stuiver et al., 1998) and correcting for a surface marine reservoir of ~400 years for core MD777-191, and ~600 years for ODP Site 723. In each core, the age model was developed by linear interpolation between ^{14}C dated control points (Figure 4). The sedimentation rates at Site 723A vary between 76 and 19 cm.kyr-1 (mean ~ 34 cm.kyr-1) during the Holocene. MD77-191 shows sedimentation rates that vary between 91 and 23 cm.kyr-1 in the Holocene (mean sedimentation rate ~61 cm.kyr-1). Owing to the high sedimentation rates at the two sites, bioturbation effects should not introduce significant biases on the paleoceanographic reconstructions (Duplessy et al., 1986; Bard, 2001).

2.2 Model and experiments

2.2.1. Simulations with the IPSL climate model

The IPSL-CM4 model couples 1/ the grid point from the LMDZ atmospheric general circulation model (Hourdin et al., 2006) developed at the Laboratoire de Météorologie Dynamique (LMD, France) to 2/ the oceanic general circulation model (Madec et al., 1998) developed at the Laboratoire d'Océanographie et du Climat (LOCEAN, ex LODYC, France). A sea-ice model (Fichefet and Morales Maqueda, 1997), which computes ice thermodynamics and dynamics, is included in the ocean model. On the continent, the land surface scheme ORCHIDEE (Krinner et al., 2005) is coupled to the atmospheric model. Only the thermodynamic component of ORCHIDEE is active in the simulations presented here. The closure of the water budget with the ocean is achieved thanks to a river routing scheme implemented in the land surface model. The ocean and atmospheric models exchange surface temperature, sea-ice cover, momentum, heat and fresh water fluxes, once a day, using the OASIS coupler (Terray et al., 1995) developed at CERFACS (France). None of these fluxes are corrected.

The atmospheric grid is regular, with a resolution of 3.75° in longitude, 2.5° in latitude, and 19 vertical levels. The ocean model grid has approximately a 2 degree-resolution (0.5 degrees near the equator) with 182 points in longitude, 149 points in latitude and 31 1evels in the ocean (Marti et al., 2010).

The reference (CTRL) is a 1,000 yr long simulation of the pre-industrial climate with trace gazes concentration in the atmosphere prescribed to those of 1860 (Dufresne et al. 2005, Marzin and Braconnot, 2009). We consider, in the following, a mean seasonal cycle

computed from 200 yr of the simulation. Figure 1 shows that this simulation captures the large-scale features of the summer (Figure 1C) and winter (Figure 1D) monsoon flow (to be compared with meteorological data from Figures 1A and 1B). Previous analyses (not shown) indicated that the characteristics of the pre-industrial simulation resemble those of modern simulations with the same version of the model, so that it makes sense to compare our pre-industrial runs with ERA interim reanalyses. In winter (DJFM) the surface flow pattern is properly reproduced. The 850 hPa wind intensity is slightly overestimated along Somalia. The larger biases are found in summer (JJAS). These biases may affect part of the model-data comparison and, therefore, need to be considered. In particular, the monsoon flow does not penetrate far enough into the Arabian Sea. Thus, wind directions and intensity are not well reproduced along the western Indian coast. The wind intensity along Somalia and the Oman margin is also underestimated, which affects the northward extent and the strength of the simulated upwelling.

Simulations of the Indian monsoon at 9 ka (early Holocene) and 6 ka (mid-Holocene) are described in Marzin and Braconnot (2009). In these simulations the date of the vernal equinox is fixed to March 21 at noon, following PMIPII protocol (Braconnot et al. 2007a). Trace gases are prescribed to the pre-industrial values, so that only the changes in the orbital parameters are accounted for. They have been computed following Berger (1978). The initial state for the atmosphere corresponds to a 1st January representative of present day climate. The model was integrated from an ocean at rest with temperature and salinity prescribed to the Levitus's (1982) climatology. The model is then run long enough (300 years for early Holocene to 700 years for mid-Holocene), so that the surface and middle ocean are equilibrated with the forcing. Previous results with these simulations described the evolution of Indian precipitation (Marzin and Braconnot. 2009), the impact of the SST response on Indian and east-Asian precipitations (Marzin and Braconnot 2009b) and the surface stratification of the Indian Ocean between the tip of India and the equator (Braconnot et al. 2008).

2.2.2 Biogeochemical model: PISCES

PISCES (Pelagic Interaction Scheme for Carbon and Ecosystem Studies) simulates the cycling of carbon, oxygen, and of the major nutrients determining phytoplankton growth (PO_4^{3-} , NO_3^- , NH_4^+ ,Si, Fe). Phytoplankton growth is limited by the availability of nutrients, temperature, and light. The model has two phytoplankton size classes (small and large), representing nanophytoplankton and diatoms, as well as two zooplankton size classes (small and large), representing microzooplankton and mesozooplankton. For all species the C:N:P ratios are assumed constant (122:16:1), while the internal ratios of Fe:C, Chl:C, and Si:C of phytoplankton are predicted by the model. There are three non-living components of organic carbon in the model: semi-labile dissolved organic carbon (DOC), with a lifetime of several weeks to years, as well as large and small detrital particles, which are fuelled by mortality, aggregation, faecal pellet production and grazing. Small detrital particles sink through the water column with a constant sinking speed of 3 m/day, while for large particles the sinking speed increases with depth from a value of 50 m/day at the depth of the mixed layer, increasing to a maximum sinking speed of 425 m/day at 5000 m depth. For a more detailed description of the PISCES model see Aumont and Bopp (2006) and Gehlen et al. (2007).

PISCES was run in its offline configuration, i.e. monthly output of the climate simulations (currents, temperature, salinity, winds, radiations,…) were used to compute biological processes, as well as advection /diffusion of the passive tracers within PISCES. Accordingly, PISCES simulations are run on a global grid, with 31 levels on the vertical (10 of which are located in the first 100m) and 2°x2°cos lat for the horizontal resolution. For this work, two biogeochemical simulations were carried out for 500 yrs, using climatologies constructed

from IPSL-CM4 runs for 6ka and Pre-industrial. The analysis is done on the last year of each of the simulation.

The modelled surface chlorophyll concentrations for pre-industrial times (Figures 2C and 2D) are compared to the SeaWiFS climatology data of Levy et al. [2007], for Summer (JJAS) and Winter (DJFM) seasons (Figures 2A and 2B). The general pattern that consists of two phytoplankton blooms (summer and winter blooms) driven by the summer southwest monsoon and the winter northeast monsoon respectively is reproduced by the biogeochemical model. The magnitude of these blooms is, however, underestimated. During the summer season in the upwelling area over the Oman Margin, for instance, the Seawifs data indicate that chlorophyll abundance is > 1mm/m^3 (Figure 2A), whereas estimated chlorophyll abundance remains around 0.3-0.4mg/m^3 in the PISCES simulation (Figure 2C). The main reason for this discrepancy is linked to the coarse resolution of both the atmosphere (LMDZ) and ocean (OPA) general circulation models that force the biogeochemical model, and that precludes a good representation of coastal upwelling zones. Indeed, a similar version of the PISCES model, coupled to OPA at 0.5° resolution and forced by reanalysis products has been compared to the same data set over the 1990-1999 period and it reproduced nicely the distribution, the seasonality and the magnitude of surface chlorophyll changes (Koné et al. 2009).

2.2.3 The FORAMCLIM ecophysiological model

The FORAMCLIM model (Lombard et al. submitted) is an eco-physiological model reproducing the growth of 8 foraminifera species (including *G. bulloides*). It is based on the assumption that a species occurrence in an ecosystem is linked to its ability to grow, depending on the environmental conditions. The model reproduces the physiological rates involved in the growth of planktonic foraminifers and is principally based on biological processes observed under controlled laboratory experiments. The calibration of the model has been presented in Lombard et al. (submitted) and uses both observed growth under laboratory conditions in function of temperature and light intensity, and observed abundance in field conditions for which hydrological characteristics have been measured.

At the two sites of interest, we forced the FORACLIM model with monthly mean outputs from the IPSL-CM4 (temperature, light) and PISCES (food) simulations performed under pre-industrial (CTRL) and Mid-Holocene (6 ka) conditions. Abundance estimates of each species were cumulated over months and depths in order to derive a signal, which could be compared to the actual sedimentary records. The modelled *G. bulloides* proportion (17.3% for the Oman Margin, and 19.3 % for the southern tip of India) are clearly underestimated, corresponding to about half of the observed *G. bulloides* proportion in the sediment (>30% at ODP Site 723, Oman Margin and >45% in core MD77-191, South of India). These low, modelled *G. bulloides* abundances likely reflect the underestimation of marine productivity and biomass by PISCES as discussed above.

3. Link between past productivity and the Indian monsoon evolution.

3.1. upwelling and wind evolution revealed by Site 723 and core MD 77-191 proxy records

Both the ODP Site 723A and MD77-191 records were re-sampled at the same, constant time-interval of 0.3 kyr. Then, in order to extract long-term evolution over the Holocene, a 5-

point window moving average has been applied to both records. Raw and smoothed data from ODP Site 723 and core MD77-191 are presented on Figure 5A and Figure 5B, respectively. The low latitude (30°N) summer insolation has been calculated for the last 12 kyr using the Analyserie Software (Paillard et al., 1996) and is displayed on Figure 5C for comparison.

3.1.1 Oman margin (site ODP 723A)

The smoothed, temporal evolution of *G. bulloides* abundance shows that, on a long-term basis (orbital scale) the Oman margin productivity was at its maximum at the beginning of the Holocene (~9 ka). Then, over the course of the Holocene, a clear tendency of decreasing *G. bulloides* abundance is observed, with the lowest inferred activity between about 2 and 1.5 ka BP. The subsequent increase in productivity since ~1.5 ka BP has been attributed to 1/ change in the date of aphelion, and/or 2/ the effects of agricultural and other human land uses on monsoon (Anderson et al., 2010).

The reduction of summer monsoon upwelling activity along the course of the Holocene deduced from the *G. bulloides* record is coherent with the $\delta^{15}N$ record of core NIOP 905, collected off the coast of Somalia from a water depth of ~1580 m (Ivanochko et al., 2005). This long-term reduction in ODP Site 723 upwelling intensity appears to mimic the progressive decrease of the northern hemisphere summer insolation, which results from the Holocene evolution of the Earth's orbital parameters (Figure 5C).

3.1.2 Southern tip of India (core MD77-191)

Opposite to what we have just observed for the Oman Margin site, the *G. bulloides* relative abundance at the southern tip of India reaches its lowest level at the beginning of the Holocene (~ 9ka BP; Figure 5B). This suggests that productivity was lower than today when low latitude boreal summer insolation was at its maximum (Figure 5C). From ~9 ka BP to the present, the *G. bulloides* relative abundance increases continuously in core MD77-191, suggesting that productivity gradually increased throughout the Holocene. The maximum in *G. bulloides* abundance is reached at the top part of the record, at around 2.1 ka BP.

3.1.3 Implication of the two G. bulloides records

The opposite evolution shown by ODP Site 723 and MD77-191 *G. bulloides* records suggest that, either, 1/ the productivity at one of these sites did not remain chiefly associated to summer monsoon upwelling activity along the course of the Holocene, or 2/ that summer wind forcing showed an opposite evolution at these two sites in response to change in insolation forcing. In order to help interpreting our paleo-productivity records and test which of these assumptions is correct, we used model simulations to look at the relationship between wind forcing and marine productivity across the Holocene.

3.2 Link between productivity and larger-scale summer monsoon wind

We first consider the 6 ka time-slice for which the simulations performed with the IPSL-CM4 and PISCES models make it possible to analyze the consistency between the changes in the monsoon flow, wind and ocean productivity.

In response to the strengthening of seasonality in the Northern hemisphere both the winter and the summer monsoons are enhanced during the mid-Holocene compared to the present (Figure 6A and 6B). As a result, northeasterly winds are stronger along the Oman margin during boreal winter and south westerly winds are stronger during summer. The larger changes are found in summer when wind speed differences with the pre industrial simulation

exceed 3 ms^{-1} at the coast (Figure 6A). The monsoon flow intensification is associated to an anomalous anticlockwise wind pattern resulting in an intensification of the wind in winter at the tip of India and to a clockwise pattern in summer leading to a reduction of the wind. Even though the changes occurring during the summer season are the largest it is important to check which season is dominant in the change of ocean export production and *G. bulloides* abundance in the marine sediments.

Figure 7 shows a map of the differences in particulate export production at 100m (Figure 7A) between 6ka and 0ka in the Arabian Sea, as well as a comparison of 6 ka and pre-industrial reconstructions of annual (monthly) evolution of export production obtained by PISCES at site ODP 723 (Figure 7B) and core MD99-171 (Figure 7C) locations. These results indicate that, using the bio-geochemical PISCES model and the ocean physics simulated by IPSL-CM4 model at 6ka BP and for the pre-industrial, we qualitatively reproduce the variations reconstructed from the *G. bulloides* productivity proxy at the ODP 723 and MD77-191 sites, that is: more export production at 6ka BP on the Arabian coast, and less export at the Southern tip of India compared to the pre-industrial simulation. South of India, this difference (less export at 6ka) seems directly related to the characteristics of the summer bloom, and thus to the intensity of the monsoon upwelling. In the western Arabian Sea, even if the simulated changes agree in average (see map on Figure 7A), the message is complicated by the seasonality of the bloom. This region is characterized by two blooms: a summer bloom related to the monsoon and upwelling, and a winter bloom linked to the deepening of the mixed layer (see Levy et al. 2007). The characteristics of these two blooms are modified during the Holocene, as opposed to the Pre-Industrial. The summer bloom is driven by the characteristics of the monsoon upwelling: its intensity increases significantly. The winter bloom is also largely impacted: its timing is modified and an earlier start also contributes to the difference in the average annual export.

Mean outputs from IPSL-CM4 (temperature, light) and PISCES (food) simulations were used to emulate the FORAMCLIM ecophysiological model (6ka and pre-industrial, control-run). As already mentioned above, the resulting *G. bulloides* proportion in the pre-industrial run is around half of the observed one in recent sediments, which is not surprising considering the coarse resolution of both the atmosphere (LMDZ) and the ocean (OPA) general circulation models that force PISCES, the biogeochemical model, precluding a good representation of coastal upwelling zones. Yet, the evolution of the *G. bulloides* proportion are reproduced in a correct way by the FORAMCLIM model, with an increase of *G. bulloides* at the southern tip of India between 6ka (16.3 %) and pre-industrial conditions (19.3%) (compared to the observed increase between ~35% and ~45%), whereas the simulated proportion decrease in the Oman margin from 19.8 to 17.3% (compared to the observed decrease from ~32% to ~25%.

3.3 Differences between the early and the mid Holocene

As seen above, the complete set of model simulations obtained at 6ka (IPSL-CM4, PISCES and FORAMCLIM) are consistent with *G. bulloides* records from ODP Site 723 and MD77-191. These simulations 1/ confirm that productivity at these two sites has always been chiefly associated to monsoon-driven, summer upwelling activity, and 2/ they reproduce the opposite, long-term evolution of productivity recorded in the *G. bulloides* records at the two sites (i.e. more export production at 6ka BP on the Arabian coast, and less export at the Southern tip of India compared to the pre-industrial simulation).

For this paper, no PISCES simulation was available at 9 ka, but simulations of surface winds obtained with the IPSL-CM4 model were available at 9 ka, 6 ka and could be compared

to the pre-industrial control run (Figure 6). These 9 and 6 ka simulations show that the inverse evolution of the Oman margin and southern India productivity recorded in the *%G. bulloides* data from sites ODP 723 and MD77-191 is fully consistent with the modelled, local evolution of summer wind forcing at these two locations (Figures 6B and 6D). Over the Somalian margin, summer monsoon winds were clearly enhanced at 9 ka compared to the pre-industrial reference (6ka showing intermediate values; Figures 6C and 6A). Over the southern tip of India the wind evolution is opposite. The western winds that prevail during the summer monsoon were lowest at 9 ka compared to today owing to the northernmost position of the ITCZ during the summer season. The northernmost position reached by the rain belt at the peak boreal summer insolation, 9 kyr ago, is independently supported by the $\delta_{18}O$ record of the Qunf Cave's speleothem (southern Oman; Fleitmann et al., 2003). On this record, the $\delta^{18}O$ values become gradually lighter over the past 10 kyr, a trend that has been interpreted as resulting from the progressive southward migration of the ITCZ as boreal summer insolation reduces over the course of the Holocene.

Figure 8 compares the evolution of %*G. bulloides* records from cores ODP 723 and MD 77-191 with the upwelling velocities modelled at these sites at 9 ka, 6 ka and 0 ka. Twenty decades of vertical velocities are individually plotted to show the decadal variability of the upwelling for each period. In the Oman Sea (core ODP 723), the changes of the upwelling velocities from 9 ka to 0 ka are significant, with a smaller change between 9 ka and 6 ka than between 6 ka and 0 ka. The decrease of the biological activity depicted by *G. bulloides* relative abundance is fully coherent with the reduction of the upwelling estimated by the IPSL-CM4 model throughout the Holocene. At the southern tip of India (core MD 77-91), the upwelling change between 6 ka and 0 ka is significant. The change between 9 ka and 6 ka is slightly smaller, with a large decadal variability, which reduces the significance. At this location also, the %*G. bulloides* sedimentary record and the modelled upwelling intensity are coherent, with a decrease of the upwelling associated to a decrease of the biological activity along the course of the Holocene.

Thus, for both cores, model and data fit well, which supports the interpretation of *G. bulloides* relative abundance as a proxy of the upwelling intensity and, therefore, wind forcing. Model and data are coherent and indicate a reduction of wind intensity since 9ka over the Oman margin, associated to the decrease of boreal summer insolation. At the Southern tip of India, summer winds increase since 9ka due to the progressive shift to the South of the regional circulation pattern.

4. Conclusion

Two summer monsoon upwellings, one over the Oman Margin and the other South of India, show opposite long-term evolution over the Holocene. While the former shows a direct response to boreal summer insolation and decreases in intensity since ~9 ka, the later shows an increase in intensity towards the recent.

Paleo-reconstructions of wind patterns, marine productivity and foraminifera assemblages were obtained using the IPSL-CM4 climate model coupled to the PISCES marine biogeochemical model and the FORAMCLIM ecophysiological model. These reconstructions are fully coherent with the marine core data. They confirm that the evolution of particulate export production and foraminifera assemblages at our two sites have been directly linked with the strength of the upwelling. The opposite, long-term evolution observed from *G. bulloides* (productivity) records at the Oman and South Indian site is correctly reproduced through modelisation. IPSL-CM4 model runs at 9 and 6 ka show that, while the Oman Margin summer wind intensity responds directly to summer insolation, the increase in wind intensity

since 9ka at the southern tip of Indian results from the southward shift of monsoon winds over the Arabian Sea.

The simulated changes are however smaller than observed due 1) to the low resolution of the climate model that does not allow to properly represent the strength of the regional upwellings and 2) to the systematic underestimation of the northward extent of the boreal summer monsoon flow in the north Arabian see in the control simulation. The good agreement on the relative evolution of the two upwellings during the Holocene provides also the important confirmation that the changes recorded in the ocean sediments are dominated by large scale changes in the atmosphere and ocean circulation and not by local processes at the scale of the upwellings. Our results also show that the combination of climate simulations with simulations of the ocean biochemistry coupled to a foraminifer, ecophysiological model offers new perspectives in model data comparisons and in the understanding of past changes. They help to refine the criteria to test the response of climate models to the insolation forcing and show how the confrontation of model results with proxy records help us to better understand the spatio-temporal evolution of Indian monsoon flow across the Holocene.

Acknowledgements

This work was supported by CEA through a CFR grant. The authors thank E. Michel, B. Malaizé and L. Labeyrie for fruitful discussions during the maturation of this research project.

References

An, Z., Porter, S.C., Kutzbach, J.E., Wu X., Wang S., Liu X., Li X. and Zhou W., 2000. Asynchronous Holocene optimum of the East Asian monsoon. *Quat. Sci. Rev*., 19(8), 743-762.

Anderson, D. and Prell, W., 1993. A 300 kyr record of upwelling off oman during the late quaternary: Evidence of the Asian Southwest monsoon. *Paleoceanography*, 8(2), 193-208.

Anderson, D.M., Baulcomb, C.K., Duvivier, A.K., and Gupta, A.K., 2010. Indian summer monsoon during the last two millennia, *J. Quat. Sci*., ISSN 0267-8179, DOI: 10.1002/jqs.1369.

Ashok, K., Guan, Z. , Saji, N. H., Yamagata, T. 2004. Individual and Combined Influences of ENSO and the Indian Ocean Dipole on the Indian Summer Monsoon. *J. Climate*, 17, 3141–3155.

Aumont and Bopp, 2006. Globalizing results from ocean in situ iron fertilization studies, *Global Biogeochem. Cycl.*, 20, GB2017, doi:10.1029/2005GB002591

Bard, E., 2001. Paleoceanographic implications of the difference in deep-sea sediment mixing between large and fine particles. *Paleoceanography*, 16(3): 235-239.

Braconnot, P., Otto-Bliesner, B., Harrison, S., Joussaume, S., Peterchmitt, J.-Y., Abe-Ouchi, A. Crucifix, M., Driesschaert, E., Fichefet, Th., Hewitt, C. D., Kageyama, M., Kitoh, A., Laîné, A., Loutre, M.-F., Marti, O., Merkel, U., Ramstein, G., Valdes, P., Weber, S. L., Yu, Y., Zhao, Y., 2007a. Results of PMIP2 coupled simulations of the Mid-Holocene and Last Glacial Maximum – Part 1: experiments and large-scale features, *Clim. Past*, 3(2), 261-277.

--- 2007b. Results of PMIP2 coupled simulations of the Mid-Holocene and Last Glacial Maximum – Part 2: feedbacks with emphasis on the location of the ITCZ and mid- and high latitudes heat budget, *Clim. Past*, 3(2), 279-296.

Braconnot, P., Marzin, C., Grégoire, L. Mosquet, E., and Marti, O., 2008. Monsoon response

to changes in Earth's orbital parameters: comparisons between simulations of the Eemian and of the Holocene, *Clim. Past* 4(2), 459-493.
Berger, A.L. 1978. Long-term variations of daily insolation and Quaternary climatic changes, *J. Atmos. Sci*, 35(12), 2362-2367.
Camberlin, P., 1997. Rainfall Anomalies in the Source Region of the Nile and Their Connection with the Indian Summer Monsoon. *J. Climate*, 10, 1380–1392.
Clemens, S., Prell, W., Murray, D., Shimmield, G. and Weedon, G., 1991. Forcing mechanisms of the Indian Ocean monsoon. *Nature*, 353(6346), 720-725.
Clemens, S. C. and Prell, W.L., 2003. A 350,000 year summer-monsoon multi-proxy stack from the Owen Ridge, Northern Arabian Sea. *Mar. Geol*., 201, 35-51.
COHMAP members, 1988. Climatic changes of the last 18,000 years: Observations and model simulations, *Science*, 241, 365-379.
Conan, S. and Brummer, G., 2000. Fluxes of planktic foraminifera in response to monsoonal upwelling on the Somalia Basin margin. *Deep-sea research, Part II: Topical studies in oceanography*, 47(9-11), 2207-2227.
Cullen, J. and Prell, W., 1984. Planktonic foraminifera of the northern Indian Ocean: distribution and preservation in surface sediments. *Mar. Micropal*., 9, 1-52.
Curry, W., Ostermann, D., Guptha, M. and Ittekkot, V., 1992. Foraminiferal production and monsoonal upwelling in the Arabian Sea: evidence from sediment traps. *Geol. Soc. London Spec. Publ*., 64(1): 93.
Dufresne, J., J. Quaas, O. Boucher, S. Denvil, and L. Fairhead, 2005. Contrasts in the effects on climate of anthropogenic sulfate aerosols between the 20th and the 21st century. *Geophys. Res. Lett,* 32, L21703, doi:10.1029/2005GL023619
Duplessy, J.C. Arnold, M., Maurice, P., Bard, E., Duprat, J. and Moyes, J., 1986. Direct dating of the oxygen-isotope record of the last deglaciation by 14C accelerator mass spectrometry. *Nature*, 320(6060), 350-352.
Durand, F., Shankar, D., Boyer de Montegut, C., et al. 2007. Modeling the barrier-layer formation in the southeastern Arabian Sea. *J.Clim*., 20(10), 2109-2120.
Emeis, K., Anderson, D., Doose, H., Kroon, D. and Schulz-Bull, D., 1995. Sea surface temperatures and history of monsoon upwelling in the northwest arabian sea during the last 500,000 years. *Quat. Res*., 43, 355-361.
Fichefet, T. and Morales Maqueda, M.A., 1997. Sensitivity of a global sea ice model to the treatment of ice thermodynamics and dynamics, *J. Geophys. Res*., 102(C6), 12,609-12,646. doi:10.1029/97JC00480
Fleitmann, D. et al., 2003. Holocene forcing of the Indian monsoon recorded in a stalagmite from Southern Oman. *Science*, 300(5626), 1737-1739.
Gehlen, M., Gangstø, R., Schneider, B., Bopp, L., Aumont, O., and Ethe, C., 2007. The fate of pelagic CaCO3 production in a high CO2 ocean: a model study, *Biogeosciences*, 4, 505–519.
Gupta, A.K., Anderson, D.M. and Overpeck, J.T., 2003. Abrupt changes in the Asian southwest monsoon during the Holocene and their links to the North Atlantic Ocean. *Nature*, 421(6921), 354-357.
Hourdin, F., Musat, I., Bony, S., Braconnot, P., Codron, F., Dufresne, J-L, Fairhead, L., Filiberti, M-A., Friedlingstein, P., Grandpeix, J-Y. et al., 2006. The LMDZ4 general circulation model: climate performance and sensitivity to parametrized physics with emphasis on tropical convection, *Clim. Dynamics*, 27(7-8), 787-813, DOI: 10.1007/s00382-006-0158-0
Ihara, C., Kushnir1, Y., Cane1, M.A., De La Peña, V.H., 2007. Indian summer monsoon rainfall and its link with ENSO and Indian Ocean climate indices. *Int. J. Climat*., 27(2), 179–187.

581 Ivanochko, T., Ganeshram, R.J., Brummer, G-J.A., Ganssen, G., Jung, S.J.A., Moreton, S.G.
582 and Kroon, D., 2005. Variations in tropical convection as an amplifier of global climate
583 change at the millennial scale. *Earth. Planet. Sci. Lett*, 235, 302-314.
584 Joussaume et al., 1999. Monsoon changes for 6000 years ago: Results of 18 simulations from
585 the Paleoclimate Modeling Intercomparison Project (PMIP), *Geophys. Res. Lett*., 26(7),
586 859-862. doi:10.1029/1999GL900126
587 Kone, V., Aumont, O., Levy, M. and Resplandy, L. 2009. Physical and biogeochemical
588 controls of the phytoplankton seasonal cycle in the Indian Ocean: a modeling study, in
589 "Indian Ocean Biogeochemical Processes and Ecological Variability", *Geophys*.
590 *Monograph Series* 185, doi:10.1029/2008GM000700,
591 Krinner,G., Viovy, N., de Noblet-Ducoudre, N., Ogée, J., Polcher,J., Friedlingstein, P., Ciais,
592 P., Sitch,S., and Prentice C., 2005. A dynamic global vegetation model for studies of
593 the coupled atmosphere-biosphere system, *Global Biogeochem. Cycl*., 19, GB1015,
594 doi:10.1029/2003GB002199.
595 Kumar, K.K., Rajagopalan, B., Hoerling, M., Bates, G. and Cane, M., 2006. Unraveling the
596 Mystery of Indian Monsoon Failure During El Niño, *Science*, 314(5796), 115 – 119,
597 doi: 10.1126/science.1131152.
598 Lee, C., Jones, B., Brink, K. and Fischer, A., 2000. The upper-ocean response to monsoonal
599 forcing in the Arabian Sea: seasonal and spatial variability. *Deep Sea Res. Part II:*
600 *Topical Studies in Oceanography*, 47(7), 1177- 1226.
601 Levitus, S. (1982) Climatological Atlas of the World Ocean, *NOAA Professional Paper*, 13,
602 pp. 191.
603 Levy, M., Shankar, D., Andre, J.M., Shenoi, S.S.C., Durand, F., DeBoyer Montegut, C. 2007.
604 Basin-wide seasonal evolution of the Indian Ocean's phytoplankton blooms, *J. Geophys*.
605 *Res*., 112; doi:10.1029/2007JC004090.
606 Liu, Z., Otto-Bliesner, B., Kutzbach, J., Li, L., and Shields, C., 2003. Coupled Climate
607 Simulation of the Evolution of Global Monsoons in the Holocene, *J. Clim*., 16, 2472-
608 2490.
609 Madec, G., P. Delecluse, M. Imbard, and C. Lévy, 1998. Ocean General Circulation Model
610 reference manual, *Notes du Pole de Modélisation de l'Institut Pierre-Simon Laplace*,
611 11, 91 pp. (Available from http:// www.lodyc.jussieu.fr/opa).
612 Mall, R.K., Singh, R., Gupta, A., Srinivasan, G., and Rathore, L. S., 2006. Impact of Climate
613 Change on Indian Agriculture: A Review. *Climatic Change*, 78(2-4), 445-478, doi:
614 10.1007/s10584-005-9042-x
615 Marti, 0., . Braconnot, P., Dufresne, J.-L., Bellier , J., Benshila, R., Bony, S., Brockmann, P.,
616 Cadule, P.,Caubel A., Codron, F., de Noblet, N., Denvil, S., Fairhead, L., Fichefet, T.,
617 Foujols M.-A., Friedlingstein, P., Goosse, H., Grandpeix, J.-Y., Guilyardi, E., Hourdin,
618 F., Idelkadi, A., Kageyama M., Krinner, G., Lévy, C., Madec, G., Mignot, J., Musat, I.,
619 Swingedouw, D. and Talandier, C., 2010. Key features of the IPSL ocean atmosphere
620 model, and its sensitivity to atmospheric resolution, *Clim Dyn*, 34:1–26, DOI
621 10.1007/s00382-009-0640-6
622 Marzin, C. and Braconnot, P., 2009. Variations of Indian and African monsoons induced by
623 insolation changes at 6 and 9.5 kyr BP, *Clim Dyn*., 33(2-3), 215-231, DOI:
624 10.1007/s00382-009-0538-3.
625 Masson, S., J. Luo, G. Madec, J. Vialard, F. Durand, S. Gualdi, E. Guilyardi, S. Behera, P.
626 Delecluse, A. Navarra, and T. Yamagata, 2005: Impact of barrier layer on winter-spring
627 variability of the southeastern Arabian Sea. *Geophys. Res. Lett*., 32, L07703,
628 doi:10.1029/2004GL021980.
629 Mléneck Vautravers, M., 1997. Sédimentation et dissolution des carbonates biogéniques aux
630 moyennes latitudes Nord et Sud. Approche quantitative et relations avec les

631 paléocirculations océaniques des derniers 150 000 ans. *PhD thesis*, Université Bordeaux
632 I, 277pp.
633 Mooley, D.A., Parthasarathy, B., Sontakke, N. A., and Munot, A.A., 1981. Annual rain-water
634 over India, its variability and impact on the economy. *Int. J. Climat*., 1(2), 167–186.
635 Naidu, P. D., 1990. Distribution of upwelling index planktonic foraminifera in the sediments
636 of the western continental margin of India. *Oceanologica Acta*, 13, 327-333.
637 Naidu, P.D., 1993. Distribution patterns of recent planktonic foraminifera in surface
638 sediments of the western continental margin of India. *Mar. Geol.,* 110, 403418.
639 Naidu, P.D. and Malmgren, B.A., 1995. A 2,200 years periodicity in the Asian monsoon
640 system. *Geophys. Res. Lett*., 22(17), 2361-2364.
641 Naidu, P.D. and Malmgren, B.A., 1996. A high-resolution record of late quaternary upwelling
642 along the Oman Margin, Arabian Sea based on planktonic foraminifera.
643 *Paleoceanography*, 11(1), 129-140.
644 Ohgaito, R., and Abe-Ouchi, A. 2007. The role of ocean thermodynamics and dynamics in
645 Asian summer monsoon changes during the Mid-Holocene, *Climate Dyn*. 29 (1), 39–50.
646 Ortiz, J. D., Mix, A. C., and Collier, R. W., 1995. Environmental control of living symbiotic
647 and asymbiotic foraminifera of the California Current. *Paleoceanography*, 10,
648 987–1009.
649 Overpeck, J., Anderson, D., Trumbore, S. and Prell, W., 1996. The southwest Indian
650 Monsoon over the last 18000 years, *Clim. Dynamics*, 12, 213-225.
651 Paillard, D., Labeyrie, L. and Yiou, P., 1996. Macintosch program performs timeseries
652 analysis - eos Trans. Electronic supplement at htt://www.agu.org.eos_elec/96097e.html.
653 AGU. 77, 379.
654 Prell, W. and Curry, W., 1981. Faunal and isotopic indices of monsoonal upwelling: western
655 Arabian Sea. *Oceanologica Acta*, 4(1), 91–98.
656 Prell, W.L. & J.E. Kutzbach, 1987. Monsoon variability over the past 150000 years - *J.*
657 *Geophys. Res*. 92: 8411-8425
658 Prell, W.L. and Kutzbach, J.E., 1992. Sensitivity of the Indian monsoon to forcing parameters
659 and implications for its evolution. *Nature*, 360, 647-652.
660 Rao, R. R., R. L. Molinari, and J. F. Festa, 1989. Evolution of the Climatological Near-
661 Surface Thermal Structure of the Tropical Indian Ocean.1. Description of Mean
662 Monthly Mixed Layer Depth, and Sea Surface Temperature, Surface Current, and
663 Surface Meteorological Fields. *J . Geophys. Res*., 94, 10801-10815.
664 Rao, R. R. and R. Sivakumar, 1999: On the possible mechanisms of the evolution of a mini-
665 warm pool during the pre-summer monsoon season and the genesis of onset vortex in
666 the south-eastern Arabian Sea. *Quart. J. Royal Meteo. Soc.*, 125, 787-809.
667 Saha, K. R., Mooley, D. A. and Saha, S., 1979. The Indian monsoon and its economic impact.
668 *GeoJournal*, 3(2), 171-178, doi: 10.1007/BF00257706.
669 Sautter, L. R. and Thunell, R. C., 1989. Seasonal succession of planktonic foraminifera:
670 results from a four-year time-series sediment trap experiment in the northeast Pacific. *J.*
671 *Foramin. Res*., 19, 253–267.
672 Schott, F.A. and McCreary Jr., J.P., 2001. The monsoon circulation of the Indian Ocean,
673 *Progr. Oceanography*, 51(1), 1-123.
674 Sharma, G. S., 1978. Upwelling off the southwest coast of India. *Indian J. Mar. Sci*., 7, 209-
675 218.
676 Shetye, S. R., Gouveia, A. D., Shenoi, S. S. C., Sundar, D., Michael, G. S., Almeida, A. M.,
677 and Santanam, K., 1990. Hydrography and circulation off the west coast of India during
678 the southwest monsoon 1987. *J. Mar. Res*., 48, 359-378.
679 Stuiver, M. and Braziunas, T.F., 1993. Modeling atmospheric C-14 influences and C-14 ages
680 of marine Samples to 10,000 Bc. *Radiocarbon*, 35(1), 137- 189.

681 Stuiver, M., Reimer, P.J., Bard, E., Beck, J.W., Burr, G.S., Highen, K.A., Kromer, B.,
682 McCormac, G., Van der Plicht, J., Spurk, M., 1998. INTCAL98 radiocarbon age
683 calibration, 24,000-0 cal BP. *Radiocarbon*, 40(3), 1041-1083.
684 Terray, L., Thual, O., Belamari, S. , Déqué, M., Dandin, P., Delecluse, P. and C. Levy, 1995.
685 Climatology and interannual variability simulated by the ARPEGE-OPA coupled
686 model, *Clim. Dyn.,* 11, 8, 487-505, DOI: 10.1007/BF00207197.
687 Watkins, J. M. and Mix, A. C., 1998. Testing the effects of tropical temperature,productivity,
688 and mixed-layer depth on foraminiferal transfer functions. *Paleoceanography*, 13,
689 96–105.
690 Zaric, S., Donner, B., Fischer, G., Mulitza, S., and Wefer, G., 2005. Sensitivity of planktic
691 foraminifera to sea surface temperature and export production as derived from sediment
692 trap data. *Mar. Micropal*., 55(1-2), 75-105.
693 Zhang, R., and Delworth, T.L., 2006. Impact of Atlantic multidecadal oscillations on
694 India/Sahel rainfall and Atlantic hurricanes. *Geophys. Res. Lett.,* 33, L17712,
695 doi:10.1029/2006GL026267.
696

Table captions

Table 1: AMS dating of core MD77-191 (for Site ODP 723, see Gupta et al., 2003).

Figure captions

Figure 1 : **A-** (upper left) summer (JJAS) wind patterns over the Arabian Sea. **B-** (upper right) winter (DJFM) wind patterns over the Arabian Sea. **C-** (lower left) summer wind pattern obtained from the Pre-industrial run of the IPSL-CM4 model. **D-** (lower right) winter wind pattern obtained from the Pre-industrial run of the IPSL-CM4 model. Wind speed scales in m/s.

Figure 2: Seasonal distribution of chlorophyll abundance (mg/m^3) in the Tropical Indian Ocean (SeaWiFs data) during the summer (**A**, upper left) and winter (**B**, lower left) seasons. PISCES simulations of chlorophyll concentration (mg/m^3) for the summer (**C**, upper right) and winter (**D**, lower right) seasons.

Figure 3: Location map of Site ODP 723 (Oman Margin) and core MD77-191 (southern tip of Indian).

Figure 4: Depth-age plots for core MD77-191 (upper panel; data from Mlaveck-Vautravers, 1997) and ODP site 723A (lower panel; data from Gupta et al., 2003).

Figure 5: Lower panel (A): *G. bulloides* percentages versus age in ODP Site 723 (Oman Margin ; Gupta et al., 2003). Middle panel (B) : *G. bulloides* percentages versus age in core MD77-191 (southern tip of Indian; Mladeck-Vautravers, 1997). Upper panel (C) : boreal summer insolation at 30°N over the last 12 kyr. In figures 4A and 4B, the triangles on the lower part of the panels represent the ^{14}C dates with their associated error bars. Dashed-line curves represent %*G. bulloides* data re-sampled at a constant, 0.3 kyr interval. The thick-line curves represent smoothed records (5-point moving average).

Figure 6: early and mid-Holocene wind simulations from the IPSL-CM4 model at the 850 hPa level. In all figures we plotted the differences with the pre-industrial run (control run) for the wind directions (vectors) and intensity (color scale, in m/s). **. A.** (upper left) Winter simulation, 6 ka BP. **B.** (lower left) Summer simulation, 6ka BP. **C** (upper right) Winter simulation, 9ka BP. **D** (lower right) Summer simulation, 9ka BP.

Figure 7: PISCES outputs. Maps showing the differences between the mid-Holocene (6ka) and the pre-industrial control-runs, for the chlorophyll concentration (left panel) and the particulate export production at 100m (right panel).

Figure 8: Data/model comparison of upwelling intensity evolution across the Holocene at the Site ODP 723 (A, upper panel) and core MD77-191 (B, lower panel) locations. Data presented are the re-scaled (0.3 kyr interpolation) and smoothed *%G. bulloides* records (a 5-point, moving average). Error bars are standard deviations estimated over the same, 5-point

744 windows. Model outputs are mean, vertical velocities estimated at grid-points near to MD77-
745 191 and ODP Site 723 location.

		14C age		Calendar Age		
Depth (m) (m)	Material	14C age (yr)	Uncertainty (1s) (yr)	Median Probability (yr) (yr)	Lower range (yr)	Upper Range (yr)
0,28	G. bulloides	1 970	60	1 453	1 341	1 540
0,76	G. bulloides	2 560	70	2 148	2 042	2 286
1,27	G. bulloides	3 020	60	2 721	2 609	2 635
1,75	G. bulloides	3 660	60	3 492	3 377	3 590
2,22	G. bulloides	4 160	60	4 139	3 991	4 261
2,71	G. bulloides	4 790	60	4 980	4 831	5 078
3,73	G. bulloides	6 150	80	6 511	6 393	6 629
4,25	G. bulloides	8 230	90	8 676	8 517	8 843
4,82	G. bulloides	8 970	80	9 589	9 452	9 702
5,94	pteropods sp.	12 630	190	14270	13 764	14 676

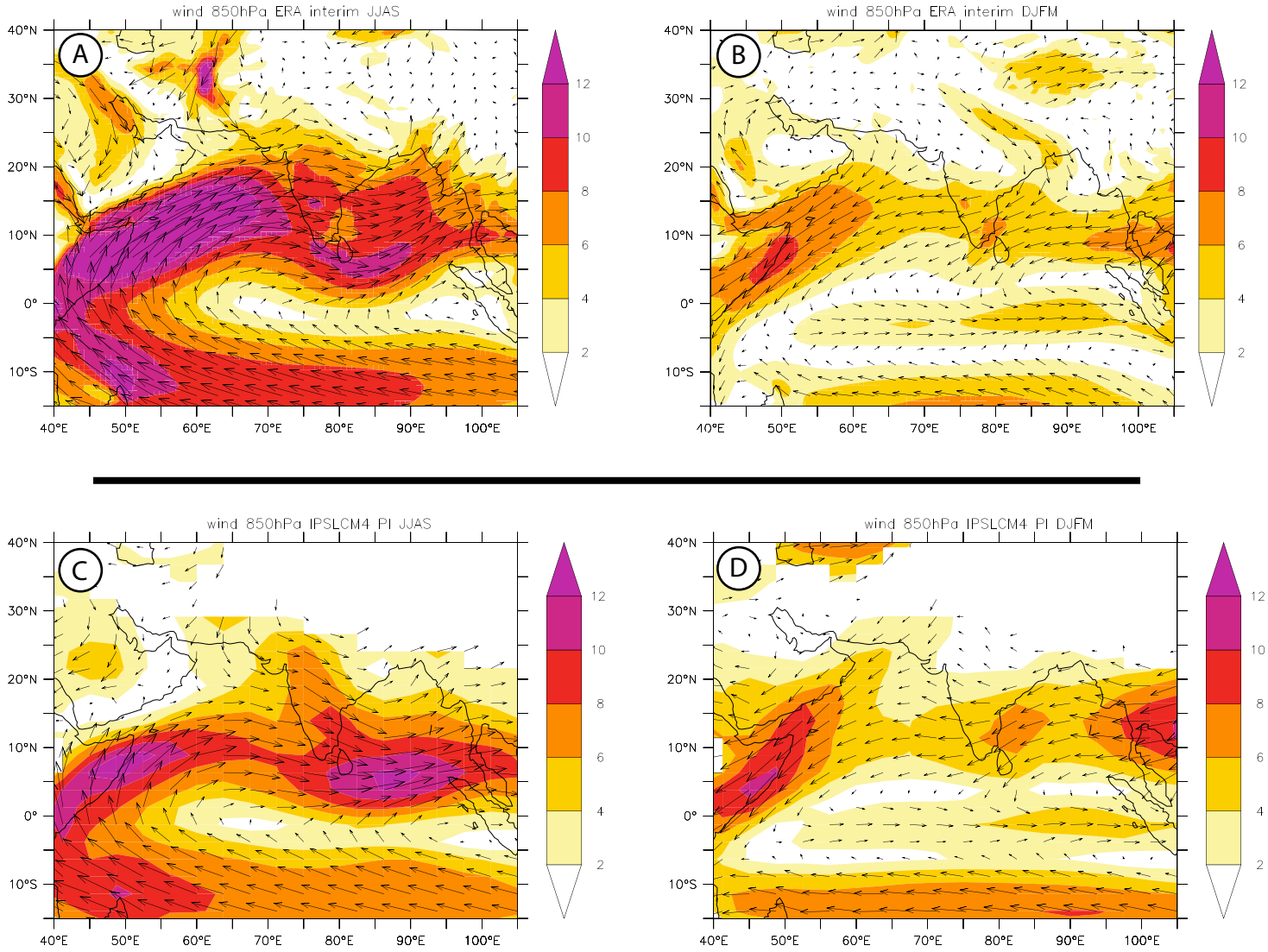
wind 850hPa ERA interim JJAS
A
wind 850hPa ERA interim DJFM
B
wind 850hPa IPSLCM4 PI JJAS
C
wind 850hPa IPSLCM4 PI DJFM
D
40°N
30°N
20°N
10°N
0°
10°S
40°E
50°E
60°E
70°E
80°E
90°E
100°E
12
10
8
6
4
2

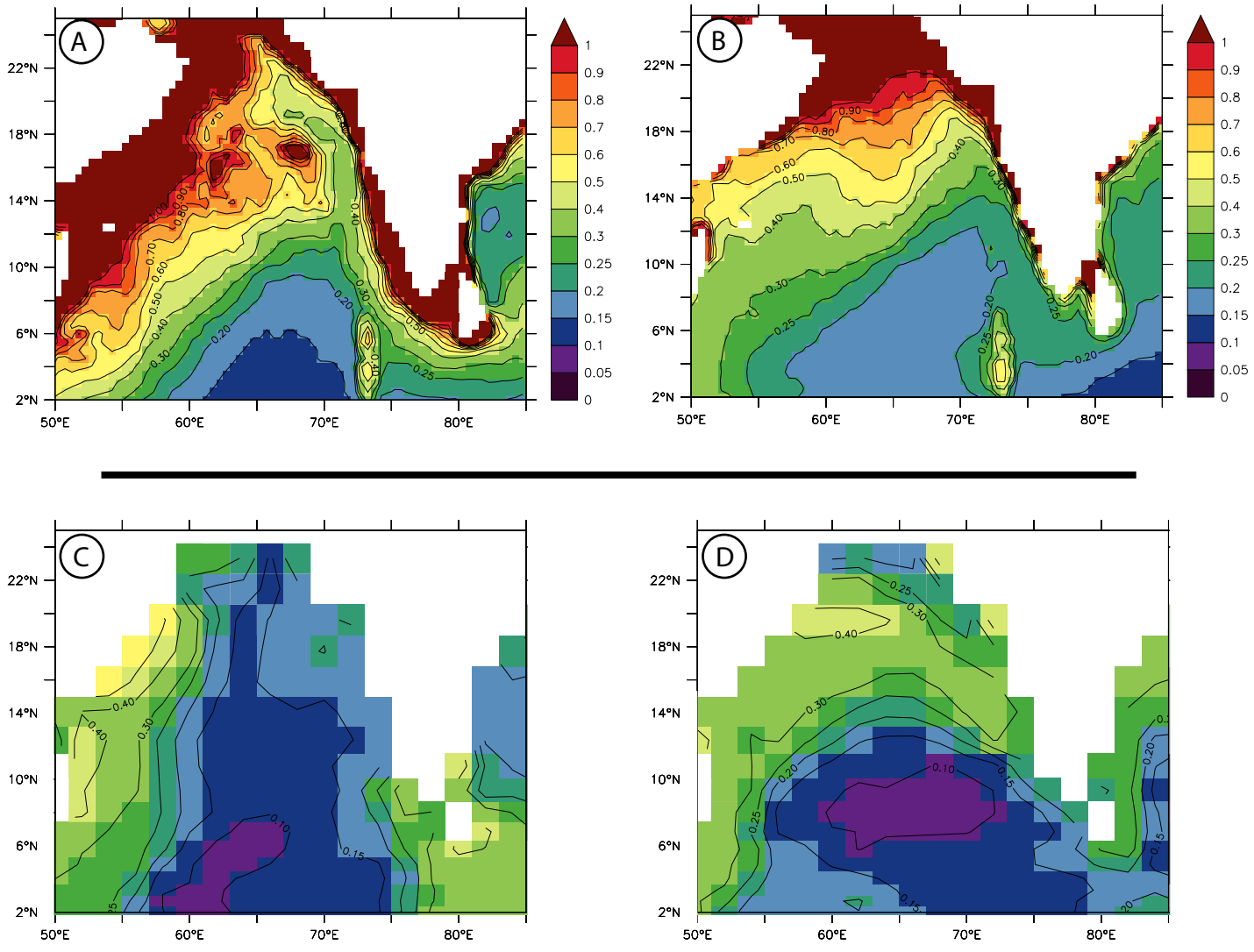
A
B
C
D
22°N
18°N
14°N
10°N
6°N
2°N
50°E
60°E
70°E
80°E
1
0.9
0.8
0.7
0.6
0.5
0.4
0.3
0.25
0.2
0.15
0.1
0.05
0

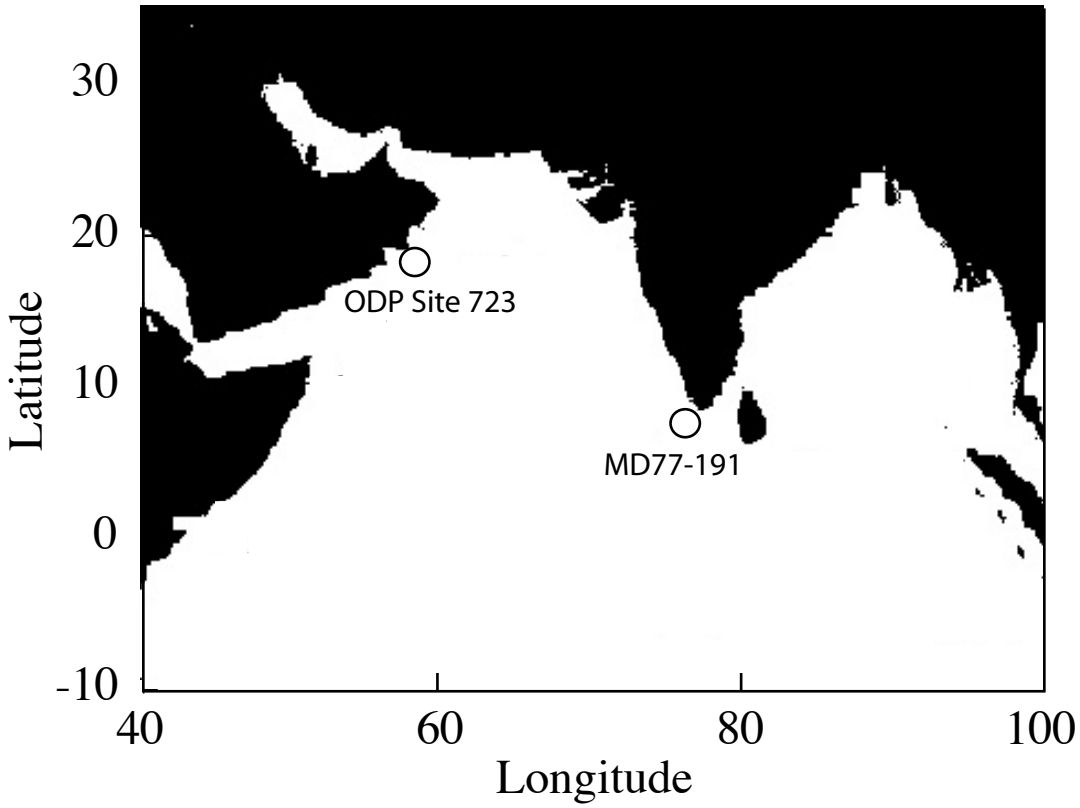
30
20
10
0
-10
Latitude
ODP Site 723
MD77-191
40
60
80
100
Longitude

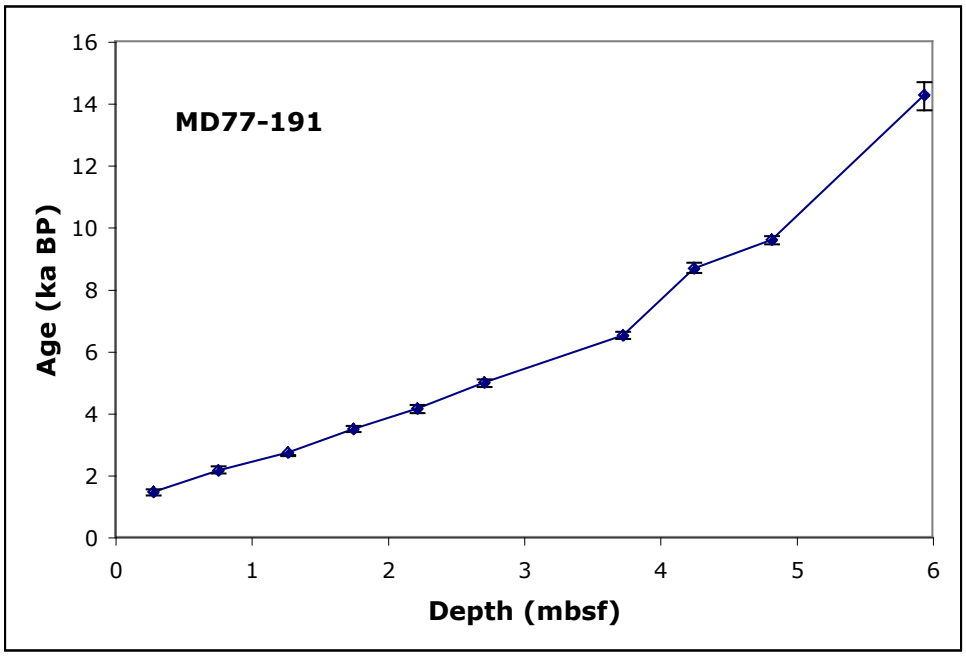
MD77-191
Age (ka BP)
Depth (mbsf)
0
2
4
6
8
10
12
14
16
0
1
2
3
4
5
6

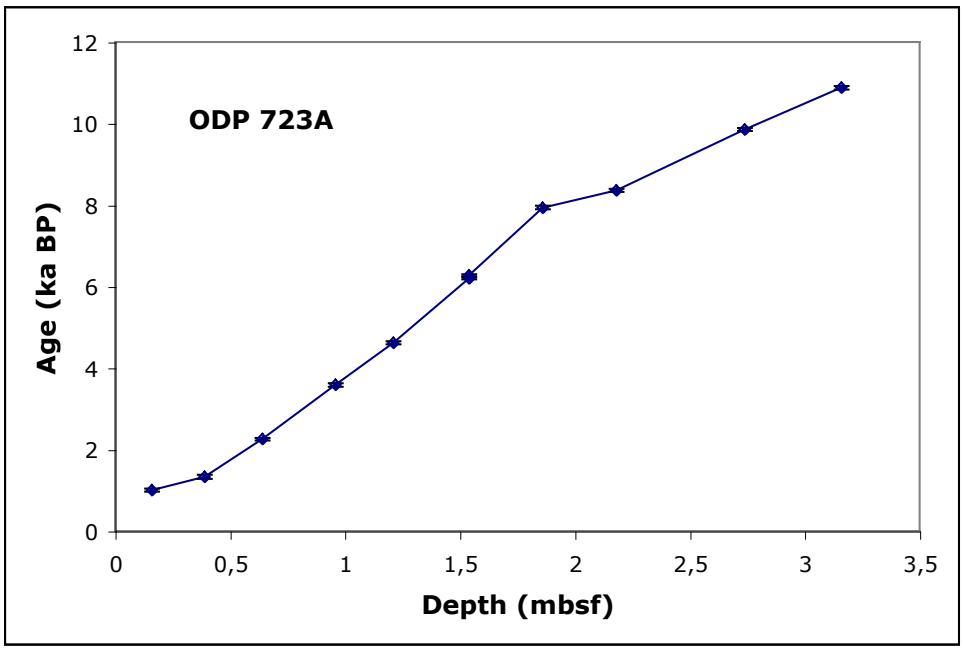
ODP 723A
Age (ka BP)
Depth (mbsf)
0
2
4
6
8
10
12
0
0,5
1
1,5
2
2,5
3
3,5

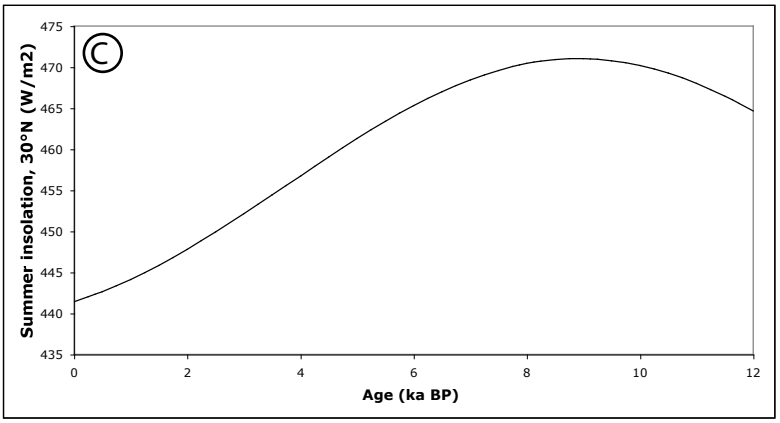
C
Summer insolation, 30°N (W/m2)
475
470
465
460
455
450
445
440
435
0
2
4
6
8
10
12
Age (ka BP)

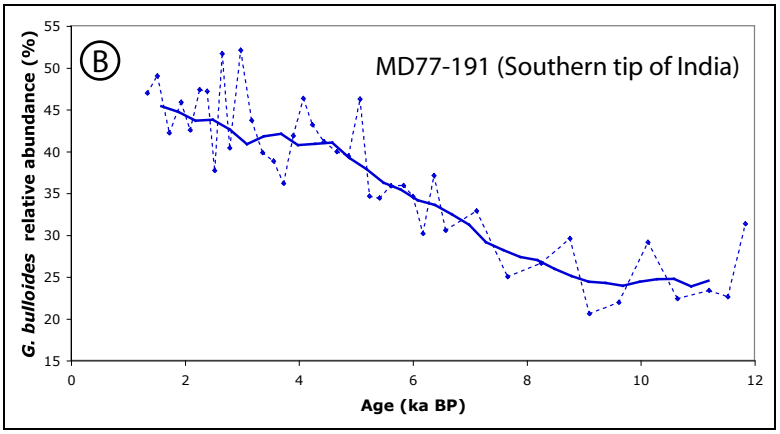
B
MD77-191 (Southern tip of India)
G. bulloides relative abundance (%)
55
50
45
40
35
30
25
20
15
0
2
4
6
8
10
12
Age (ka BP)

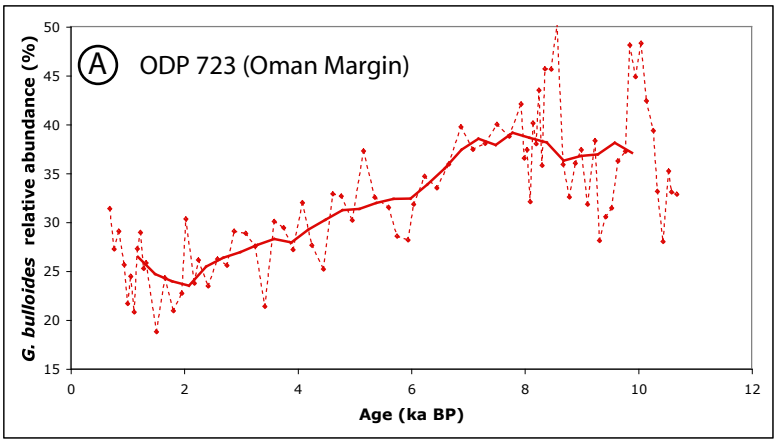
A
ODP 723 (Oman Margin)
G. bulloides relative abundance (%)
50
45
40
35
30
25
20
15
0
2
4
6
8
10
12
Age (ka BP)

6 ka - CTRL

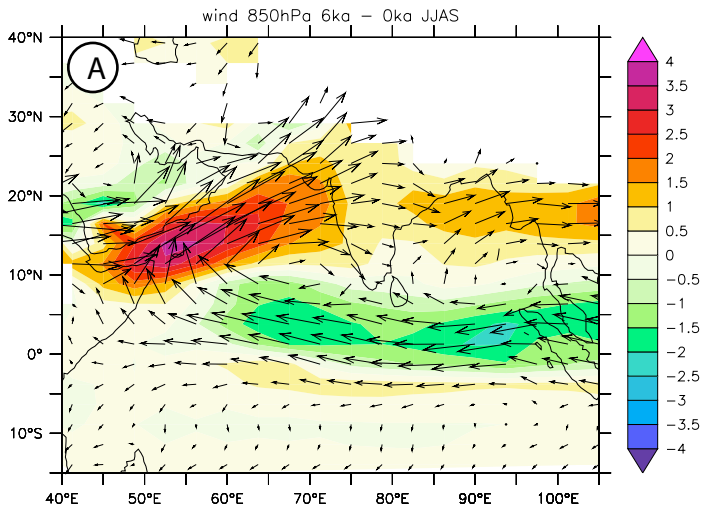

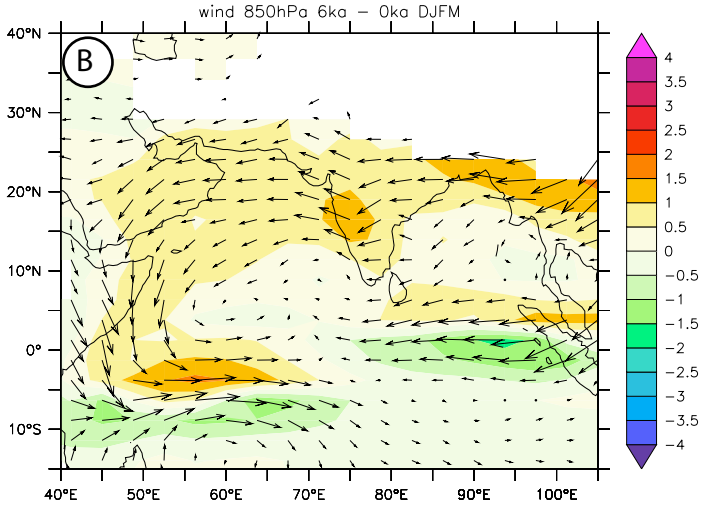

9 ka - CTRL

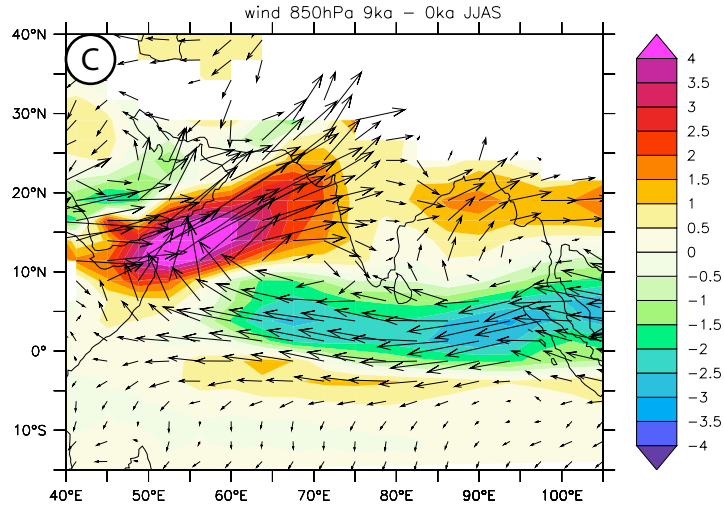

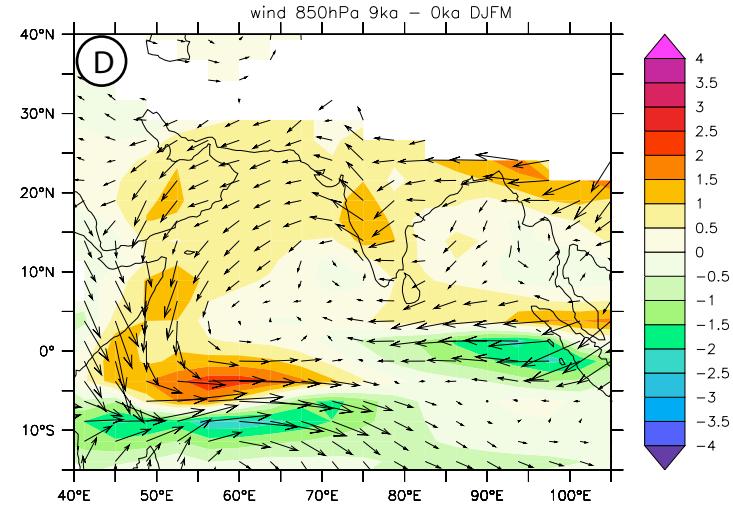

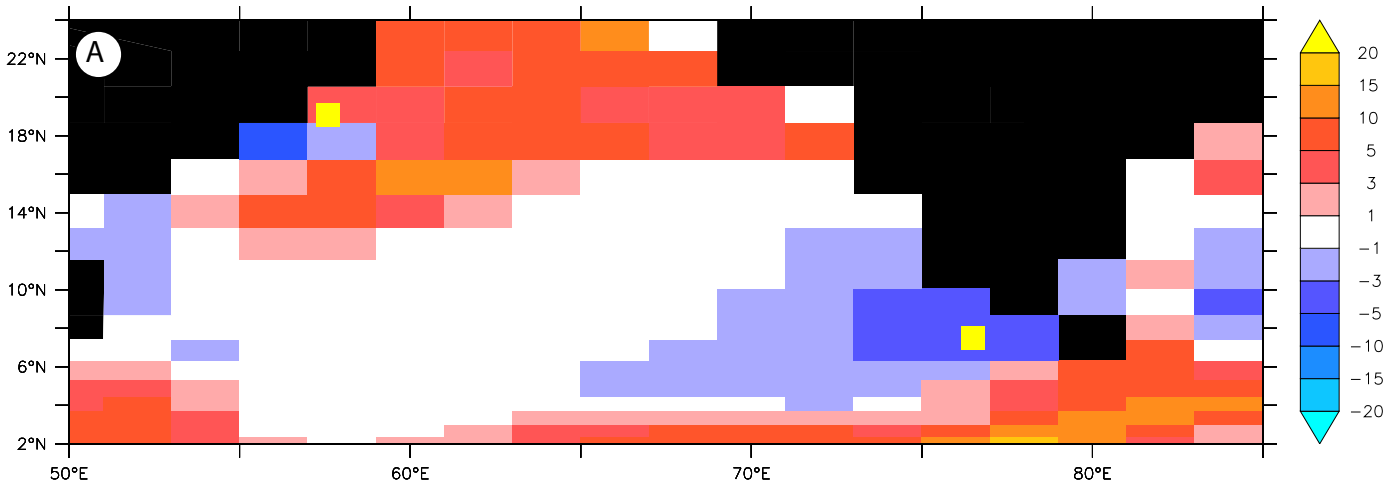
A
22°N
18°N
14°N
10°N
6°N
2°N
50°E
60°E
70°E
80°E
20
15
10
5
3
1
−1
−3
−5
−10
−15
−20

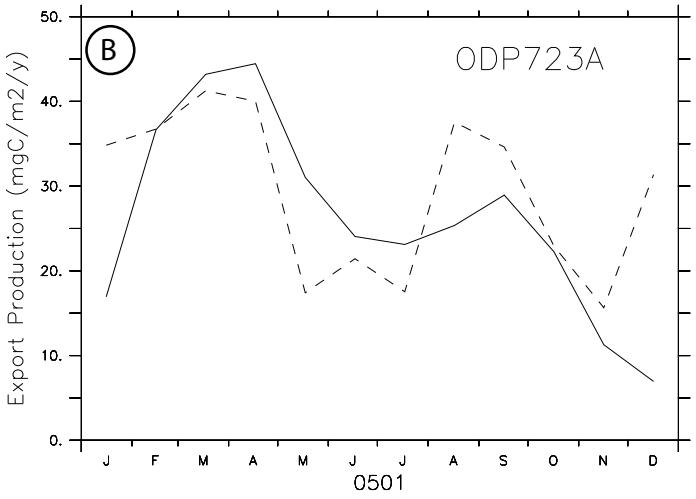
B
ODP723A
Export Production (mgC/m2/y)
50.
40.
30.
20.
10.
0.
J F M A M J J A S O N D
0501

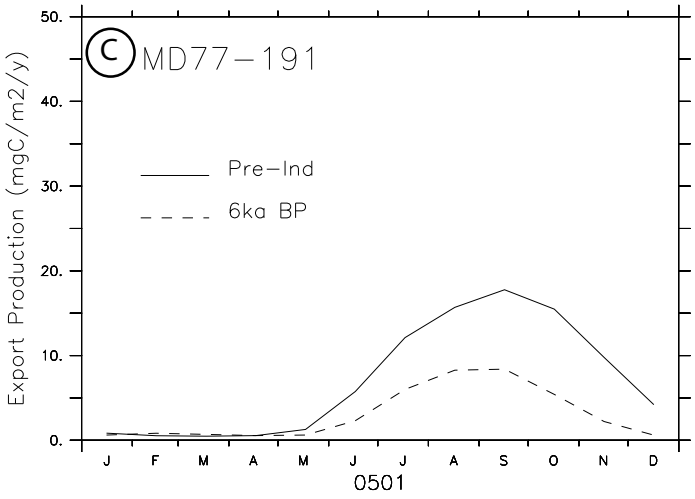
C
MD77−191
Pre−Ind
6ka BP
Export Production (mgC/m2/y)
50.
40.
30.
20.
10.
0.
J F M A M J J A S O N D
0501

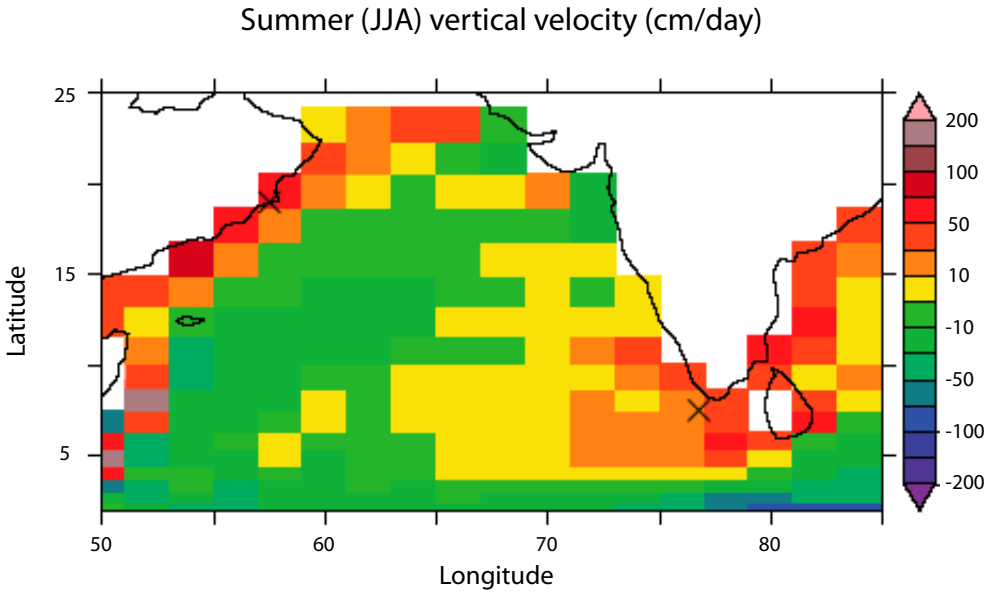
Summer (JJA) vertical velocity (cm/day)
Latitude
Longitude
25
15
5
50
60
70
80
200
100
50
10
-10
-50
-100
-200

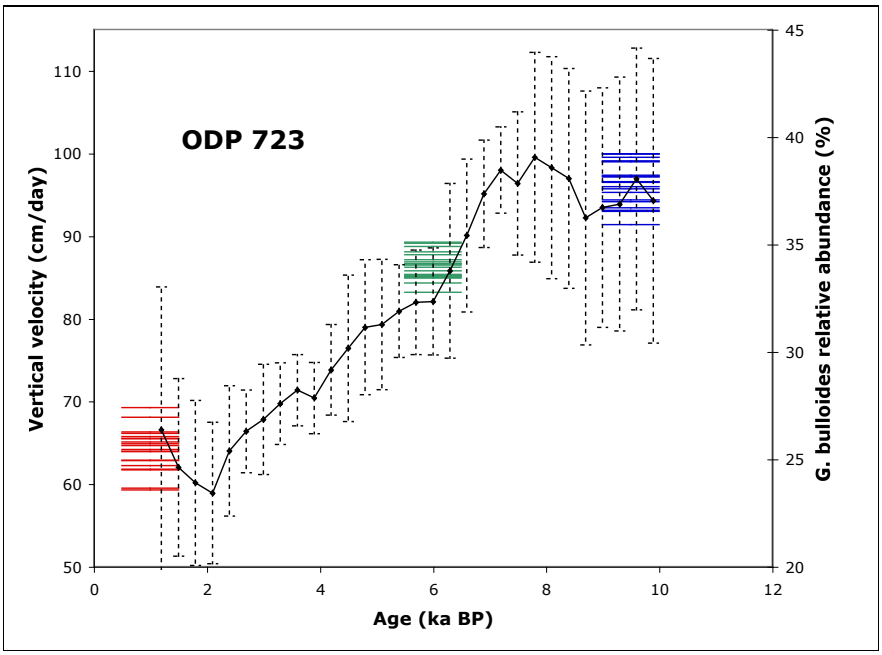
ODP 723
Vertical velocity (cm/day)
G. bulloides relative abundance (%)
Age (ka BP)
110
100
90
80
70
60
50
45
40
35
30
25
20
0
2
4
6
8
10
12

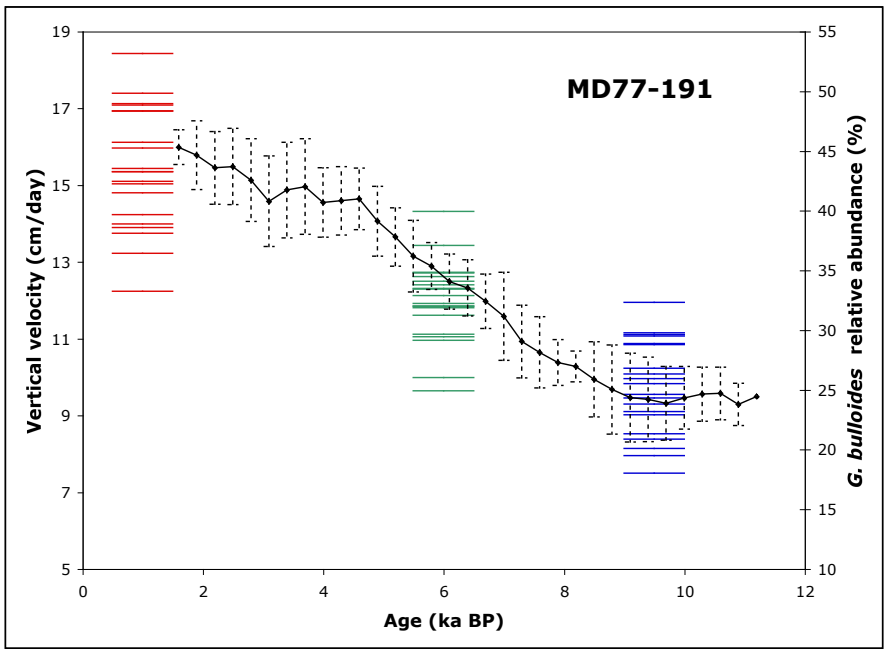
MD77-191
Vertical velocity (cm/day)
G. bulloides relative abundance (%)
Age (ka BP)
19
17
15
13
11
9
7
5
55
50
45
40
35
30
25
20
15
10
0
2
4
6
8
10
12

A.3 Sensibilité du climat glaciaire à différents états de la circulation thermohaline : résultats du modèle de l'IPSL

Clim. Past, 5, 551–570, 2009
www.clim-past.net/5/551/2009/

Climate of the Past

Glacial climate sensitivity to different states of the Atlantic Meridional Overturning Circulation: results from the IPSL model

M. Kageyama[1], **J. Mignot**[2], **D. Swingedouw**[3], **C. Marzin**[1], **R. Alkama**[1,4], **and O. Marti**[1]

[1]LSCE/IPSL, UMR CEA-CNRS-UVSQ 1572, CE Saclay, L'Orme des Merisiers, Bât. 701, 91191 Gif-sur-Yvette Cedex, France
[2]LOCEAN, Universite Pierre et Marie Curie, Case courrier 100, 4 place Jussieu, 75252 Paris Cedex 05, France
[3]CERFACS, 42 Avenue Gaspard Coriolis 31057 Toulouse, France
[4]CNRM, 42 av Coriolis, 31057 Toulouse cedex 1, France

Received: 22 December 2008 – Published in Clim. Past Discuss.: 18 March 2009
Revised: 6 August 2009 – Accepted: 6 August 2009 – Published: 30 September 2009

Abstract. Paleorecords from distant locations on the globe show rapid and large amplitude climate variations during the last glacial period. Here we study the global climatic response to different states of the Atlantic Meridional Overturning Circulation (AMOC) as a potential explanation for these climate variations and their possible connections. We analyse three glacial simulations obtained with an atmosphere-ocean coupled general circulation model and characterised by different AMOC strengths (18, 15 and 2 Sv) resulting from successive ∼0.1 Sv freshwater perturbations in the North Atlantic. These AMOC states suggest the existence of a freshwater threshold for which the AMOC collapses. A weak (18 to 15 Sv) AMOC decrease results in a North Atlantic and European cooling. This cooling is not homogeneous, with even a slight warming over the Norwegian Sea. Convection in this area is active in both experiments, but surprisingly stronger in the 15 Sv simulation, which appears to be related to interactions with the atmospheric circulation and sea-ice cover. Far from the North Atlantic, the climatic response is not significant. The climate differences for an AMOC collapse (15 to 2 Sv) are much larger and of global extent. The timing of the climate response to this AMOC collapse suggests teleconnection mechanisms. Our analyses focus on the North Atlantic and surrounding regions, the tropical Atlantic and the Indian monsoon region. The North Atlantic cooling associated with the AMOC collapse induces a cyclonic atmospheric circulation anomaly centred over this region, which modulates the eastward advection of cold air over the Eurasian continent. This can explain why the cooling is not as strong over western Europe as over the North Atlantic. In the Tropics, the southward shift of the Inter-Tropical Convergence Zone appears to be strongest over the Atlantic and Eastern Pacific and results from an adjustment of the atmospheric and oceanic heat transports. Finally, the Indian monsoon weakening appears to be connected to the North Atlantic cooling via that of the troposphere over Eurasia. Such an understanding of these teleconnections and their timing could be useful for paleodata interpretation.

Correspondence to: M. Kageyama
(masa.kageyama@lsce.ipsl.fr)

1 Introduction

Since the discovery of abrupt oceanic and climate changes in marine records from the North Atlantic (Heinrich, 1988) and glaciological records from Greenland (Dansgaard et al., 1993), numerous studies have contributed to better describe this large amplitude millennial scale variability during glacial periods. In a first step, Bond et al. (1993) suggested the simultaneity between the abrupt changes in the North Atlantic surface conditions and the Greenland ice core records. These authors showed that glacial millennial variability is organised as follows in this area: after a cold period associated with a massive iceberg discharge from the Laurentide ice-sheet to the mid-latitude North Atlantic Ocean (a "Heinrich event"), an abrupt and large amplitude warming event (a "Dansgaard-Oeschger event") occurs, followed by a progressive slow cooling (a "Greenland interstadial") ended by an abrupt cooling leading to a cold period (a "Greenland stadial"). Several

Published by Copernicus Publications on behalf of the European Geosciences Union.

of these Dansgaard-Oeschger cycles occur, with Greenland interstadial peaks decreasing each time, until, during a stadial, a Heinrich event occurs again. Further studies of marine proxies sensitive to the ocean ventilation (e.g. ^{13}C, Elliot et al., 2002) or circulation (e.g. paleomagnetic properties of the marine sediments, see Kissel, 2005, for a recent review) show that the North Atlantic water ventilation and circulation strongly decreased during Heinrich events, but not so much during stadials. The Atlantic Meridional Overturning Circulation (AMOC) has then been proposed to play a key role in rapid climatic changes both around and far from the North Atlantic, and in particular in the Southern Hemisphere and Antarctica (e.g. Blunier et al., 1998; EPICA community members, 2006). Other invoked mechanisms for glacial millennial climate variability include those related to sea-ice cover, especially in the Northern Hemisphere, and to changes in the characteristics of tropical interannual variability, which, at present, do have significant impacts on the extratropical climate (for a complete review, see Clement and Peterson, 2008).

Our objective here is to investigate the most commonly invoked mechanism for this millennial glacial variability, namely the climate differences related to different states of the AMOC. We use a global coupled ocean-atmosphere general circulation model run under glacial boundary conditions to study the sensitivity of the AMOC to the fresh water balance (or imbalance) imposed at the atmosphere-ocean interface and to study the climate differences related to three different states of the AMOC, which we briefly compare to available proxy records. Our main objective is to analyse the mechanisms for climate changes related to AMOC differences over 3 regions where the model compares qualitatively well with data: the northern extra-tropics, the tropical Atlantic and Indian monsoon region.

1.1 Palaeorecords of of millennial-scale climate changes

Pollen records retrieved in marine sediment cores off the European coast, and in particular around the Iberian Peninsula, show that simultaneous to abrupt changes in sea surface conditions, the composition of the vegetation on the nearby land changed significantly (Combourieu Nebout et al., 2002; Sánchez-Goñi et al., 2002; Sánchez-Goñi et al., 2008), with more forests during interstadials, characterized by relatively warm sea surface temperatures and more semi-desert or steppic vegetation during stadials, characterized by relatively cold ocean surface conditions. Other types of continental records, such as the speleothem record from Villars Cave in Southwestern France (Genty et al., 2003), confirm the abrupt and large amplitude climatic and vegetation changes during the last glacial period. Schematically, these records suggest cold and dry stadials, and warmer and wetter interstadials over Southwest Europe. Additional information on the atmospheric circulation of this region has been obtained from a clay mineral record from the Alboran Sea (Bout-Roumazeilles et al., 2007) which shows more export of dust from Morocco to the Mediterranean Sea during stadials and even more prominently during Heinrich events, which can be related to a more southerly circulation during these periods in this region. This signature associated with cold conditions over the North Atlantic constrasts with the warm, wet conditions found during Heinrich events on the other side of the Atlantic, in Florida (Grimm et al., 2006). This shows that even around the North Atlantic, the continental climate response to cold oceanic conditions which could be due to a weakening of the AMOC is far from being spatially homogeneous. Furthermore, studying an apparent mismatch between reconstructions of the Greenland temperatures based on ice core and on snowline changes, Denton et al. (2005) show that abrupt climate variations are likely to be dependent on the season, with the strongest cooling occuring in winter.

Abrupt climatic variations have also been recorded, on the same type of time-scales as for the events occuring around the North Atlantic, away from from this region. Records from the tropical Atlantic (e.g. Cariaco Basin, Peterson et al., 2000; González et al., 2008) show dry events during Greenland stadials, while to the South of these sites, in North East Brazil, wet events are recorded (Wang et al., 2004). Taken together, these records can be interpreted as showing a southward migration of the Intertropical convergence zone (ITCZ) during stadials over the Atlantic Basin. This is confirmed for the other side of the tropical Atlantic by dusty events recorded off the northwestern African margin during Heinrich events (Jullien et al., 2007), which suggest southward shifts of the ITCZ during those events. Leduc et al. (2007) further suggest this southward migration to be associated with a decrease in moisture transport from the Atlantic to the Pacific, due to the topographic barrier of the Andes. The southward migration of the ITCZ during stadials is therefore supported by many records. Such a migration is also suggested for the Western Pacific during Heinrich events from records from North East Australia (Turney et al., 2004; Muller et al., 2008).

Speleothem and loess records from China show that the East Asian monsoon also shows strong millennial scale variations, with decreases in the summer monsoons during Heinrich events and stadials (Porter and An, 1995; Wang et al., 2001). Ruth et al. (2007), analysing the dust content from the ice cores retrieved by the North Greenland Ice Core Project, suggest a very tight temporal correspondence between the climatic changes recorded in Greenland and the East Asian monsoon activity, which modulates the dust archived in Greenland. Several records show that the Indian monsoon intensity also changes in glacial times, simultaneous with Greenland stadials and interstadials (Schulz et al., 1998; Leuschner and Sirocko, 2000; Altabet et al., 2002; Rashid et al., 2007). In addition, Sánchez-Goñi et al. (2008) show a correspondence between the impacts of Dansgaard-Oeschger events in western Europe and in Asia. Variations in Asian monsoon strength could be responsible for the abrupt

changes in atmospheric methane concentration recorded in ice cores both from Greenland and Antarctica (Blunier et al., 1998; EPICA community members, 2006).

In summary, millennial-scale variability, first revealed in records of North Atlantic surface conditions and in Greenland ice core records, is traced in many paleo-records around the world. Here we will examine if different states of the AMOC can be responsible for these teleconnections and if so, the mechanisms underlying these teleconnections.

1.2 Insights from numerical models: fresh water hosing under present boundary conditions

Nearly from the time it was discovered, glacial abrupt climate variability has been related to model results showing that the thermohaline circulation (here assimilated to the AMOC) is characterised by several equilibria (Stommel, 1961) and that transitions between these equilibria, i.e. between situations in which the AMOC is slow or shut-down and situations with strong AMOC, can be rapid (Rahmstorf, 1994). Using an atmospheric-ocean coupled General Circulation Model (AOGCM) and, thanks to an anomalous freshwater input into the northern North Atlantic, forcing its AMOC from an "on" state, similar to the present one, to an "off" state, and back to an "on" state, Manabe and Stouffer (1995) show that it is possible to simulate an abrupt climate change in the North Atlantic, which they relate to be similar to the Younger Dryas ($\sim$12 000 years ago). They show that a strong temperature anomaly develops over and around the North Atlantic in response to a weakening of the thermohaline circulation but that no strong temperature anomaly develops elsewhere. This type of experiments, termed "water-hosing experiments", have been run by many groups since then, with models of different complexities. Stouffer et al. (2006) compile the results from 14 models in which fresh water fluxes of 0.1 and 1 Sv are applied in the North Atlantic between 50 and 70° N. All models simulate, to various degrees, a weakening of the AMOC and a cooling of the North Atlantic in response to the 0.1 Sv fresh water flux, but some models also simulate a warming in the Nordic and/or Barents Sea. The response to the 1.0 Sv fresh water flux in the North Atlantic, Nordic Seas and Arctic Ocean is a general cooling, which is maximum over the North Atlantic and Nordic Seas between 50 and 80° N. The cooling propagates over Eurasia, but it is not as strong over North America. This shows the sensitivity of the climate response to different fresh water forcings and different states of the thermohaline circulation.

In terms of atmospheric circulation, the response to the 0.1 Sv anomaly shows that the North Atlantic sea surface temperature (SST) anomaly is associated with a cyclonic sea-level pressure anomaly, which constitutes a modulation of the mid-latitude westerlies. A weakening in the AMOC therefore has an impact on the Northern Hemisphere stationary wave pattern. Vellinga and Wood (2002) show that this response appears within decades of their initial (very strong) perturbation. They also obtain a cyclonic anomaly over the northern North Atlantic, with southwesterly surface wind anomalies over western Europe. This could explain why the temperature anomalies over this region are not as strong as over the North Atlantic: relatively warmer air is advected by the anomalous circulation forced by the North Atlantic cooling.

The SST response in areas remote from the North Atlantic is dominated by a warming of the South Atlantic and of the Southern Ocean. This follows the classical interhemispheric (bipolar) see-saw effect (Crowley, 1992; Stocker, 1998), which appears more prominently in the Atlantic. It creates, around the Equator, a temperature anomaly dipole, with colder waters to the North and warmer waters to the South when the AMOC is weaker. This dipole is associated with a southward shift of the ITCZ (e.g. Stouffer et al., 2006; Chiang et al., 2008). The development of such a dipole is due to a decrease in interhemispheric transport of heat by the Atlantic ocean. The atmosphere also plays a role. Chiang and Bitz (2005) and Yang and Liu (2005) show that an imposed cooling in the North Atlantic propogates towards the Equator and cools the SST to the South through a Wind-Evaporation-SST feedback (Chiang et al., 2008).

The Indian monsoon response to an AMOC weakening is consistent with a southward shift of the ITCZ. However, specific mechanisms have been suggested for the monsoon variations concomitant with the millennial scale events occuring in the North Atlantic. On the basis of observational data from 1871 to 2003, Goswami et al. (2006) propose that the Indian summer monsoon and Atlantic Multidecadal Oscillation (AMO) could be linked via a modification of the meridional gradient of the temperature of the upper half of the troposhere (which they term "TT"). They show that for a warm North Atlantic, there is an increase in the meridional gradient of TT, which, in turn, favours a stronger monsoon. Using a coupled ocean-atmosphere model on which they impose a positive sea surface temperature anomaly in the North Atlantic, Lu et al. (2006) show that in addition to the atmospheric connection via the TT meridional gradient, coupled ocean-atmosphere feedbacks in the Indian and Western Pacific Ocean help instensifying the monsoon. Indeed, the warm anomaly in the North Atlantic is associated with warm anomalies in the Indian and western Pacific oceans, which help producing more precipitation and induce an enhanced monsoon circulation. Zhang and Delworth (2005) show that the weakening of the East Asian monsoon in their coupled GCM with a weaker AMOC is related to a change of the Pacific Walker circulation and the Rossby wave response to the resulting dampened convection over Indonesia acts to weaken the Indian monsoon.

1.3 Fresh water hosing in glacial conditions

All the experiments cited above were run in the present-day or pre-industrial contexts, i.e. for present or pre-industrial

greenhouse gas concentrations and ice-sheet extent and topography. On the other hand, millennial scale variability is largest during glacial times. Using the climate model of intermediate complexity CLIMBER-2, Ganopolski and Rahmstorf (2001) show that a glacial climate is much more sensitive to fresh water fluxes in the North Atlantic than an interglacial climate. Using a fully coupled ocean-atmosphere general circulation model, Hu et al. (2008) show that when the Bering Strait is closed, the recovery of the AMOC from an "off" to an "on" state is slower, due to the fact that the fresh water introduced in the North Atlantic takes a longer time to be removed from this region when the Arctic and Pacific oceans are not connected. Bitz et al. (2007) also obtain a much slower recovery of the AMOC in a glacial world but instead ascribe it to more extensive sea-ice cover in the North Atlantic and Nordic Seas. Finally, Weber and Drijfhout (2007) show that the glacial AMOC is more sensitive to fresh water discharges than the present one, and that the recovery timescales from the collapse are much longer.

In terms of glacial surface climate response to a collapse in the AMOC, Ganopolski and Rahmstorf (2001), along with the follow-up studies of Claussen et al. (2003) and Jin et al. (2007), show a cooling of the North Atlantic, extending over Eurasia, and a smaller cooling over the Pacific and North America. The response in the Southern Hemisphere is an overall warming, consistent with the bipolar see-saw mechanism. In addition, using the same model, Jin et al. (2007) show that the decrease in Eurasian temperatures associated with a weakening of the AMOC can be responsible for a weakening of the Asian monsoon. The thermal response to a collapse of the AMOC simulated by the HadCM3 fully coupled atmosphere-ocean general circulation model (Hewitt et al., 2006) is broadly consistent with the results of the CLIMBER-2 climate model of intermediate complexity.

Using the coupled ocean-atmosphere model ECBILT-CLIO forced with full glacial boundary conditions, Timmermann et al. (2005) and Krebs and Timmermann (2007) investigate the mechanisms for the teleconnections between the North Atlantic oceanic state and equatorial Pacific temperatures and salinities, during a transient meltwater pulse experiment in which the AMOC shuts down and recovers. Analysing fully coupled as well as partially coupled atmosphere-ocean simulations, they examine the respective roles of the atmosphere and the ocean in the response to the AMOC collapse. They find that the North Atlantic cooling associated with the AMOC collapse is advected downstream over the Eurasian continent and is largely responsible, on its own, for the atmospheric circulation changes simulated in their coupled experiments. This includes a weakening of the Asian monsoon and an intensification of the trade winds over the northern tropical Pacific, both related to changes in the meridional temperature gradient. In addition, the sea-level increase associated to the oceanic response has a global impact on the thermocline structure via a standing wave pattern. In the Western Pacific, this adjustment involves the transport of cold and salty waters in the Pacific warm pool. The response is further amplified by the fact that trade winds intensify and precipitation decreases in this area.

Flückiger et al. (2008) use the same model to show that the surface climate response to an increase in AMOC is not linear with respect to the AMOC strength. In addition, the simulated surface climate response to an AMOC intensification is dependent on the season, with the high northern latitudes undergoing the maximum climate changes in winter while the differences over the mid-latitude Eurasian continent are largest in spring due to a shift of the period of snow retreat. This, in turn, is responsible for an earlier break of the Siberian high pressure and an earlier setup of the Asian monsoon. The dependence of the climate response on the season has important implications for the interpretation of proxy data, as they are often more sensitive to the climate of one particular period of the year.

1.4 Objectives of the present study

Hence, to our knowledge, there are not many fresh water hosing experiments run in a glacial climatic context with fully coupled ocean-atmosphere general circulation models. In this study, we report on new results obtained with the IPSL_CM4 model. We consider the surface climate sensitivity to a weak change in an active AMOC (18 vs. 15 Sv) and to a collapse of the AMOC (15 vs. 2 Sv). We first describe the model and simulations (Sect. 2). Then we analyse the reasons for differences in the AMOC of the three simulations (Sect. 3.1) and briefly examine their impact on global heat transports (Sect. 3.2). In Sect. 3.3, we present the signature of these AMOC states in terms of surface climate and compare it with the available paleo-records and in Sect. 4, we study the timing of the climate changes in the simulation in which the AMOC collapses. This leads us to postulate on mechanisms for these climate changes, which we investigate further for three regions: the northern extratropics, the tropical Atlantic and the Indian monsoon region (Sect. 5). This analysis is the main objective of the present study. It is not our goal here to compare the climatic sensitivity to changes in AMOC between the glacial and the present states. This issue is treated in a companion study (Swingedouw et al., 2009).

2 Description of the climate model simulations

The model used in the present study is the coupled ocean-atmosphere IPSL_CM4 model (Marti et al., 2006, 2009). The atmospheric component of this coupled model is LMDZ.3.3, with resolution $96\times71\times19$ in longitude$\times$latitude$\times$altitude. The horizontal grid is regular, while the vertical levels are more numerous near the surface. This atmospheric module includes the land surface scheme ORCHIDEE which includes a complex river routing scheme. The ocean module is

ORCA2, which uses an irregular horizontal grid of 182×149 points with a resolution of ca. 2°, refined over key regions such as the North Atlantic and near the Equator. This model has 31 depth levels. The sea-ice module is the Louvain Ice Model (LIM). The coupling of these components is performed using the OASIS (version 3) coupler.

The performance of the model in its representation of the modern climate is described in detail in Marti et al. (2009). At the resolution used in the present study, the AMOC simulated for pre-industrial boundary conditions is weak (11 Sv) but its strength increases with resolution. This bias is partly related to the fact that there is no convection in the Labrador Sea in this model, for these boundary conditions (Swingedouw et al., 2007a). This is due to an excess of precipitation in the North Atlantic and North Atlantic westerlies located too much to the South (Marti et al., 2009). Nevertheless the model's sensitivity to prescribed freshwater fluxes such as in Stouffer et al. (2006) is similar to other models (Swingedouw et al., 2009), as is the case for its sensitivity to freshwater fluxes in climate projections (Swingedouw et al., 2007b; Schneider et al., 2007).

In the present study, we analyse three simulations of the IPSL_CM4 model with boundary conditions for the Last Glacial Maximum, as defined by the PMIP2 protocol (Braconnot et al., 2007a, http://pmip2.lsce.ipsl.fr): we use the ICE-5G ice-sheet reconstruction (Peltier, 2004), CO_2, CH_4 and N_2O atmospheric concentrations of 185 ppm, 350 ppb and 200 ppb respectively (Monnin et al., 2001; Dallenbach et al., 2000; Flückiger et al., 1999), and orbital parameters relevant for 21 ky BP (Berger, 1978). The river routing has been adapted for Last Glacial Maximum (LGM) conditions (Alkama et al., 2007). The vegetation is kept at its present-day distribution.

With such an experimental set up, snow accumulates over the ice sheets and this freshwater sink has to be compensated in order to obtain stable simulations. This compensation is performed in three latitude bands, with limits at 90° S/50° S/40° N/90° N. In each latitude band, the excess of freshwater accumulating as snow on the ice sheets, which we define as "calving", is integrated and supplied to the ocean in the same latitude band. The 40° N limit roughly represents the southernmost latitude reached by icebergs during ice ages. Freshwater fluxes due to calving collected North of this limit are delivered to the Atlantic and Arctic oceans but not to the Pacific since observations suggest that these are the regions were ice rafted detritus are most abundant. In spite of this procedure, the first LGM simulation performed with our model had a remaining imbalance in the freshwater budget due to a slightly non conservative atmospheric convection scheme. Therefore two additional simulations in which the freshwater budget is closed using different methods prolong this first, unbalanced, 200-year-long simulation: in LGMa, the bias is compensated by multiplying global precipitations by 2.1% over the oceans. In LGMb, the "calving" flux is multiplied by 44% in the three latitude bands defined above. Both methods lead to a closed fresh water budget at the atmosphere-ocean interface. LGMa has been run for 300 years and LGMb for 1000 years. An additional sensitivity experiment, LGMc, is performed, where the calving fluxes in the three regions defined above have been multiplied by 100% (as compared to 44% for LGMb). In this simulation, which has been integrated for 420 years starting from year 150 of LGMb, the freshwater balance is not closed.

In terms of differences of fresh water fluxes over the ocean, the largest differences between the experiments are in the North Atlantic/Artic region, which receives 0.08 Sv more fresh water in LGMb than LGMa, and 0.1 Sv more in LGMc compared to LGMb. These figures remain stable throughout the simulations. The differences in fresh water forcing are comparatively very small over the Austral Ocean: the calving is 0.012 Sv less in LGMb compared to LGMa and 0.015 Sv less in LGMc compared LGMb. Hence, even though our experiments do not follow the classical fresh water hosing experimental set-up, as described for example by Stouffer et al. (2006), the freshwater flux differences in the North Atlantic/Arctic regions are of the same order of magnitude as in many other fresh water hosing experiments (cf. Sects. 1.2 and 1.3), if not on the low side compared to the 1 Sv used in some extreme experimental set-ups.

It is not our goal here to perform a detailed comparison of our model results with Last Glacial Maximum paleo-data. Within the PMIP2 project, an earlier LGM simulation with the same model has been extensively compared to paleo-records and to other model results. This simulation of the LGM climate was very much in line with results from other models (e.g. Masson-Delmotte et al., 2006; Kageyama et al., 2006; Braconnot et al., 2007a,b; Ramstein et al., 2007; Otto-Bliesner et al., 2009). A surprising result from our LGMa or LGMb simulations compared to the pre-industrial one is the increase in AMOC. This is in contradiction with paleodata (e.g. Lynch-Stieglitz et al., 2007) but it is found in several models (Weber et al., 2007). In our model, it is partly related to its under-evaluation for the pre-industrial case. This was an additional motivation to obtain a LGM simulation with a collapsed AMOC, but a more detailed comparison between all the LGM simulations presented here and the pre-industrial basic state is left for a forthcoming study, as our goal here is to better understand the differences between these three LGM simulations.

3 Large-scale oceanic and climatic adjustments of the AMOC to different freshwater perturbations

3.1 Evolution of the AMOC and North Atlantic deep water formation

The perturbation in fresh water flux into the northern North Atlantic and Arctic are of 0.08 Sv between LGMa and LMGb and of 0.1 Sv between LGMb and LGMc. Yet, while

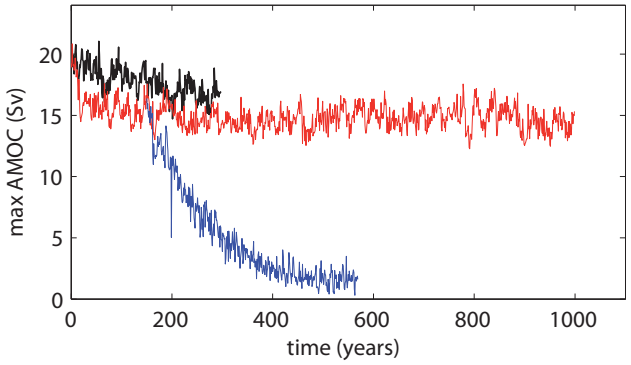

Fig. 1. Time evolution of the maximum of the Atlantic Meridional Overturning Circulation (in Sv, 1 Sv=10^6 m^3/s) in runs LGMa (black), b (red) and c (blue).

LGMa and LGMb present strong and stable AMOCs, with strengths of 18 and 15 Sv respectively, and strong North Atlantic Deep Water (NADW) formation that reaches the bottom of the North Atlantic Ocean in the northern mid-latitudes, the AMOC collapses to 2 Sv by the end of simulation LGMc (Figs. 1 and 2). We can therefore conclude that the atmosphere-ocean state in LGMb is probably close to a North Atlantic fresh water threshold for which the AMOC collapses: although the additional fresh water in the North Atlantic is rather small in LGMc compared to other fresh water hosing experiments, the AMOC collapses within 300 years. We therefore obtain two simulations with extreme AMOCs, one in the "on" state (LGMa) and one in the "off" state (LGMc) and a simulation (LGMb) with an active AMOC slightly smaller than the LGMa maximum. LGMa and LGMb are therefore reminiscent of Greenland interstadials, while the extreme LGMc simulation, especially at its end when the AMOC has completely collapsed, is to first order relevant for a comparison to a Heinrich event, e.g. Heinrich events 2 or 1 which are close to the LGM.

To understand the differences in the AMOCs of our simulations, we further study the characteristics of the NADW formation. In LGMa, it essentially takes place North of Newfoundland and South of Iceland (Fig. 2), immediately South of the winter ice edge, as well as in the Arctic Ocean beneath the sea ice. Some relatively deep mixed layers are also detected along the Norwegian coast. In LGMb, deep water formation disappears from the Arctic Ocean while it tends to increase in the northern North Atlantic areas. Since this occurs simultaneously with a global reduction in AMOC strength, this suggests that deep water formed in the Arctic in the LGMa simulation actually plays an important role in this interhemispheric water transport. Figure 3 illustrates that in the Southern Labrador Sea, an anomalous mixed layer depth pattern, consisting in a southward shift of the convection site (black contours) develops in LGMb compared to LGMa. This is associated with an increase of sea ice cover in the northwestern part of the area (pink contours) that leads to negative anomalous ice to ocean freshwater flux due to brine rejection and thus to a net oceanic freshwater loss further South of this ice formation area (blue colours). This freshwater loss locally overwhelms the freshwater input due to the experimental set-up (not shown). Thus, surface water density tends to increase locally and this favours deep water formation. A similar process is at play Southwest of Iceland, although the sea ice anomaly and the ice to ocean freshwater flux are much weaker. Along the Norwegian coast, deep water formation clearly decreases at around 75° N while it increases locally around 65° N. Indeed, in this area, sea ice cover, largely capping the ocean from intense atmospheric cooling and thus preventing deep water formation, is pushed by anomalous southerly winds and thus decreases around 65° N while it increases further North (not shown). We will show that the anomalous deepening of deep convection in this area has an important climatic implication.

Figure 4 (l.h.s.) illustrates the timescale on which these deep convection changes set up in LGMb. The shallowing of the mixed layer in the Arctic area (Site 5) and off the Norwegian coast (Site 2) settles within the first years of the simulation. On the other hand, changes in the Labrador Sea (Site 3) and in the Norwegian Sea's southern site (Site 4) are delayed and settle after several decades. In these areas, the interannual variability also clearly increases. This suggests a link with a change in atmospheric variability but the coupled simulations make it difficult to isolate the exact mechanism. However, it raises the possibility for delayed climatic responses to changes in the North Atlantic freshwater budget that can have important regional consequences.

As expected from Fig. 1, NADW formation is practically shut off in LGMc (Figs. 2 and 4). This results from a direct capping of the deep water formation sites by the freshwater. The AMOC reduction is also associated with a southward displacement of the winter sea-ice edge (Fig. 2). As above however, all convection sites do not cease their activity at the same time (Fig. 4, r.h.s): while the Norwegian Sea convective activity immediately decreases after the start of the run and completely ceases in less than 100 years, the Labrador Sea site remains very variable, sometimes reaching the activity levels of LGMb over the first hundred years of LGMc, before shutting off. The slowest site to react is the one in the Irminger Sea and South of Iceland, which finally shuts off after 200 years of simulation. The time series of mixed layer depth for this site in LGMb also shows more stability than for the two other sites, probably because it is much larger. The open area South of Iceland and along Greenland is wide, and allows convection to adjust and shift slightly according to changes in the forcing, while the location of convection is probably much more constrained in the Labrador Sea and off Norway. This might explain the greater persistence of this site. Eventually, its time scale for shutting down is very close to that of the AMOC itself (Fig. 1), suggesting that it controls the strength of the AMOC. This is consistent with findings of

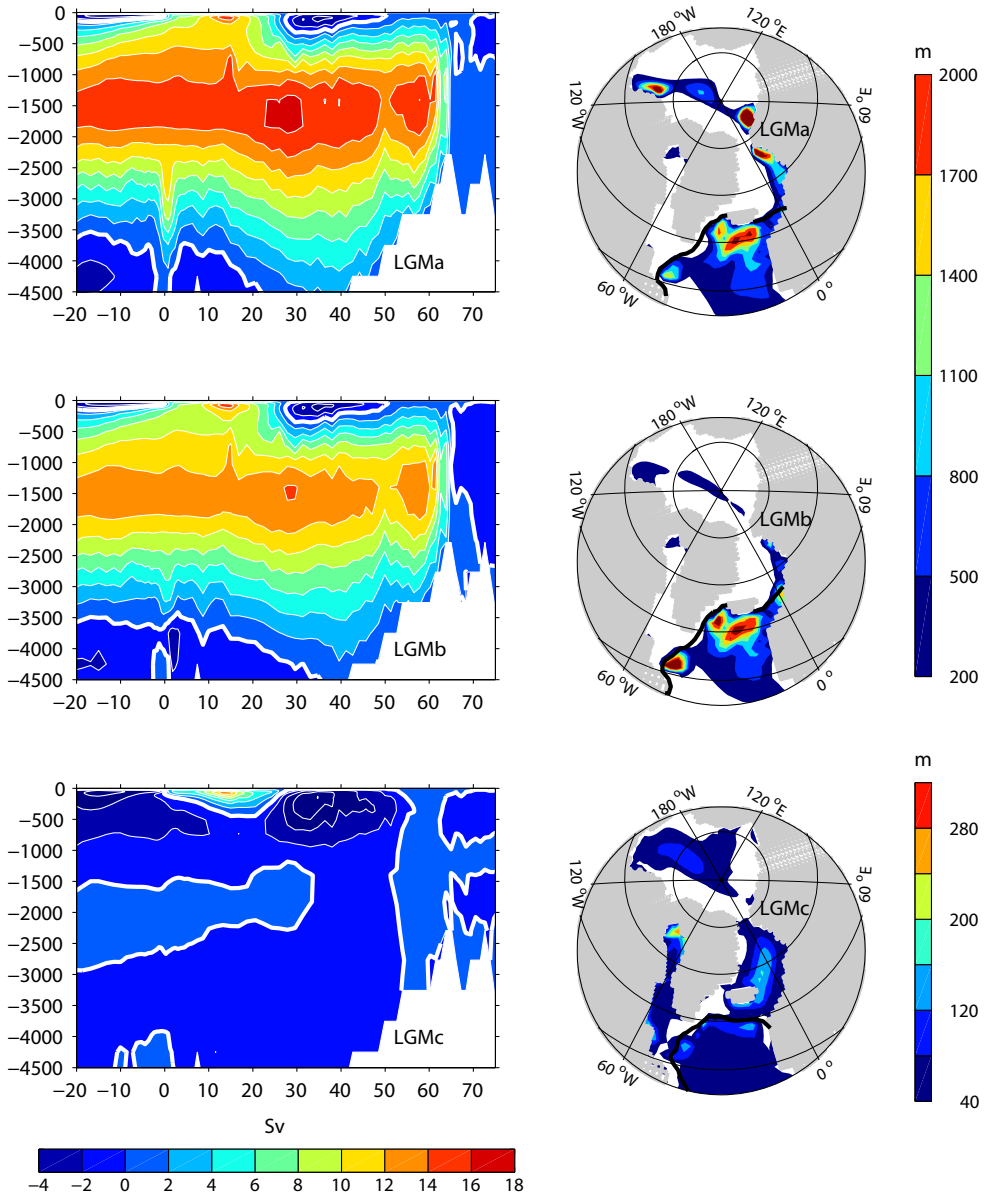

Fig. 2. Atlantic meridional streamfunction (l.h.s) and maximum mixed layer depth reached over the winter months (February to April) (r.h.s) for LGMa (top), LGMb (middle), LGMc (bottom), years 201–250 for LGMa and b, 521–570 for LGMc. The thick black line on the mixed layer depth plots shows the limit of a 10% sea ice coverage in March.

Msadek and Frankignoul (2009) who showed that the multi-decadal fluctuations of the AMOC are mostly driven by deep convection south of Iceland in this model under modern climate.

3.2 Global heat transport adjustements

The shutdown of the AMOC in LGMc induces an important weakening in oceanic heat transport. The global meridional oceanic heat transport is reduced by more than 0.32 PW between 10° S and 60° N. This decrease is lower than the 0.45 PW reduction in the Atlantic alone. The other basins therefore compensate part of the reduction in the Atlantic heat transport. The reduction is maximum at 17° N where it reaches more than 0.68 PW, i.e. a 70% decrease in LGMc compared to LGMb at the end of each simulation (Fig. 5). The atmospheric meridional heat transport increases in response to the decrease in oceanic meridional heat transport, showing that the "Bjerknes compensation" effect (Bjerknes, 1964; Shaffrey and Sutton, 2006) is at work here. However, a perfect compensation would require a constant radiative

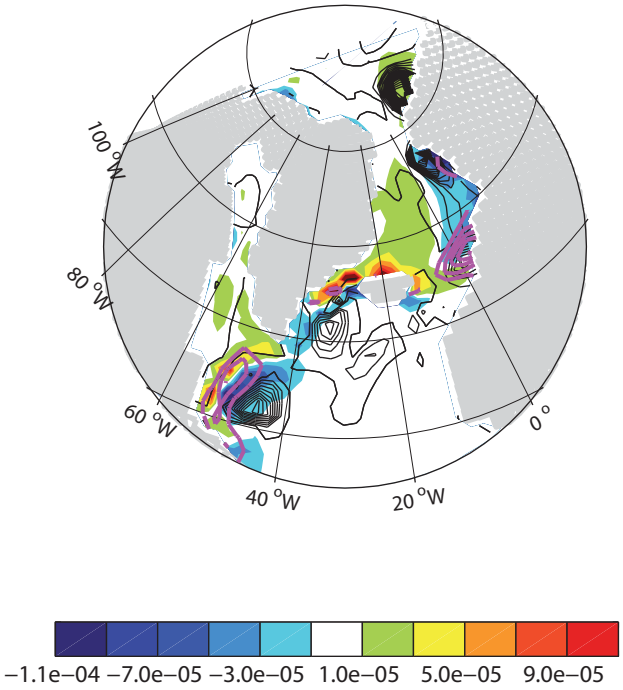

Fig. 3. Colours: ice to ocean winter (January-February-March) anomalous (LGMb–LGMa) freshwater budget (in kg/m^2/s). Black contours: anomalous (LGMb–LGMa) winter (JFM) mixed layer depth. Continuous (dashed) contours show positive (negative) anomalies. Contour interval is 150 m. The contour of zero anomaly is omitted. Pink contours: anomalous (LGMb–LGMa) winter (JFM) ice coverage. Continuous (dashed) contours show positive (negative) anomalies. Contour interval: 0.1.

budget and no storage in any heat reservoirs. These hypotheses are scarcely verified (see also Swingedouw et al., 2009), and Fig. 5 shows that the Bjerknes compensation is not total: it amounts to ca. 64% in terms of meridional heat transport at 17° N. Changes in ocean and atmosphere heat transports between LGMa and LGMb are small compared to those associated with a collapse of the AMOC. At this scale, there is no compensation between the anomalies in oceanic and atmospheric heat transports.

3.3 Global surface climate adjustments

As expected from previous model results and from the heat transport changes discussed above, the North Atlantic Ocean is cooler when the AMOC is weaker. In LGMb, compared to LGMa (Fig. 6, middle), this cooling is only significant at mid-latitudes, is rather constant along the year and does not exceed 2°C (Fig. 7). Cooling is also simulated over the northern continents at mid- to high latitudes, with significant anomalies only during autumn and winter. Eurasia is slightly cooler in LGMb compared to LGMa, with a maximum difference of 1°C centred over Eastern Europe. It is therefore surprising to obtain a warmer (by ∼1°C in annual mean) surface air temperature over the Norwegian Sea, a feature which is mainly significant during the transition seasons (Fig. 7). This is linked to an anomalous warming of the ocean associated with the reinforcement of the convective activity in this area. Finally, a cooling of around 1°C is also found over the Southeastern Pacific and East of the Antarctic Peninsula.

The cold anomaly over the North Atlantic is associated with changes in the stationary waves, as shown by the presence of a cyclonic anomaly over the zone of cooling. This structure can be traced from the sea surface to the 200 hPa level and is shown for the 500 hPa level on Fig. 8 (middle). If we compare the location of this cyclonic anomaly to the mean flow on Fig. 8 (top), we can see that it corresponds to a southward shift of the jet-stream, which is consistent with the cooling inducing the strongest meridional temperature gradient more to the South than its position in LGMa. This anomaly can explain that the North Atlantic cooling does not expand over western Europe, which undergoes southerly wind anomalies.

Over northern Eurasia, another cyclonic anomaly develops, bringing cold air from the North over central and eastern Europe. This cyclonic anomaly occurs for autumn and winter, consistent with the cooling simulated over these regions for these seasons. It is not possible, from our experiments only, to determine if the cyclonic anomaly over the North Atlantic is responsible for the Eurasian cyclonic anomaly via a disturbance of the autumn and winter stationary waves, or if the Eurasian cyclonic anomaly develops as a response to the cooling over this area. However, the surface temperature anomaly and associated atmospheric circulation anomalies seem to act as if they sustain each other. The warming over the Norwegian Sea does not correspond to an anomaly in the sensible heat transport (which structure, not shown, is very similar to the 500 hPa wind), hence confirming the rather local mechanism, developed in Sect. 3.1, based on changes in sea ice cover and surface winds. Precipitation differences between LGMa and LGMb are scarcely significant and will not be discussed further.

In LGMc, the whole Arctic Ocean and the North Atlantic, from 10° N northward, are much colder than in LGMb (Fig. 6, bottom). The surface air temperature cools by more than 5°C over regions in which sea ice appears in LGMc, i.e. just south of Iceland, and by up to 4°C in the mid-latitude North Atlantic. Over Eurasia, the simulated LGMc-LGMb cold anomaly is twice as strong as the LGMb–LGMa one in amplitude, but nearly covers the whole Eurasian continent. Nevertheless, some regions still experience a warming in LGMc compared to LGMb. Western Europe does not cool as much as the surrounding regions, to the West or to the East. The northeastern Pacific and northwestern North America experience a warming of 1°C in LGMc compared to LGMb. In addition, the South Atlantic Ocean warms up by as much as 2°C, which, together with the North Atlantic cooling, constitutes a classical bipolar see-saw response. The Indian and Western Pacific sections of the Southern Ocean also

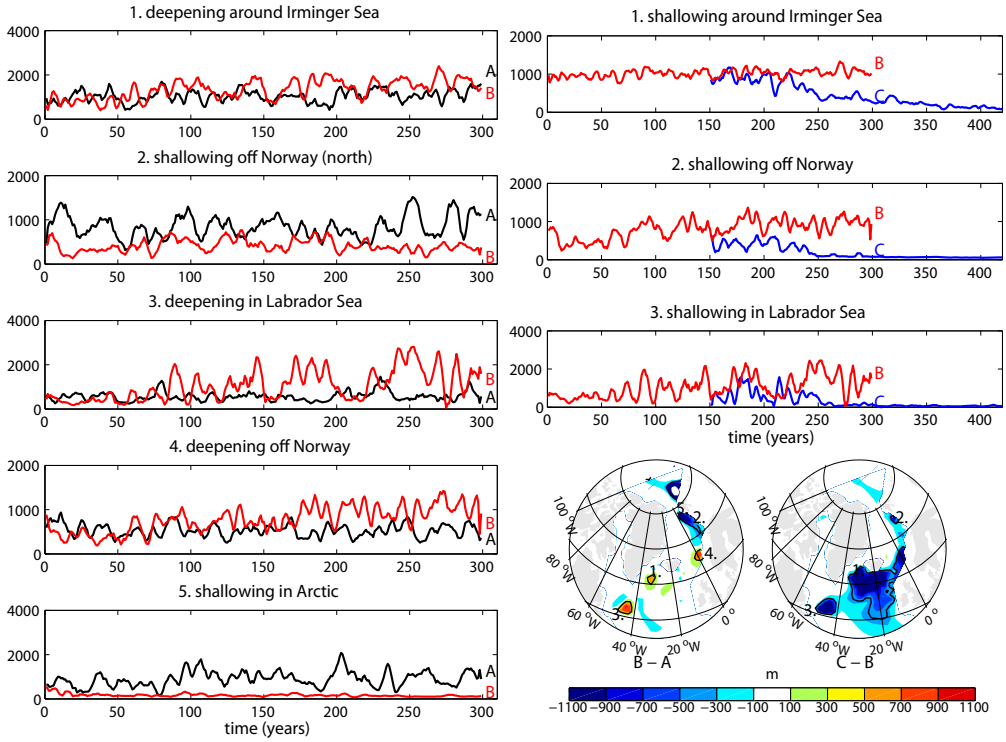

Fig. 4. Timeseries of winter mean mixed layer depth (m) averaged over areas of anomalous deep convection (indicated on the maps below the time series). Black line: LGMa, red line: LGMb, blue line: LGMc. All annual time series have been low-passed filtered using a 5-point running mean.

warm up in LGMc compared to LGMb, while the eastern Pacific section of the Southern Ocean cools by as much as 2°C. To conclude, a weak reduction of the AMOC from 18 Sv (LGMa) to 15 Sv (LGMb) is associated with significant temperature anomalies of regional extent, while a strong reduction of the AMOC, from 15 Sv (LGMb) to 2 Sv (LGMc), has a global imprint on the mean annual temperatures. The temperature response is clearly not linear w.r.t the AMOC strength.

In terms of mean annual precipitation in LGMc compared to LGMb (Fig. 9, bottom), there is a significant drying of the North Atlantic mid-latitudes, Western Europe and the northern Mediterranean coast, by up to 0.6 mm/day, which represents a 20% reduction in annual rainfall over these regions. The Gulf of Mexico and surrounding regions, as well as the Atlantic Ocean off Florida, also experience a major decrease in precipitation. The pattern of this anomaly, which straddles Central America over the adjacent Pacific and Atlantic oceans (Fig. 9), is not associated with an underlying temperature anomaly (Fig. 6). This suggests a change in atmospheric dynamics to be responsible for the large precipitation reduction. Over the Northeastern Pacific and the northwestern North American coast, the precipitation increases by up to 0.8 mm/day. Over the Indian sub-continent and surrounding ocean, the rainfall also decreases, indicating a weakened Indian monsoon. Finally, the largest change in hydrological

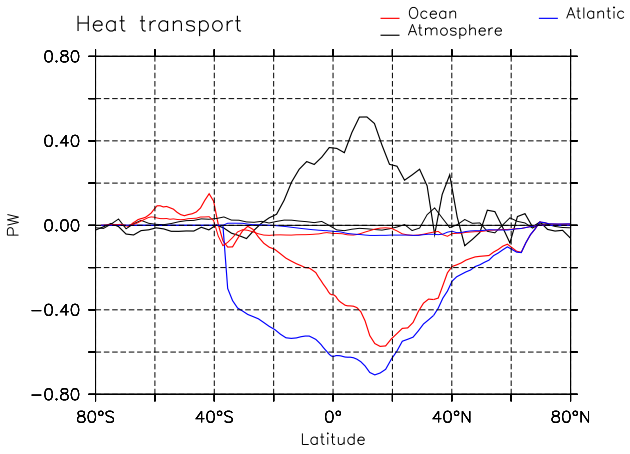

Fig. 5. Difference in zonally averaged northward meridional heat transports (in PW), between LGMa and LGMb (thin lines) and between LGMc and LGMb (thick lines). In red: the oceanic heat transport difference, in black: the atmospheric heat transport difference and in blue: the Atlantic heat transport difference. The time averages are taken over years 201–250 for LGMa and LGMb, and over years 521–570 for LGMc.

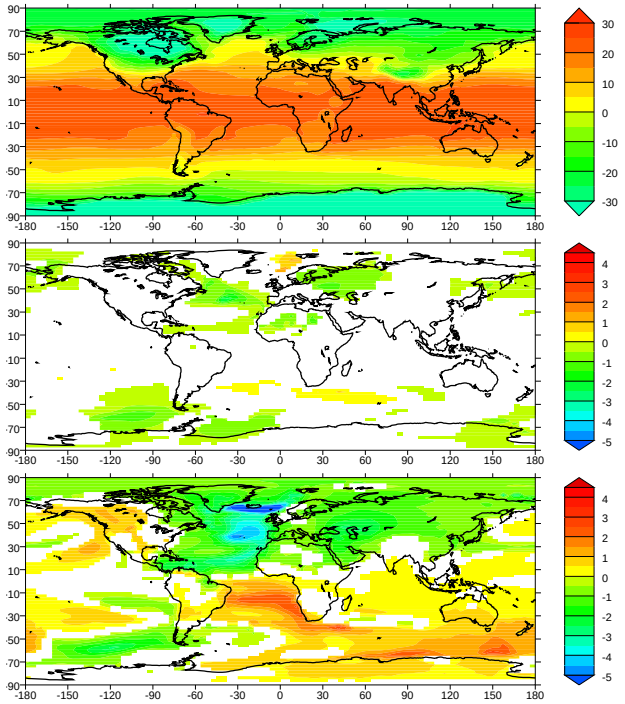

Fig. 6. Mean annual surface air temperature (°C). Top: LGMa; middle: LGMb–LGMa; bottom: LGMc-LGMb. The differences have been masked where not significant at the 95% level in a standard Student-T test. The time averages are taken over years 201–250 for LGMa and LGMb, and over years 521–570 for LGMc. Note that although this figure (and all maps hereafter) shows present coastlines, all simulations have actually used LGM coastlines.

cycle is found in the tropical Atlantic where the ITCZ clearly shifts southward. Indeed, a drying centered at around 10° N, the mean ITCZ location in LGMb, is accompanied by a wettening centered at around 10° S and extending over eastern Brazil (cf. Sect. 5.2).

How do these climate differences compare to the proxy evidence of abrupt millennial scale variability presented in Sect. 1.1? As discussed above, if we want to test the hypothesis that the recorded climatic changes are indeed due to AMOC variations, simulations LGMa and b would best compare to interstadials, while LGMc would be relevant for a Heinrich event. Qualitatively, the simulated climatic changes between an AMOC-off state, such as in LGMc, and an AMOC-on state, such as in LGMa and b, are in agreement with the records (1) over the North Atlantic, Greenland and Europe, which experience a strong cooling and drying; (2) over the tropical Atlantic, which undergoes a clear southward shift of the ITCZ; (3) over the Indian Peninsula and surrounding ocean, which are characterised by a decreased Indian monsoon. However, our model does not simulate a decrease of the South East Asian monsoon (precipitation is similar over China in the three simulations). Furthermore, although it does simulate an Atlantic bipolar see-saw, it does not produce a clear warming over Antarctica for a collapsed AMOC. Possible reasons for these discrepancies will be discussed in Sect. 6. The mechanisms for climate changes over the northern extratropics, the tropical Atlantic and the Indian monsoon region, where our model results appear to be relevant for interpreting the proxy records will be discussed further in Sect. 5.1.

4 Timing of the response in the AMOC "off" state simulation

The timing of the heat transport change while the AMOC weakens in LGMc is fast both for the ocean and for the atmosphere. Figure 10 shows that it appears in both transports within a few decades. The global heat transport at 17° N has decreased by more than 0.27 PW, i.e. a half of its final decrease in around a 60 years. The decrease in oceanic heat transport is partly compensated by the atmosphere after a few years. This timing pleads for a very rapid atmospheric adjustment to the North Atlantic cooling as modelled by Yang and Liu (2005) and by Shaffrey and Sutton (2006).

We can compare this timing of atmospheric and oceanic transport changes to the timing of the appearance of surface climate anomalies. Indeed, the difference in annual mean surface temperature associated with a collapse of the AMOC depicted on Fig. 6 does not appear at the same rate in every region of the globe. Fig. 11 (top) shows, for each point, the year after which half of the final anomaly represented on Fig. 6 is reached, and for which the anomaly remains larger than this threshold for at least 50 years. The first regions which experience climate changes in LGMc compared to LGMb are the mid-latitude western and central North Atlantic and the coastal areas of the Arctic Ocean. In these regions, the threshold of 50% of the final response is reached in less than 60 years after the beginning of the run (regions in blue). By this time, the AMOC is reduced by about 30% (to ca. 10 Sv) and the Atlantic heat transport by half. Temperature anomalies over in the North Atlantic from 30° N northward, the Arctic Ocean, Greenland, Eurasia, pass the 50% threshold by 120 years (regions in green), suggesting a relatively fast adjustement of the continental temperatures to the oceanic changes via the atmospheric circulation. Further South, the tropical Atlantic off the African coast as well as Africa North of 10° N pass the threshold at around the same time. This could be related to the advection of the cold surface ocean anomaly along the subtropical gyre or faster adjustements such as the Wind-Evaporation-SST feedback as proposed by Chiang et al. (2008). At the same time, the mean annual temperature response over the tropical South Atlantic also starts to appear. The next regions for which climate anomalies pass over the 50% threshold are the tropical North Atlantic and the South Atlantic between 10 and 20° S (by year 200). By that time, the AMOC is already less than

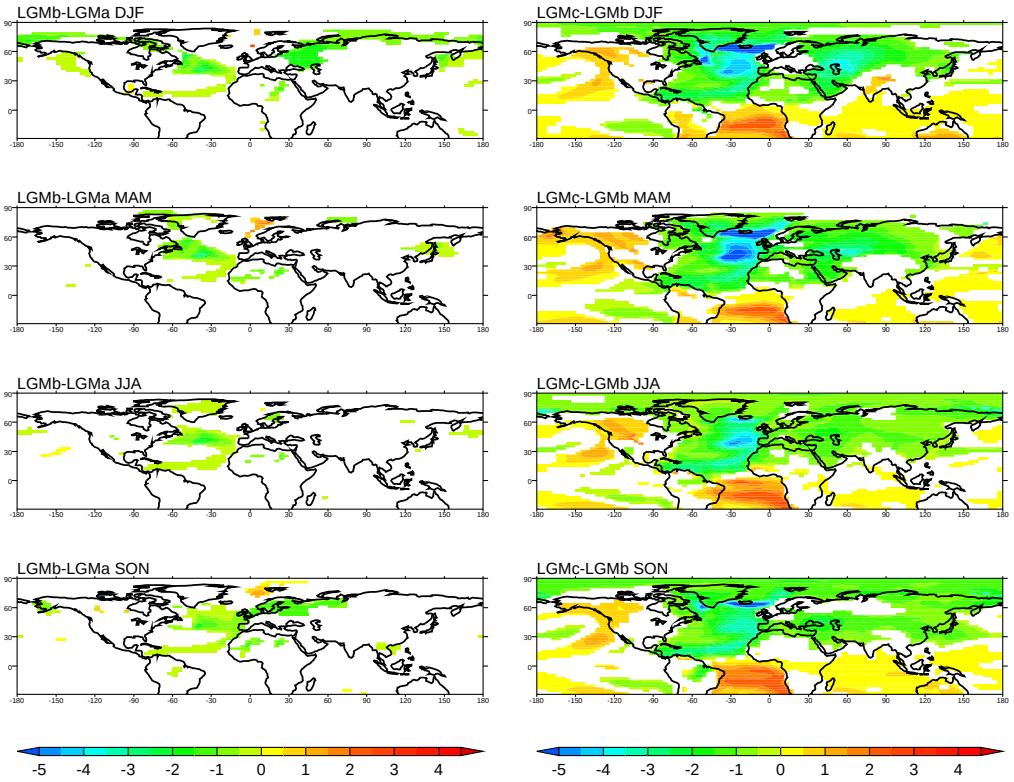

Fig. 7. LGMb–LGMa anomalies (l.h.s.) and LGMc-LGMb anomalies (r.h.s) in 2 m temperatures (in °C) for the 4 seasons. The differences have been masked where not significant at the 95% level in a standard Student-T test. The time averages are taken over years 201–250 for LGMa and LGMb, and over years 521–570 for LGMc.

5 Sv. This suggests that either the Atlantic bipolar seesaw is quite slow to establish, or that the AMOC change needs to be strong enough for it to appear. Anomalies of the northern subtropics need an extra 30 to 60 years to reach the Equator. The anomalies over the small region of the North Atlantic south of Greenland and Iceland, i.e. near the main convection sites (Irminger and Labrador Seas) in LGMb, only pass the 50% threshold at around year 240. This corresponds to the shut down of these sites (Fig. 4). Finally the Northeastern Pacific and Northwestern America undergo the warming shown on Fig. 6 after up to 300 yrs, which excludes an exclusive role of changes in atmospheric stationary waves in setting up this temperature anomaly.

Over the North Atlantic and Western Europe, the timing of the precipitation response (Fig. 11, bottom) is generally very much in phase with the temperature one (Fig. 11, top). The precipitation anomaly passes over the 50% threshold before year 60 for the western and central North Atlantic, before year 150 for the rest of the mid-latitude North Atlantic and the latest response occurs over the Greenland-Iceland convection site by year 240. This suggests a direct role of temperature anomalies on precipitation, the most simple mechanism for this link being via a reduction in evaporation. This is further discussed in Sect. 5.1. This type of response also occurs in an IPSL_CM4 glacial ocean-atmosphere simulation in response to changes in river run-off (Alkama et al., 2007). The response over Central America, the Gulf of Mexico and the eastern equatorial Pacific appears by year 120–180 of LGMc, i.e. before the temperature anomaly passes the 50% threshold. Over the northeastern Pacific and northwestern America, the precipitation anomaly appears in two stages. The southern part of the anomaly appears by year 120, while its northern part appears quite late, by year 240, similar to the temperature anomalies. This suggests a first response related to atmospheric circulation changes, before a response to the later temperature anomalies sets in. Over the Arabian Sea and Indian sub-continent, which are the Indian monsoon regions in our simulation (Fig. 9a), the main drying appears by year 120, but a secondary decrease occurs around the Bay of Bengal by year 240. Again, this suggests a first response related to changes in atmospheric circulation (cf. Sect. 5.3) before a second, more local mechanism, adds on to this first anomaly. Changes in precipitation in the tropical Atlantic also appear gradually, with the dipole associated with the shift of the ITCZ finally setting in at around year 200 (red colour bands across Northern South America and red zone over Eastern Brazil). The mechanisms and timing of the ITCZ shift are detailed further in Sect. 5.2.

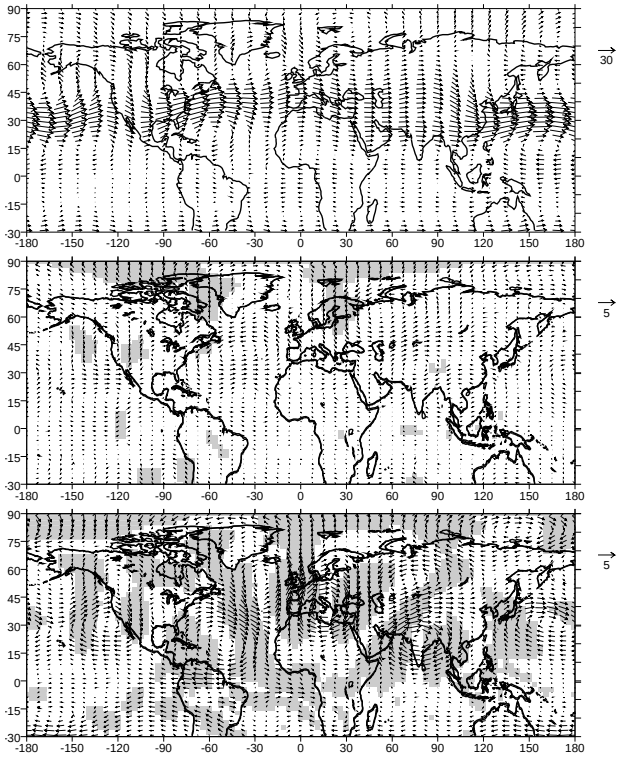

Fig. 8. December-January-February 500 hPa winds (m/s). Top: LGMa; middle: LGMb–LGMa; bottom: LGMc-LGMb. The shading indicated points for which changes in both components of the wind are significant at the 95% level in a standard Student-T test. The time averages are taken over years 201–250 for LGMa and LGMb, and over years 521–570 for LGMc.

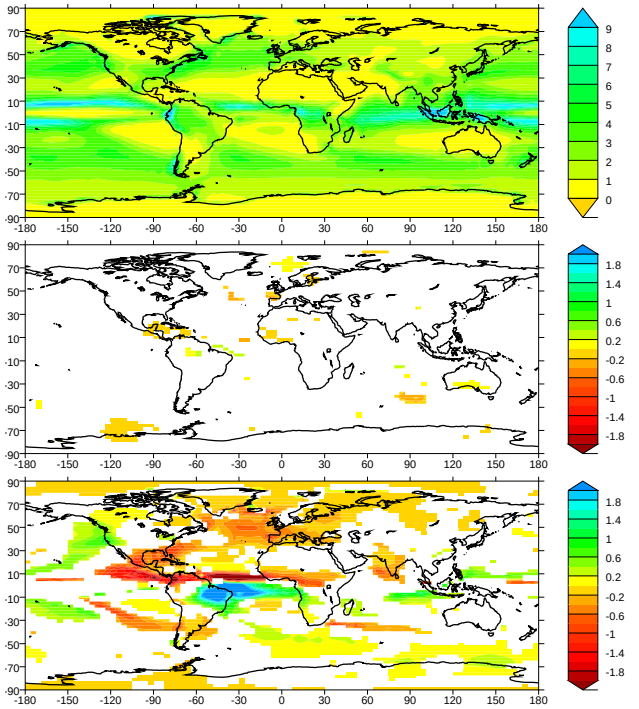

Fig. 9. Mean annual precipitation (mm/day). Top: LGMa; middle: LGMb–LGMa; bottom: LGMc–LGMb. The differences have been masked where not significant at the 95% level in a standard Student-T test. The time averages are taken over years 201–250 for LGMa and LGMb, and over years 521–570 for LGMc.

Hence, the timing of the temperature and precipitation responses to the AMOC collapse simulated in LGMc suggest: (1) over the northern extratropics, a fast (of order decades) response of the North Atlantic which propagates over Eurasia, but a much slower (of order centuries) response over North America; (2) a fast response of the Indian monsoon, which might be related to the fast adjustement over the Eurasian continent; (3) an adjustement of the tropical Atlantic consistent for temperatures and precipitation, which occurs on slightly longer time-scales. In the next section, we investigate the mechanisms underlying these climate changes for these three regions.

5 Mechanisms for the climatic response in the AMOC "off" simulation over selected areas

Our objective here is to understand the major features of the annual mean changes due to a collapse of the AMOC shown on Figs. 6 and 9 and introduced in Sects. 3.3 and 4. In particular, as indicated above, we will focus successively on the northern extratropics, the tropical Atlantic and the Indian monsoon region. We will concentrate on the response to a strong AMOC perturbation. Unless explicitely indicated, all figures and discussion will relate here to differences LGMc-LGMb.

5.1 Northern extratropics

In this region, as for the difference induced by a weak change in the AMOC (Sect. 3.2), changes in atmospheric circulation appear to play an active role in setting up the thermal response to a strong decrease in AMOC. A cyclonic anomaly develops over the region of strongest cooling of the North Atlantic, i.e. over the northeastern North Atlantic. This anomaly brings energy to northwestern Europe, hence explaining the relatively low cooling over this region (Fig. 8, bottom). Consistently, an anticyclonic anomaly centered over the Central Mediterranean brings colder air to central and eastern Europe, explaining the local maximum cooling there (Figs. 6 – bottom – and 7, r.h.s – top). Hence the cooling of Eurasia is not only explained by advection of cold air from the North Atlantic by the westerlies. Superimposed to this response, the cyclonic circulation forced by the initial cooling over the North Atlantic ocean brings warmer air to western Europe and limits the cooling there, while the cooling is amplified by cold air advection further east over eastern

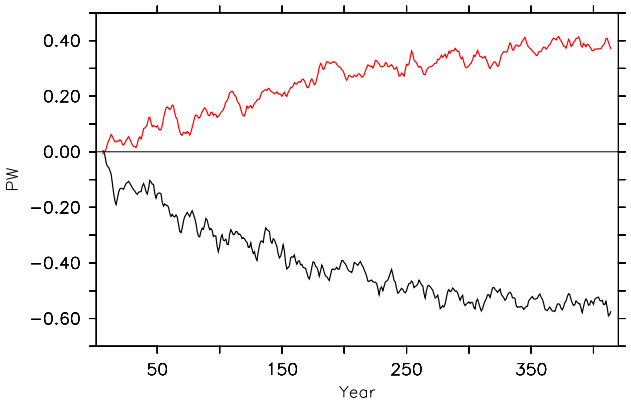

Fig. 10. Difference (LGMc-LGMb) in meridional northward heat transport at 17° N by the atmosphere (in red) and the ocean (in black).

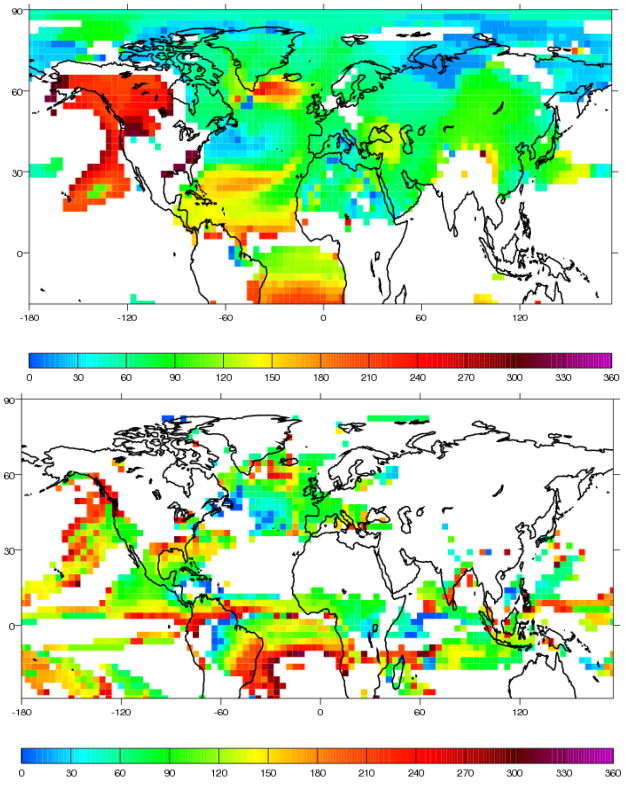

Fig. 11. Top: Timing of the appearance of significant anomalies in mean annual temperature in LGMc, as compared to LGMb, defined as the first year in which the anomaly reaches at least half of the final anomaly for at least 50 years (the "final" anomaly is taken as the difference between years 521–570 of LGMc and years 100–150 of LGMb). Bottom: Same as for top but for the mean annual precipitation (cf. final response Fig. 9).

Europe, North of the Black Sea. This behaviour is more pronounced in winter and spring in the temperature response shown on Fig. 7. This is consistent with the atmospheric circulation behaviour, which is similar for winter and spring (cf. Fig. 8, bottom) but with much less pronounced stationary waves over Eurasia in summer and autumn (not shown).

The precipitation response over the North Atlantic and Europe also depends on the season, partly because the precipitation in LGMb, as for the present observed situation, is highly seasonal (not shown). Over the North Atlantic Ocean, the decrease in precipitation is maximum, in extent and amplitude, in winter and minimum in summer. This drying is strongest over the eastern side of the basin, where the cooling is also the largest. This points to a simple relationship between North Atlantic temperature and precipitation anomalies, via a decrease in evaporation (Fig. 12). Over the northern Mediterranean area, the decrease in precipitation is strongest in winter, while in western to central Europe, North of the Mediterranean Sea, the drying is strongest in autumn. For these two regions, the strongest response therefore occurs at the season for which the precipitation is maximum in the reference run.

The temperature response to an AMOC collapse is rather constant throughout the year over the Eastern Pacific and Northwestern America, which undergo a warming (Fig. 7). There are no temperature differences in the rest of the extratropical Pacific. This warming can be explained by a cyclonic anomaly, present at all seasons, extending from the dateline to the West American coast and from ca. 30 to 60° N. However, the slow timing of the response suggests that its establishment also needs the surface ocean to adjust first. The precise position and intensity of this cyclonic anomaly slightly change from season to season but its net effect is that southwesterly winds bring warmer air to the Northeastern Pacific and Northwestern America. This warming is accompanied by an increase in precipitation, which is strongest, in amplitude and extent, in summer and autumn. This phenomenon is not only related to evaporation anomalies, as for the North Atlantic Ocean (Fig. 12), but also to the southward shift of the westerlies and storm-tracks which is prominent in summer and autumn (not shown).

5.2 Tropical Atlantic

The modifications in atmospheric heat transport between LGMb and LGMc described in Sect. 3.2 occur via an adjustment of the meridional cells in the atmosphere. In LGMb, the atmospheric zonally averaged meridional streamfunction (Fig. 13, contours) shows a near symmetry about the Equator, with two Hadley cells spreading from ca. 4° N to 30° N or S. Poleward of the Hadley cells, the Ferrel cells, between 30 and 50° N or S and finally the polar cells, mostly active in the Northern Hemisphere, are simulated. The differences between LGMc and LGMb affect every cell (Fig. 13, colour shading). The largest differences are nonetheless located near the Equator where a large positive (clockwise) anomaly implies a southward shift of the limit between the two Hadley cells. This shift amounts to around 10° of latitude. This type

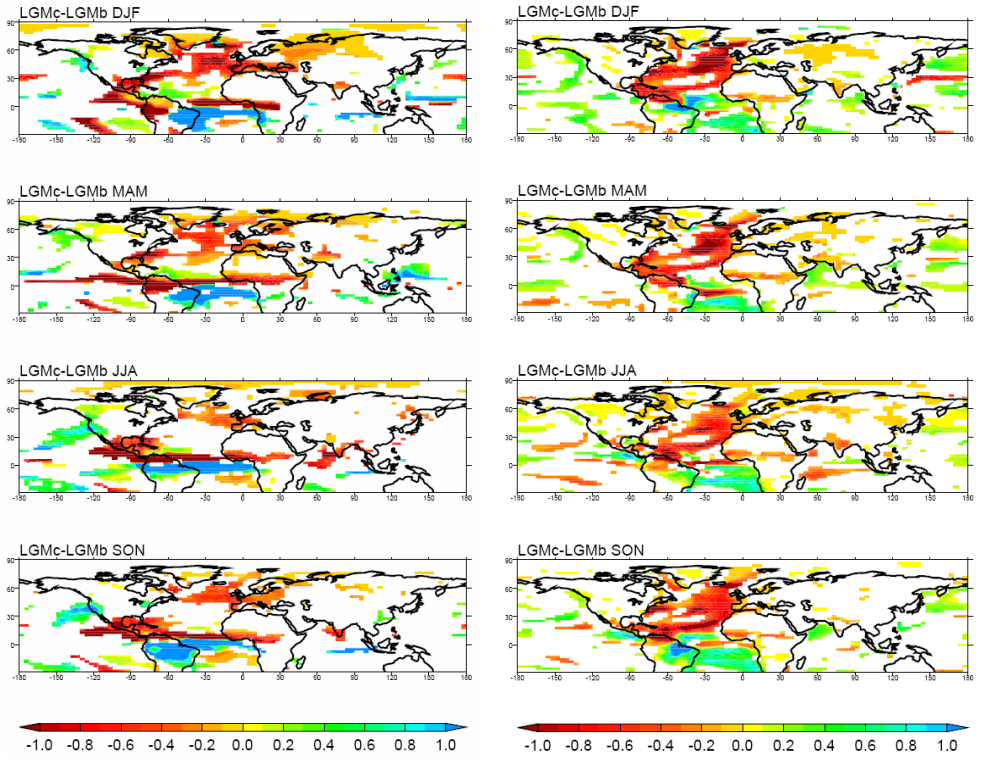

Fig. 12. LGMc-LGMb precipitation (l.h.s) and evaporation (r.h.s) anomalies in mm/day for the 4 seasons. The differences have been masked where not significant at the 95% level in a standard Student-T test. The time averages are taken over years 201–250 for LGMb and over years 521–570 for LGMc.

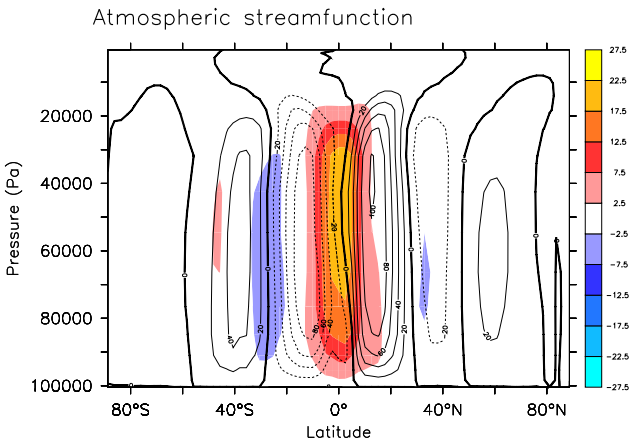

Fig. 13. Meridional atmospheric overturning streamfunction (10^{12} kg/s). The contours represent for the averaged value for LGMb (years 201–250), with a clockwise rotation when positive. Red shaded zones stand for positive (clockwise) differences between LGMc and LGMb (years 521–570 for LGMc, years 201–250 for LGMb). Blue shaded zones stand for negative (anticlockwise) ones.

of adjustment in response to an imposed Northern Hemisphere cooling is in agreement with several studies, (e.g. Zhang and Delworth, 2005; Chiang and Bitz, 2005; Broccoli et al., 2006).

This has a direct impact on the precipitation near the Equator, with the southward shift of the main precipitation belt, by 10° or more, in the tropical Atlantic. In winter, the negative anomaly of the anomalous precipitation dipole pattern shown on Fig. 12 is located at the Equator and the positive anomaly at ca. 10° S. In boreal summer this pattern is shifted North by ca. 10°. The anomaly pattern therefore follows the seasonal course of the main precipitation belt, which further proves the relationship between the shift in ITCZ and the tropical Atlantic precipitation anomalies. A close comparison of the precipitation fields for LGMb (not shown) and the corresponding LGMc-LGMb anomalies (Fig. 12, l.h.s) shows that the strong precipitation decrease off the Pacific coast of Central America can also be related to the southward shift of the ITCZ, although there is not as distinct a corresponding positive anomaly to the South, except in June-July-August (JJA). Over the Amazon region, the increase in precipitation in September-October-November (SON) and December-January-February (DJF) is further amplified by a positive feedback involving increased evaporation (Fig. 12, r.h.s). Finally, the strong precipitation decrease over the Gulf

of Mexico also appears to be associated with the southward shift of the ITCZ, or to an increase of the subsidence of the winter Hadley cell, since the anomalies are stronger in boreal autumn and winter and are not related to evaporation anomalies.

The impact of a strong weakening of the AMOC between the simulations LGMb and LGMc on the June to September (JJAS) precipitation is shown on Fig. 14a. The southward shift of the ITCZ in the Equatorial Atlantic is accompanied by a significant reduction in precipitation over the African monsoon region during the monsoon season. Other modeling experiments (e.g. Chang et al., 2008) have highlighted the sensitivity of the African monsoon system to an additionnal fresh water flux in the North Atlantic and Arctic. In our experiments, this impact is verified under glacial conditions.

5.3 Indian monsoon

The Indian monsoon precipitation is reduced by approximately 0.5 to 2 mm/day in the Southwest of the subcontinent and in the northern Bay of Bengal in LGMc compared to LGMb. No changes are observed over land since in the reference (LGMb) simulation, the largest monsoon signal is over the ocean. The reduction of the Indian monsoon intensity is also reflected in the weakened cross-equatorial flux from the Indian Ocean to the Arabian Sea (Fig. 14a). Hence our experiments show that under glacial conditions a collapse of the AMOC is associated with a significant remote impact on the Indian summer monsoon activity. As stated in Sect. 1.2, this teleconnection has been investigated for different time scales and there are several pathways by which the Indian monsoon rainfall may be influenced. The connection with the extratropics can find support in an atmospheric bridge with the changes over the North Atlantic (Goswami et al., 2006). The influence of a weakening of the AMOC can also modify the (tropical) Walker circulation (e.g. Lu et al., 2006). Local ocean-atmosphere feedbacks, e.g. through changes in SSTs and evaporation, can amplify the changes.

Here we use a physical indicator of the Indian monsoon based on the upper tropospheric temperature meridional gradient (Xavier et al., 2007; He et al., 2003). We compute the average of tropospheric temperature from 200 to 500 hPa (TT) for the JJAS season. The difference of TT between the simulations LGMc and LGMb (Fig. 14b) indicates a significant seasonal cooling over the mid-latitudes. Over India, the meridional gradient of TT is reduced, as well as the sensitive heating over the Tibetan Plateau (not shown), resulting in weaker Indian monsoon precipitation. This mechanism is in agreement with the teleconnection observed between the Atlantic Multidecadal Oscillation and the Indian monsoon variability by Goswami et al. (2006) and Feng and Hu (2008). The anomaly of SSTs in the Northern Atlantic are passed in the upper troposphere over the whole Eurasian continent (cf. Sect. 5.1), creating an atmospheric bridge between the North Atlantic and the Asian region. Since the SST

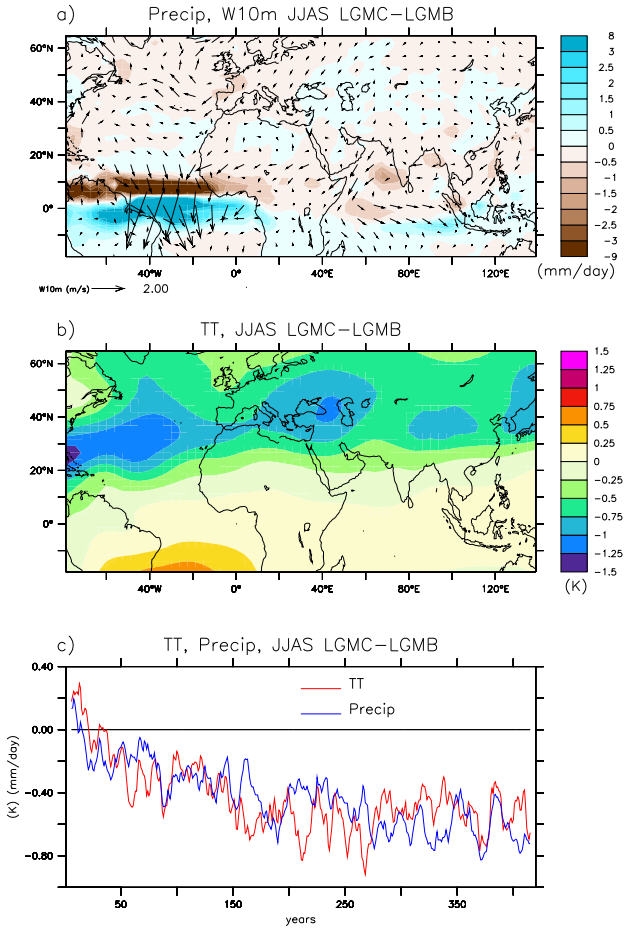

Fig. 14. (a) Difference of precipitation (mm/day) averaged for JJAS (June-July-August-September) between the simulations LGMc and LGMb (colours), and of surface winds at 10 m (m/s) (vectors); **(b)** Difference of temperature averaged from 200 to 500 hPa (TT) for JJAS between LGMc and LGMb; for (a) and (b) the time averages are taken over years 201–250 LGMb, and over years 521–570 for LGMc, for comparison to other figures; **(c)** Evolution of TT averaged over the region (50° E–100° E, 20° N–50° N) (red) and of precipitation averaged over the region (60° E–80° E, 5° N–15° N) (blue) for LGMc minus LGMb (average over years 101–150).

anomalies over the Indian Ocean and the Pacific are small, this mechanism appears to be predominant in these simulations. In addition, the evolution of the TT anomaly over the region (50° E–100° E, 20° N–50° N) and of the precipitation anomaly at the southwest of the Indian peninsula is plotted on Fig. 14c. A 10 years boxcar smoothing is applied on the time series to remove the large interannual variability. The precipitation evolution follows that of TT anomalies and is stable after ca. 200 years. These evolutions are similar to the one of the maximum of AMOC (Fig. 1).

6 Summary and discussion

The present study analyses three glacial coupled atmosphere-ocean simulations characterised by different Atlantic Meridional Overturning Circulations (AMOC). In response to an 0.08 Sv increase in North Atlantic fresh water flux, the AMOC reduces from 18 Sv (LGMa) to 15 Sv (LGMb). The climate differences between these runs are restricted to the northern North Atlantic, Nordic Seas and Europe. The cooling anomaly over the Northern North Atlantic associated with this slightly slower AMOC is strong enough to force a cyclonic anomaly in the atmospheric circulation over this region, which could take part in the slight warming over the Norwegian Sea. However, the main element explaining this surprising warm anomaly is the reinforcement of the oceanic convective activity in this area, partly resulting from the sea ice edge pushed further North by surface winds. An anomalous cooling appears further east in winter, due to northerly winds appearing as part of the stationary wave response to the SST changes over the North Atlantic and Nordic Seas. It is not possible to disentangle the roles of the atmosphere, ocean and sea ice in the temperature difference between the two simulations. Further experiments, using partial coupling of the model components, would be needed to test if the atmospheric circulation changes and oceanic/sea ice response indeed reinforce each other, especially over the Norwegian Sea, as suggested by our first analyses. The difference in precipitation, on the other hand, is hardly significant for these simulations.

A further 0.1 Sv fresh water flux into the North Atlantic induces a collapse of the AMOC in LGMc, compared to LGMb. As noted by Flückiger et al. (2008), the climatic response to this shutdown does not appear to be a simple amplification of the climate anomalies simulated as a response to a weak AMOC perturbation. This has important implications for paleo-record interpretations, which could otherwise a priori assume a linear reponse w.r.t the forcing, i.e. in our case a change in AMOC. The surface climate anomalies are of global extent, and qualitatively agree with the interpretation of paleorecords for the northern extratropics (in particular, the North Atlantic and surrounding regions such as Greenland and Europe), the tropical Atlantic, with the southward shift of the ITCZ and the Indian monsoon region, over which the monsoon decreases. However, the model does not simulate a warming over Antarctica (despite a warming over most of the Southern Ocean) or a weakening of the East Asian monsoon. It could simply be that the model is not sensitive enough to a collapse of the AMOC compared to the climatic changes suggested by the different paleo-records, or that the model is missing crucial feedbacks (from dust, vegetation or biogeochemical cycles, for instance), or that some of these climatic changes are not related to AMOC differences. However, before drawing any conclusion of this type, further experiments would have to be performed. Indeed, although it is probably legitimate to claim that LGM boundary conditions are closer to the boundary conditions which prevailed during times of strong millennial abrupt changes (Marine Isotope Stage 3 (MIS3) from ca. 60 to 30 ky BP) than present conditions, these are far from being entirely realistic for this period (for a recent study, see e.g. Van Meerbeeck et al., 2009). In particular, MIS3 is characterised by a stronger Northern Hemisphere summer insolation than during the LGM or the present, which would favour stronger Indian and South-East Asian monsoons in the basic state, as shown by the numerous studies of the Holocene climate (e.g. Braconnot et al., 2007a,b). This monsoon could then be more sensitive to AMOC changes. Also, for quantitative comparisons, including proxies such as water isotopes in the model would certainly bring a lot of precise understanding of the proxy records.

Our main objective here was to investigate the mechanisms for possible teleconnections with the North Atlantic changes. We have focussed our study on the three regions for which the results simulated by our model appeared relevant compared to the proxy records: the northern extratropics, the tropical Atlantic and the Indian monsoon region. The climate response in the northern extratropics is dominated by large changes in stationary waves, with a strong cyclonic anomaly over the northern North Atlantic persistent throughout the year, but stronger in winter and spring. These changes in stationary waves explain the smaller cooling over western Europe, as compared to the North Atlantic, because this region is affected by southwesterly wind anomalies. They also explain a warming over the Northeastern Pacific and America's northwestern coast, affected by southwesterly wind anomalies too. However in this latter case, the long timing for the set up of this anomaly pleads for a role of the Pacific Ocean in forcing the associated atmospheric circulation anomaly. The precipitation anomalies over the Atlantic extratropics are mostly related to a strong evaporation decrease due to the cooling there and not so much to atmospheric circulation changes, such as in other regions. Indeed, over the Northeastern Pacific/Northwestern America, for example, they appear to be also related with a southward shift of the westerlies/storm-tracks.

The collapse of the AMOC is accompanied by a decrease in meridional oceanic heat transport, strongest in the Atlantic basin, and only partly compensated by an increase of the transport in the other ocean basins and by an increase in atmospheric heat transport. The atmospheric meridional heat transport increase occurs via an adjustment of the meridional circulation, and most notably of the Hadley cells. The structure of the atmospheric meridional circulation shifts southward by around 10° in the Tropics. This is accompanied by a dipole in the precipitation anomalies, with a drying North of the thermal equator and a wettening South of it, which constitutes the hydrological signature of the southward shift of the ITCZ. This signature is most prominent in the tropical Atlantic, but part of the precipitation anomalies in the eastern tropical Pacific can also be ascribed to this mechanism. The

increase in precipitation over the Amazon region appears to be amplified by a local evaporation-precipitation feedback. Finally, we analyse the weakening of the Indian monsoon in response to the AMOC collapse as a consequence of an atmospheric bridge between the North Atlantic and the monsoon area, which involves the large cooling of the upper troposphere over Eurasia, and the subsequent decrease in the tropospheric meridional gradient between India and Northern Eurasia.

These surface climate changes associated with an AMOC shutdown do not appear simultaneously in all regions of the globe. The timing of the response is of the order of a hundred years over the Atlantic, Eurasia and for the Indian monsoon. The response over the northwestern Pacific is the slowest to appear, with a timescale of around 250 years. The tropical Atlantic responds with intermediate timescales compared to these extremes. This timing suggests (1) a very fast climatic response over the Arctic and Northern Eurasia, which is probably related to an atmospheric stationary wave change amplified by the sea-ice and snow-albedo feedbacks; (2) an extension of this cooling over most of Eurasia and North Africa; (3) a propagation of the temperature anomalies from the central North Atlantic along the subtropical gyre along the coasts of Africa, before the temperature cools down in the North Atlantic low latitudes; (4) relatively slower ocean responses for the largest convection site of the northwestern North Atlantic, for the South Atlantic and, finally, for the Northwestern Pacific. Comparing these results to paleodata with sufficient temporal resolution and chronological control would therefore be a good test of the model's sensitivity to freshwater forcings and states of the AMOC.

Each step in the climatic response depicted above corresponds to a precise AMOC value (Fig. 1). However, this does not mean that the AMOC has to pass below this value to obtain the described response. Indeed, the climatic response over some regions such as the North Atlantic sub-tropical gyre are indirectly related to the slow down of the AMOC, via the propagation (by different possible mechanisms) of the initial cooling of the mid-latitude Western and Central Atlantic. It is therefore not possible, from our experiments, to strictly disentangle the direct and immediate response to an AMOC decrease from the propagation of a signal advected from another region because the AMOC decrease and the climate signal propagation can occur with similar timescales. Further experiments, with different speeds of AMOC collapse and/or in which the atmosphere and the ocean are only partially coupled, would be necessary to pin down the exact roles of the ocean or the atmosphere, as has been performed by other models (e.g. Krebs and Timmermann, 2007; Yang and Liu, 2005).

Concerning the sensitivity of the AMOC under LGM conditions, a companion paper shows that the model we use, the IPSL_CM4 model, is actually more sensitive to freshwater input in the North Atlantic in the glacial context analysed here than under various interglacial climates (Swingedouw et al., 2009). This is in line with the analyses from Ganopolski and Rahmstorf (2001). This difference in sensitivity sheds light on the necessity of comparing proxy data and simulations that are under the most possible realistic boundary conditions. The reason for these differences is however not elucidated yet and will be the subject of a future study.

A final remark is related to the hydrological cycle, which is deeply affected by a collapse in the AMOC. Following Leduc et al. (2007), we can wonder whether this constitutes a positive or a negative feedback compared to the freshwater anomaly which is the initial cause of the AMOC collapse. The study of these feedbacks and of the conditions needed for a recovery of the AMOC from the "off" state obtained in our third simulation is complementary to the present study and will be presented in a forthcoming paper.

Acknowledgements. All simulations presented in this work were run on the Commissariat A l'Energie Atomique super-computing facilities. This study has been partly funded by ANR-BLANC IDEGLACE (ANR-05-BLAN-0310-01).

Edited by: H. Renssen

The publication of this article is financed by CNRS-INSU.

References

Alkama, R., Kageyama, M., Ramstein, G., Marti, O., Ribstein, P., and Swingedouw, D.: Impact of a realistic river routing in coupled ocean-atmosphere simulations of the Last Glacial Maximum climate, Clim. Dynam., 30, 855–869, doi:10.1007/s00382-007-0330-1, 2007.

Altabet, M. A., Higginson, M. J., and Murray, D. W.: The effect of millennial-scale changes in Arabian Sea denitrification on atmospheric CO_2, Nature, 415, 159–162, 2002.

Berger, A. L.: Long-term variations of daily insolation and Quaternary climatic changes, J. Atmos. Sci., 35, 2362–2367, 1978.

Bitz, C. M., Chiang, J. C. H., Cheng, W., and Barsugli, J. J.: Rates of thermohaline recovery from freshwater pulses in modern, Last Glacial Maximum, and greenhouse warming climates, Geophys. Res. Lett., 34, L07708, doi:10.1029/2006GL029237, 2007.

Bjerknes, J.: Atlantic air-sea interaction, Academic Press, 10, 1–82, 1964.

Blunier, T., Chappellaz, J., Schwander, J., Dällenbach, A., Stauffer, B., Stocker, T. F., Raynaud, D., Jouzel, J., Clausen, H. B., Hammer, C. U., and Johnsen, S. J.: Asynchrony of Antarctic and Greenland climate change during the last glacial period, Nature, 394, 739–743, 1998.

Bond, G., Broecker, W., Johnsen, S., McManus, J., Labeyrie, L., Jouzel, J., and Bonani, G.: correlations between climate records

from North Atlantic sediments and Greenland ice, Nature, 365, 143–147, 1993.

Bout-Roumazeilles, V., Nebout, N. C., Peyron, O., Cortijo, E., Landais, A., and Masson-Delmotte, V.: Connection between South Mediterranean climate and North African atmospheric circulation during the last 50 000 yr BP North Atlantic cold events, Quaternary Sci. Rev., 26, 3197–3215, 2007.

Braconnot, P., Otto-Bliesner, B., Harrison, S., Joussaume, S., Peterchmitt, J.-Y., Abe-Ouchi, A., Crucifix, M., Driesschaert, E., Fichefet, T., Hewitt, C. D., Kageyama, M., Kitoh, A., Lan, A., Loutre, M.-F., Marti, O., Merkel, U., Ramstein, G., Valdes, P., Weber, S. L., Yu, Y., and Zhao, Y.: Results of PMIP2 coupled simulations of the Mid-Holocene and Last Glacial Maximum - Part 1: experiments and large-scale features, Clim. Past, 3, 261–277, 2007a,
http://www.clim-past.net/3/261/2007/.

Braconnot, P., Otto-Bliesner, B., Harrison, S., Joussaume, S., Peterchmitt, J.-Y., Abe-Ouchi, A., Crucifix, M., Driesschaert, E., Fichefet, Th., Hewitt, C. D., Kageyama, M., Kitoh, A., Loutre, M.-F., Marti, O., Merkel, U., Ramstein, G., Valdes, P., Weber, L., Yu, Y., and Zhao, Y.: Results of PMIP2 coupled simulations of the Mid-Holocene and Last Glacial Maximum - Part 2: feedbacks with emphasis on the location of the ITCZ and mid- and high latitudes heat budget, Clim. Past, 3, 279–296, 2007b,
http://www.clim-past.net/3/279/2007/.

Broccoli, A. J., Dahl, K. A., and Stouffer, R. J.: Response of the ITCZ to Northern Hemisphere cooling, Geophys. Res. Lett., 33, L01702, doi:10.1029/2005GL024546, 2006.

Chang, P., Zhang, R., Hazeleger, W., Wen, C., Wan, X. Q., Ji, L., Haarsma, R. J., Breugem, W. P., and Seidel, H.: Oceanic link between abrupt changes in the North Atlantic Ocean and the African monsoon, Nature Geosci., 1, 444–448, 2008.

Chiang, J. C. H. and Bitz, C. M.: Influence of high latitude ice cover on the marine Intertropical Convergence Zone, Clim. Dynam., 25, 477–496, 2005.

Chiang, J. C. H., Cheng, W., and Bitz, C. M.: Fast teleconnections to the tropical Atlantic sector from Atlantic thermohaline adjustment, Geophys. Res. Lett., 35, L07704, doi:10.1029/2008GL033292, 2008.

Claussen, M., Ganopolski, A., Brovkin, V., Gerstengarbe, F.-W., and Werner, P.: Simulated global-scale response of the climate system to Dansgaard/Oeschger and Heinrich events, Clim. Dynam., 21, 361–370, 2003.

Clement, A. C. and Peterson, L. C.: Mechanisms of abrupt climate change of the last glacial period, Rev. Geophys., 46, RG4002, doi:10.1029/2006RG000204, 2008.

Combourieu Nebout, N., Turon, J.-L., Zhan, R., Capotondi, L., Londeix, L., and Pahnke, K.: Enhanced aridity and atmospheric high-pressure stablity over the western Mediterranean during the North Atlantic cold events of the past 50 k.y., Geology, 30, 863–866, 2002.

Crowley, T. J.: North Atlantic deep water cools the Southern Hemisphere, Paleoceanography, 7, 489–497, 1992.

Dallenbach, A., Blunier, T., Fluckiger, J., Stauffer, B., Chappellaz, J., and Raynaud, D.: Changes in the atmospheric CH_4 gradient between Greenland and Antarctica during the Last Glacial and the transition to the Holocene, Geophys. Res. Lett., 27, 1005–1008, 2000.

Dansgaard, W., Johnsen, S. J., Clausen, H. B., Dahl-Jensen, D., Gundestrup, N. S., Hammer, C. U., Hvidberg, C. S., Steffensen, J. P., Sveinbjörnsdottir, A. E., Jouzel, J., and Bond, G.: Evidence for general instability of past climate from a 250-kyr ice-core record, Nature, 364, 218–220, 1993.

Denton, G. H., Alley, R. B., Comer, G. C., and Broecker, W. S.: The role of seasonality in abrupt climate change, Quaternary Sci. Rev., 24, 1159–1182, 2005.

Elliot, M., Labeyrie, L., and Duplessy, J.-C.: Changes in North Atlantic deep-water formation associated with the Dansgaard-Oeschger temperature oscillations (60–10 ka), Quaternary Sci. Rev., 21, 1153–1165, 2002.

EPICA community members: One-to-one coupling of glacial climate variability in Greenland and Antarctica, Nature, 444, doi:10.1038/nature05301, 2006.

Feng, S. and Hu, Q.: How the North Atlantic Multidecadal Oscillation may have influenced the Indian summer monsoon during the past two millennia, Geophys. Res. Lett., 35, L01707, doi:10.1029/2007GL032484, 2008.

Flückiger, J., Dällenbach, A., Blunier, T., Stauffer, B., Stocker, T. F., Raynaud, D., and Barnola, J.-M.: Variations in atmospheric N_2O concentration during abrupt climatic changes, Science, 285, 227–230, 1999.

Flückiger, J., Knutti, R., White, J. W. C., and Renssen, H.: Modeled seasonality of glacial abrupt climate events, Clim. Dynam., 31, 633–645, doi:10.1007/s00382-008-0373-y, 2008.

Ganopolski, A. and Rahmstorf, S.: Rapid changes of glacial climate simulated in a coupled climate model, Nature, 409, 153–158, 2001.

Genty, D., Blamart, D., Ouahdi, R., Gilmour, M., Baker, A., Jouzel, J., and Van-Exter, S.: Precise dating of Dansgaard-Oeschger climate oscillations in western Europe from stalagmite data, Nature, 421, 833–937, 2003.

González, C., Dupont, L. M., Behling, H., and Wefer, G.: Neotropical vegetation response to rapid climate changes during the last glacial period: Palynological evidence from the Cariaco Basin, Quaternary Res., 69, 217–230, 2008.

Goswami, B. N., Madhusoodanan, M. S., Neema, C. P., and Sengupta, D.: A physical mechanism for North Atlantic SST influence on the Indian summer monsoon, Geophys. Res. Lett., 33, L02706, doi:10.1029/2005GL024803, 2006.

Grimm, E. C., Watts, W. A., Jacobson, Jr., G. L., Hansen, B. C. S., Almquist, H. R., and Dieffenbacher-Krall, A. C.: Evidence for warm wet Heinrich events in Florida, Quaternary Sci. Rev., 25, 2197–2211, 2006.

He, H. Y., Sui, C. H., Jian, M. Q., Wen, Z. P., and Lan, G. D.: The evolution of tropospheric temperature field and its relationship with the onset of Asian summer monsoon, J. Meteorol. Soc. Jpn, 81, 1201–1223, 2003.

Heinrich, H.: Origin and consequences of cyclic ice rafting in the Northeast Atlantic ocean during the past 130 000 years, Quaternary Res., 29, 142–152, 1988.

Hewitt, C. D., Broccoli, A. J., Crucifix, M., Gregory, J. M., Mitchell, J. F. B., and Stouffer, R. J.: The effect of a large freshwater perturbation on the glacial North Atlantic ocean using a coupled General Circulation Model, J. Climate, 19, 4436–4447, 2006.

Hu, A., Otto-Bliesner, B. L., Meehl, G. A., Han, W., Morrill, C., Brady, E. C., and Briegleb, B.: Response of Thermohaline Circulation to Freshwater Forcing under Present Day and LGM Con-

ditions, J. Climate, 21, 2239–2258, 2008.

Jin, L., Chen, F., Ganopolski, A., and Claussen, M.: Response of East Asian climate to Dansgaard-Oeschger and Heinrich events in a coupled model of intermediate complexity, J. Geophys. Res., 112, D06117, doi:10.1029/2006JD007316, 2007.

Jullien, E., Grousset, F., Malaize, B., Duprat, J., Sanchez-Goni, M. F., Eynaud, F., Charlier, K., Schneider, R., Bory, A., Bout, V., and Flores, J. A.: Low-latitude "dusty events" vs. high-latitude "icy Heinrich events", Quaternary Res., 68, 379–386, 2007.

Kageyama, M., Laîné, A., Abe-Ouchi, A., Braconnot, P., Cortijo, E., Crucifix, M., de Vernal, A., Guiot, J., Hewitt, C. D., Kitoh, A., Kucera, M., Marti, O., Ohgaito, R., Otto-Bliesner, B., Peltier, W. R., Vettoretti, G., Weber, S. L., and MARGO project members: Last Glacial Maximum temperatures over the North Atlantic, Europe and western Siberia: a comparison between PMIP models, MARGO sea-surface temperatures and pollen-based reconstructions, Quaternary Sci. Rev., 25, 2082–2102, 2006.

Kissel, C.: Magnetic signature of rapid climatic variations in glacial North Atlantic, a review, Comptes-RendusGeoscience, 337, 908–918, 2005.

Krebs, U. and Timmermann, A.: Tropical air-sea interactions accelerate the recovery of the Atlantic Meridional Overturning Circulation after a major shutdown, J. Climate, 20, 4940–4956, 2007.

Leduc, G., Vidal, L., Tachikawa, K., Rostek, F., Sonzogni, C., Beaufort, L., and Bard, E.: Moisture transport across Central America as a positive feedback on abrupt climatic changes, Nature, 445, 908–911, 2007.

Leuschner, D. C. and Sirocko, F.: The low-latitude monsoon climate during Dansgaard-Oeschger cycles and Heinrich Events, Quaternary Science Reviews, 19, 243–254, 2000.

Lu, R., Dong, B., and Ding, H.: Impact of the Atlantic Multidecadal Oscillation on the Asian summer monsoon, Geophys. Res. Lett., 33, L24701, doi:10.1029/2006GL027655, 2006.

Lynch-Stieglitz, J., , Adkins, J. F., Curry, W. B., Dokken, T., Hall, I. R., Herguera, J. C., Hirschi, J. J.-M., Ivanova, E. V., Kissel, C., Marchal, O., Marchitto, T. M., McCave, I. N., McManus, J. F., Mulitza, S., Ninnemann, U., Peeters, F., Yu, E.-F., and Zahn, R.: Atlantic Meridional Overturning Circulation During the Last Glacial Maximum, Science, 316, 66–69, doi:10.1126/science.1137127, 2007.

Manabe, S. and Stouffer, R. J.: Simulation of abrupt climate change induced by freshwater input to the North Atlantic Ocean, Nature, 378, 165–167, 1995.

Marti, O., Braconnot, P., Bellier, J., Benshila, R., Bony, S., Brockmann, P., Cadule, P., Caubel, A., Denvil, S., Dufresne, J.-L., Fairhead, L., Filiberti, M.-A., Foujols, M.-A., Fichefet, T., Friedlingstein, P., Goosse, H., Grandpeix, J.-Y., Hourdin, F., Krinner, G., Lévy, C., Madec, G., Musat, I., de Noblet, N., Polcher, J., and Talandier, C.: The new IPSL climate system model: IPSL-CM4, Tech. Rep. 26, IPSL, Note du Pôle de Modélisation, iSSN 1288–1619, 84 pp., 2006.

Marti, O., Braconnot, P., Dufresne, J.-L., Hourdin, F., Denvil, S., Friedlingstein, P., Swingedouw, D., Mignot, J., Goosse, H., Fichefet, T., Codron, F., Guilyardi, E., Bellier, J., Benshila, R., Bony, S., Brockmann, P., Cadule, P., Caubel, A., Fairhead, L., Foujols, M.-A., Grandpeix, J.-Y., Hourdin, F., Kageyama, M., Krinner, G., Lévy, C., Madec, G., Musat, I., de Noblet, N., and Talandier, C.: Key features of the IPSL ocean atmosphere model and its sensitivity to atmospheric resolution, Clim. Dynam., accepted, 2009.

Masson-Delmotte, V., Kageyama, M., Braconnot, P., Charbit, S., Krinner, G., Ritz, C., Guilyardi, E., Jouzel, J., Abe-Ouchi, A., Crucifix, M., Gladstone, R. M., Hewitt, C. D., Kitoh, A., LeGrande, A. N., Marti, O., Merkel, U., Motoi, T., Ohgaito, R., Otto-Bliesner, B., Peltier, W. R., Ross, I., Valdes, P. J., Vettoretti, G., Weber, S. L., Wolk, F., and Yu, Y.: Past and future polar amplification of climate change: climate model intercomparisons and ice-core constraints, Clim. Dynam., 26, 513–529, 2006.

Monnin, E.and Indermuhle, A., Dallenbach, A., Fluckiger, J., Stauffer, B., Stocker, T. F.and Raynaud, D., and Barnola, J.-M.: Atmospheric CO_2 concentrations over the last glacial termination, Science, 291, 112–114, 2001.

Msadek, R. and Frankignoul, C.: Atlantic multidecadal oceanic variability and its influence on the atmosphere in a climate model, Clim. Dynam., 33, 45–62, 2009.

Muller, J., Kylander, M., Wüst, R. A. J., Weiss, D., Martinez-Cortizas, A., LeGrande, A. N., Jennerjahn, T., Behling, H., Anderson, W. T., and Jacobson, G.: Possible evidence for wet Heinrich phases in tropical NE Australia: the Lynchs Crater deposit, Quaternary Sci. Rev., 27, 468–475, 2008.

Otto-Bliesner, B. L., Schneider, R., Brady, E. C., Kucera, M., Abe-Ouchi, A., Bard, E., Braconnot, P., Crucifix, M., Hewitt, C. D., Kageyama, M., Marti, O., Paul, A., Rosell-Mele, A., Waelbroeck, C., Weber, S. L., Weinelt, M., and Yu, Y.: A comparison of PMIP2 model simulations and the MARGO proxy reconstruction for tropical sea surface temperatures at last glacial maximum, Clim. Dynam., 32, 799–815, doi:{10.1007/s00382-008-0509-0}, 2009.

Peltier, W. R.: Global glacial isostasy and the surface of the ice-age earth: The ICE-5G (VM2) Model and GRACE, Annual Review of Earth and Planetary Science, 32, 111–149, doi:10.1146/annurev.earth.32.082503.144359, 2004.

Peterson, L. C., Haug, G. H., Hughen, K. A., and Röhl, U.: Rapid changes in the hydrologic cycle of the tropical North Atlantic during the last glacial, Science, 290, 1947–1951, 2000.

Porter, S. and An, Z.: Correlation between climate events in the North Atlantic and China during the last glaciation, Nature, 375, 305–308, 1995.

Rahmstorf, S.: Rapid climate transitions in a coupled ocean-atmosphere model, Nature, 372, 82–85, 1994.

Ramstein, G., Kageyama, M., Guiot, J., Wu, H., Hély, C., Krinner, G., and Brewer, S.: How cold was Europe at the Last Glacial Maximum? A synthesis of the progress achieved since the first PMIP model-data comparison, Clim. Past, 3, 331–339, 2007, http://www.clim-past.net/3/331/2007/.

Rashid, H., Flower, B. P., Poore, R. Z., and Quinn, T. M.: A similar to 25 ka Indian Ocean monsoon variability record from the Andaman Sea, Quaternary Sci. Rev., 26, 2586–2597, 2007.

Ruth, U., Bigler, M., Röthlisberger, R., Siggard-Andersen, M.-L., Kipfstuhl, S., Goto-Azuma, K., Hansson, M. E., Johnsen, S. J., Lu, H., and Steffensen, J. P.: Ice core evidence for a very tight link between North Atlantic and east Asian glacial climate, Geophys. Res. Lett., 34, L03706, doi:10.1029/2006GL027876, 2007.

Sánchez-Goñi, M. F., Landais, A., Fletcher, W. J., Naughton, F., Desprat, S., and Duprat, J.: Contrasting impacts of Dansgaard-Oeschger events over a western European latitudinal transect modulated by orbital parameters, Quaternary Sci. Rev., 27, 1136–1151, 2008.

Sánchez-Goñi, M.-F., Cacho, I., Turon, J.-L., Guiot, J., Sierro, F. J., Peypouquet, J.-P., Grimalt, J. O., and Shackleton, N. J.: Synchroneity between marine and terrestrial responses to millennial scale climatic variability during the last glacial period in the Mediterranean region, Clim. Dynam., 19, 95–105, 2002.

Schneider, B., Latif, M., and Schmittner, A.: Evaluation of Different Methods to Assess Model Projections of the Future Evolution of the Atlantic Meridional Overturning Circulation, J. Climate, 20, 2121–2132, 2007.

Schulz, H., von Rad, U., and Erlenkeuser, H.: Correlation between Arabian Sea and Greenland climate oscillations of the past 110 000 years, Nature, 393, 54–57, 1998.

Shaffrey, L. and Sutton, R.: Bjerknes compensation and the decadal variability of the energy transports in a coupled climate model, J. Climate, 19, 1167–1181, 2006.

Stocker, T. F.: Climate change – The seesaw effect, Science, 282, 61–62, 1998.

Stommel, H. M.: Thermohaline convection with two stable regimes of flow, Tellus, 13, 224–230, 1961.

Stouffer, R. J., Yin, J., Gregory, J. M., Diwon, K. W., Spelman, M. J., Hurlin, W., Weaver, A. J., Eby, M., Flato, G. M., Hasumi, H., Hu, A., Jungclaus, J. H., Kamenovich, I. V., Levermann, A., Montoya, M., Murakami, S., Nawrath, S., Oka, A., Peltier, W. R., Robitaille, D. Y., Sokolov, A., Vettoretti, G., and Weber, S. L.: Investigating the causes of the response of the thermohaline circulation to past and future climate changes, J. Climate, 19, 1365–1387, 2006.

Swingedouw, D., Braconnot, P., Delecluse, P., Guilyardi, E., and Marti, O.: The impact of global freshwater forcing on the thermohaline circulation: adjustment of North Atlantic convection sites in a CGCM, Clim. Dynam., 28, 291–305, 2007a.

Swingedouw, D., Braconnot, P., Delecluse, P., Guilyardi, E., and Marti, O.: Quantifying the AMOC feedbacks during a 2xCO2 stabilization experiment with land-ice melting, Clim. Dynam., 29, 521–534, 2007b.

Swingedouw, D., Mignot, J., Braconnot, P., Mosquet, E., Kageyama, M., and Alkama, R.: Impact of freshwater release in the North Atlantic under different climate conditions in an OAGCM, J. Climate, accepted, 2009.

Timmermann, A., Krebs, U., Justino, F., Goosse, H., and Ivanochko, T.: Mechanisms for millennial-scale global synchronization during the last glacial period, Paleoceanography, 20, PA4008, doi:10.1029/2004PA001090, 2005.

Turney, C. S. M., Kershaw, A. P., Clemens, S. C., Branch, N., Moss, P. T., and Fifield, L. K.: Millennial and orbital variations of El Niño/Southern Oscillation and high-latitude climate in the last glacial period, Nature, 428, 306–310, 2004.

Van Meerbeeck, C. J., Renssen, H., and Roche, D. M.: How did Marine Isotope Stage 3 and Last Glacial Maximum climates differ? - Perspectives from equilibrium simulations, Clim. Past, 5, 33–51, 2009, http://www.clim-past.net/5/33/2009/.

Vellinga, M. and Wood, R. A.: Global climatic impacts of a collapse of the Atlantic thermohaline circulation, Clim. Change, 54, 251–267, 2002.

Wang, X., Auler, A. S., Edwards, R. L., Cheng, H., Cristalli, P. S., Smart, P. L., Richards, D. A., and Shen, C.-C.: Wet periods in northeastern Brazil over the past 210 kyr linked to distant climate anomalies, Nature, 432, 740–743, 2004.

Wang, Y. J., Cheng, H., Edwards, R. L., An, Z. S., Wu, J. Y., Shen, C.-C., and Dorale, J. A.: A high-resolution absolute-dated late Pleistocene monsoon record from Hulu Cave, China, Science, 294, 2345–2348, 2001.

Weber, S. L. and Drijfhout, S. S.: Stability of the Atlantic Meridional Overturning Circulation in the Last Glacial Maximum climate, Geophys. Res. Lett., 34, L22706, doi:10.1029/2007GL031437, 2007.

Weber, S. L., Drijfhout, S. S., Abe-Ouchi, A., Crucifix, M., Eby, M., Ganopolski, A., Murakami, S., Otto-Bliesner, B., and Peltier, W. R.: The modern and glacial overturning circulation in the Atlantic ocean in PMIP coupled model simulations, Clim. Past, 3, 51–64, 2007, http://www.clim-past.net/3/51/2007/.

Xavier, P. K., Marzin, C., and Goswami, B. N.: An objective definition of the Indian summer monsoon season and a new perspective on the ENSO-monsoon relationship, Q. J. Roy. Meteor. Soc., 133, 749–764, 2007.

Yang, H. and Liu, Z.: Tropical-extra-tropical climate interaction as revealed in idealized coupled climate model experiments, Clim. Dynam., 24, 863–879, 2005.

Zhang, R. and Delworth, T. L.: Simulated tropical response to a substantial weakening of the Atlantic thermohaline circulation, J. Climate, 18, 1853–1860, 2005.

Bibliographie

Adkins, J., P. Demenocal, and G. Eshel, 2006 : The "African humid period" and the record of marine upwelling from excess Th-230 in Ocean Drilling Program Hole 658C. *Paleoceanography*, **21 (4)**, PA4203.

Altabet, M. A., M. J. Higginson, and D. W. Murray, 2002 : The effect of millennial-scale changes in Arabian Sea denitrification on atmospheric CO2. *Nature*, **415 (6868)**, 159–162.

An, Z. S., S. C. Porter, J. E. Kutzbach, X. H. Wu, S. M. Wang, X. D. Liu, X. Q. Li, and W. J. Zhou, 2000 : Asynchronous Holocene optimum of the East Asian monsoon. *Quatern. Sci. Rev.*, **19 (8)**, 743–762.

Aumont, O. and L. Bopp, 2006 : Globalizing results from ocean in situ iron fertilization studies. *Global Biogeochemical Cycles*, **20 (2)**, GB2017.

Berger, A. L., 1978 : Long-Term Variations Of Daily Insolation And Quaternary Clim. Changes. *J. Atmos. Sci.*, **35 (12)**, 2362–2367.

Bielli, S., H. Douville, and B. Pohl, 2010 : Understanding the West African monsoon variability and its remote effects : an illustration of the grid point nudging methodology. *Climate Dyn.*, **35 (1)**, 159–174.

Blanford, H., 1886 : Rainfall of India. *Mem. India Met. Dep.*, **3**, 658.

Blanke, B. and P. Delecluse, 1993 : Variability Of The Tropical Atlantic-Ocean Simulated By A General-Circulation Model With 2 Different Mixed-Layer Physics. *J. Phys. Oceanogr.*, **23 (7)**, 1363–1388.

Bond, G., et al., 1997 : A pervasive millennial-scale cycle in North Atlantic Holocene and glacial climates. *Science*, **278 (5341)**, 1257–1266.

Bond, G., et al., 2001 : Persistent solar influence on north Atlantic climate during the Holocene. *Science*, **294 (5549)**, 2130–2136.

Bony, S. and K. A. Emanuel, 2001 : A parameterization of the cloudiness associated with cumulus convection ; Evaluation using TOGA COARE data. *Journal Of The Atmospheric Sciences*, **58 (21)**, 3158–3183.

Box, G. E. P. and N. R. Draper, 1987 : *Empirical Model-Building and response Surfaces*. Wiley.

Braconnot, P., S. Joussaume, N. de Noblet, and G. Ramstein, 2000a : Mid-holocene and Last Glacial Maximum African monsoon changes as simulated within the Paleoclimate Modelling Intercomparison Project. *Global And Planetary Change*, **26 (1-3)**, 51–66.

Braconnot, P., S. Joussaume, O. Marti, and N. de Noblet, 1999 : Synergistic feedbacks from ocean and vegetation on the African monsoon response to mid-Holocene insolation. *Geophys. Res. Lett.*, **26 (16)**, 2481–2484.

Braconnot, P., M. F. Loutre, B. Dong, S. Joussaume, and P. Valdes, 2002 : How the simulated change in monsoon at 6 ka BP is related to the simulation of the modern climate : results from the Paleoclimate Modeling Intercomparison Project. *Climate Dyn.*, **19 (2)**, 107–121.

Braconnot, P. and O. Marti, 2003 : Impact of precession on monsoon characteristics from coupled ocean atmosphere experiments : changes in Indian monsoon and Indian ocean climatology. *Marine Geology*, **201 (1-3)**, 23–34.

Braconnot, P., O. Marti, S. Joussaume, and Y. Leclainche, 2000b : Ocean feedback in response to 6 kyr BP insolation. *J. Climate*, **13 (9)**, 1537–1553.

Braconnot, P., C. Marzin, L. Gregoire, E. Mosquet, and O. Marti, 2008 : Monsoon response to changes in Earth's orbital parameters : comparisons between simulations of the Eemian and of the Holocene. *Clim. Past Discuss.*, **4**, 459–493.

Braconnot, P., et al., 2007a : Results of PMIP2 coupled simulations of the Mid-Holocene and Last Glacial Maximum - Part 1 : experiments and large-scale features. *Clim. Past*, **3 (2)**, 261–277.

Braconnot, P., et al., 2007b : Results of PMIP2 coupled simulations of the Mid-Holocene and Last Glacial Maximum - Part 2 : feedbacks with emphasis on the location of the ITCZ and mid- and high latitudes heat budget. *Clim. Past*, **3 (2)**, 279–296.

Brown, E. T., T. C. Johnson, C. A. Scholz, A. S. Cohen, and J. W. King, 2007 : Abrupt change in tropical African climate linked to the bipolar seesaw over the past 55,000 years. *Geophys. Res. Lett.*, **34 (20)**, L20 702.

Brown, J., M. Collins, A. W. Tudhope, and T. Toniazzo, 2008 : Modelling mid-Holocene tropical climate and ENSO variability : towards constraining predictions of future change with palaeo-data. *Climate Dyn.*, **30 (1)**, 19–36.

Camberlin, P., 1995 : June-September Rainfall In North-Eastern Africa And Atmospheric Signals Over The Tropics - A Zonal Perspective. *International Journal Of Climatology*, **15 (7)**, 773–783.

Camberlin, P., 1997 : Rainfall anomalies in the source region of the Nile and their connection with the Indian summer monsoon. *J. Climate*, **10 (6)**, 1380–1392.

Camberlin, P., B. Fontaine, S. Louvut, P. Oettli, and P. Valimba, 2010 : Climate Adjustments over Africa Accompanying the Indian Monsoon Onset. *J. Climate*, **23 (8)**, 2047–2064.

Chang, P., et al., 2008 : Oceanic link between abrupt changes in the North Atlantic Ocean and the African monsoon. *Nature Geoscience*, **1 (7)**, 444–448.

Chatfield, R. B., H. Guan, A. M. Thompson, and J. C. Witte, 2004 : Convective lofting links Indian Ocean air pollution to paradoxical South Atlantic ozone maxima. *Geophys. Res. Lett.*, **31 (6)**, L06 103.

Chen, F. H., et al., 2008 : Holocene moisture evolution in arid central Asia and its out-of-phase relationship with Asian monsoon history. *Quatern. Sci. Rev.*, **27 (3-4)**, 351–364.

Chiang, J. C. H., 2009 : The Tropics in Paleoclimate. *Annual Review Of Earth And Planetary Sciences*, **37**, 263–297.

Chou, C. and J. D. Neelin, 2003 : Mechanisms limiting the northward extent of the northern summer monsoons over North America, Asia, and Africa. *J. Climate*, **16 (3)**, 406–425.

Claussen, M. and V. Gayler, 1997 : The greening of the Sahara during the mid-Holocene : results of an interactive atmosphere-biome model. *Global Ecology And Biogeography Letters*, **6 (5)**, 369–377.

Claussen, M., C. Kubatzki, V. Brovkin, A. Ganopolski, P. Hoelzmann, and H. J. Pachur, 1999 : Simulation of an abrupt change in Saharan vegetation in the mid-Holocene. *Geophys. Res. Lett.*, **26 (14)**, 2037–2040.

Clemens, S., W. Prell, D. Murray, G. Shimmield, and G. Weedon, 1991 : Forcing Mechanisms Of The Indian-Ocean Monsoon. *Nature*, **353 (6346)**, 720–725.

Clemens, S. C., W. L. Prell, Y. B. Sun, Z. Y. Liu, and G. S. Chen, 2008 : Southern Hemisphere forcing of Pliocene delta O-18 and the evolution of Indo-Asian monsoons. *Paleoceanography*, **23 (4)**, PA4210.

Clement, A. C. and L. C. Peterson, 2008 : Mechanisms of abrupt climate change of the last glacial period. *Rev. Geophys.*, **46 (4)**, RG4002.

COHMAP Members, ., 1988 : Clim. Changes of the Last 18,000 Years : Observations and Model Simulations. *Science*, **241**, 1043–1052.

Cole, J., 2001 : Paleoclimate - A slow dance for El Nino. *Science*, **291 (5508)**, 1496–1497.

Cook, K. H. and E. K. Vizy, 2006 : Coupled model simulations of the west African monsoon system : Twentieth- and Twenty-First-century simulations. *J. Climate*, **19 (15)**, 3681–3703.

deMenocal, P., J. Ortiz, T. Guilderson, J. Adkins, M. Sarnthein, L. Baker, and M. Yarusinsky, 2000 : Abrupt onset and termination of the African Humid Period : rapid climate responses to gradual insolation forcing. *Quatern. Sci. Rev.*, **19 (1-5)**, 347–361.

deNoblet, N., P. Braconnot, S. Joussaume, and V. Masson, 1996 : Sensitivity of simulated Asian and African summer monsoons to orbitally induced variations in insolation 126, 115 and 6kBP. *Climate Dyn.*, **12 (9)**, 589–603.

Djamali, M., et al., 2010 : Indian Summer Monsoon variations could have affected the early-Holocene woodland expansion in the Near East. *Holocene*, **20 (5)**, 813–820.

Douville, H., F. Chauvin, and H. Broqua, 2001 : Influence of soil moisture on the Asian and African monsoons Part I : mean monsoon and daily precipitation. *J. Climate*, **14**, 2381—-2403.

Duplessy, J. C., 1982 : Glacial to interglacial contrasts in the northern Indian Ocean. *Nature*, **295 (5849)**, 494–498, URL `http://dx.doi.org/10.1038/295494a0`.

Emanuel, K. A., 1991 : A Scheme For Representing Cumulus Convection In Large-Scale Models. *Journal Of The Atmospheric Sciences*, **48 (21)**, 2313–2335.

Fein, J. S. and P. L. Stephens, (Eds.) , 1987 : *Monsoons*. Wiley-Interscience Publication, 632 pp, John Wiley and Sons, New York.

Feng, S. and Q. Hu, 2008 : How the North Atlantic Multidecadal Oscillation may have influenced the Indian summer monsoon during the past two millennia. *Geophys. Res. Lett.*, **35 (1)**, L01 707.

Fichefet, T. and M. A. M. Maqueda, 1997 : Sensitivity of a global sea ice model to the treatment of ice thermodynamics and dynamics. *J. Geophys. Res.*, **102 (C6)**, 12 609–12 646.

Fleitmann, D., S. J. Burns, M. Mudelsee, U. Neff, J. Kramers, A. Mangini, and A. Matter, 2003 : Holocene forcing of the Indian monsoon recorded in a stalagmite from Southern Oman. *Science*, **300 (5626)**, 1737–1739.

Fleitmann, D., et al., 2007 : Holocene ITCZ and Indian monsoon dynamics recorded in stalagmites from Oman and Yemen (Socotra). *Quatern. Sci. Rev.*, **26 (1-2)**, 170–188.

Fontaine, B., et al., 2010 : Impacts of warm and cold situations in the Mediterranean basins on the West African monsoon : observed connection patterns (1979-2006) and climate simulations. *Climate Dyn.*, **35 (1)**, 95–114.

Gadgil, S., 2003 : The Indian monsoon and its variability. *Annual Review Of Earth And Planetary Sciences*, **31**, 429–467.

Gasse, F., 2000 : Hydrological changes in the African tropics since the Last Glacial Maximum. *Quatern. Sci. Rev.*, **19 (1-5)**, 189–211.

Gasse, F. and E. Vancampo, 1994 : Abrupt Postglacial Climate Events In West Asia And North-Africa Monsoon Domains. *Earth And Planetary Science Letters*, **126 (4)**, 435–456.

Gehlen, M., R. Gangsto, B. Schneider, L. Bopp, O. Aumont, and C. Ethe, 2007 : The fate of pelagic CaCO3 production in a high CO2 ocean : a model study. *Biogeosciences*, **4 (4)**, 505–519.

Giannini, A., R. Saravanan, and P. Chang, 2003 : Oceanic forcing of Sahel rainfall on interannual to interdecadal time scales. *Science*, **302 (5647)**, 1027–1030.

Gill, A. E., 1980 : Some simple solutions for heat-induced tropical circulation. *Quart. J. Roy. Meteor. Soc.*, **106**, 447–462.

Goni, M. F. S., A. Landais, W. J. Fletcher, F. Naughton, S. Desprat, and J. Duprat, 2008 : Contrasting impacts of Dansgaard-Oeschger events over a western European latitudinal transect modulated by orbital parameters. *Quatern. Sci. Rev.*, **27 (11-12)**, 1136–1151.

Goswami, B. N., 2005 : South Asian Monsoon. *Intraseasonal variability in the Atmosphere-Ocean climate system*, Praxis. Springer Berlin Heidelberg.

Goswami, B. N., M. S. Madhusoodanan, C. P. Neema, and D. Sengupta, 2006 : A physical mechanism for North Atlantic SST influence on the Indian summer monsoon. *Geophys. Res. Lett.*, **33 (2)**, L02 706.

Guilyardi, E., 2006 : El Nino-mean state-seasonal cycle interactions in a multi-model ensemble. *Climate Dyn.*, **26 (4)**, 329–348.

Gupta, A. K., 2004 : Origin of agriculture and domestication of plants and animals linked to early Holocene climate amelioration. *Current Science*, **87 (1)**, 54–59.

Gupta, A. K., D. M. Anderson, and J. T. Overpeck, 2003 : Abrupt changes in the Asian southwest monsoon during the Holocene and their links to the North Atlantic Ocean. *Nature*, **421 (6921)**, 354–357.

Gupta, A. K., D. M. Anderson, D. N. Pandey, and A. K. Singhvi, 2006 : Adaptation and human migration, and evidence of agriculture coincident with changes in the Indian summer monsoon during the Holocene. *Current Science*, **90 (8)**, 1082–1090.

Hall, N. M. J. and P. Peyrille, 2006 : Dynamics of the west African monsoon. *Journal De Physique Iv*, **139**, 81–99.

Halley, E., 1686 : An historical account of the trade winds, and monsoons, observable in the seas between and near the Tropicks, with an attempt to assign the physical cause of said winds. *Phil. Trans. of the Royal Soc. of London*, **26**, 153–168.

Harrison, S. P., et al., 1998 : Intercomparison of simulated global vegetation distributions in response to 6 kyr BP orbital forcing. *J. Climate*, **11 (11)**, 2721–2742.

Haug, G. H., K. A. Hughen, D. M. Sigman, L. C. Peterson, and U. Rohl, 2001 : Southward migration of the intertropical convergence zone through the Holocene. *Science*, **293 (5533)**, 1304–1308.

He, H. Y., C. H. Sui, M. Q. Jian, Z. P. Wen, and G. D. Lan, 2003 : The evolution of tropospheric temperature field and its relationship with the onset of Asian summer monsoon. *J. Meteor. Soc. Japan*, **81 (5)**, 1201–1223.

Hely, C., P. Braconnot, J. Watrin, and W. P. Zheng, 2009 : Climate and vegetation : Simulating the African humid period. *Comptes Rendus Geoscience*, **341 (8-9)**, 671–688.

Hewitt, C. D. and J. F. B. Mitchell, 1998 : A fully coupled GCM simulation of the climate of the mid-Holocene. *Geophys. Res. Lett.*, **25 (3)**, 361–364.

Hoelzmann, P., D. Jolly, S. P. Harrison, F. Laarif, R. Bonnefille, and H. J. Pachur, 1998 : Mid-Holocene land-surface conditions in northern Africa and the Arabian Peninsula : A data set for the analysis of biogeophysical feedbacks in the climate system. *Global Biogeochemical Cycles*, **12 (1)**, 35–51.

Hoskins, B., R. Neale, M. Rodwell, and G. Y. Yang, 1999 : Aspects of the large-scale tropical atmospheric circulation. *Tellus Series A-Dynamic Meteorology And Oceanography*, **51 (1)**, 33–44.

Hoskins, B. J. and M. J. Rodwell, 1995 : A Model Of The Asian Summer Monsoon .1. The Global-Scale. *Journal Of The Atmospheric Sciences*, **52 (9)**, 1329–1340.

Hourdin, F., et al., 2006 : The LMDZ4 general circulation model : climate performance and sensitivity to parametrized physics with emphasis on tropical convection. *Climate Dyn.*, **27 (7-8)**, 787–813.

Hsu, H.-H., 2005 : East Asian Monsoon. *Intraseasonal variability in the Atmosphere-Ocean climate system*, Praxis. Springer Berlin Heidelberg.

Ivanochko, T. S., R. S. Ganeshram, G. J. A. Brummer, G. Ganssen, S. J. A. Jung, S. G. Moreton, and D. Kroon, 2005 : Variations in tropical convection as an amplifier of global climate change at the millennial scale. *Earth And Planetary Science Letters*, **235 (1-2)**, 302–314.

Janicot, S., 2009 : A comparison of Indian and African monsoon variability at different time scales. *Comptes Rendus Geoscience*, **341 (8-9)**, 575–590.

Janicot, S., J. Lafore, and C. Thorncroft, 2010 : The West African Monsoon. Tech. rep., WMO report.

Janicot, S., F. Mounier, N. M. J. Hall, S. Leroux, B. Sultan, and G. N. Kiladis, 2009 : Dynamics of the West African Monsoon. Part IV : Analysis of 25-90-Day Variability of Convection and the Role of the Indian Monsoon. *J. Climate*, **22 (6)**, 1541–1565.

Janicot, S., S. Trzaska, and I. Poccard, 2001 : Summer Sahel-ENSO teleconnection and decadal time scale SST variations. *Climate Dyn.*, **18 (3-4)**, 303–320.

Jolly, D., et al., 1998 : Biome reconstruction from pollen and plant macrofossil data for Africa and the Arabian peninsula at 0 and 6000 years. *Journal Of Biogeography*, **25 (6)**, 1007–1027.

Joly, M., A. Voldoire, H. Douville, P. Terray, and J. F. Royer, 2007 : African monsoon teleconnections with tropical SSTs : validation and evolution in a set of IPCC4 simulations. *Climate Dyn.*, **29 (1)**, 1–20.

Joussaume, S. and P. Braconnot, 1997 : Sensitivity of paleoclimate simulation results to season definitions. *J. Geophys. Res.*, **102 (D2)**, 1943–1956.

Joussaume, S. and K. E. Taylor, 1995 : *Proceedings of the First International AMIP Scientific Conference, 15- 19 May 1995*, chap. Status of the Paleoclimate Modeling Intercomparison Project (PMIP), 425–430. World Clim. Res. Prog., Monterey, Calif.

Joussaume, S., et al., 1999 : Monsoon changes for 6000 years ago : Results of 18 simulations from the Paleoclimate Modeling Intercomparison Project (PMIP). *Geophys. Res. Lett.*, **26 (7)**, 859–862.

Kageyama, M., J. Mignot, D. Swingedouw, C. Marzin, R. Alkama, and O. Marti, 2009 : Glacial climate sensitivity to different states of the Atlantic Meridional Overturning Circulation : results from the IPSL model. *Clim. Past*, **5 (3)**, 551–570.

Kalnay, E., et al., 1996 : The NCEP/NCAR 40-year reanalysis project. *Bulletin Of The American Meteorological Society*, **77 (3)**, 437–471.

Kistler, R., et al., 2001 : The NCEP-NCAR 50-year reanalysis : Monthly means CD-ROM and documentation. *Bulletin Of The American Meteorological Society*, **82 (2)**, 247–267.

Koutavas, A., P. B. Demenocal, G. C. Olive, and J. Lynch-Stieglitz, 2006 : Mid-Holocene El Nino-Southern Oscillation (ENSO) attenuation revealed by individual foraminifera in eastern tropical Pacific sediments. *Geology*, **34 (12)**, 993–996.

Krinner, G., et al., 2005 : A dynamic global vegetation model for studies of the coupled atmosphere-biosphere system. *Global Biogeochemical Cycles*, **19 (1)**, GB1015.

Kripalani, R. H., J. H. Oh, A. Kulkarni, S. S. Sabade, and H. S. Chaudhari, 2007 : South Asian summer monsoon precipitation variability : Coupled climate model simulations and projections under IPCC AR4. *Theor. Appl. Climatol.*, **90 (3-4)**, 133–159.

Kropelin, S., et al., 2008 : Climate-driven ecosystem succession in the Sahara : The past 6000 years. *Science*, **320 (5877)**, 765–768.

Kucharski, F., A. Bracco, J. H. Yoo, A. M. Tompkins, L. Feudale, P. Ruti, and A. Dell'Aquila, 2009 : A Gill-Matsuno-type mechanism explains the tropical Atlantic influence

on African and Indian monsoon rainfall. *Quarterly Journal Of The Royal Meteorological Society*, **135 (640)**, 569–579.

Kutzbach, J. E., 1981 : Monsoon Climate Of The Early Holocene - Climate Experiment With The Earths Orbital Parameters For 9000 Years Ago. *Science*, **214 (4516)**, 59–61.

Kutzbach, J. E. and R. G. Gallimore, 1988 : Sensitivity Of A Coupled Atmosphere Mixed Layer Ocean Model To Changes In Orbital Forcing At 9000 Years Bp. *J. Geophys. Res.*, **93 (D1)**, 803–821.

Kutzbach, J. E. and Z. Liu, 1997 : Response of the African monsoon to orbital forcing and ocean feedbacks in the middle Holocene. *Science*, **278 (5337)**, 440–443.

Kutzbach, J. E. and B. L. Ottobliesner, 1982 : The Sensitivity Of The African-Asian Monsoonal Climate To Orbital Parameter Changes For 9000 Years Bp In A Low-Resolution General-Circulation Model. *Journal Of The Atmospheric Sciences*, **39 (6)**, 1177–1188.

Lafore, J., C. Flamand, F. Giraud, F. Guichard, P. Knippertz, J. Mahfouf, P. Mascart, and E. Williams, 2010 : Editorial Introduction to the AMMA Special Issue on Advances in understanding atmospheric processes over West Africa through the AMMA field campaign. *Quart. J. Roy. Meteor. Soc.*, **136(s1)**, 2–7.

Lavaysse, C., C. Flamant, S. Janicot, LaforeJ-.P., D. Parker, and J. Pelon, 2009 : Seasonal cycle of the West African heat low : a climatological perspective. *Climate Dyn.*, **33**, 313–330.

Leuschner, D. C. and F. Sirocko, 2000 : The low-latitude monsoon climate during Dansgaard-Oeschger cycles and Heinrich Events. *Quatern. Sci. Rev.*, **19 (1-5)**, 243–254.

Levitus, S., 1998 : World Ocean Database 1998, vol. 1, Introduction. Tech. rep., NOAA Atlas NESDIS 18.

Levy, M., D. Shankar, J. M. Andre, S. S. C. Shenoi, F. Durand, and C. Boyer de Montegut, 2007 : Basin-wide seasonal evolution of the Indian Ocean's phytoplankton blooms. *J. Geophys. Res.-Oceans*, **112 (C12)**, C12 014.

Lezine, A. M., 2009 : Timing of vegetation changes at the end of the Holocene Humid Period in desert areas at the northern edge of the Atlantic and Indian monsoon systems. *Comptes Rendus Geoscience*, **341 (8-9)**, 750–759.

Lezine, A. M. and J. Casanova, 1991 : Correlated Oceanic And Continental Records Demonstrate Past Climate And Hydrology Of North-Africa (0-140-Ka). *Geology*, **19 (4)**, 307–310.

Lezine, A. M., J. J. Tiercelin, C. Robert, J. F. Saliege, S. Cleuziou, M. L. Inizan, and F. Braemer, 2007 : Centennial to millennial-scale variability of the Indian monsoon during the early Holocene from a sediment, pollen and isotope record from the desert of Yemen. *Palaeogeography Palaeoclimatology Palaeoecology*, **243 (3-4)**, 235–249.

Liebmann, B. and C. A. Smith, 1996 : Description of a complete (interpolated) outgoing longwave radiation dataset. *Bulletin Of The American Meteorological Society*, **77 (6)**, 1275–1277.

Liu, X. D. and Z. G. Shi, 2009 : Effect of precession on the Asian summer monsoon evolution : A systematic review. *Chinese Science Bulletin*, **54 (20)**, 3720–3730.

Liu, Z., S. P. Harrison, J. Kutzbach, and B. Otto-Bliesner, 2004 : Global monsoons in the mid-Holocene and oceanic feedback. *Climate Dyn.*, **22 (2-3)**, 157–182.

Liu, Z., et al., 2007 : Simulating the transient evolution and abrupt change of Northern Africa atmosphere-ocean-terrestrial ecosystem in the Holocene. *Quatern. Sci. Rev.*, **26 (13-14)**, 1818–1837.

Losada, T., B. Rodriguez-Fonseca, I. Polo, S. Janicot, S. Gervois, F. Chauvin, and P. Ruti, 2010 : Tropical response to the Atlantic Equatorial mode : AGCM multimodel approach. *Climate Dyn.*, **35 (1)**, 45–52.

Lott, F., 1999 : Alleviation of stationary biases in a GCM through a mountain drag parameterization scheme and a simple representation of mountain lift forces. *Monthly Weather Review*, **127 (5)**, 788–801.

Lu, R. Y. and B. W. Dong, 2008 : Response of the Asian Summer Monsoon to Weakening of Atlantic Thermohaline Circulation. *Advances In Atmospheric Sciences*, **25 (5)**, 723–736.

Madec, G., P. Delecluse, M. Imbard, and C. Levy, 1998 : *OPA version 8.1 ocean general circulation model reference manual*. Paris, France, LODYC/IPSL, 11.

Maher, B. A., 2008 : Holocene variability of the East Asian summer monsoon from Chinese cave records : a re-assessment. *Holocene*, **18 (6)**, 861–866.

Maloney, E. D. and J. Shaman, 2008 : Intraseasonal variability of the West African monsoon and Atlantic ITCZ. *J. Climate*, **21 (12)**, 2898–2918.

Marti, O., et al., 2005 : The New IPSL Climate System Model : IPSL-Cm4. *Note du Pôle de Modélisation*, **n26**, ISSN 1288–1619.

Marti, O., et al., 2010 : Key features of the IPSL ocean atmosphere model and its sensitivity to atmospheric resolution. *Climate Dyn.*, DOI 10.1007/s00 382–009–0640–6.

Marzin, C. and P. Braconnot, 2009a : The role of the ocean feedback on Asian and African monsoon variations at 6 kyr and 9.5 kyr BP. *Comptes Rendus Geoscience*, **341 (8-9)**, 643–655.

Marzin, C. and P. Braconnot, 2009b : Variations of Indian and African monsoons induced by insolation changes at 6 and 9.5 kyr BP. *Climate Dyn.*, **33 (2-3)**, 215–231.

Mathien-Blard, E., 2009 : Révision du paléothermomètre Mg/Ca et son application sur l'hydrologie de surface de l'Océan Indien Tropical au cours de l'Holocène. Ph.D. thesis, Université Paris XI.

Mathien-Blard, E. and F. Bassinot, 2009 : Salinity bias on the foraminifera Mg/Ca thermometry : Correction procedure and implications for past ocean hydrographic reconstructions. *Geochemistry Geophysics Geosystems*, **10**, Q12 011.

Meehl, G. A., C. Covey, T. Delworth, M. Latif, B. McAvaney, J. F. B. Mitchell, R. J. Stouffer, and K. E. Taylor, 2007 : The WCRP CMIP3 multimodel dataset - A new era in climate change research. *Bull. Amer. Meteor. Soc.*, **88 (9)**, 1383–+.

Mitchell, J. F. B., N. S. Grahame, and K. J. Needham, 1988 : Climate Simulations For 9000 Years Before Present - Seasonal-Variations And Effect Of The Laurentide Ice-Sheet. *J. Geophys. Res.-Atmospheres*, **93 (D7)**, 8283–8303.

Ohgaito, R. and A. Abe-Ouchi, 2007 : The role of ocean thermodynamics and dynamics in Asian summer monsoon changes during the mid-Holocene. *Climate Dyn.*, **29 (1)**, 39–50.

Okumura and Xie, 2004 : Interaction of the Atlantic Equatorial Cold Tongue and the African Monsoon. *J. Climate*, **17**, 3589–3602.

Overpeck, J., D. Anderson, S. Trumbore, and W. Prell, 1996 : The southwest Indian Monsoon over the last 18000 years. *Climate Dyn.*, **12 (3)**, 213–225.

Petit-Maire, N., 1999 : Natural variability of the Earth's environments : the last two climatic extremes (18000 +/- 2000 and 8000 +/- 1000 yrs BP). *Comptes Rendus De L Academie Des Sciences Serie Ii Fascicule A-Sciences De La Terre Et Des Planetes*, **328 (4)**, 273–+.

Porter, S. C. and Z. S. An, 1995 : Correlation Between Climate Events In The North-Atlantic And China During Last Glaciation. *Nature*, **375 (6529)**, 305–308.

Prasad, S. and Y. Enzel, 2006 : Holocene paleoclimates of India. *Quat. Res.*, **66 (3)**, 442–453.

Prell, W. L. and J. E. Kutzbach, 1987 : Monsoon Variability Over The Past 150,000 Years. *J. Geophys. Res.*, **92 (D7)**, 8411–8425.

Prentice, I. C., J. Guiot, B. Huntley, D. Jolly, and R. Cheddadi, 1996 : Reconstructing biomes from palaeoecological data : A general method and its application to European pollen data at 0 and 6 ka. *Climate Dyn.*, **12 (3)**, 185–194.

Prentice, I. C. and T. Webb, 1998 : BIOME 6000 : reconstructing global mid-Holocene vegetation patterns from palaeoecological records. *Journal Of Biogeography*, **25 (6)**, 997–1005.

Raicich, F., N. Pinardi, and A. Navarra, 2003 : Teleconnections between Indian monsoon and Sahel rainfall and the Mediterranean. *International Journal Of Climatology*, **23 (2)**, 173–186.

Ramesh, R., 2001 : High resolution Holocene monsoon records from different proxies : An assessment of their consistency. *Current Science*, **81 (11)**, 1432–1436.

Rashid, H., B. P. Flower, R. Z. Poore, and T. M. Quinn, 2007 : A similar to 25 ka Indian Ocean monsoon variability record from the Andaman Sea. *Quatern. Sci. Rev.*, **26 (19-21)**, 2586–2597.

Roca, R., J. P. Lafore, C. Piriou, and J. L. Redelsperger, 2005 : Extratropical dry-air intrusions into the West African monsoon midtroposphere : An important factor for the convective activity over the Sahel. *Journal Of The Atmospheric Sciences*, **62 (2)**, 390–407.

Rodwell, M. J. and B. J. Hoskins, 1996 : Monsoons and the dynamics of deserts. *Quart. J. Roy. Meteor. Soc.*, **122 (534)**, 1385–1404.

Rodwell, M. J. and B. J. Hoskins, 2001 : Subtropical anticyclones and summer monsoons. *J. Climate*, **14 (15)**, 3192–3211.

Rowell, D. P., 2001 : Teleconnections between the tropical Pacific and the Sahel. *Quarterly Journal Of The Royal Meteorological Society*, **127 (575)**, 1683–1706.

Rowell, D. P., 2003 : The impact of Mediterranean SSTs on the Sahelian rainfall season. *J. Climate*, **16 (5)**, 849–862.

Ruddiman, W. F., 2006 : What is the timing of orbital-scale monsoon changes ? *Quatern. Sci. Rev.*, **25 (7-8)**, 657–658.

Sadourny, R. and K. Laval, 1984 : January and July performance of the LMD general circulation model. *New perspectives in Climate Modeling*, 173–197.

Sarkar, A., R. Ramesh, B. L. K. Somayajulu, R. Agnihotri, A. J. T. Jull, and G. S. Burr, 2000 : High resolution Holocene monsoon record from the eastern Arabian Sea. *Earth And Planetary Science Letters*, **177 (3-4)**, 209–218.

Schulz, H., U. von Rad, and H. Erlenkeuser, 1998 : Correlation between Arabian Sea and Greenland climate oscillations of the past 110,000 years. *Nature*, **393 (6680)**, 54–57.

Solomon, S., D. Qin, M. Manning, Z. Chen, M. Marquis, K. B. Averyt, M. Tignor, and H. L. Miller, (Eds.) , 2007 : *IPCC 2007 : Climate Change 2007 : The Physical Basis. Contribution of Working Group I to the Fourth Assessment Report of the Intergovernmental Panel on Climate Change*. Cambridge University Press, Cambridge, United Kingdom and New York, NY, USA.

Srinivasan, J., 2006 : Holocene precipitation and theories of monsoon. *Journal Of The Geological Society Of India*, **68 (3)**, 527–532.

Staubwasser, M., 2006 : An overview of Holocene South Asian monsoon records - Monsoon domains and regional contrasts. *Journal Of The Geological Society Of India*, **68 (3)**, 433–446.

Sultan, B., S. Janicot, and A. Diedhiou, 2003 : The West African monsoon dynamics. Part I : Documentation of intraseasonal variability. *J. Climate*, **16 (21)**, 3389–3406.

Swingedouw, D., 2006 : Origine et impact climatique d'un changement de circulation thermohaline au cours des prochains siècles dans le modèle IPSL-CM4. Ph.D. thesis, Université Pierre et Marie Curie (Paris 6).

Swingedouw, D., P. Braconnot, P. Delecluse, E. Guilyardi, and O. Marti, 2007 : The impact of global freshwater forcing on the thermohaline circulation : adjustment of North Atlantic convection sites in a CGCM. *Climate Dyn.*, **28 (2-3)**, 291–305.

Swingedouw, D., P. Braconnot, and O. Marti, 2006 : Sensitivity of the Atlantic Meridional Overturning Circulation to the melting from northern glaciers in climate change experiments. *Geophys. Res. Lett.*, **33 (7)**, L07 711.

Swingedouw, D., J. Mignot, P. Braconnot, E. Mosquet, M. Kageyama, and R. Alkama, 2009 : Impact of Freshwater Release in the North Atlantic under Different Climate Conditions in an OAGCM. *J. Climate*, **22 (23)**, 6377–6403.

Terray, L., E. Sevault, E. Guilyardi, and O. Thual, 1995 : *The OASIS coupler user guide version 2.0.*

Texier, D., N. de Noblet, and P. Braconnot, 2000 : Sensitivity of the African and Asian monsoons to mid-Holocene insolation and data-inferred surface changes. *J. Climate*, **13 (1)**, 164–181.

Texier, D., et al., 1997 : Quantifying the role of biosphere-atmosphere feedbacks in climate change : coupled model simulations for 6000 years BP and comparison with palaeodata for northern Eurasia and northern Africa. *Climate Dyn.*, **13 (12)**, 865–882.

Torrence, C. and P. J. Webster, 1999 : Interdecadal changes in the ENSO-monsoon system. *J. Climate*, **12 (8)**, 2679–2690.

Trenberth, K. E., D. P. Stepaniak, and J. M. Caron, 2000 : The global monsoon as seen through the divergent atmospheric circulation. *J. Climate*, **13 (22)**, 3969–3993.

Tuenter, E., S. L. Weber, F. J. Hilgen, L. J. Lourens, and A. Ganopolski, 2005 : Simulation of climate phase lags in response to precession and obliquity forcing and the role of vegetation. *Climate Dyn.*, **24 (2-3)**, 279–295.

Tzedakis, P. C., 2007 : Seven ambiguities in the Mediterranean palaeoenvironmental narrative. *Quatern. Sci. Rev.*, **26 (17-18)**, 2042–2066.

Tzedakis, P. C., H. Palike, K. H. Roucoux, and L. de Abreu, 2009 : Atmospheric methane, southern European vegetation and low-mid latitude links on orbital and millennial timescales. *Earth And Planetary Science Letters*, **277 (3-4)**, 307–317.

Vellinga, M. and R. A. Wood, 2002 : Global climatic impacts of a collapse of the Atlantic thermohaline circulation. *Clim. Change*, **54 (3)**, 251–267.

Vizy, E. K. and K. H. Cook, 2003 : Connections between the summer east African and Indian rainfall regimes. *J. Geophys. Res.-Atmospheres*, **108 (D16)**, 4510.

Voss, R. and U. Mikolajewicz, 2001 : The climate of 6000 years BP in near-equilibrium simulations with a coupled AOGCM. *Geophys. Res. Lett.*, **28 (11)**, 2213–2216.

Walker, G., 1910 : On the meteorological evidence for supposed changes of climate in India. *Mem. India Met. Dep.*, **21 :1**, 1–21.

Wang, B., (Ed.) , 2006 : *The Asian Monsoon*. Springer/Praxis Publishing Co.

Wang, B., S. C. Clemens, and P. Liu, 2003 : Contrasting the Indian and East Asian monsoons : implications on geologic timescales. *Marine Geology*, **201 (1-3)**, 5–21.

Wang, B. and Q. H. Ding, 2006 : Changes in global monsoon precipitation over the past 56 years. *Geophys. Res. Lett.*, **33 (6)**, L06 711.

Wang, B. and Q. H. Ding, 2008 : Global monsoon : Dominant mode of annual variation in the tropics. *Dynamics Of Atmospheres And Oceans*, **44 (3-4)**, 165–183.

Wang, B., R. G. Wu, and K. M. Lau, 2001a : Interannual variability of the Asian summer monsoon : Contrasts between the Indian and the western North Pacific-east Asian monsoons. *J. Climate*, **14 (20)**, 4073–4090.

Wang, P. X., S. Clemens, L. Beaufort, P. Braconnot, G. Ganssen, Z. M. Jian, P. Kershaw, and M. Sarnthein, 2005 : Evolution and variability of the Asian monsoon system : state of the art and outstanding issues. *Quatern. Sci. Rev.*, **24 (5-6)**, 595–629.

Wang, Y. J., H. Cheng, R. L. Edwards, Z. S. An, J. Y. Wu, C. C. Shen, and J. A. Dorale, 2001b : A high-resolution absolute-dated Late Pleistocene monsoon record from Hulu Cave, China. *Science*, **294 (5550)**, 2345–2348.

Ward, M. N., 1998 : Diagnosis and short-lead time prediction of summer rainfall in tropical North Africa at interannual and multidecadal timescales. *J. Climate*, **11 (12)**, 3167–3191.

Watrin, J., A. M. Lezine, and C. Hely, 2009 : Plant migration and plant communities at the time of the "green Sahara". *Comptes Rendus Geoscience*, **341 (8-9)**, 656–670.

Webster, P. J., V. O. Magana, T. N. Palmer, J. Shukla, R. A. Tomas, M. Yanai, and T. Yasunari, 1998 : Monsoons : Processes, predictability, and the prospects for prediction. *J. Geophys. Res.-Oceans*, **103 (C7)**, 14 451–14 510.

Weldeab, S., D. W. Lea, R. R. Schneider, and N. Andersen, 2007 : 155,000 years of West African monsoon and ocean thermal evolution. *Science*, **316 (5829)**, 1303–1307.

Wick, L., G. Lemcke, and M. Sturm, 2003 : Evidence of Lateglacial and Holocene climatic change and human impact in eastern Anatolia : high-resolution pollen, charcoal, isotopic and geochemical records from the laminated sediments of Lake Van, Turkey. *Holocene*, **13 (5)**, 665–675.

Wright, H., J. Kutzbach, T. Webb III, W. Ruddiman, F. Street-Perrot, and P. Bartlein, (Eds.) , 1993 : *Global Climates since the Last Glacial Maximum*. University of Minnesota Press.

Wu, G. X., Y. Liu, X. Zhu, W. Li, R. Ren, A. Duan, and X. Liang, 2009 : Multi-scale forcing and the formation of subtropical desert and monsoon. *Annales Geophysicae*, **27 (9)**, 3631–3644.

Xavier, P. K., J. P. Duvel, P. Braconnot, and F. J. Doblas-Reyes, 2010 : An Evaluation Metric for Intraseasonal Variability and its Application to CMIP3 Twentieth-Century Simulations. *J. Climate*, **23 (13)**, 3497–3508.

Xavier, P. K., C. Marzin, and B. N. Goswami, 2007 : An objective definition of the Indian summer monsoon season and a new perspective on the ENSO-monsoon relationship. *Quart. J. Roy. Meteor. Soc.*, **133 (624)**, 749–764.

Xie, P. P. and P. A. Arkin, 1997 : Global precipitation : A 17-year monthly analysis based on gauge observations, satellite estimates, and numerical model outputs. *Bulletin Of The American Meteorological Society*, **78 (11)**, 2539–2558.

Yanai, M. H., C. F. Li, and Z. S. Song, 1992 : Seasonal Heating Of The Tibetan Plateau And Its Effects On The Evolution Of The Asian Summer Monsoon. *J. Meteor. Soc. Japan*, **70 (1B)**, 319–351.

Zeist, W. v. and S. Bottema, 1991 : *Late Quaternary vegetation of the Near East*. Wiesbaden.

Zhang, R. and T. L. Delworth, 2005 : Simulated tropical response to a substantial weakening of the Atlantic thermohaline circulation. *J. Climate*, **18 (12)**, 1853–1860.

Zhao, Y., P. Braconnot, S. P. Harrison, P. Yiou, and O. Marti, 2007 : Simulated changes in the relationship between tropical ocean temperatures and the western African monsoon during the mid-Holocene. *Climate Dyn.*, **28 (5)**, 533–551.

Zhao, Y., et al., 2005 : A multi-model analysis of the role of the ocean on the African and Indian monsoon during the mid-Holocene. *Climate Dyn.*, **25 (7-8)**, 777–800.

Zheng, W., P. Braconnot, E. Guilyardi, U. Merkel, and Y. Yu, 2008 : ENSO at 6ka and 21ka from ocean-atmosphere coupled model simulations. *Climate Dyn.*, **30 (7-8)**, 745–762.

Ziv, B., H. Saaroni, and P. Alpert, 2004 : The factors governing the summer regime of the eastern Mediterranean. *International Journal Of Climatology*, **24 (14)**, 1859–1871.